# Dynamic Patterned Electrospun Fibres for 3D Cell Culture

**Afnan Mohammed Aladdad**
**B.Pharm.Sc (Second Honor)**

Supervisors:

Dr. Felicity Rose
Prof. Cameron Alexander
Drug Delivery and Tissue Engineering




School of Pharmacy
University of Nottingham
March 2016

# Declaration

I hereby declare that all the work described in this thesis is my own, unless otherwise stated, and that this thesis has not been submitted, neither in whole or in part, elsewhere for another degree.

---

Afnan Mohammed Aladdad

PhD Student

Drug Delivery and Tissue Engineering

University of Nottingham

March 2016

## Abstract

Current culture methods to generate large quantities of cells destined for tissue engineering and regenerative medicine commonly use enzymatic digestion. However, this method is not desirable for subsequent cell transfer to the body due to the destruction of important cell-surface proteins and the risk of enzymatic contamination [1]. Therefore, research has led to the development of thermo-responsive surfaces for the continued culture of mammalian cells, with passaging achieved via a drop in the culture temperature. Recognising that the three-dimensional (3D) culture environment influences the cell phenotype, our aim was to generate a thermo-responsive 3D fibre-based scaffold, using electrospinning, to create an enzyme-free 3D culture surface for mammalian cell expansion that would be suitable for cells destined for the clinic.

Thermo-responsive poly (poly (ethylene glycol) methacrylate), poly ($PEGMA_{188}$), with lower critical solution temperature (LCST) of 26°C has been proposed for use within this thesis. It was used in combination with poly (lactic-co-glycolic acid) (PLGA) and poly (ethylene terephthalate) (PET) polymers in order to create 3D thermo-responsive non-woven electrospun fibrous scaffolds, on which different cell types could be cultured and passaged. Poly ($PEGMA_{188}$) was prepared by free radical polymerization, and then incorporated with PLGA and PET polymers via four different methods: (i) surface adsorption, (ii) NaOH surface treatment, (iii) surface entrapment and (iv) blend-electrospinning. Blend-electrospinning was chosen over the other methods as it produced nano-PET and micro-PLGA bead-less fibres with responsive behaviour.

The biocompatibility was assessed via the adhesion and proliferation of different mammalian cell types, including (i) red fluorescent protein (RFP)-expressing 3T3 fibroblasts, (ii) green fluorescent protein (GFP)-expressing primary immortalized human mesenchymal stem cells (ihMSCs), (iii) human colon adenocarcinoma cells (Caco2) and (iv) primary human corneal stromal stem cells (hCSSCs). The cell viability (Alamar Blue assay) was determined to measure the difference in cell populations adherent to the scaffolds while changing the culture temperature. These thermo-responsive scaffolds were able to support cell adhesion and proliferation at 37°C (hydrophobic surface). Furthermore, it was possible to detach the cells from the scaffolds by decreasing the temperature to 17°C (hydrophilic surface). Irrespective of the concentration of poly ($PEGMA_{188}$) used, all scaffolds exhibited thermo-responsive proprieties; the cells were viable and proliferated in a similar manner to those cultured on control surfaces (PLGA or PET scaffolds).

Finally, the effects of the thermo-responsive polymer and 3D culture environment on the hCSSC phenotype were assessed by quantitative reverse transcription-polymerase chain reaction (RT-qPCR) and immunocytochemistry. The application of 3D environments can promote the reversion of activated corneal stromal cells' 'fibroblastic phenotype' to a desirable quiescent keratocyte phenotype. Therefore, seven thermal and enzymatic passages on responsive 3D scaffolds and 2D TCPS, respectively, were performed. Cell culture on the 3D scaffolds promoted the quiescent keratocyte phenotype, with the increased expression of the keratocyte markers, *CD34* and *ALDH*, and decreased expression of the myofibroblast marker, *ACTA2*, when compared with cells cultured on the 2D culture flasks.

In this thesis, the preparation and application of first generation, biocompatible thermo-responsive fibrous scaffolds are described. The combination of ease of preparation, positive cell response and the expansion of a desirable cell phenotype make the thermo-responsive fibres promising as a new class of materials for application in cell culture. The materials developed and studied in this thesis are believed to represent a significant contribution to the fields of biomaterials and tissue engineering.

## Publications and presentations:

Some of the work reported in this thesis has been presented in the following meetings:

**Conference paper in (TCES, Newcastle, UK, 2014):** Dynamic Patterned Electrospun Fibres for 3D Cell Growth, European cells and materials Vol. 28. Suppl. 4, 2014 (page 57).

**Conference paper in (TCES, Southampton, UK, 2015):** Creating thermo-responsive co-electrospun fibres for 3D cell growth, European cells and materials Vol. 29. Suppl. 3, 2015 (page 24).

**Conference paper in (4$^{th}$ TERMIS world congress, Boston, USA, 2015):** Creating thermo-responsive co-electrospun fibres for 3D cell growth, Tissue engineering part A, Sep 2015.

**Conference paper in (4$^{th}$ TERMIS world congress, Boston, USA, 2015):** A 3D Thermo-responsive Scaffold System for the Continued Culture and Passaging of Primary Human Corneal Stromal Cells, Tissue engineering part A, Sep 2015.

**Conference paper in (MSCA Young Investigators Workshop & MSCA Annual Scientific Meeting, Sheffield, UK, 2015):** A 3D thermo-responsive fibre-based scaffold for the culture and enzyme-free passage of quiescent primary human corneal stromal stem cells, 6th MSCA Annual Meeting Programme, December 8th, 2015.

**Conference paper in (TCES, London, UK, 2016):** Extended culture and passage of primary human corneal stromal stem cells (hCSSCs) on 3D thermo-responsive co-electrospun scaffolds. European cells and materials Vol. 30, 2016.

## Acknowledgments

First and foremost, all praise and thanks are due to **Allah**, the Most Gracious and the Most Merciful for all his blessings, and for giving me the ability to produce this PhD thesis.

I would like to express gratitude to my supervisors, Dr. Felicity Rose and Professor Cameron Alexander for their constructive criticism, inspiration, guidance and support during the course of this PhD. I would also like to thank Dr. Lisa White for her supervision during the second year of PhD. Many thanks go to my internal examiner, Dr. Giuseppe Mantovani, for his criticism, useful comments and guidance during the course of this PhD, especially during my first and second year viva. Thanks to Carol Turrill for organising my meetings, as well as her support.

I am deeply appreciative of the help I received from my colleagues in the Tissue Engineering and Drug Delivery groups from 2012 to 2016, especially Catherine, James, Gavin, Aram, Hilary, Omar and Glen who were willing to provide help and advice in the lab whenever I needed. Special thanks go to Laura Sidney for her friendship and support with hCSSCs culture, PCR and immunocytochemistry training. Thanks also to Teresa Marshall and Christy Grainger-Boultby for all the technical help. Thanks to Emily Smith for her XPS training and guidance throughout this project. I would also like to thank Lee, Nora Francini, Alshaimaa and Marta for their help with NMR training and analysis.

I sincerely thank my dear friends for their great support during stressful times, especially Sheraz, Saba, and Ligia. Also, huge thanks go to Yamina Boukari for her

help with reading my thesis and friendship. Heartfelt thanks go to Mr. Hadi Hameed for his continuous support during the writing-up period and stressful times.

Thanks to all my family (Aladdad, Alttyar and Hameed), especially my wonderful father (Mohammed) for his financial and emotional support. Big love and thanks go to my great grandma for her prayers and love all my life (Mama Lolo). Great thanks to my aunt Eng. Iqbal for her support and encouragement. Thanks to my mom (Manal) and I hope that she will be proud of me. Thanks to my brothers, sister (Latifa), and cousin (Dana).

Lastly, I would like to acknowledge the funding and financial support I received throughout my postgraduate study at the University of Nottingham from the Saudi Arabian government.

I dedicate this PhD work to the best partner in the whole world, Mr. Hadi Hameed.

# Table of content

**Abstract…… ..... iii**

**Publications and presentations: .....vi**

**Acknowledgments ..... viii**

**Table of content .....x**

**List of figures .....xix**

**List of tables..... xxxiii**

**Abbreviations .....xxxv**

**Chapter 1. General introduction.....1**

1.1 Regenerative medicine and tissue engineering .....1

1.2 Stem cell-based therapy for regenerative medicine .....5

1.3 *In vitro* culture methods for cell expansion in regenerative medicine.....10

1.3.1 Importance of scaffolds in cell culture for regenerative medicine.....10

1.3.2 Importance of 3D culture for mammalian cells .....11

1.3.3 Properties required in scaffolds intended for 3D cell culture .....14

1.3.4 Common materials used for scaffolding in tissue engineering .....16

1.3.4.i Natural materials.....16

1.3.4.ii Synthetic materials.....17

1.4 Different types and designs of scaffolds used to create 3D cell-culture environments for cell therapies/regenerative medicine .....19

1.4.1 Hydrogel scaffolds ..... 19

1.4.2 Microparticles ..... 20

1.4.3 Specially designed porous scaffolds ..... 21

1.4.3.i Alvetex® ..... 21

1.4.3.ii High-pressure processing ..... 21

1.4.4 Fibrous scaffolds ..... 22

1.4.5 Electrospinning ..... 23

1.4.5.i Setup and principle ..... 25

1.4.5.ii Process parameters ..... 26

1.4.5.ii.a Solution parameters ..... 26

1.4.5.ii.b Processing parameters ..... 27

1.4.5.ii.c Ambient conditions ..... 27

1.4.5.iii Characteristics of electrospun scaffolds ..... 28

1.4.5.iii.a Non-woven fibre scaffolds (unordered mesh scaffolds) ..... 28

1.4.5.iii.b Aligned-fibre scaffolds (ordered fibre scaffolds) ..... 28

1.5 Applications of electrospun fibre-based scaffolds in regenerative medicine and tissue engineering ..... 29

1.6 Responsive surfaces for mammalian cell culture ..... 34

1.6.1 Disadvantages of enzyme treatment.....35

1.6.2 Thermo-responsive surfaces .....36

1.6.3 Cell-sheet engineering.....40

1.7 Aims and objectives .....43

**Chapter 2. Electrospinning and creation of thermo-responsive fibrous scaffolds…….....46**

2.1 Introduction.....46

2.2 Aims and objectives .....54

2.3 Materials and methods .....55

2.3.1 Scaffold fabrication.....55

2.3.1.i Preparation of PLGA and PET polymer solutions.....55

2.3.1.ii Electrospinning process .....56

2.3.2 Synthesis of the thermo-responsive polymer poly (poly (ethylene glycol) methacrylate), poly ($PEGMA_{188}$), via the free radical polymerization technique .....57

2.3.2.i Gel Permeation Chromatography (GPC).....57

2.3.2.ii Proton and carbon nuclear magnetic resonance characterisation of poly ($PEGMA_{188}$) ($^{1}H$ NMR, $^{13}C$ NMR) .....58

2.3.2.iii Determination of the cloud point (lower critical solution temperature [LCST]) of poly ($PEGMA_{188}$).....58

2.3.3 Scaffold surface modification .....59

2.3.3.i Surface adsorption of poly ($PEGMA_{188}$) onto the PLGA and PET fibre surfaces .....59

2.3.3.ii NaOH Hydrolysis modification of the PLGA and PET fibres .....59

2.3.3.iii Surface entrapment of poly ($PEGMA_{188}$) into PLGA and PET scaffolds via solvent swelling .....60

2.3.3.iv Co-electrospinning of poly ($PEGMA_{188}$) and PLGA or PET polymers…..61

2.3.3.iv.a Preparation of the co-polymer solutions.....61

2.3.3.iv.b Co-electrospinning of co-polymer solutions .....61

2.3.4 Scaffold characterisation.....62

2.3.4.i Scanning electron microscopy (SEM) .....62

2.3.4.ii Water contact angle measurements (WCA).....62

2.3.4.iii Proton nuclear magnetic resonance ($^1H$ NMR) .....63

2.3.5 Statistical analysis .....63

2.4 Results and discussion .....64

2.4.1 Electrospun scaffold characterization .....64

2.4.1.i Fibre diameter and beads in the electrospun scaffolds .....64

2.4.1.ii Surface wettability of the scaffolds .....71

2.4.2 Scaffold surface modification by poly ($PEGMA_{188}$) .....74

2.4.2.i Surface adsorption of poly ($PEGMA_{188}$) onto the 18.5% *(w/v)* PLGA and 30% *(w/v)* recycled PET scaffold surface .....78

2.4.2.ii Hydrolysis modification of the PLGA and PET scaffolds surface by NaOH treatment .....82

2.4.2.iii Surface entrapment of poly ($PEGMA_{188}$) polymer into PLGA and PET scaffolds by solvent swelling .....86

2.4.2.iv Co-electrospinning of poly ($PEGMA_{188}$) and PLGA or PET polymers in a single step .....88

2.5 Conclusions .....96

**Chapter 3. Development of a novel thermo-responsive electrospun scaffold and initial mammalian cell response .....98**

3.1 Introduction .....98

3.2 Aims and objectives .....105

3.3 Materials and methods .....106

3.3.1 Synthesis of the thermo-responsive poly ($PEGMA_{188}$).....106

3.3.2 Preparation of the co-polymer poly ($PEGMA_{188}$)-PLGA and poly ($PEGMA_{188}$)-PET solutions .....106

3.3.3 Blend electrospinning (co-electrospinning) .....106

3.3.4 Surface characterization of the thermo-responsive scaffolds.....107

3.3.4.i Scanning electron microscopy (SEM) .....107

3.3.4.ii Water contact angle measurements (WCA) .....107

3.3.4.iii Proton nuclear magnetic resonance ($^1$H NMR) .....108

3.3.4.iv X-ray photoelectron spectroscopy (XPS). .....108

3.3.5 Maintenance and passage of red fluorescent protein (RFP)-expressing 3T3 fibroblast cells.....109

3.3.6 Scaffold sterilization and seeding .....110

3.3.7 Cell response to culture on the thermo-responsive scaffolds.....111

3.3.7.i Assessing cell viability using the AlamarBlue® (AB) assay .....111

3.3.7.ii Cell imaging and image analysis .....113

3.3.7.iii Cell fixation and preparation for SEM .....113

3.3.8 Statistical analysis .....114

3.4 Results and discussion .....115

3.4.1 Preparation and characterisation of thermo-responsive co-electrospun scaffolds .....115

3.4.2 Application of the thermo-responsive scaffolds to 3T3 fibroblast cell culture….....135

3.5 Conclusions.....144

**Chapter 4. Evaluation of thermo-responsive co-electrospun scaffolds for human colon adenocarcinoma cells (Caco2), immortalized human mesenchymal stem cells (ihMSCs) and prolonged passaging of mouse 3T3 fibroblasts .....146**

4.1 Introduction .....146

4.2 Aims and objectives .....148

4.3 Materials and methods .....150

4.3.1 Preparation of the co-polymer 18.5% PLGA-4% poly ($PEGMA_{188}$) and 30% PET-4% poly ($PEGMA_{188}$) (*w/v*) solutions and co-electrospinning.....150

4.3.2 Maintenance and passage of 3T3 fibroblast cells, ihMSCs and Caco2 cells…… .....150

4.3.3 Scaffold sterilization and seeding .....151

4.3.4 Determination of 3T3 mouse fibroblast cell attachment and detachment.. .....151

4.3.5 Determination of ihMSC and Caco2 cell attachment and detachment…. .....153

4.3.6 Cell imaging and image analysis.....154

4.3.6.i Cell fixation and preparation for SEM .....154

4.3.7 Statistical analysis .....154

4.4 Results and discussion .....155

4.5 Conclusions.....170

**Chapter 5. Extended culture and passage of primary human corneal stromal stem cells (hCSSCs) on thermo-responsive co-electrospun scaffolds.....172**

5.1 Introduction ..... 172

5.2 Aims and objectives ..... 177

5.3 Materials and methods ..... 178

5.3.1 Preparation of the co-polymer 18.5% PLGA-4% poly ($PEGMA_{188}$) and 30% PET-4% poly ($PEGMA_{188}$) (*w/v*) solutions and co-electrospinning..... 178

5.3.2 Cell culture media and maintenance for primary human corneal stromal stem cells (hCSSCs) ..... 178

5.3.3 Scaffold sterilization and seeding ..... 179

5.3.4 Determination of cell confluence using the Live-Dead™ assay..... 179

5.3.5 Effect of poly ($PEGMA_{188}$) on corneal stromal stem cell viability assessed using the AB assay ..... 180

5.3.6 Prolonged (seven) thermal and enzymatic passages of corneal stromal stem cells on thermo-responsive PET-poly ($PEGMA_{188}$) scaffolds and TCPS respectively ..... 182

5.3.7 RNA extraction and quantitative reverse transcription-polymerase chain reaction (RT-qPCR)..... 184

5.3.7.i Reverse transcription (RT)..... 184

5.3.7.ii Polymerase chain reaction (PCR) ..... 186

5.3.8 Immunofluorescent staining for CD34 and alpha-smooth muscle actin (α-SMA) ..... 187

5.3.9 Statistical analysis ..... 188

5.4 Results and discussion .....189

5.5 Conclusions .....215

**Chapter 6. General discussion, conclusions and future works .....217**

**References… .....230**

**Appendixes…..254**

## List of figures

Figure 1.1: Tissue engineering approaches are classified into three categories: (i) cells alone, (ii) scaffolds alone and (iii) cells with scaffolds. Each one of these approaches can be enhanced by *in vitro* micro-environmental factors before application as a tissue substitute. Taken from [9]. ..... 2

Figure 1.2: The difference in cell growth on 2D and 3D surfaces. Cells flatten and spread when cultured on 2D surfaces, while larger surface areas and an increased number of binding sites are offered to cells cultured in 3D environments such as the ECM, modified from [89]. ..... 12

Figure 1.3: A schematic representing the basic electrospinning setup. Inset images show the electrified Taylor cone and a scanning electron microscopy (SEM) image of an electrospun fibre-based scaffold on the collecting plate, modified from [167]. ..... 25

Figure 1.4: Potential applications of electrospun fibres, modified from [164]. ..... 30

Figure 1.5: Examples of different areas in regenerative medicine where electrospun scaffolds are being used, modified from [200]. ..... 34

Figure 1.6: Schematic of ‘smart’ polymer response to temperature, modified from [203] ..... 36

Figure 1.7: Cell adhesion onto the PNIPAAm-grafted surface and the release of cells as a continuous cell sheet when the temperature is lowered below 32°C, taken from [219]. ..... 37

Figure 1.8: Molecular structure of standard linear PEG and nonlinear PEG-analogues constructed with oligo (ethylene glycol) macro monomers. (Red: hydrophobic methacrylate portion; blue: the hydrophilic PEG portion), taken from [224].....38

Figure 2.1: Molecular structure of A) poly (lactic-co-glycolic acid) (x is the number of lactic acid units and y is number of glycolic acid units) and B) poly (ethylene terephthalate) (PET), (n is the number of repeating units in the PET polymer) .....55

Figure 2.2: Schematic representing the setup of electrospinning process. .....56

Figure 2.3: Schematic representing the five different areas of the same electrospun scaffolds used for WCA measurements. .....63

Figure 2.4: Representative SEM images and histogram charts of PLGA fibres showing the surface morphology at magnification powers of x500, and frequency of fibre diameter (µm), of five different polymer solution concentrations A-B) 17%, C-D) 17.5%, E-F) 18.5%, G-H) 20% and I-J) 23% (*w/v*). For histogram charts 20 measurements from each SEM image were recorded (100 in total), n = 5, n represent the number of replicates were taken from one batch of each scaffolds. .....65

Figure 2.5: Representative SEM images and histogram charts of recycled PET fibres showing the surface morphology at two magnification powers of x1000 and x3000, and frequency of fibre diameter (nm), of two different polymer solution concentrations A-B) 10%, C-D) 30% (*w/v*). For histogram charts 20 measurements from each SEM image were recorded (100 in total), n = 5, n represents the number of replicates were taken from one batch of each scaffolds. .....67

Figure 2.6: WCA measurements for PLGA and PET scaffolds. The error bars represent the mean with standard deviation (SD), n = 3, n represents the number of replicates that were taken from one batch of each scaffold type. .....72

Figure 2.7: Image showing the molecular structure of A) Poly ($PEGMA_{188}$) and B) Di (ethylene glycol) methyl ether methacrylate ($PEGMA_{188}$) monomer with the vinyl group highlighted (box). In C) GPC chromatogram showing the molar mass distribution of poly ($PEGMA_{188}$). .....74

Figure 2.8: Images showing A) $^{1}H$ NMR and B) $^{13}C$ NMR of poly ($PEGMA_{188}$), and the highlighted box indicating the purity of the polymer from any remaining $PEGMA_{188}$ monomer.....75

Figure 2.9: Cloud point analysis of poly ($PEGMA_{188}$) polymer, assessed by UV-VIS at 550 nm over controlled change in the temperature at rate of 1°C / minute. The error bars represent the mean with SD, n = 2, n represent the number of replicates were taken from each batch. Insert images, showing the LCST for poly ($PEGMA_{188}$) polymer solution by changing the environment temperature above and below 26°C. .....76

Figure 2.10: Representative SEM images showing surface adsorption of two different concentrations 3% and 5% (*w/v*) of poly ($PEGMA_{188}$) onto A) PLGA and B) PET scaffolds at different time periods 1 h, 5 h, 12 h and 24 h.....79

Figure 2.11: Change in hydrophobicity of the scaffolds after the addition of thermo-responsive poly ($PEGMA_{188}$) by surface adsorption, indicated by water contact angle measurements, before and after washing with distilled water A) PLGA and B) PET

over 10 seconds time period. The error bars represent the mean ± SD; experiments were conducted three times for each scaffold type. (n = 9 total, three scaffolds from three different batches).....81

Figure 2.12: Representative SEM images show the hydrolysis effect of NaOH treatment on A) PLGA and B) PET scaffolds with 0.5% and 1% (*w/v*) NaOH concentrations at different time periods (5 minutes and 10 minutes). The arrows are representing the surface hydrolysis as small grooves on individual fibre's surface.. 84

Figure 2.13: Change in hydrophobicity over 10 seconds time period, of PLGA and PET scaffolds respectively before and after treatment with 0.5% (*w/v*) NaOH for 10 minutes. The error bars represent the mean ± SD, experiment were conducted three times for each scaffolds (n = 9 total, three scaffolds from three different batches)...85

Figure 2.14: Representative SEM images of 18.5% (*w/v*) PLGA and recycled 30% (*w/v*) PET scaffolds treated with different concentrations of TFE and acetone as swelling solvents respectively for 1h. .....87

Figure 2.15: SEM shows the decrease in fibres diameters of A) PET and B) PLGA, after addition of non-solvent (distilled water) to the treated scaffolds (poly ($PEGMA_{188}$) present in the swelling solvents).....87

Figure 2.16: SEM images representing the co-electrospun fibrous scaffolds of poly ($PEGMA_{188}$) with PLGA polymer and co-electrospinning parameters for each SEM Image, with the changeable parameters highlighted in blue. .....90

Figure 2.17: SEM images representing the co-electrospun fibrous scaffolds of poly ($PEGMA_{188}$) with PET polymer and co-electrospinning parameters for each SEM Image, with the changeable parameters highlighted in blue. .....92

Figure 2.18: $^{1}H$ NMR of A) electrospun poly (lactic-co-glycolic acid) (PLGA) scaffolds and B) blend electrospun PLGA with poly ($PEGMA_{188}$) scaffolds. .....93

Figure 2.19: $^{1}H$ NMR of A) electrospun for poly (ethylene terephthalate) (PET) scaffolds and B) blend electrospun for PET with poly ($PEGMA_{188}$) scaffolds. .....94

Figure 3.1: A schematic of the thermo-responsive 3D scaffolds synthesis route. a) Synthesis of the thermo-responsive polymer; 1-dodecanethiol chain transfer agent was used in the free radical polymerization of 2-(2-methoxyethoxy) ethyl methacrylate ($MEO_2MA$) monomers to make thermo-responsive poly ($PEGMA_{188}$) polymer. b) Co-electrospinning of synthesised poly ($PEGMA_{188}$) with PET or PLGA polymers. Insert image modified from [348] c) Application of responsive scaffolds for cell culture; cell attachment (above LCST) and detachment (below LCST) to/from thermo-responsive co-electrospun fibres. Thermo-responsive polymer chains at temperatures below the LCST are shown as chain extended, forming a 'cell-resistant' surface, whereas collapse of the polymer chain above the LCST results in a surface more favourable for cell attachment. Note: cells, polymer chains and fibres were shown out of scale. .....104

Figure 3.2: AlamarBlue® assay principle, modified from [351].....112

Figure 3.3: Schematic representing the AB experiment timeline for cultured 3T3 fibroblast cells .....113

Figure 3.4: Representative SEM images and histogram charts of co-electrospun PLGA-poly ($PEGMA_{188}$) fibres showing the surface morphology at magnification powers of x1000, and frequency of fibre diameter (µm), of six different polymer solution concentrations ratios A-B) 18.5%: 0% (*w/v*), C-D) 18.5%: 2% (*w/v*), E-F) 18.5%: 4% (*w/v*), G-H) 18.5%: 6% (*w/v*), I-J) 18.5%: 8% (*w/v*) and k-L) 18.5%: 10% (*w/v*). For histogram charts 20 measurements from each SEM image were recorded (100 in total), n = 5, n represent the number of replicates were taken from one batch of each scaffolds. Scale bars = 10 µm except image A) = 50 µm. .....117

Figure 3.5: Representative SEM images and histogram charts of co-electrospun PET-poly ($PEGMA_{188}$) fibres showing the surface morphology at magnification powers of x500, and frequency of fibre diameter (nm), of six different polymer solution concentrations ratios A-B) 30%: 0% (*w/v*), C-D) 30%: 2% (*w/v*), E-F) 30%: 4% (*w/v*), G-H) 30%: 6% (*w/v*), I-J) 30%: 8% (*w/v*) and k-L) 30%: 10% (*w/v*). For histogram charts 20 measurements from each SEM image were recorded (100 in total), n = 5, n represent the number of replicates were taken from one batch of each scaffolds. Scale bars = 50 µm. .....120

Figure 3.6: Differences in wettability represented by measuring the WCA of five different areas of the same co-electrospun scaffold A) 18.5% PLGA-8% poly ($PEGMA_{188}$) and B) 30% PET-6% poly ($PEGMA_{188}$) (*w/v*). The error bars represent the mean of 20 measurements in that area with standard deviation; the experiment was conducted two times for each scaffold type (n=2 batches).....124

Figure 3.7: $^{1}H$ NMR of A) PLGA scaffolds, B) PET scaffolds co-spun with different poly ($PEGMA_{188}$) concentrations of (2, 4, 6, 8 and 10% [*w/v*]), and the highlighted

box indicating the presence of poly ($PEGMA_{188}$) polymer in the blend-electrospun scaffolds. .....128

Figure 3.8: XPS C1s-peak of electrospun scaffolds of 18.5% PLGA and 30% PET, co-electrospun with different concentrations of poly ($PEGMA_{188}$), 0 %, 2% and 10% (*w/v*). Typical PLGA, PET and poly ($PEGMA_{188}$) carbon peaks are visible.....130

Figure 3.9: Representative fluorescence microscopy images showing 3T3 cells attachment to co-spun scaffolds of 18.5% PLGA with different concentration of poly ($PEGMA_{188}$); A) 2% B) 4%, C) 6%, D) 8%, E) 10% and F) 0% (*w/v*) after 6 h at varying temperature/time regimes. In day 0 and day 2 cells were allowed to attach to the surfaces at 37°C, whereas, cell detachment took place over 10 minutes at 17°C (passage 1). In day 4, re-attachment of cells occurred at 37°C on the same scaffolds. Scale bars = 50 µm.....138

Figure 3.10: Representative fluorescence microscopy images showing 3T3 cells attachment to co-spun scaffolds of 30% PET with different concentration of poly ($PEGMA_{188}$); A) 2% B) 4%, C) 6%, D) 8%, E) 10% and F) 0% (*w/v*) after 6 h at varying temperature/time regimes. In day 0 and day 2 cells were allowed to attach to the surfaces at 37°C, whereas, cell detachment took place over 10 minutes at 17°C (passage 1). In day 4, re-attachment of cells occurred at 37°C on the same scaffolds. Scale bars = 50 µm.....139

Figure 3.11: Representative SEM images showing 3T3 cells attachment to A) PLGA- 4% poly ($PEGMA_{188}$) and B) PLGA scaffolds (control) surfaces after 6 h at varying temperature/time regimes. In day 0 and day 2 cells were allowed to attach to

the surfaces at 37°C, whereas, cell detachment took place over 10 minutes at 17°C (passage 1). In day 4, re-attachment of cells occurred at 37°C. Scale bars = 50 µm. The inset images show a higher magnification view of the 3T3 cells on the scaffolds, scale bars 10 = µm. .....140

Figure 3.12: AB assay representing the change in cell number over the initial culture time (up to 6 h - 54 h /day 0 - day 2). Following detachment (10 minutes at 17°C / passage 1 (56 hrs)) and subsequent re-attachment (48 h at 37°C/ day 4) of 3T3 cells, on A) PLGA scaffolds and B) PET scaffolds, with different concentrations of poly ($PEGMA_{188}$). Error bars represent mean ± SD; n = 9. Statistical significance, Day 0 versus Day 2, Day 2 versus passage 1 and passage 1 versus Day 4: (ns) $p > 0.05$, (*) $P \leq 0.05$ and (****) $p \leq 0.0001$, (Two-way ANOVA). .....143

Figure 4.1: Schematic representing the passaging experiment timeline for cultured A) 3T3 fibroblast cells over ten passages on new co-electrospun thermo-responsive scaffolds each passage and B) Caco2 or ihMSCs over two passages on same co-electrospun thermo-responsive scaffold each passage. .....149

Figure 4.2: The 3T3 cell detachment using trypsin/EDTA from tissue culture flask and temperature from thermo-responsive co-electrospun 18.5% PLGA-4% poly ($PEGMA_{188}$) and 30% recycled PET-4% poly ($PEGMA_{188}$) scaffolds (*w/v*) after 6 h in cell culture. Error bars represent mean ± SD; (n = 9, three scaffolds from three different batches). Statistical significance versus tissue culture flask: (ns) $p > 0.05$ and (*) $p \leq 0.05$, (one-way ANOVA). .....156

Figure 4.3: Representative A) Bright field and B) Fluorescence microscopy images showing 3T3 fibroblast cells after thermal detachment process at 17°C from thermo-responsive scaffolds and enzymatic detachment from TCPS. C) Cell following dissociation using a gentle pipetting for 5-10 minutes, following detachment from the scaffold. Scale bars = 50 µm. .....160

Figure 4.4: Graphs showing A) 3T3 fibroblast cell number and B) growth curve for 3T3 fibroblasts, which they were serially passaged, over 10 passages, using trypsin and temperature from TCPS or co-electrospun scaffolds containing poly ($PEGMA_{188}$) respectively. Error bars represent mean ± SD; (n = 9, three scaffolds from three different batches). Statistical significance versus tissue culture flask: (ns) $p > 0.05$ and (****) $p \leq 0.0001$, (two -way ANOVA). .....164

Figure 4.5: Representative fluorescence microscopy showing ihMSCs cell attachment to PLGA, PLGA-4% poly ($PEGMA_{188}$), PET and PET-4% poly ($PEGMA_{188}$) scaffolds for 5 days at 37°C. In day 5 detachment, cell detachment took place over 7 minutes at 17°C on scaffolds containing thermo-responsive polymer only. Cells were allowed to reattach to the same scaffolds by returning the culture plate to the incubator at 37°C. The cells were cultured for a further 10 days when they were detached again from the scaffold by reducing the temperature to 17°C again, illustrating the reversible nature of the thermo-responsive polymer. Scale bars = 50 µm. .....166

Figure 4.6: Representative scanning electron microscope images showing ihMSCs and Caco2 cell detachment over 7 minutes at 17°C from PLGA-4% poly ($PEGMA_{188}$) and PET-4% poly ($PEGMA_{188}$) scaffolds after ten days in cell culture.

While, cells remained attached on PLGA and PET scaffolds (control). Scale bars = 10 µm. .....167

Figure 4.7: Alamar blue assay representing the change in cell fluorescence intensity over the initial culture time (up to 6 h - 126 h /day 0 - day 5), following detachment (7 minutes at 17°C/ passage 1) and subsequent re-attachment and culture (246 h at 37°C/ day 10), following detachment (7 minutes at 17°C/ passage 2) of A) ihMSCs and B) Caco2 cells on PLGA, PLGA-poly ($PEGMA_{188}$), PET and PET-poly ($PEGMA_{188}$) scaffolds. Error bars represent mean ± SD; (n = 9, three scaffolds from three different batches). Statistical significance, Day 0 versus Day 5, Day 5 versus passage 1, passage 1versus Day 10 and Day 10 versus passage 2: (ns) $p > 0.05$, (*) $p \leq 0.05$, (**) $p \leq 0.01$, (***) $p \leq 0.001$ and (****) $p \leq 0.0001$, (Two-way ANOVA). .....169

Figure 5.1: Corneal structure, modified from [409].....173

Figure 5.2: Schematic diagram of human eye showing limbus cornea in A) horizontal section and B) anterior section, taken from [431].....175

Figure 5.3: Schematic representing the AB experiment timeline for cultured hCSSCs .....181

Figure 5.4: Schematic representing the prolonged seven thermal passages experiment timeline for cultured hCSSCs.....183

Figure 5.5: Representative fluorescence microscopy images showing hCSSCs attachment, proliferation and confluency using live-dead assay on PET, PET-4%

poly ($PEGMA_{188}$), PLGA, PLGA-4% poly ($PEGMA_{188}$) (*w/v*) and control (TCPS) over six days of cell culture at 37°C. In day 0, cells were round in shape after 6 h of attachment. In day 3 and day 6, cells adopted a more spread morphology. Scale bars = 50 µm. .....193

Figure 5.6: Representative fluorescence microscopy images showing hCSSCs detachment after six days of culture from PET-4% poly ($PEGMA_{188}$) and PLGA-4% poly ($PEGMA_{188}$) (*w/v*) in the culture media after reducing the culture temperature to 17°C for 7 minutes. Images were taken on three different areas in the well plate. Scale bars = 50 µm. .....194

Figure 5.7: Alamar blue assay representing the significant change in fluorescence intensity of hCSSCs over the culture time (up to 6 h – 78h – 126 h /Day 0 – Day3 – Day 5) at 37°C on A) TCPS, PLGA and PLGA-poly ($PEGMA_{188}$) and B) TCPS, PET, PET-poly ($PEGMA_{188}$). Error bars represent mean ± SD; n = 9. Statistical significance, Day 0 versus Day 3 and Day 3 versus Day 5: (***) $p \leq 0.001$ and (****) $p \leq 0.0001$, (Two-way ANOVA). .....195

Figure 5.8: Alamar blue assay representing the change in fluorescence intensity in response to change of hCSSCs culture temperature. After five days of cell culture (126 h / Day 5 and Day 5 post passage, reseeded scaffolds), detachment occurred (for 7 minutes at 17°C/ passage 1 and passage 2) on A) TCPS, PLGA and PLGA-poly ($PEGMA_{188}$) and B) TCPS, PET, PET-poly ($PEGMA_{188}$). Error bars represent mean ± SD; n = 9. Statistical significance, Day 5 versus passage 1 and Day 5 post passage, reseeded scaffolds versus passage 2: (ns) $p > 0.05$, (***) $p \leq 0.001$ and (****) $p \leq 0.0001$, (Two-way ANOVA). .....197

Figure 5.9: Comparative effects of culture environment (TCPS, PLGA scaffolds alone and PLGA-4% poly ($PEGMA_{188}$)) and thermo-responsive polymer on gene expression of hCSSCs at passage 3. Relative levels of mRNA were determined by means of RT-qPCR for the following genes: (A) *CD34*, (B) *ALDH3A1*, (C) *THY1* and (D) *ACTA2*. Expression of each target gene is normalized to *GAPDH* (housekeeping gene) and represented relative to mRNA expression in TCPS. Data are shown as mean ± standard error of the mean of three independent experiments (n = 3), each with two replicates, one donor. Statistical significance versus TCPS: (ns) $p > 0.05$, (*) $P \leq 0.05$ (one-way ANOVA). .....201

Figure 5.10: Comparative effects of culture environment (TCPS, PET scaffolds alone and PET-4% poly ($PEGMA_{188}$)) and thermo-responsive polymer on gene expression of hCSSCs at passage 3. Relative levels of mRNA were determined by means of RT-qPCR for the following genes: (A) *CD34*, (B) *ALDH3A1*, (C) *THY1* and (D) *ACTA2*. Expression of each target gene is normalized to *GAPDH* (housekeeping gene) and represented relative to mRNA expression in TCPS. Data are shown as mean ± SEM of three independent experiments (n = 3), each with two replicates, one donor. Statistical significance versus TCPS: (ns) $p > 0.05$, (*) $P \leq 0.05$, (**) $P \leq 0.01$ (one-way ANOVA).....202

Figure 5.11: Images showing the effect of culture media on thermo-responsive PET and PLGA co-electrospun scaffolds after 6 h of incubation in cell culture media at $37^{o}$C. Scale bars = 1 cm. .....204

Figure 5.12: Comparative effects of culture environment TCPS and PET-4% poly ($PEGMA_{188}$) on gene expression of hCSSCs at different thermal (3D scaffold) and

enzymatic (2D TCPS) passages of 3, 6 and 9. Relative levels of mRNA were determined by means of RT-qPCR for the following genes: (A) *CD34*, (B) *ALDH3A1*, (C) *THY1* and (D) *ACTA2*. Expression of each target gene is normalized to *GAPDH* (housekeeping gene) and represented relative to mRNA expression in TCPS of each passage. Data are shown as mean ± SEM of three independent experiments (n = 3), each with two replicates. Statistical significance versus TCPS: (ns) $p > 0.05$, (*) $P \leq 0.05$, (**) $P \leq 0.01$, (***) $P \leq 0.001$ (Student's t-test). Note: after passage 3, *CD34* gene expression of TCPS is equal to n = 2 for passage 6 and passage 9. .....206

Figure 5.13: Comparative effects of increasing passage number on gene expression of hCSSCs culture on TCPS and PET-4% poly ($PEGMA_{188}$) at different thermal (3D scaffold) and enzymatic (2D TCPS) passages of 3, 6 and 9. Relative levels of mRNA were determined by means of RT-qPCR for the following genes: (A) *CD34*, (B) *ALDH3A1*, (C) *THY1* and (D) *ACTA2*. Expression of each target gene is normalized to *GAPDH* (housekeeping gene) and represented relative to mRNA expression in TCPS of passage 3. Data are shown as mean ± SEM of three independent experiments (n = 3), each with two replicates. Statistical significance versus TCPS at passage 3: (ns) for $p > 0.05$, (*) $P \leq 0.05$, (****) $P \leq 0.0001$ (one-way ANOVA). Note: after passage 3, *CD34* gene expression of TCPS is equal to n = 2 for passage 6 and passage 9. .....208

Figure 5.14: Representative fluorescence microscopy images showing the effects of culture environment of TCPS and PET-4% poly ($PEGMA_{188}$) scaffolds on keratocyte and myofibroblast markers of hCSSCs. Immunocytochemistry was

performed for CD34 (green) and α-SMA (green) after five days in cell culture at passages 3, 6 and 9 from one donor. Negative control images (secondary antibody only) of donkey anti-mouse immunoglobulin (Ig)G Alexa Fluor-488. All images shown with PI counterstain (red), scale bar = 50 μm.....212

Figure 5.15: Graphs showing A) hCSSCs number and B) growth curve for hCSSCs, which they were serially passaged, over 9 passages, using trypsin and temperature from TCPS or co-electrospun scaffolds containing poly ($PEGMA_{188}$) respectively. Data are shown as mean ± standard error of the mean of three independent experiments (n = 3). Statistical significance versus TCPS: (ns) $p > 0.05$, (*) $P \leq 0.05$, (**) $p \leq 0.01$, (***) $p \leq 0.001$, (****) $P \leq 0.0001$ (two-way ANOVA).....214

## List of tables

Table 2-1: A summary table of electrospinning parameters for PLGA and PET polymers and fibre characterizations .....73

Table 2-2: A summary table of poly ($PEGMA_{188}$) synthesis and characterization....77

Table 2-3 A summary table of creating thermo-responsive scaffolds .....95

Table 3-1: Co-electrospinning parameters of PLGA-poly ($PEGMA_{188}$) and PET-poly ($PEGMA_{188}$).....107

Table. 3-2 WCA measurements (θw), of co-electrospun scaffolds surfaces. Data shown for each surface are the mean of five independent measurements ± standard deviation.....123

Table 3-3: Molar ratio (Mole) of PLGA or PET with poly ($PEGMA_{188}$) in co-electrospun scaffolds.....127

Table 3-4: Carbon ratio of poly ($PEGMA_{188}$), PLGA and PET polymers in PLGA, PET and their co-electrospun with 2% and 10% (*w/v*) poly ($PEGMA_{188}$) scaffolds determined by XPS. SD represents seven different areas of each scaffold. .....132

Table 3-5: A summary tables of characterisation of thermo-responsive scaffolds of 18.5% (*w/v*) PLGA and 30% (*w/v*) PET co-electrospun with poly ($PEGMA_{188}$)....134

Table 4-1: A summary of the experimental work of Chapter 4 .....171

Table 5-1: Reverse transcription mixture volumes used for both cells collected from the thermo-responsive scaffolds and TCPS surfaces. .....185

Table 5-2: Polymerase chain reaction mixture volumes used for both cells collected from the thermo-responsive scaffolds and TCPS surfaces. .....186

Table 5-3: Details of antibodies used in immunocytochemistry.....188

Table 5-4: A summary of the experimental finding of Chapter 5.....216

## Abbreviations

| | |
|---|---|
| **AB** | Alamar Blue |
| **AFM** | Atomic force microscopy |
| **ALDH** | Aldehyde dehydrogenase |
| **α-SMA** | α-smooth muscle actin |
| **ATRP** | Atom transfer radical polymerisation |
| **BMSCs** | Bone marrow-derived stromal stem cells |
| **BSA** | Bovine serum albumin |
| **Caco2** | Human colon adenocarcinoma cells |
| **3D** | Three dimensional |
| **DCM** | Dichloromethane |
| **DMEM** | Dulbecco's modified Eagle's medium |
| **EDTA** | Ethylenediaminetetraacetic acid |
| **ECM** | Extracellular matrix |
| **ESCs** | Embryonic stem cell |
| **FBS** | Foetal bovine serum |
| **FDA** | Food and drug administration |
| **GPC** | Gel permeation chromatography |
| **hCSSCs** | Human corneal stroma-derived stem cells |
| **hESCs** | Human embryonic stem cells |
| **$^{1}$H-NMR** | Proton nuclear magnetic resonance |
| **h** | Hour (s) |

| | |
|---|---|
| **HUVECs** | Human umbilical vein endothelial cells |
| **ihMsc** | Immortalized human mesenchymal stem cells |
| **K-SFM** | Serum-free keratinocyte medium |
| **LCST** | Lower critical solution temperature |
| **LIF** | Leukaemia Inhibitory Factor |
| **M199** | Medium 199 |
| **$MEO_2MA$** | 2-(2-methoxyethoxy) ethyl methacrylate |
| **mESCs** | Mouse embryonic stem cell |
| **mL** | Millilitre |
| **µL** | Microlitre |
| **Mn** | Number average molecular weight |
| **Mw** | Weight average molecular weight |
| **nm** | Nanometre |
| **OEGMA** | Oligo (ethylene glycol) methacrylate |
| **PBS** | Phosphate buffered saline |
| **PCL** | Poly caprolactone |
| **PEG** | Polyethylene glycol |
| **PEGMA** | Poly (ethylene glycol) methacrylate |
| **PEGPLA** | Poly (ethylene glycol)-poly(L-lactic acid) |
| **PEO** | Polyethylene oxide |
| **PEVA** | Poly (ethylene-co-vinyl acetate) |
| **PGA** | Poly (glycolic acid) |

| | |
|---|---|
| **PLA** | Poly (lactic acid) |
| **PLCL** | Poly(l-lactide-co-ε-caprolactone) |
| **PLGA** | Poly (lactic-co-glycolic acid) |
| **PNIPAAm** | Poly (N-isopropylacrylamide) |
| **Poly (PEGMA-EE246)** | Poly (polyethylene glycol methacrylate ethyl ether) |
| **Poly (MEO2MA-co-OEGMA))** | Poly (methoxyethoxyethylmethacrylate-co-oligoethyleneglycolmethacrylate) |
| **ppAAI** | Plasma polymerised allyl alcohol |
| **PU** | Polyurethane |
| **RT** | Room temperature |
| **RT-qPCR** | Quantitative reverse transcription polymerase chain reaction |
| **S** | Second |
| **SEM** | Scanning electron microscopy |
| **SCM** | Stem cell medium |
| **TCPS** | Tissue culture polystyrene |
| **TFA** | Trifluoroacetic acid |
| **ToF-SIMS** | Time of flight secondary ion mass spectroscopy |
| **W** | Watts |
| **WCA** | Water contact angle ($^{o}$) |
| **XPS** | X-ray photoelectron spectroscopy |

# Chapter 1. General introduction

## 1.1 Regenerative medicine and tissue engineering

Patients who suffer from severely injured or damaged organs are treated by organ or tissue transplantation with the use of various drug molecules. However, there are difficulties associated with these procedures, including organ shortages, the quality of the tissue and complications arising from the body's immune system after transplantation. Furthermore, there are increasing demands for organ transplants to treat chronic diseases such as diabetes, stroke, muscular dystrophy, liver cirrhosis and renal failure. All of these facts have led scientists to apply the principles of regenerative medicine to restore, maintain or improve the organ's function. Regenerative medicine is a multidisciplinary field that involves the use of combined approaches, including cell therapy, tissue engineering, gene therapy and the usage of medical devises [2-5].

The concept of tissue engineering was first introduced in 1933 by Biscgelie when mouse tumour cells survived in a biocompatible polymer membrane, and were then implanted into the abdominal cavity of chick embryos [6]. The term 'tissue engineering' was then first used in 1985 by Y. C. Fung, based on the definition of a 'tissue' as a fundamental level of living organisms between cells and organs [7]. After that, Langer and Vacanti (1993) defined tissue engineering as an 'interdisciplinary field that applies the principles of engineering and the life sciences toward the development of biological substitutes that restore, maintain, or improve

tissue function' [8]. Tissue engineering involves the following different approaches: (i) to use isolated cells, (ii) to use acellular biomaterials capable of inducing tissue regeneration and (iii) to use a combination of cells and materials, as summarised in Figure 1.1 [9]. Traditionally, the process starts by harvesting cells from a patient, expanding them *in vitro* and then seeding them onto a scaffold to provide a biomechanical environment that supports tissue formation. The tissue can be grown on a scaffold that will completely degrade as the new tissue grows, or on a permanent scaffold and the bio-composite would then be implanted. After implantation, the tissue-engineered construct must be able to survive, restore normal function and integrate with the surrounding tissues [10].

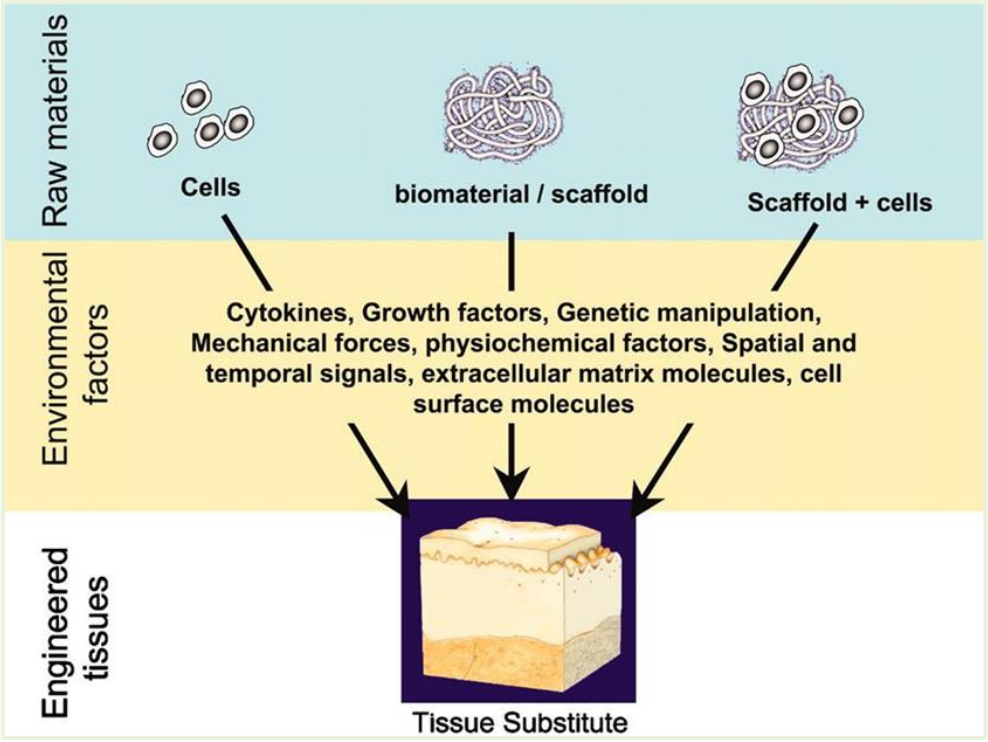



Figure 1.1: Tissue engineering approaches are classified into three categories: (i) cells alone, (ii) scaffolds alone and (iii) cells with scaffolds. Each one of these approaches can be enhanced by *in vitro* micro-environmental factors before application as a tissue substitute. Taken from [9].

Cell biology and material science are considered fundamental components in regenerative medicine [11]. Cells are grouped into stem cells, autologous cells, allogeneic cells or xenogeneic cells. Autologous cells, which originate from the recipient's body rather than from a donor, have the advantage of lower immune rejection for clinical applications. However, autologous cells are not always available in the numbers or quality required, and they may be incapable of proliferation *in vitro* [12, 13]. Using allogeneic cells from a living donor is an option, for example, human pancreatic islet transplantation in patients with type I diabetes reduced insulin requirements; however, a disadvantage is that it can cause an immune response [14]. Xenogeneic cells obtained from a different species have been used to deliver specific chemicals within the engineered tissue with impaired function [15]. For example, foetal porcine islet-like cell clusters (ICC) were transplanted into insulin-dependent diabetic kidney-transplant patients and resulted in positive staining for insulin and glucagon [16]. However, the problems associated with the rejection of transplanted foreign tissue into the human body and the difficulties with a prolonged regimen of immunosuppressants are still present with xenogeneic grafts [17]. Primary cells derived from the original tissue have been used widely due to their immunological compatibility; however, their finite lifespans and limited potential for generating sufficient numbers for clinical purposes are considered to be major obstacles associated with the use of primary cells. Additionally, the tendency of some cell types to de-differentiate during *ex-vivo* cultivation and express an inappropriate phenotype, such as articular chondrocytes in culture often producing fibrocartilage, as opposed to hyaline cartilage [18], is also an

obstacle. In addition, harvesting some phenotypes, such as spinal cord neurons from patients or donors, is not practical [5]. Therefore, multi-potent stem cells are seen as a good alternative for use in the field of tissue engineering due to their ability to grow in high numbers and differentiate into different lineages, including cells of the cardiovascular system, spinal cord, lung, retina, bone marrow, liver, adipose tissue, placenta and pancreas. However, a particular challenge associated with the use of stem cells is the ability to direct cell differentiation towards a particular phenotype [19].

In addition to optimising cell isolation, proliferation and, in the case of stem cells, differentiation, a key challenge facing tissue engineers is the design of supporting matrices or scaffolds for the culture and expansion of different cell types. Scaffolds are either natural or synthetic materials serving as an artificial extra cellular matrix (ECM) for the cells. To regenerate tissues, scaffolds should have adequate mechanical strength to support cell attachment, growth, differentiation and function. Moreover, scaffolds should be biocompatible and biodegradable at a controlled rate once implanted into the human body [11], or non-biodegradable once used for the *in vitro* expansion of cells [20].

Combining cell-based therapy and engineered scaffolds offers the potential for complex tissue reconstruction in the future. However, a better understanding of organ morphogenesis is needed to fully exploit this possibility. Despite the bright future of regenerative medicine and its promise for replacing various damaged tissues and organs [11], there are still challenges that need to be solved. Some

examples of these challenges include stem cell differentiation, administration techniques, scaffolds' compatibility, cell-number shortages, scaffold design, cost of goods and industrial scale-up [2]. Therefore, this review aims to describe the recent literature reported with regard to cell-based therapy and *in vitro* 3D supporting culture systems for the expansion of cells destined for regenerative medicine applications, which then leads on to the main aims and objectives of this research project.

## 1.2 Stem cell-based therapy for regenerative medicine

The lack of suitable donor organs and tissues is an urgent problem in transplantation medicine; therefore, cell replacement can act as an alternative technique for the repair or replacement of diseased tissue. The human body has an endogenous system for regeneration and repair via stem cells, which can be found in almost every type of tissue [21]. Therefore, it is logical that the restoration of function is best accomplished by these cells. Stem cells were first studied by Becker *et al*. in 1963 [22]. They have the capacity of self-renewal, giving rise to more stem cells, and the ability to differentiate into different cell lineages under appropriate conditions. Therefore, stem cells hold great promise for the improvement of healthcare by either augmenting the body's own regenerative potential, or for the development of new therapies. Thus, they represent an important building block in regenerative medicine and tissue engineering [23, 24].

Stem cells are broadly classified as embryonic (germinal) or somatic (foetal or adult) according to their origin. They are also classified into totipotent, pluripotent or multipotent according to their ability to differentiate further into other cells [25]. Embryonic stem cells (ESCs) were first described by Martin in 1981, and derived from the inner cell mass (ICM) of 5–6-day-old blastocysts [26]. They are pluripotent and, accordingly, they can differentiate into all three embryonic germ layers, i.e. the ectoderm, mesoderm and endoderm, with the potential of forming various body tissues [27]. Cardiomyocyte grafts derived from mouse ESCs (m-ESCs) were present for as long as 7 weeks after implantation into the ventricular myocardium of adult dystrophic mice [28]. ES-derived neural cells also demonstrated their potential use for the treatment of rat models of Parkinson's disease [29], Alzheimer's disease [30] and spinal cord injuries [31]. In addition, ESCs have also been used for the treatment of diabetes. Insulin-secreting cells were derived from ESCs and normalised glycaemia in streptozotocin-induced diabetic mice [32]. Additionally, human embryonic neural stem cells from ectodermal origin have been transplanted bilaterally to the putamen of 40 patients suffering from Parkinson's disease. The standardised tests for Parkinson's disease revealed a significant improvement in the symptoms when patients aged 60 years old or younger were tested in the morning, before receiving medication, in comparison with elderly patients who underwent a sham-surgery [33]. Despite the great differentiation potential of ESCs, their use is still limited by several ethical and scientific considerations regarding the isolation of these cells from *in vitro*-fertilised human embryos, as well as their tumour-forming potential [34].

Recently, induced pluripotent stem cells (iPSCs) were reported, in which adult cells were genetically reprogrammed by viruses to an embryonic stem cell-like state by being forced to express genes and factors important for maintaining the defining properties of ESCs. In animal studies, the virus used to introduce the stem-cell factors sometimes causes cancers and mutation [35]. Researchers are currently investigating non-viral delivery strategies [36]. However, this breakthrough discovery has created a powerful new way to "de-differentiate" cells whose developmental fates had been previously assumed to be determined. In addition, tissues derived from iPSCs will be a nearly identical match to the cell donor and, thus, will probably avoid rejection by the immune system and be capable of generating cell characteristic of all three germ layers [37, 38].

On the other hand, non-embryonic stem cells (non-ESCs), also known as adult stem cells, possess a multipotent differentiation potential [39]. They can be derived from several sources, including the amniotic fluid [40], umbilical cord tissue (Wharton's jelly) [41], fat tissue [42], central nervous system [43], bone marrow [44], retina [45], and skin [46] and many more. The use of bone marrow-, umbilical cord-, adipose tissue-, skin- and amniotic fluid-derived mesenchymal stem cells (MSCs) might be an adequate alternative for translational practice [47]. The most widespread adult stem cell therapies are for the treatment of malignancies, immuno-deficiency and leukaemia using stem cells from the bone marrow of the patient or a donor, which rebuild the haematopoietic system [48, 49]. In particular, bone marrow-derived stem cells (BMSCs) have been used successfully for enhancing

many organs' functions and healing. For example, improved bone formation and the curing of bone defects were observed when BMSCs were implanted in mice [50]. Furthermore, they also showed positive results in osseous defects [51] and treatment of large bony defects [52]. Moreover, good cross-sectional collagen fibre formation was observed when BMSCs were seeded onto 1 cm rabbit Achilles tendon experimental defects [53]. Another studies reported xonal regeneration and functional recovery in animal models of spinal cord injury following BMSC implantation, and the formation of neural and myelin-producing cells [54]. Additionally, BMSCs were successfully differentiated into cardiomyocytes [55]; therefore, they have been used for the regeneration of cardiac tissue in a mice model of ischaemic heart disease [56]. Moreover, intramyocardial injection of endogenous cardiac stem cells after infarction in mice promoted cardiomyocyte and vascular-cell formation, with improved systolic function [57]. This suggests that these cells could be used for cardiac tissue repair. Another study in which the bladder domes of rats were replaced with bladder acellular matrix grafts, showed that the transplanted BMSCs were able to migrate to these bladder grafts and differentiate into smooth muscle cells [58]. Autologous BMSC transplantation was used as a treatment approach in articular cartilage defects in the osteoarthritic knee joints of 24 patients. Six weeks after BMSC transplantation, the defects were covered with white to pink soft tissue, in which metachromasia was partially observed. Forty-two weeks after transplantation, the defects were covered with white soft tissue, in which metachromasia was observed in almost all areas of the sampled tissue, and hyaline cartilage-like tissue was partially observed [59]. In another example of an adult stem

cell therapy, MSCs were differentiated into hepatocytes under suitable culture conditions, and their transplantation into the parenchyma of the liver with no immune rejection was observed [60]. Human MSCs isolated from the iliac crest of healthy human donors were able to undergo myogenic differentiation after injection into the left ventricle of adult mice. This indicates the potential of these cells for augmenting the function of diseased myocardium [61]. Another study showed that human MSCs underwent site-specific differentiation into chondrocytes, adipocytes, myocytes and cardiomyocytes, bone marrow stromal cells and thymic stroma after transplantation into foetal sheep in the early gestation period [62]. Moreover, human MSCs were isolated and implanted into critical-sized segmental defects in the femurs of adult athymic rats; evidence of new bone was apparent by 8 weeks and histomorphometry demonstrated increasing bone formation after 12 weeks [63]. Other therapies are being tested for their ability to treat autoimmune diseases such as rheumatoid arthritis [64]. These studies demonstrate that stem cells can regenerate organ or function defects and may, therefore, provide an alternative to autogenous grafts.

Despite much interest in stem cell biology, there are a few challenges for their clinical use. These include problems associated with extensive *in vitro* cell expansion (including the limited cell supply and trans-differentiation potential) [65-67], cell apoptosis following implantation [68], difficulties in achieving vascularization [69], and problems with carrier biomaterials. Additionally, moral concerns and ethical issues associated with the use of ESCs hinder their clinical

applications [34]; furthermore, the cost associated with prolonged cell culture is also an obstacle.

## 1.3 *In vitro* culture methods for cell expansion in regenerative medicine

### 1.3.1 Importance of scaffolds in cell culture for regenerative medicine

In tissues, cells connect to each other, as well as to the ECM. Receptor complexes on the surfaces of cells facilitate interactions with their neighbours, the ECM and other exogenous factors. The 3D ECM microenvironment is thought to be involved in the regulation of the intracellular complex signalling cascade that influences phenotypic fate by altering the gene, and ultimately protein expression, of the stem cells, i.e. self-renewal or development to committed cells. Additionally, the ECM provides the cells with the required mechanical support [70-74]. Therefore, one challenge in tissue engineering is the design of reproducible 3D scaffolds that can mimic the structure and biological functions of the natural ECM for the purposes of *in vitro* cell expansion [75].

The importance of using scaffolds *in vivo* arose from the limited success of cell therapy when free cells in suspension were injected to an area of impaired function or structure. This is mainly due to poor cell engraftment, which was as low as 1–5% of the injected cells in certain conditions [76]. Post-injection, all control over cell fate is lost and since the cells lack a template to guide the restructuring, they become incapable of histological reorganisation and tissue formation, leading eventually to

the death of the vast majority [77, 78]. Furthermore, a lack of cell attachment is known to induce cell apoptosis [79].

Supporting biomaterial scaffolds are also important *in vitro* for the 3D culture of cells. Traditionally cells have been cultured on planar surfaces, a practice that does not mimic the cells natural environment. Various studies have emphasised the importance of 3D culture environments, especially with regards to stem cells, where temporal and special cues are critical in deciding the cell fate [80].

### 1.3.2 Importance of 3D culture for mammalian cells

The culture of mammalian cells *in vitro* provides a defined platform for investigating cell and tissue physiology and pathophysiology outside of the organism. Traditionally, in the past four decades, this has been achieved by culturing individual cell types on two-dimensional (2D) substrates such as tissue culture polystyrene (TCPS) [81]. TCPS flasks are convenient for routine work; however, these cultures do not provide an accurate representation of the ECM found in native 3D tissues. Only a segment of the cell's membrane can interact with the culture surface and neighbouring cells, while the rest of the cell is exposed to the bulk culture media [82]. As a result, many complicated biological mechanisms, such as stem cell differentiation [83] and tissue morphogenesis [84], are known to differ from those of *in vivo* organs or tissues [19]. On the other hand, larger surface areas and more binding sites are offered to cells cultured in 3D environments when compared to 2D cultures, as shown in Figure 1.2. Therefore, many methods have been investigated

for the development of a 3D growth environment that mimics the original tissue as closely as possible [85-88]. A good review of 3D cell culture by John W. Haycock includes 3D culture methods, design, fabrication techniques and the importance of these cultures for clinical applications [13].

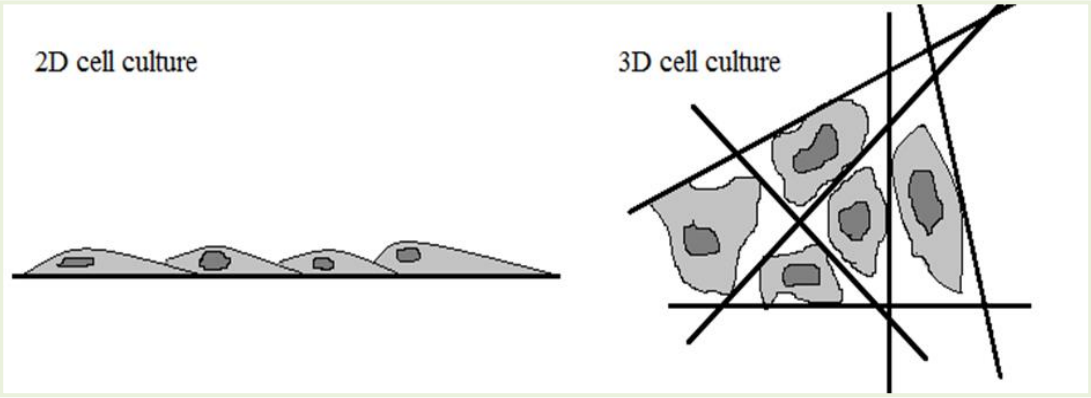



**Figure 1.2:** The difference in cell growth on 2D and 3D surfaces. Cells flatten and spread when cultured on 2D surfaces, while larger surface areas and an increased number of binding sites are offered to cells cultured in 3D environments such as the ECM**,** modified from [89].

Many cell-culture studies have shown that the growth and differentiation of cells is highly dependent on the context in which a cell is grown, and that changing the environment can radically alter the behaviour of cells [75, 90]. These findings are related to the cell-cell and cell-substrate interaction patterns; in 2D cell cultures, unequal integrin binding occurs, which affects the intracellular signalling and phenotypic fate of cells [91, 92]. For example, human liver carcinoma (HepG2) cells cultured in 3D cell culture, displayed excellent morphological characteristics and formed numerous bile canaliculi that were rarely seen in 2D cell culture. Furthermore, during the toxicological test, HepG2 cells grown in a 3D environment

maintained their structural integrity, possessed greater viability and were less susceptible to cell death at higher levels of the cytotoxin (methotrexate) when compared with cells grown in 2D cultures [92]. Similar findings were observed when human dermal fibroblasts and endothelial cells were cultured in a 3D (Azowipes®) environment when compared with cells cultured on 2D TCPS; the cells were significantly more resistant to oxidative stress (hydrogen peroxide) and to a potentially toxic heavy metal (silver nitrate) [93]. Cell differentiation is also responsive to changes in the culture environment, for example improved chondrogenesis was observed when murine embryonic stem cells were cultured in 3D when compared to 2D cell culture [94]. Furthermore, the rates of adhesion, proliferation and migration of fibroblast cells in 3D cell culture are high; additionally, the cells display an elongated shape, as in native tissues [95, 96]. Another study showed the ability of 3D culture to enhance the osteoblastic differentiation of human mesenchymal stem cells (hMSCs), where bone morphogenetic protein 2 (BMP-2), bone sialoprotein (BSP) and ALP gene expression were modified by the 3D culture substrate [73]. Experiments have also shown that growing cancerous breast cells in a 3D culture resulted in changes in their patterns of gene expression and other biological activities, which more closely reflected the activities of cells in living tissues [97]. Another study showed the influence of 3D culture on the phenotype, gene expression and epidermal growth factor receptor (EGFR) inhibition of colorectal cancer (CRC) cell lines, with 3D culture offering the opportunity to investigate CRC cell lines under more physiological-related conditions, when compared to 2D culture [98]. Moreover, 3D

culture has been used in lung tumour cellular models, and resulted in the reduction in EGFR and cMET protein expression; in addition to an altered cell-proliferation response to hepatocyte growth factor (HGF), when compared with a monolayer culture [99].

As a consequence of these findings, there is a requirement for *in vitro* culture systems that represent the cellular environment in native tissues, which in turn will help our understanding of complex biological phenomena.

### 1.3.3 Properties required in scaffolds intended for 3D cell culture

The ECM is a complex composite of interwoven protein fibres, such as fibronectin, collagen and elastin, with diameters ranging from tens to hundreds of nano-metres (nm). ECM proteins serve as a signalling route between the cells and the ECM by providing binding sites for integrins on the cell surfaces [100]. Therefore, the main aim of creating different scaffolds for culturing the cells is to mimic the real environment of the ECM in order to control the normal behaviour, growth, proliferation, differentiation, migration and function of the cells [101]. Many parameters need to be considered when designing a 3D culture, such as the choice of materials (natural or synthetic), biocompatibility, cell-culture additives (e.g. growth factors), culture conditions (temperature, oxygen level and pH) and culture methods [13].

Three-dimensional cell cultures should allow the continuous exchange of nutrients, oxygen and waste metabolites in order to minimize the aggregation and death of the

cells [19]. This has been addressed by designing highly porous scaffolds with controlled mass transfer rates and specific binding sites for the cells [87, 102]. Moreover, different growth factors and nutrients were encapsulated in different layers of the 3D structure to support cell growth and differentiation [89, 103]. The scaffold should also possess adequate mechanical properties, ideally matching those of the original tissue, that allow for sufficient cell ingrowth and the maintenance of the appropriate ECM. Additionally, some level of bioactivity should be provided by the scaffold surface to accommodate cell adhesion and migration [104]. The length scale of the scaffolds, which differs from the macro- to the nano- scale, is also considered as one of the most important parameters for designing scaffolds for 3D cell culture [105].

Scaffolds used in clinical applications should be biocompatible and, after implantation into the defected region of the body, degrade gradually to aid the integration of the cells that they carry within the existing host tissues, as well as only generating non-toxic or non-immunogenic metabolites [106-108]. However, the improper storage of such biodegradable scaffolds can render them useless due to degradation and changes in their properties that can directly influence the quality and reproducibility of results. Furthermore, biodegradation itself is not necessarily required for scaffolds that can be routinely used for investigating cell differentiation *in vitro* [109].

### 1.3.4 Common materials used for scaffolding in tissue engineering

The last half a century of biomaterials research has witnessed a shift from the use of permanent metallic and ceramic implants, to biocompatible synthetic materials, which have contributed to the current tissue-engineering ideology [109, 110]. Some of the natural and synthetic materials that have been successfully employed in tissue engineering are listed below.

#### 1.3.4.i Natural materials

These are advantageous due to their inherent properties of biological recognition and their susceptibility to cell-triggered proteolytic degradation and remodelling. However, their application has been limited due to the complexities associated with sourcing, processing and purification, limited mechanical strength, loss of their morphology in aqueous environments, immunogenicity and potential of disease transmission [13, 111].

Naturally occurring ECM proteins, such as collagen, gelatin and elastin, are the most commonly used materials for tissue engineering due to their good biocompatibility [112, 113]. Collagen is a well-established and Food and Drug Administration (FDA)-approved material for wound healing for the treatment of burns and chronic wounds. Many collagen types have been used; however, the main types are type I (found in the skin and bone), type II (cartilage) and type III (blood-vessel walls). Collagen type I and type III account for nearly one-third of the proteins in the human body [114]. Due to their biocompatibility, aligned collagen electrospun fibres were

shown to support fibroblast cell growth by offering them a similar environment to that found *in vivo* [115]. Hyaluronic acid [116], gelatin [117], chitosan [118] and alginates [119] also been widely studied as scaffolds for tissue engineering.

### 1.3.4.ii Synthetic materials

Synthetic materials have been widely used for tissue engineering. Polymers have been employed due to their reproducibility, adaptable chemistries, mechanical strength, lack of infection transmission and lower costs [13]. These polymers can be processed into highly porous 3D scaffolds of variable designs, such as fibres, sheets, blocks or microspheres [120].

The poly (α-hydroxy acid) polymers are among the best characterised and most studied polyesters for tissue-engineering applications due to their low toxicity, biocompatibility and FDA-approval for human use. Examples include poly (lactic acid) (PLA), poly (glycolic acid) (PGA) and their co-polymer PLGA [121, 122]. PGA non-woven scaffolds seeded with chondrocytes formed cartilage-like tissue after 20 weeks in culture, with relatively high resistance to loading [123]. PLGA scaffolds have also been widely used for various tissue-engineering applications [124].

Aliphatic polycaprolactone (PCL) is polyester, with a slower degradation rate than PLGA, which makes it suitable for the design of prolonged cell-culture systems. Moreover, its mechanical stability and low cost make PCL a desirable choice for

scaffold fabrication [125]. For example, the combination of PCL with collagen led to an increase in the fibrous scaffolds' tensile strength after electrospinning [126].

Non-biodegradable polyesters such as poly (ethylene terephthalate) (PET) have also been used for the preparation of supportive scaffolds for cell culture *in vitro* [103]. PET is known to be bio-stable, has excellent mechanical strength and is amenable to various surface modifications [127-129]. PET nano-fibres were able to support endothelial cell (EC) spreading and proliferation, in addition to preserving the ECs' phenotype [130].

The use of synthetic materials can be limited by the hydrophobicity of the resultant surfaces, which affects the ability of cells to attach to the scaffolds. However, surface-modification techniques have led to significant improvements in cell adhesion and further aspects of cell behaviour [131]. Other groups combined synthetic materials with biological substances to yield superior materials tailored to induce cell responses [132]. Another challenge associated with using synthetic materials is the change in culture pH as a result of the accumulation of degradation products, which can also be detrimental to cells [110]. Moreover, in some cases, scaffolds intended for clinical use are recognized as foreign substances and cause significant immune responses and inflammation when implanted into the human body [133].

## 1.4 Different types and designs of scaffolds used to create 3D cell-culture environments for cell therapies/regenerative medicine

Tissue engineers and cell biologists have been developing a number of 3D cell cultures that mimic the native environment. Some of the common scaffold fabrication techniques and scaffold designs are listed below.

### 1.4.1 Hydrogel scaffolds

Hydrogels represent a proper environment for isolated cells due to their highly hydrated 3D network of polymers that provides a place for cells to adhere, proliferate and differentiate [134]. In addition to their biocompatibility, their low interfacial tension and minimal mechanical and frictional irritation are all appealing features that favour their application in tissue engineering [135]. Gelation can occur through a change in temperature, via chemical or ionic crosslinking or the formation of an insoluble complex. Hydrogels made of a fibrinogen backbone and crosslinked with difunctional polyethylene glycol (PEG) side chains were able to support smooth-muscle cell adhesion, their penetration through the hydrogel material and the formation of interconnecting networks of cells [136]. Thermo-responsive hydrogels were also used as 3D cell culture environments. Photo-crosslinked hydrogels made of a co-polymer of 4-(N-cinnamoylcarbamide) methylstyrene (CCMS) and poly (N-isopropylacrylamide) (PNIPAAm) were able to support bovine endothelium and human retinal pigmented epithelium cell attachment at 37°C. In response to a decrease in the culture temperature, these cells detached and transplanted to another culture surface, without functional and structural changes [137].

### 1.4.2 Microparticles

Microparticles have also been used as a 3D culture system. PLA microparticles containing poly (vinyl alcohol) (PVA) in the matrix structure (PLA-PVA) provided a 3D environment for breast cancer cell adhesion and growth. A cell density of $1.5 \times 10^6$ cells per mg of microparticles was achieved after 9 days of culture, which was a 7-fold increase from the initial seeding cell density. In addition to tissue engineering applications, microparticles with cancer cells grown into a tissue-like structure *in vitro* could be potentially used as a model system for the preclinical evaluation of the cytotoxic effects of anticancer agents [138]. Another study evaluated the antiproliferative effects of three anticancer drugs, doxorubicin, paclitaxel and tamoxifen, on breast cancer cells cultured on 3D porous microparticles versus cells cultured as a 2D monolayer. The antiproliferative effect of the drugs in the 3D model was significantly lower than of that on the 2D monolayer, which was evident from the 12- to 23-fold differences in their $IC_{50}$ values. Doxorubicin accumulation in the cells grown on 3D microparticles was ~2.6-fold lower than in the cells grown as a 2D monolayer. Furthermore, the collagen content of the cells grown on the 3D microparticles was 2-fold greater than that of the cells grown in 2D, suggesting greater synthesis of ECM in the 3D model, which acted as a barrier to drug diffusion [139]. The aggregations of prepared microparticles by physical or thermal means have been studied by different groups in order to create 3D porous structures. Chitosan particle aggregated scaffolds were seeded with hMSCs and demonstrated

no toxic effects on the cells, in addition to the potential for osteochondral bilayered scaffold development [140].

### 1.4.3 Specially designed porous scaffolds

#### 1.4.3.i Alvetex®

Alvetex® is a rigid, highly porous polystyrene scaffold designed specifically to enable routine 3D cell culture. The scaffold is formed by polymerisation in a biphasic emulsion consisting of an aqueous and a non-aqueous monomer/surfactant phase, termed a high-internal-phase emulsion (HIPE). The resulting polymer (poly-HIPE) consists of a relatively homogeneous porous network of voids, linked by interconnecting pores, which provides the environment for routine cells to grow, spread and differentiate *in vitro* [141, 142]. The suitability of the Alvetex® system for use with human HaCaT keratinocytes was demonstrated, and it was shown to support the formation of a basic stratum corneum. Therefore, it proposed that it is a useful tool for testing epidermal barrier function [143].

#### 1.4.3.ii High-pressure processing

High-pressure processing, also known as supercritical-fluid technology, involves applying a gas, such as carbon dioxide, to dry a polymer under a high pressure, which forms a single polymer/gas phase. As the pressure is decreased, pore formation occurs in the polymer matrix based on the amount and the reduction rate of the pressure. This technique was pioneered by Mooney *et al.* who utilised it to fabricate highly porous PLGA sponges [144]. The main advantage of this technique

is the avoidance of organic solvents, the remnants of which might lead to inflammatory responses after implantation. Additionally, the approach allows for the incorporation of growth factors into 3D scaffolds, without the risk of solvent-induced denaturation [145].

The scaffolds fabricated using this method have pore sizes of 100–500 μm. The main drawback, however, is their closed-pore morphology. Harris *et al.* showed that this could be addressed through the incorporation of leaching particles [146].

### 1.4.4 Fibrous scaffolds

There are different techniques used to fabricate polymers into nano-metre (nm) or micro-metre (μm) scale fibres, which include drawing, template synthesis, phase separation, self-assembly and electrospinning [71, 147, 148]. The drawing process starts by dipping a micropipette near to the contact line of a polymer droplet by using a micromanipulator. The micropipette is then withdrawn at specific speeds, resulting in fibre diameters that range from 2 to 100 nm and fibre lengths of up to 10 μm. The drawing process requires minimal equipment; however, it is a non-continuous and time-consuming process. Moreover, the materials should be viscoelastic in order to withstand the strong deformation applied to the droplet during the pulling process, without the breakage of the fibres [149]. In the template synthesis method, the polymer solution is pushed through a metal-oxide porous membrane (e.g. an aluminium-oxide membrane) under the application of pressurized water. The polymer will then come into contact with a solidifying solution, resulting in fibre

formation with diameters that depend on the pore size of the membrane, e.g. 100 nm and 10 µm in length [105, 149]. Phase separation consists of five steps; polymer dissolution in a proper solvent, gelation, solvent extraction, freezing and freeze-drying to produce fibres with diameters ranging from 50 to 500 nm. Phase separation gives good batch-to-batch consistency and the fibre porosity and diameter can be controlled; however, it has been applied to a limited range of polymers and takes a relatively long period of time to transfer the solid polymer into the porous fibres [150]. Self-assembly is a complex technique that involves the use of smaller engineered polymer molecules as building blocks for nano-scale fibres (1 to 100 nm). The resultant scaffold morphologies depend on the shape and the intermolecular forces between the smaller molecules, which in turn determine the shape of the nano-fibres [149, 151]. More recently, electrospinning has also been widely investigated for the production of meshes of submicrometric fibres for different tissue engineering applications [152, 153].

### 1.4.5 Electrospinning

Electrospinning, derived from ‘‘electrostatic spinning’’, was invented by Formhals in 1934 via the use of an electrostatic field to produce a polymer filament [149]. In 1969, Taylor described the formation of the ‘Taylor cone’, which is the conical-shaped droplet of the polymer solution formed when the applied electric field overcomes the surface tension of the solution, as shown in Figure 1.3 [154]. In 1971 and 1987, the effects of electrospinning parameters on the electrospun fibres were studied, such as the investigation of the effects of the solution concentration by

Baumgarten [155], applied voltage by Hayat *et al.* [156] and viscosity and working distance by Simons, *et al.* [157, 158]. The relationship between surface beads and the applied voltage was later studied by Deitzel *et al*. [159]. Further studies into electrospinning were carried out by different scientists such as Hohman *et al.,* Yarin *et al.,* Warner *et al.* and many others [160-162].

Electrospinning is considered a cost-effective process that is capable of producing continuous fibres, ranging from a few hundred nano-metres to a few microns in diameter, through an electrically charged polymer jet [152, 153]. Furthermore, a wide range of polymers (natural and synthetic) have been fabricated by electrospinning [163, 164]. The shape, size and porosity of the electrospun fibres can be controlled by changing different electrospinning parameters [165, 166]. In comparison with other fabrication methods, electrospinning is a less-complex process than self-assembly. It is also a contactless procedure, unlike the drawing method, and can be applied to a variety of polymers when compared with phase separation [167]. Moreover, electrospun fibres have a large surface area, with a highly porous structure that provides the basic design for cell adhesion sites and allows the flow of gases, nutrients and metabolites [13]. These fibres can be applied in many fields such as medicine, industry and in pharmaceutical applications [114, 168, 169]. However, further understanding is needed to study the influence of multiple parameters on the resultant fibre morphology.

### 1.4.5.i Setup and principle

Electrospinning requires four major components: a conductive spinneret (hypodermic needle), a syringe pump to eject the polymer solution out of the spinneret at a controlled rate, a voltage supply (one electrode is applied onto the spinneret and the other electrode onto the collecting plate) ranging from 0 to 30 kV and a collector (metallic plate or rotating mandrel) at a defined distance from the spinneret to collect the fibre mat, as shown in Figure 1.3 [103]. After applying the electric field onto the spinneret, charges of the same sign will build up on the droplet surface. The Taylor cone will then be formed when the electrostatic charge overcomes the surface tension, followed by polymer-jet elongation, thinning and solvent evaporation, leaving the electrically charged nonwoven fibres on the collecting plate [167, 170, 171].

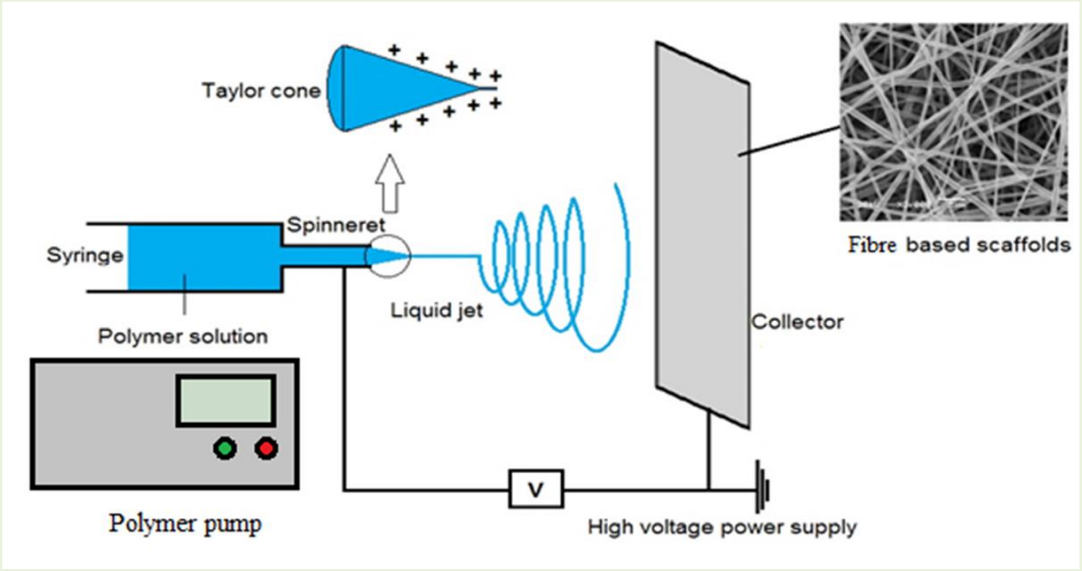



**Figure 1.3:** A schematic representing the basic electrospinning setup. Inset images show the electrified Taylor cone and a scanning electron microscopy (SEM) image of an electrospun fibre-based scaffold on the collecting plate, modified from [167].

### 1.4.5.ii Process parameters

Many parameters can influence the transformation of polymer solutions into fibres through electrospinning. These parameters include (i) the solution properties, such as viscosity, elasticity, conductivity and surface tension; (ii) processing parameters and (iii) ambient parameters [158].

#### 1.4.5.ii.a Solution parameters

The first consideration when forming a polymer solution is to choose a suitable solvent for each polymer [149]. The polymer-solution viscosity should not be too high as to prevent the jet formation, nor too low in order to allow the polymer solution to drain freely from the syringe [149, 158]. For example, the electrospinning of poly (ethylene oxide) (PEO) dissolved in ethanol-to-water solutions was prohibited when solution viscosities were above 20 poises, due to the instability of flow caused by the high cohesiveness of the solution. However, droplets were formed when the viscosity was too low (<1 poise) [172]. The polymer-solution concentration is proportional to the polymer-solution viscosity and is considered one of the most important parameters in the electrospinning process because it affects the fibre diameters, fibre morphology and bead formation [173]. Additionally, the surface tension of the polymer droplet is another parameter that affects fibre formation and morphology. For example, Fong *et al.* showed that the modification of the surface tension via the addition of a surfactant resulted in thin

fibres of 100 nm [174]. Moreover, the polymer-solution conductivity also affects the fibre diameter and formation of beads in the fibre matrix [175, 176].

#### 1.4.5.ii.b Processing parameters

The voltage, distance between the spinneret and the collector plate and flow rate are the three main processing parameters that determine fibre formation and morphology. The electric field and flow rate should be high enough to overcome the viscosity and surface tension of the polymer solution, hence, resulting in the formation and maintenance of the jet elongation from the spinneret [149, 169]. In general, higher applied voltages and flow rates eject more fluid in a jet, resulting in a larger fibre diameter [177]. The gap between the syringe and the collecting surfaces must be large enough to allow fibre formation and prevent the formation of electric sparks between the two electrodes [149, 178].

#### 1.4.5.ii.c Ambient conditions

There have not been many reports discussing the influence of environmental conditions on the electrospinning process and the resultant electrospun fibres. However, a useful attempt to understand the effect of the environmental temperature on electrospun fibres was made by Demir *et al.* [177]. They showed that the fibre diameters obtained from the polymer solution at a high temperature (70°C) were much more uniform than those obtained at room temperature (25°C). The mechanisms involved, however, were not fully understood. It should be noted that

the viscosity of the polyurethane solution at the same concentration at a higher temperature was significantly lower than that at room temperature. This is also supported by Kim *et al.*, who found that high temperatures resulted in an increase in the evaporation rate of the solvents, which in turn decreased the polymer solution viscosity [174]. Humidity also affects the fibre formation; when humidity is high, the fibre diameter and beading is increased due to the incomplete solvent evaporation from the fibres that reached the collecting plate [179].

#### 1.4.5.iii Characteristics of electrospun scaffolds

##### 1.4.5.iii.a Non-woven fibre scaffolds (unordered mesh scaffolds)

Non-woven fibres possess a high range of porosity, are well suited for the exchange between nutrients and waste in cell culture and have a large surface area to volume ratio, which enable the loading of different bioactive molecules to influence cell activity [176]. These fibres greatly supported the contraction of cardiac myocytes when cultured on PCL meshes [180]. Another study reported a good infiltration rate of chondrocytes when they were cultured on non-woven type II collagen mats for the purpose of replacing damaged cartilage [181].

##### 1.4.5.iii.b Aligned-fibre scaffolds (ordered fibre scaffolds)

Scaffolds with directional cues are important for many tissues requiring this type of orientation, such as blood vessels [182], tendons, bone [183], nerve bundles [184] and cardiac muscle [185]. A number of methods have been developed to create

aligned fibres that depend on the force applied, such as mechanical, electrostatic and magnetic forces [103]. The application of 3D aligned scaffolds for neural stem cell culture showed similar elongation and extension of the neurites parallel to the fibres, as in the human body [186, 187]. Aligned scaffolds for smooth muscle cells (SMCs) also displayed a spindle-like contractile phenotype that is similar to the native vessels [188]. Moreover, tendon-specific genes were up-regulated in human tendon stem progenitor cells (hTSPCs) cultured on aligned PLLA scaffolds, when compared with non-woven PLLA scaffolds [183]. Faster wound healing was also observed with the use of aligned fibres when compared to non-woven fibres [189].

## 1.5 Applications of electrospun fibre-based scaffolds in regenerative medicine and tissue engineering

Electrospun scaffolds have been used for variable applications, as illustrated in Figure 1.4. However, in this chapter, the main focus is on the application of these electrospun fibrous scaffolds in tissue engineering and regenerative medicine.

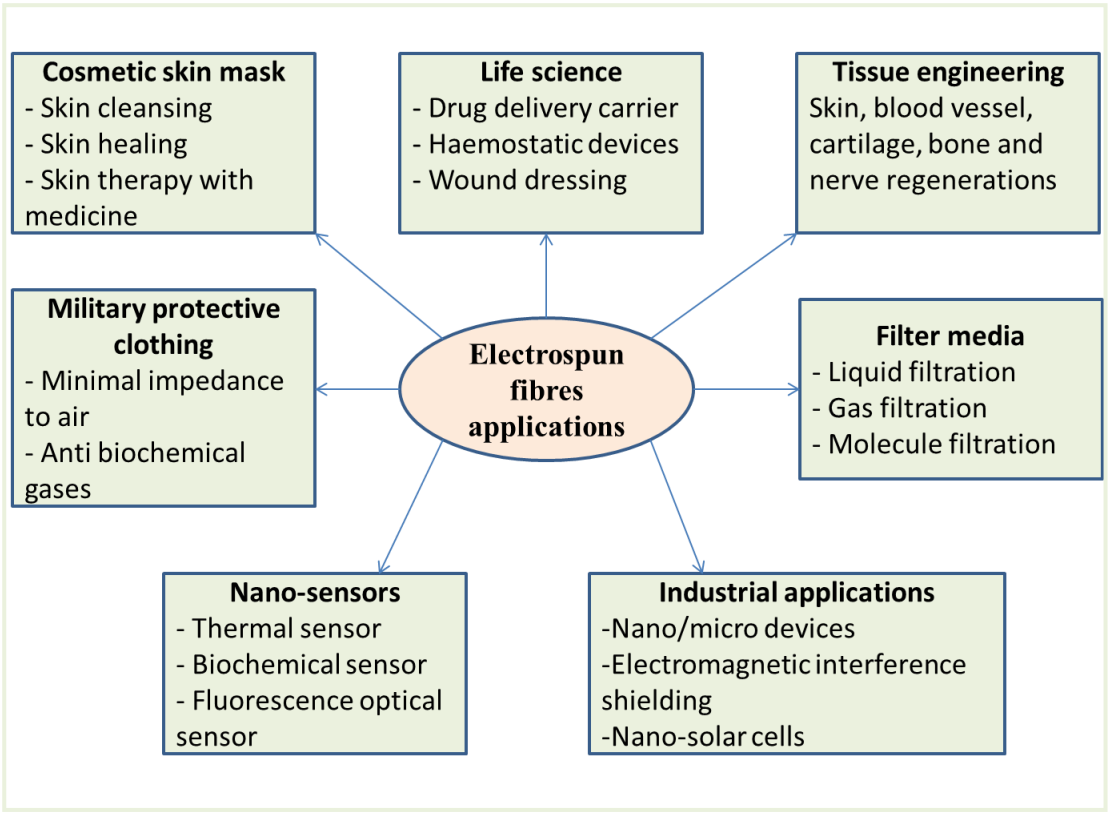



**Figure 1.4:** Potential applications of electrospun fibres, modified from [164].

The applications of electrospun fibres in tissue engineering often involve several considerations, including the choice of materials, fibre orientation, porosity, surface modification and type of tissue. Progress has been made in applying electrospun scaffolds to different human tissues for regenerative medicine, as shown in Figure 1.5 [96]. Electrospun scaffolds have been used in vascular tissue engineering, for example, poly (L-lactic-co-ε-caprolactone) electrospun nano-fibres were used for human coronary artery smooth muscle cell (HCASMCs) culture by Xu *et al.* [190]. The results showed that SMCs proliferated well and reached 90% confluency, in addition to maintaining their phenotypic properties. Human vascular ECs have also

been cultured on electrospun PLA fibrous scaffolds and the cells reached 75% confluency and maintained their differentiated phenotype, which indicates that the scaffolds have good biocompatibility [191]. Another study by Jeong *et al.* demonstrated the use of collagen-PLGA hybrid scaffolds for the co-culturing of SMCs and ECs. The results showed that electrospun scaffolds supported cellular alignment, the enhancement of vascular EC development and the retention of a differentiated cell phenotype [192]. Electrospun silk fibroin scaffolds were also used by Zhang *et al.* for *in vitro* vascular cell growth, where human aortic endothelial cells (HAECs) and HCASMCs were seeded on these scaffolds. The data showed that cells were aligned, elongated and proliferated on the scaffolds with the formation of ECM for the HCASMCs based on the quantification of collagen type I expression at the protein and transcription levels [193]. Heart tissue engineering is also considered an important application of electrospun fibres, for example, the culturing of cardiomyocytes (CMs) on electrospun poly (L-lactide) (PLLA) scaffolds resulted in the development of mature contractile machinery (sarcomeres) [185].

Electrospun fibres also play an important role in neural tissue engineering, in particular, aligned nano-fibre scaffolds. These scaffolds can be used to regenerate peripheral nervous system (PNS) and central nervous system (CNS) injuries by providing directional cues for neuron cell extension and orientation [179]. For example, neonatal mouse cerebellum C17.2 stem cells (NSCs) were cultured on aligned PLLA fibrous scaffolds. They showed good attachment to the fibres, with neurite-like growth, and they elongated in the same direction as the aligned fibres

[194]. Moreover, the large surface area of the nano-fibres provided an excellent differentiation environment for the NSCs by accommodating a higher concentration of neurotropic factors. Non-aligned electrospun nano-fibrous and radial alignment nano-fibrous-based scaffolds have also gained large importance in recent years as dural substitutes, due to their high rate of cell infiltration [103].

Furthermore, experiments showed that electrospun fibres have the ability to acts as a good substrate for cartilage and bone tissue development. Electrospun PCL nano-fibres greatly supported MSCs derived from the bone marrow; growth and secretion of type I collagen was observed after 4 weeks [195, 196]. Another study showed that co-electrospun PLGA-collagen scaffolds could be useful for the treatment of skeletal joint defects [197]. Moreover, the similarities between the microstructure of the fibrous scaffolds and the native collagen matrix enabled them to support the chondrogenesis of the human bone marrow-derived MSCs [198]. Ouyang *et al.* showed that aligned PLLA fibrous scaffolds were suitable for human tendon progenitor stem cell (hTSPC) culture, as the cells aligned themselves along the same direction of the fibres and expressed tendon-specific genes [198].

Electrospun fibres have also been used in urethral regeneration. A study reported the seeding of autologous bladder cells on PLGA scaffolds, which were then implanted into five boys in order to repair urethral defects. These implants stimulated sufficient repair such that the urinary flow rate was restored and the post-operative development of naturally appearing urothelial and bladder tissues was observed [199]. Moreover, studies are being conducted to establish the efficacy and safety of

the use of tissue-engineered electrospun scaffolds in the female reproductive system and in oesophageal tissue repair [11, 200].

The field of wound dressings is another potentially significant application of electrospun fibres. Powell and co-workers grafted bovine collagen nano-fibrous scaffolds into athymic mice; the rate of engrafting was 100% and histological studies showed that no bovine collagen nano-fibres were present after 8 weeks in the wound area [201]. Polyurethane (PU) is also frequently used in wound dressings because of its unique properties, which include good barrier properties and oxygen permeability. Khil and co-workers fabricated an electrospun PU membrane for wound dressing applications and the data showed a controlled evaporative water loss, excellent oxygen permeability and the promotion of fluid-drainage ability. Neither toxicity nor permeability to exogenous microorganisms was observed with the nano-fibrous membrane. The histological examination confirmed that there was an increased epithelialisation rate, and that the exudate in the dermis was well controlled by covering the wound with the electrospun membrane [202].

To conclude, electrospun fibrous scaffolds are considered as promising substitutes for many tissue-engineering applications and for the regeneration of various body organs and tissues or the restoration of their function.

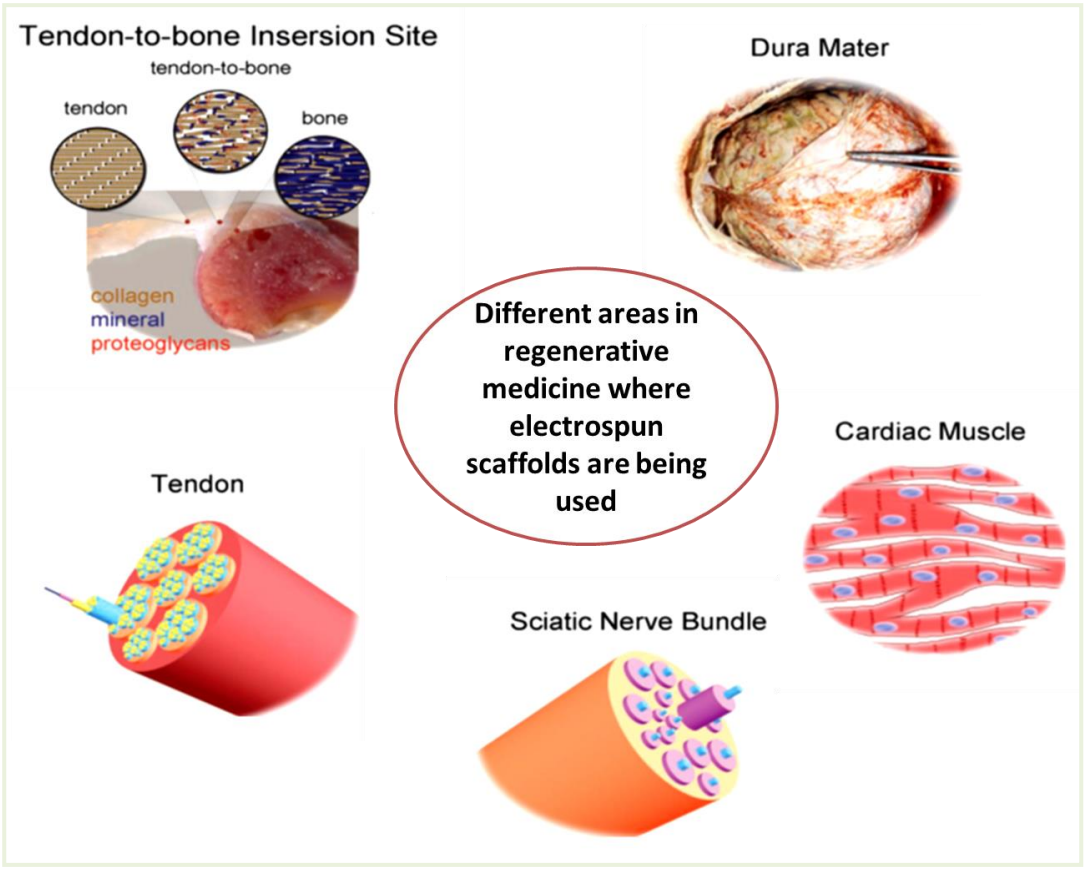



**Figure 1.5:** Examples of different areas in regenerative medicine where electrospun scaffolds are being used, modified from [200].

## 1.6 Responsive surfaces for mammalian cell culture

Many cell types behave differently on hydrophobic compared to hydrophilic substrates. This has led scientists to design and apply responsive polymer surfaces. These responsive 'smart biomaterials' can change their physical proprieties in response to external stimuli such as light, temperature, pH and enzymes. They are being extensively studied as they provide promising materials that can support cell adhesion, proliferation, differentiation and detachment [203].

### 1.6.1 Disadvantages of enzyme treatment

Normally, cells are harvested from the cell-culture environment with the use of chelating agents, such as ethylenediaminetetraacetic acid (EDTA), and a protease enzyme, such as trypsin. Trypsin-EDTA treatment disrupts the cell-substratum and cell-cell interactions. These interactions are mediated by various proteins (mostly integrins and ECM proteins like fibronectin or vitronectin) and their interactions are strengthened by divalent cationic metals (e.g. fibronectin-integrin interactions are promoted by $Ca^{2+}$). Trypsin disrupts these interactions by proteolysis and EDTA chelates divalent cationic metals. This results in the loss of interactions between cell-cell and cell-substratum, thereby, causing the destruction of cell-membrane proteins, such as ion channels and growth-factor receptors [204]. Furthermore, enzymatic passage using the digestive enzyme, trypsin, damaged the mammalian cells internally via the degradation of polyribosomes [205]. In addition, transmission electron microscopy examination of keratinocytes revealed that desmosomes were destroyed during dispase treatment; however, they remained intact when cells were harvested by lowering the culture temperature on thermo-responsive substrates [206]. Therefore, there is a persisting need to develop new responsive systems that enable the easy removal of the cultured cells, without affecting the cell integrity or viability. As a result, many intelligent systems have been developed to avoid or reduce the utilisation of digesting enzymes for cell-culture studies, in particular for those destined for the clinic.

### 1.6.2 Thermo-responsive surfaces

Thermo-responsive polymers have been used over the past three decades for different mammalian cell cultures. Their thermo-responsive activity arises due to a change in their chain configuration, which is manifested in a transformation from a hydrophobic to hydrophilic state. The temperature at which this transformation happens is defined as the lower critical solution temperature (LCST) for water-soluble polymers, as shown in Figure 1.6. This enables cell adhesion to the hydrophobic surface at temperatures above the LCST, with the spontaneous release of the cells from the hydrophilic surface at temperatures below the LCST, as shown in Figure 1.7 [190].

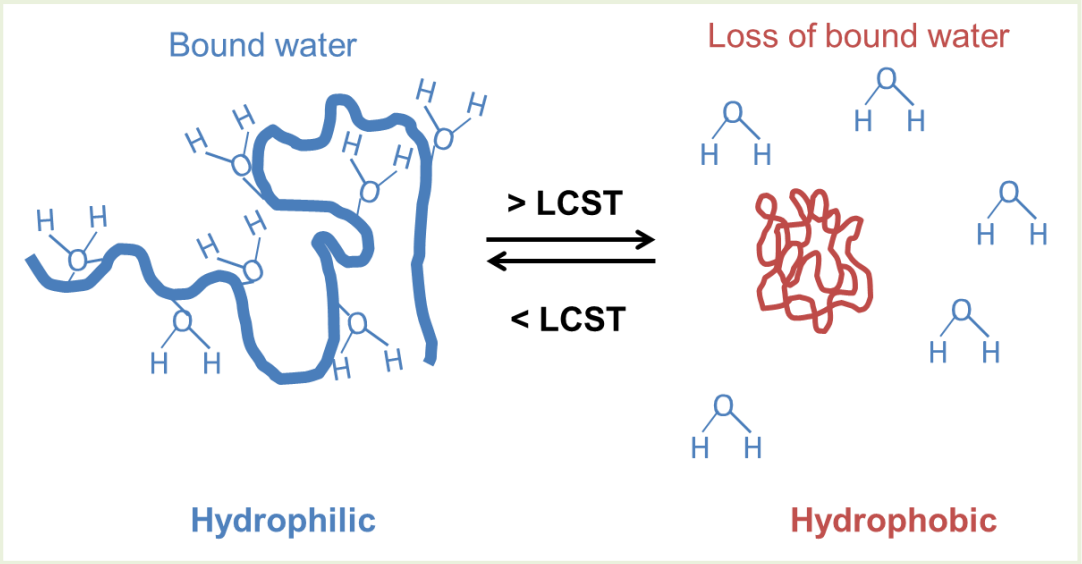



**Figure 1.6:** Schematic of 'smart' polymer response to temperature, modified from [203]

Thermo-responsive surfaces have potential applications in the biomedical field as a surface for *in vitro* cell culture for tissue engineering and regenerative medicine. A classic example of a responsive synthetic polymer is PNIPAAm, which is considered as the gold standard in this research area. It has been used over the last few decades as a thermo-responsive polymer for cell adhesion and detachment, and has a LCST of approximately 32°C. Surfaces coated with PNIPAAm have been widely used as smart substrates for cell-culture studies, as shown in Figure 1.7 [204, 207-210]. By using PNIPAAm-coated surfaces, cells are noninvasively harvested as intact cell sheets with critical cell-surface proteins, growth-factor receptors and cell-to-cell junction proteins remaining intact [90, 211]. To date, many cell types have been cultured on PNIPAAm-coated 2D surfaces such as keratinocytes [206, 212], cardiac myocytes [213], mouse embryonic stem cells (mESCs) [205, 214], human corneal endothelial cells [215, 216], human SMCs [217] and vascular ECs [218].

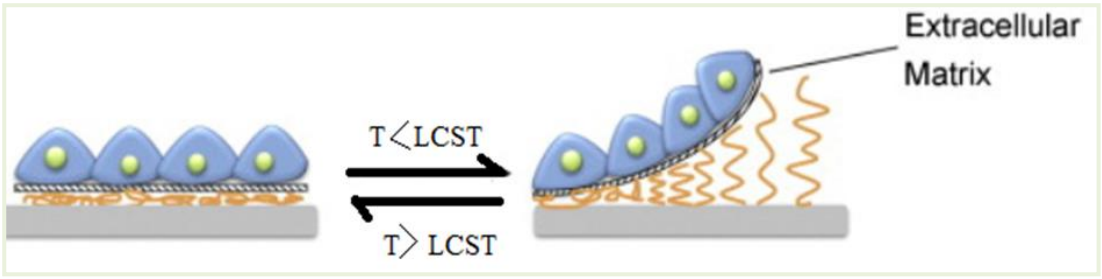



**Figure 1.7:** Cell adhesion onto the PNIPAAm-grafted surface and the release of cells as a continuous cell sheet when the temperature is lowered below 32°C, taken from [219].

Despite the widespread popularity of PNIPAAm in materials science, it has some disadvantages such as an irreversible phase transition, which is due to the significant influence of its end-groups [220, 221]. Moreover, the presence of multiple amide

functionalities in the molecular structure of PNIPAAm may lead to the formation of H-bonding interactions with other polyamides such as proteins [222]. Such behaviour raises doubts over the use of PNIPAAm in some biotechnology applications [223].

Polymers of poly (ethylene glycol) methacrylate have also been recently shown to possess thermo-responsive properties. The non-linear PEG polymers are composed of up to 85% in weight of PEG and are, therefore, water soluble and biocompatible [194]. Their LCST in water was found to increase with the length of the poly (ethylene glycol) side chain and could be tuned to around physiological temperature. These polymers are considered ideal structures, which combine the lack of toxicity and immunogenicity of PEG, and the environment-independent thermosensitivity of PNIPAAm in a single macromolecule [224], (Figure 1.8).

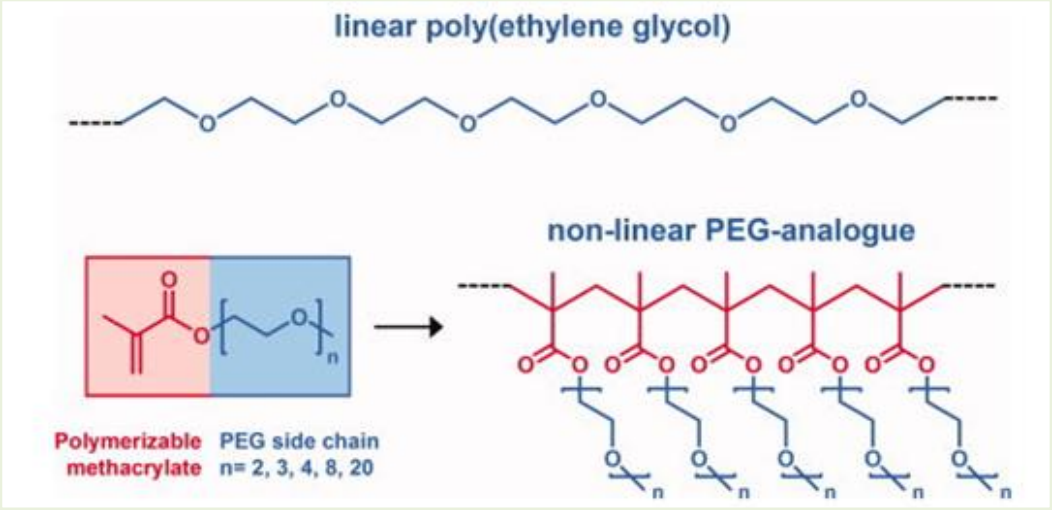



**Figure 1.8:** Molecular structure of standard linear PEG and nonlinear PEG-analogues constructed with oligo (ethylene glycol) macro monomers. (Red: hydrophobic methacrylate portion; blue: the hydrophilic PEG portion), taken from [224].

Huck and co-workers were the first to report the preparation of thermo-responsive brushes consisting of 2-(2-methoxyethoxy) ethyl methacrylate ($MEO_2MA$) and oligo (ethylene glycol) methacrylate (OEGMA). These 2D brushes exhibited clear thermo-responsive behaviour and displayed LCST values roughly similar to those observed for the copolymers in solution [225]. This co-polymer was successfully grafted to gold surfaces, offering temperature control over cell adhesion to the underlying substrate, and showed promising results for cell-sheet engineering [226]. Another study, showed that these grafted surfaces supported mouse mESC adhesion and proliferation at 37°C (above the LCST) and detachment from the surface by decreasing the temperature to 20°C (below the LCST) [205]. Thermo-responsive scaffolds with 3D features have also been introduced for cell-culture studies. A recent study described the use of a 3D non-woven fibre scaffold fabricated from poly (propylene) (PP), PET and nylon via needle-punching, which was grafted with PNIPAAm for HC04 hepatocyte culture. The cell number increased over the seven-day culture period and the thermal release of the cells was observed after 2 hrs of reducing the temperature to 20°C [90]. Another study reported that biodegradable thermo-responsive microparticles prepared with the co-polymer PEGMA and poly (propylene glycol) methacrylate (PPGMA) were also able to maintain mouse myoblast cells (C2C12) throughout ten days of cell culture [227]. Furthermore, the blend-electrospinning process has been used to fabricate 3D thermo-responsive fibres. Human endothelial cells adhered and proliferated on cross-linked electrospun thermo-responsive fibres made of poly (ethylene glycol) methacrylate (PEGMA) and PU scaffolds, with low cell-death rates, which indicate that PEGMA/PU scaffolds

were highly biocompatible and non-cytotoxic. However, no cell-detachment studies were conducted on these electrospun responsive scaffolds [228].

### 1.6.3 Cell-sheet engineering

Cell-sheet engineering without scaffolds is an alternative approach for tissue engineering and regenerative medicine and it has been suggested that by using this approach, better results than the conventional regenerative therapies of cell injection and tissue reconstruction with biodegradable scaffolds can be achieved [229]. It involves three main aspects; the first is the non-invasive harvest of cultured cells and cell sheets, e.g. using temperature-responsive cultures. The second aspect is the harvest of viable cell sheets that can be transferred to other culture-dish surfaces or directly transplanted to host tissues, as in the cases of the skin, corneal epithelium, bladder urothelium and periodontal ligament (2D cell-sheet manipulation). The third aspect involves the piling of the recovered cell sheets to reconstruct complex stratified tissue architectures such as the liver lobule, kidney glomeruli, and blood vessels (3D cell sheet manipulation) [230].

The Okano group has pioneered the application of thermo-responsive surfaces for cell-sheet-engineering applications. For example, endothelial cells were cultured on 2D thermo-responsive PNIPAAm surfaces, and when the culture temperature was decreased after cells proliferated to confluency, the cells spontaneously detached from the PNIPAAm-grafted surfaces. The cell-to-cell junctions were intact, with viable monolayer cell sheets and the recovery of intact ECM, which was deposited

during cell culture [231]. Recovered ECM adherent to the basal side of the harvested cell sheets can function as a natural substance to attach cell sheets onto other surfaces. Therefore, harvested viable cell sheets can be transferred to other culture dishes or device surfaces (2D cell-sheet manipulation) [232]. Another example reported by the same group showed the potential of using monolayered MSCs detached from responsive culture dishes for the treatment of a scarred myocardium. Four weeks after the transplantation of the MSC monolayer, the engrafted sheet gradually grew to form a thick stratum that included newly formed vessels, undifferentiated cells and a few cardiomyocytes [233]. Sheets of hepatic tissue were also recovered from PNIPAAm-grafted surfaces and then transplanted into the subcutaneous space. Efficient engraftment to the surrounding cells was observed, with the formation of 2D hepatic tissues that persisted in a stable form for longer than 200 days, as well as exhibiting several characteristics of liver-specific functionality [234].

The problems associated with corneal-donor deficiencies, rejection after corneal transplantation and the risk of infection associated with biological carrier substrates such as amniotic membrane [235] and fibrin gel [236] have made the use of thermo-responsive surfaces in corneal disease extremely important. A recent study reported the culture of normal rabbit corneal epithelial cells on PNIPAAm-grafted dishes in order to prepare cell sheets. The cell sheets were then transplanted to a rabbit with corneal erosion; after three weeks of implantation, the epithelial cell sheet was well-accepted into the injured area, without the use of a suture [237]. Moreover,

functional human corneal endothelial cell sheets harvested from temperature-responsive culture surfaces were shown to possess morphologically and functionally similar characteristics to the native corneal endothelium *ex vivo*. These sheets can be used clinically in patients with ocular endothelial defects [238].

Multiple layers of recovered cell sheets from 2D thermo-responsive surfaces have also been layered and used for cell-sheet transplantation for different tissues (3D cell sheet manipulation). A good review illustrated the development of myocardial tissue engineering using cell sheets harvested from temperature-responsive culture surfaces and discussed their usage [239]. The use of overlaid neonatal rat cardiomyocyte sheets detached from PNIPAAm-grafted surfaces to construct cardiac grafts was reported. After 4 weeks of *in vitro* culture, these layered sheets began to pulse simultaneously. After 3 weeks of implantation of the layered cardiomyocyte sheets into subcutaneous tissues of nude rats, spontaneous beating was macroscopically observed and the histological studies showed characteristic structures of heart tissue and neovascularisation within contractile tissues [240]. Similar *in vitro* results were observed when cardiomyocyte cell sheets constructed from chicken embryos beat strongly after being detached from the thermo-responsive surface [241]. A recent study demonstrated that after transplantation, human induced pluripotent stem cell-derived cardiomyocyte (hiPS-CMs) sheets detached from responsive surfaces to myocardial infarcts in a porcine model of ischemic cardiomyopathy. Transplantation significantly improved cardiac performance and attenuated left ventricular remodelling. hiPS-CMs were detectable 8 weeks after transplantation, with no

teratoma formation observed in animals that received the hiPS-CM sheets [242]. Cell sheets have also been used for periodontal regeneration, where three layered sheets of periodontal ligament (PDL)-derived cells were transplanted to dental root surfaces with three-wall periodontal defects. Cell-sheet transplantation regenerated new bone with well-oriented collagen fibres, while only limited bone regeneration was observed in the control group, which did not receive a cell-sheet transplantation [243].

To conclude, the use of synthetic smart thermo-responsive electrospun scaffolds for the expansion of mammalian cell cultures, including stem cells, is proposed for the first time in this project. The use of temperature as an alternative to trypsinization for cell detachment from the culture substrates is proposed, and this is further described below in the aims and objectives of this research project.

## 1.7 Aims and objectives

Cell and tissue-based therapies offer alternative treatments for a number of diseases and the regeneration of a range of tissues and organs. However, they are dependent on the culture system to generate large quantities of the desired cell phenotypes. They are compatible with good manufacturing practice, physically and chemically stable, reproducible and of a well-defined chemical composition. Moreover, the supply of good-quality cell types in appropriate numbers is considered an important factor for cell and tissue therapies. This supply can be achieved by creating 3D culture environments as it has been proven that 3D substrates are important for the

maintenance of many required cell phenotypes and for the improvement of the yields of desired cell phenotypes for clinical use [19]. Moreover, surfaces responsive to temperature can help to eliminate the use of digestive enzymes for cell passaging, which may render cell populations unsuitable for clinical use due to the risk of contamination. Evidence from the literature suggests that using smart surfaces can reduce the damage incurred to cells during passaging, providing a better starting cell quality for clinical applications.

The thermo-responsive polymer, poly ($PEGMA_{188}$), was considered for use as a responsive polymer in this study as it is composed of FDA-approved oligo (ethylene glycol) segments [244] and has an LCST of 26°C. Moreover, electrospinning was chosen in order to create 3D responsive fibrous scaffolds for mammalian cell culture as it considered an efficient method for the fabrication of fibrous scaffolds with controlled diameters, porosity, morphology and composition [245]. Fibrous scaffolds mimic the native fibrous nature of the ECM, in addition to possessing good mechanical support, offering large surface areas for cell attachment and the loading of biomaterials or growth factors.

The aim of this research project was to fabricate temperature-responsive fibre-based scaffolds by electrospinning in order to eliminate the need for enzymes to detach the cells from the culture surface. The thermo-responsive polymer, poly ($PEGMA_{188}$) was chosen for co-electrospinning with PLGA and PET polymers for mammalian cell culture, which included primary human corneal stromal stem cells (hCSSCs) and other cell types.

The aim of this project was achieved through the following objectives:

- To establish electrospinning and blend-electrospinning parameters, then characterize the electrospun fibres in terms of their diameter, morphology, integrity, composition and surface wettability.
- To assess different ways of incorporating a thermo-responsive poly ($PEGMA_{188}$) into the electrospun PET or PLGA fibres, either as part of the electrospinning process or as a post-electrospinning step.
- To investigate mammalian cell adhesion and detachment using 3T3 fibroblasts (Chapter 3), ihMSCs and Caco2 cells (Chapter 4) and hCSSCs (Chapter 5).
- To determine the effect of multiple thermal passages when cultured in 3D on the hCSSC cell phenotype and viability compared to 2D TCPS culture using enzymatic passage (Chapter 5).

# Chapter 2. Electrospinning and creation of thermo-responsive fibrous scaffolds

## 2.1 Introduction

Polymer surface engineering and smart biomaterials, in which the bio-adhesive properties of the surface can be altered by environmental factors or external controls, are important in the development of tuneable artificial substrates for cell growth [246]. Thermo-responsive substrates, which enable the culturing of cells and subsequent recovery of cell sheets using a small drop in the culture temperature, have been used over the past three decades for the *in vitro* culture of different cell lines in tissue engineering and regenerative medicine [206, 213-216]. To date, many cell types have been cultured on thermo-responsive PNIPAAm-coated surfaces, in which the polymer chains exhibit a lower critical solution temperature (LCST) of approximately 32°C [207, 209, 212, 217]. Despite extensive research into PNIPAAm thermo-responsive surfaces for cell culture, there remain some concerns that this polymer can damage cells when it transforms from its hydrophilic structure into its hydrophobic conformation. This is due to the presence of multiple secondary amide functional groups in the molecular structure of PNIPAAm, which may form hydrogen-bond interactions with proteins on the cell membrane [247]. Additionally, PNIPAAm can undergo irreversible phase transitions, primarily due to inter chain entanglement via the amide groups of PNIPAAm and intermolecular NH$^{\cdots}$O=C hydrogen bonding interactions above the polymer phase transition temperatures. Hence, during the cooling process, the rehydration of PNIPAAm is hindered by these additional interactions, leading to a marked hysteresis in transition temperatures [248].

Poly ethylene glycol (PEG) based polymers have recently been investigated for their use in biomedical applications, such as copolymers of 2-(2-methoxyethoxy) ethyl methacrylate ($MEO_2MA$) and oligo (ethylene glycol) methacrylate (OEGMA). These co-polymers have been used to produce a thermo-responsive 2D surface to support mESC adhesion, proliferation and detachment [226, 249]. They are related to FDA-approved oligo (ethylene glycol), but also exhibit LCST behaviour. The LCST of these polymers can be adjusted by altering the co-monomer compositions in order to obtain chain conformation changes at temperatures close to those of normal biological systems [226, 250, 251]. For example, cloud points of either 32°C, 37°C or 39°C were observed in pure water for copolymers having on average 5, 8 or 10% of OEGMA units per chain, respectively [226]. In contrast to PNIPAAm, poly (oligo ethylene glycol) methyl ether methacrylates exhibit a reversible dehydration due to the absence of a strong H-bond donor in the molecular structure of these polymers; therefore, there is no possibility of forming stabilizing H-bonds in the collapsed state. This makes switchable PEG-based substrates intended for cell culture applications more advantageous. This is particularly the case where the process of cell attachment on the hydrophobic surface (above the LCST) and subsequent detachment of cells from the hydrophilic surface (below the LCST) is continuous and unhindered by irreversible hydration [248].

Electrospinning is an efficient fabrication method used to produce 3D nano or micro fibrous scaffolds with controlled morphology, porosity and composition. The equipment required to successfully electrospin a variety of natural and synthetic polymers is relatively simple and was reviewed by Huang *et al.* [164], Teo *et al.* and Ramakrishnaet *et al.* [245]. A comprehensive summary of the various studies on

electrospinning, its nano-fibres and their references can be found in the book by Ramakrishna *et al.* [252]. While there is now an extensive literature on the use of thermo-responsive polymer surfaces for cell culture, very few studies have been conducted on the creation of thermo-responsive electrospun fibre based-scaffolds [253-258]. Different methods have been investigated for the incorporation of a thermo-responsive polymer in an electrospun matrix. Post-electrospinning modification is one of these methods [200, 259, 260]. Its principal benefit is that the polymer is not exposed to the spinning process, which can result in its deactivation due to prolonged exposure to high voltages and harsh organic solvents such as trifluoroacetic acid (TFA). Moreover, post surface modification is a method that enables the thermo-responsive polymer or any added agents to be chemically bound to or physically entrapped within the fibre via adding or exposing specific functional groups on the fibre surface, while the chemical bulk properties of the electrospun matrix remain unchanged [261]. However, for electrospinning to be a viable manufacturing process, time and costs need to be kept low. Therefore, the higher the number of steps required to functionalise the fibres, the less viable the process becomes for scale-up [200].

One of the simplest ways to modify electrospun fibres after electrospinning is via the physical adsorption of molecules of interest onto the surface of the electrospun fibres. This is a two-step method; firstly the fibres are electrospun, then then they exposed to an aqueous solution containing the desired grafting material, which binds to the fibre surface by electrostatic interaction, hydrogen bonding, hydrophobic interaction and van der Waals interactions. This method has been successfully used to adsorb different drugs, growth factors, nucleic acids and cytokines onto electrospun scaffolds

[200]. However, non-specific binding, uncontrolled release profiles and washing off of the adsorbed agents from the electrospun surfaces are the main disadvantages of this approach [200]. For example, 75% of bone morphogenetic protein-2 (BMP2) adsorbed onto poly (lactic-co-glycolic acid) (PLGA) scaffolds was released within 5 days, with a nearly complete release within just 20 days. This release rate was much faster than that of the same amount of protein loaded in PLGA scaffolds prepared using blend-electrospinning [262]. A similar trend was observed for gene delivery using electrospun PLGA/hydroxylapatite (HAp) nanoparticles scaffolds loaded with naked DNA and DNA/chitosan nanoparticles. A burst release (80–85%) of adsorbed naked and encapsulated DNA occurred, and over 95% of the incorporated DNA was released within 10 days [263]. In contrast, no burst release occurred (< 80%) of DNA/chitosan nanoparticles when blended with PLGA/HAp before electrospinning. Furthermore, the sustained release was better than that of scaffolds prepared using the surface adsorption method. This is due to the presence of the fibre matrix, which forms a dominant barrier and increases the diffusion resistance of DNA/chitosan nanoparticles until a significant proportion of the PLGA polymer has degraded [263].

A more challenging route is the chemical immobilization of modification agents on the surface of electrospun fibres. This is often a multistep, time-consuming process and may require surface chemistry modifications before the desired molecules can attach. However, this approach is favoured over physical adsorption due to the covalent bond formed between the surface-modification agent and the scaffolds, which prevents the leaching of the surface-modification agent from the fibres during use. Additionally, a variety of active molecules can be attached using this method, thereby, offering high surface-modification specificity and control [200, 264, 265]. For example, the

surfaces of electrospun poly (glycolic acid) (PGA), poly (L-lactic acid) (PLLA) and PLGA nano-fibres were chemically modified using oxygen plasma treatment and *in situ* grafting of hydrophilic acrylic acid (AA). This modification resulted in the spreading of fibroblast cells over a larger surface area after seeding on the AA-grafted surface when compared with the unmodified scaffolds [266]. Primary amine and carboxylate groups have been most extensively employed to immobilize bioactive molecules on the surface of nano-fibres. Carboxylic groups on the surface of polymeric nano-fibres containing different amounts of polyacrylic acid were employed for conjugation with collagen [267]. In other studies, acrylic acid-immobilized nano-fibres were conjugated to amine groups to prepare aminated nano-fibres [268]. However, it should be noted that partial inactivation of the immobilized molecules can occur upon covalent modification when active sites are chemically modified [200].

Partial surface hydrolysis of biodegradable aliphatic polyester scaffolds under acidic or basic conditions has been widely used to modify the surface wettability or to create new functionalities post-electrospinning [269, 270]. This is based on the random chemical scission of ester linkages on the polymer backbones located on the surface, resulting in the surface generation of carboxylic and hydroxyl groups from degraded, yet water-insoluble, polymer fragments. The duration of hydrolysis and the concentration of hydrolysing agents are important in order to produce surface functional groups with minimal changes to the bulk properties [271]. Polycaprolactone (PCL) membranes have been coated with PCL electrospun nano-fibres in order to mimic the architecture of the natural ECM and create nano-topography for enhanced cellular attachment. When these modified membranes were treated with 5 M NaOH, the surface wettability was dramatically enhanced, with a

water contact angle of almost zero due to the capillary action on the highly rough surface. When NIH 3T3 cells were cultured on the surface of the modified nano-topographical membrane, a favourable spindle-shaped morphology was evident, while they remained in isolated spherical shaped entities on the non-treated fibrous surfaces [272].

The properties of the resultant electrospun fibres can be modified before the electrospinning process. Pre-electrospinning modification is desirable mainly due to the fewer number of steps required in the process, which is beneficial for cost, time and scale-up processes. In addition, the fewer modifications the scaffold undertakes, the greater the retention of its integrity in terms of structure, morphology and function, which improves the potential of the technique [261]. Additionally, less chemicals are required for making the functional fibres as compared with post-electrospinning modification [273]. A way to do this is to functionalise the polymer solution before it is electrospun through pre-modification techniques such as (i) the addition of drugs or portions to the polymer solution [274], (ii) atmospheric plasma treatment of pre-electrospinning solutions [275] and (iii) blending different polymers or co-polymers before electrospinning [275, 276]. However, the main concern is that this pre-modification could influence the properties of the polymer solution, such as its viscosity, conductivity and surface tension, which may affect the electrospinning parameters, such as voltage, spinning distance and flow rate, that are required to achieve the desired fibre morphologies [261].

Blend electrospinning is a method that has been investigated for the incorporation of different polymers with different chemical properties into one solution for electrospinning. Therefore, this is a one-step method with the ability to incorporate

the desired components into the fibres. Many polymer mixtures have been successfully co-electrospun using this method. Examples include PNIPAAm with polyethylene oxide (PEO), which was used as a thermo-responsive drug carrier system for VB12 [277]; PLGA blended with PLGA-b-PEG-$NH_2$ di-block copolymer, used as a cell culture template [278] and PLA with poly (ethylene-co-vinyl acetate) (PEVA) electrospun fibres, used for the controlled release of tetracycline hydrochloride, which resulted in a steady drug release over approximately 5 days [279].

Emulsion spinning is where a mix of two different solutions are used; a polymer solution in an organic solvent, and the active molecule or a polymer in an aqueous solution. The two immiscible solutions are electrospun, resulting in a core sheath structure, with the aqueous solution encapsulated inside the organic solution. The solvent in the organic solution evaporates quickly, leading to an increased viscosity that forces the aqueous solution to become encapsulated [200]. For example, core sheath fibres prepared via emulsion electrospinning were generated, where the aqueous phase consisted of a PEO solution in water, and the oil phase was a chloroform solution of an amphiphilic PEG-PLLA diblock copolymer. The obtained fibres were composed of a PEO core and a PEG-PLLA sheath, with a sharp boundary in between. This process, therefore, is suitable for fabricating composite fibres that contain water-soluble drugs, which are difficult to electrospin alone [280].

Co-axial electrospinning is also a one-step process that was first employed by Sung et al. in 2003 [281]. This method allows two separate mixtures to be electrospun in one process. The solutions are kept in separate reservoirs until their release through the same needle. Similarly to the emulsion spinning technique, it results in a core/sheath

fibre. The potential benefits of such methods include protecting an unstable biological agent from an aggressive environment, preventing the decomposition of a labile compound under a certain condition, delivering a bio-molecular drug in a sustained way and functionalizing the surface of nanostructures without affecting the core material [282]. A wide variety of polymers and polymer blends can be electrospun using this technique.

PCL has predominantly been used in coaxial studies principally due to its history within the field of being able to be spun into robust, porous non-woven mats, which could be useful for biomedical applications [283-285]. PCL-gelatin type A was successfully electrospun to form a core-shell nano-fibre mat, suggested to be useful for application in controlled drug release, bioactive tissue scaffolds and highly sensitive biochemical sensors [282]. PCL-collagen, in the form of core-shell nano-fibres, has also been produced by co-axial electrospinning, and is used as a substrate for human dermal fibroblasts (HDF). These coated fibres enhanced cell proliferation and migration compared to PCL scaffolds alone. Moreover, the cell density increased on these core-sheath fibres by 19.5% (2 days), 22.9% (4 days) and 31.8% (6 days) compared to physically coating collagen on PCL fibres, whereby the cell density increased by only 5.5% (2 days), 11.0% (4 days) and 21.0% (6 days) [286].

## 2.2 Aims and objectives

The main aim of this chapter was to create bead-less fibres of PLGA and PET polymers using electrospinning, and to assess different ways of incorporating a thermo-responsive polymer, poly ($PEGMA_{188}$) into the fibres. Incorporation of poly ($PEGMA_{188}$) into the electrospun fibres, either as part of the electrospinning process or as a post-electrospinning step, was explored in order to generate thermo-responsive fibres suitable for cell culture and thermo-responsive passage.

The aim of this chapter was achieved through the following objectives:

- To establish electrospinning parameters for PLGA and PET.
- To characterise the electrospun fibres in terms of their diameter, morphology and surface wettability.
- To synthesise, purify and characterise the thermo-responsive polymer, poly ($PEGMA_{188}$).
- To incorporate poly ($PEGMA_{188}$) into the electrospun fibre surface via surface adsorption, NaOH treatment, solvent swelling and co-electrospinning.
- To evaluate the change in the hydrophobicity and morphology of the fibres in the presence of the incorporated poly ($PEGMA_{188}$).

## 2.3 Materials and methods

### 2.3.1 Scaffold fabrication

#### 2.3.1.i Preparation of PLGA and PET polymer solutions

PLGA polymer, shown in Figure 2.1 A, (Sigma-Aldrich, lactide/glycolide ratio 75/25, $M_n$ [gel permeation chromatography, GPC] = 68 kDa, Đ = 1.7), was used in this study in different ratios to afford solutions of 17, 17.5, 18.5, 20 and 23% *(w/v)* of the polymer in 5 mL of dichloromethane (DCM). The solutions were stirred continuously at room temperature (RT) for 24 h to achieve full dissolution.

PET polymer, shown in Figure 2.1 B, in the form of pellets (Sigma, molecular weight of repeat unit: 192.2 g/mole) and recycled PET collected from drinks bottles were used in this study. Different concentrations of PET polymer solutions were prepared to make 5 mL of a 9, 10, 10.5, 11.5 and 30% *(w/v)* mixture of the polymer in DCM and trifluoroacetic acid (TFA; TFA 99%, DCM 99.99% Sigma). The mixtures were stirred continuously at RT for 24 h to achieve full dissolution.

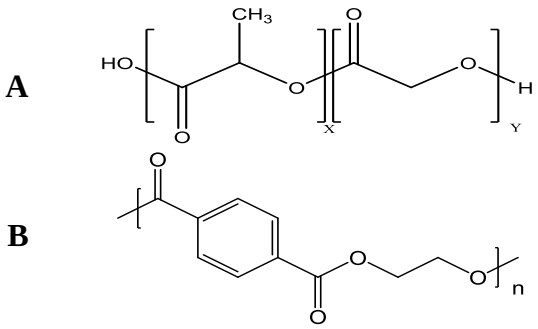



**Figure 2.1:** Molecular structure of A) poly (lactic-co-glycolic acid) (x is the number of lactic acid units and y is number of glycolic acid units) and B) poly (ethylene terephthalate) (PET), (n is the number of repeating units in the PET polymer)

### 2.3.1.ii Electrospinning process

For the electrospinning process shown in Figure 2.2, each 5 mL of the polymer solutions prepared in section 2.3.1.i were taken into a 10 mL plastic syringe fitted with an 18-gauge blunt needle. The loaded syringe was then mounted onto a syringe pump (Harvard) and the polymer solution was pumped through the needle at rates ranging between 0.5 and 4.0 mL/h until regular dripping occurred. A voltage of 14–19 kV was then applied to the needle tip (positive electrode) using a high-voltage unit (Glassman High Voltage Inc.). The solution was spun onto a rectangular stainless-steel collector plate, with an area of 6 $cm^2$, which was grounded via an earthed electrode. The working distance between the needle and the collector plate was set to approximately 15 cm. The entire 5 mL polymer solution was spun and the plate was rotated at 90° every 20 minutes at RT (25°C). The resultant non-woven mats were air-dried for 48 h at RT, and then peeled off the collector plate manually prior to storage at 25°C.

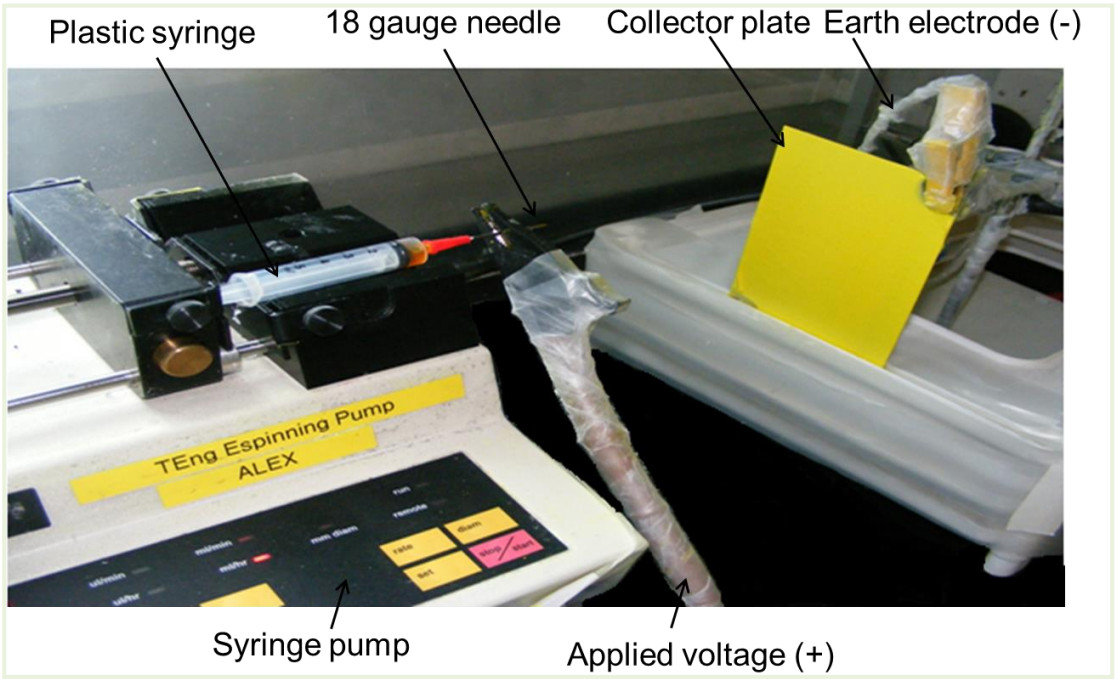



**Figure 2.2:** Schematic representing the setup of electrospinning process.

### 2.3.2 Synthesis of the thermo-responsive polymer poly (poly (ethylene glycol) methacrylate), poly ($PEGMA_{188}$), via the free radical polymerization technique

Poly ($PEGMA_{188}$) was prepared by free radical polymerization following a published method [251]. Di (ethylene glycol) methyl ether methacrylate (98%, Sigma, 188), (22 g, 0.12 moles) was weighed into a round-bottom flask, to which 1-dodecanethiol (chain transfer agent; 98%, Sigma; 0.225 g, 0.001 moles) and 15 mL of 2-butanone were added. Azobisisobutyronitrile (AIBN; 0.15 g, 0.001 moles) was added last and the mixture was degassed with nitrogen for 15 minutes. The flask was then placed on a hot plate (Stuart®) and the polymerization reaction was conducted at 70°C for 1 h. The prepared poly ($PEGMA_{188}$) was precipitated three times in 500 mL of hexane and re-dissolved in 50 mL of 2-butanone to remove any residual $PEGMA_{188}$ monomer. The precipitated poly ($PEGMA_{188}$) was placed in a desiccator for 48 h to remove any remaining solvent.

#### 2.3.2.i Gel Permeation Chromatography (GPC)

The number average molecular weight ($M_n$), weight average molecular weight ($M_w$) and polydispersity ($Đ = M_w/M_n$) of the synthesized poly ($PEGMA_{188}$) polymers were determined using a Polymer Labs GPC 50 Plus instrument with triple detection (differential refractive index, differential capillary viscometer and dual angle [15° and 90°] light scattering). Chromatograms were run at 35°C using chloroform as the eluent with a flow rate of 1 mL/minute and a sample concentration of 2–5 mg polymer/mL of chloroform. All samples were filtered using a syringe filter of 0.2 µm.

The columns (2) used were 30 cm PLgel Mixed-B. The machine was calibrated with linear polystyrene ($M_w$ = 162–371100 Da).

### 2.3.2.ii Proton and carbon nuclear magnetic resonance characterisation of poly ($PEGMA_{188}$) ($^1$H NMR, $^{13}$C NMR)

Poly ($PEGMA_{188}$) was characterised by proton ($^1$H NMR) and carbon ($^{13}$C NMR) NMR using a 400 Bruker MHz NMR spectrometer at 399.8 MHz (1H). All chemical shifts were reported in ppm relative to tetramethylsilane (TMS) and the MestReNova software was used to process the data. Samples were prepared by dissolving 10 mg and 40 mg of each sample in 600 µl of chloroform-d, for $^1$H NMR and $^{13}$C NMR, respectively. $^1$H NMR (400 MHz, $CDCl_3$): δ 0.9 (br s, 3H, $CH_{3\ backbone}$), 1.9 (br s, 2H, $CH_{2\ backbone}$), 3.4 (br s, 3H, $OCH_3$), 3.6 (br m, 6H, $OCH_2$) and 4.2 (br s, 2H, $COOCH_2$). $^{13}$C NMR (400 MHz, $CDCl_3$): δ 17 ($CH_{3\ backbone}$), 20 ($CH_{2\ backbone}$), 46 ($C_{\ backbone}$), 60 ($OCH_3$), 72 ($OCH_2$) and 178 (*CO*OCH2).

### 2.3.2.iii Determination of the cloud point (lower critical solution temperature [LCST]) of poly ($PEGMA_{188}$)

The cloud point temperatures of 1% (*w/v*) polymer solutions (poly ($PEGMA_{188}$) in distilled water) were initially estimated by heating the polymer to 37°C using a hot plate (Stuart®); they were then cooled to 15°C using ice. The cloud point temperature was defined as the temperature at which the first signs of turbidity occurred.

A more detailed cloud-point analysis was performed by measuring the absorbance of the polymer solutions at 550 nm as a function of temperature using a UV/VIS Spectrophotometer-Beckman, DU 800, coupled with a temperature controller. The

1% (*w/v*) polymer solution was prepared in 1 mL of distilled water. The heating rate was set at 1°C/minute, with a starting temperature of 15°C and an end temperature of 37°C. The LCST, approximated by the cloud point, was considered to be the temperature at which the first signs of turbidity occurred. Temperature-turbidity measurements were repeated three times for all individual batches (5 batches) of poly ($PEGMA_{188}$).

### 2.3.3 Scaffold surface modification

#### 2.3.3.i Surface adsorption of poly ($PEGMA_{188}$) onto the PLGA and PET fibre surfaces

PET and PLGA electrospun fibres were cut into discs with areas of 1 $cm^2$ using a trephine (stainless-steel cylinders with a diameter of 1 cm) and placed into 24 non-tissue-culture well plates. Then, 1 mL of the 3, 5 and 7% [*w/v*] solutions of poly ($PEGMA_{188}$) was added onto the scaffolds for different time periods (1, 5, 12 and 24 h) at RT (25°C). Controls included scaffolds incubated in 1 mL of distilled water for the same time periods. (n = 9 total, three scaffolds of each polymer were used per treatment and the experiment was repeated three times).

#### 2.3.3.ii NaOH Hydrolysis modification of the PLGA and PET fibres

PET and PLGA electrospun fibres were cut into discs with areas of 1 $cm^2$ using a trephine (stainless steel cylinders with 1 cm diameter) and placed into 24 non-tissue-culture well plates. Different concentrations of 1 N NaOH (97%, Sigma; 0.5, 1, 2, 3, 4, 5, 6, 7, 8, 9 and 10% [*w/v*]) were prepared in distilled water to make 4 mL of solution for each concentration. One millilitre of each solution was added into the

scaffold wells for different time periods (1, 5, 12 and 24 h) at RT (25°C); another set of scaffolds were incubated in 1 mL of distilled water as a control for the same time periods. (n = 9 total, three scaffolds of each polymer were used per treatment and the experiment was repeated three times).

### 2.3.3.iii Surface entrapment of poly ($PEGMA_{188}$) into PLGA and PET scaffolds via solvent swelling

PET and PLGA electrospun fibres were cut into discs with areas of 1 $cm^2$ using a trephine (stainless steel cylinders with a diameter of 1 cm) and placed into 24 non-tissue-culture well plates. Different concentrations of acetone (99%, Sigma) as a solvent for PET and 2,2,2-trifluoroethanol (TFE, 99.8%, Sigma) as a solvent for PLGA (0.5, 1, 2 and 5% [*w/v*]) were prepared in distilled water to make 6 mL of solution for each concentration. Then, 1 mL of each solution was added into the scaffold wells for different time periods (10 min, 20 min, 30 min, 1 h, 2 h and 3 h) at RT (25°C); another set of scaffolds were incubated in 1 mL of distilled water as a control for the same time periods. (n = 9 total, three scaffolds of each polymer were used per treatment and the experiment was repeated three times).

After determining the concentration and time period at which the fibres swelled and did not dissolve or break, the surface-modifying solution was prepared by first dissolving poly ($PEGMA_{188}$) in distilled water, resulting in a final concentration of 5% (*w/v*), and then adding the solvent (acetone and TFE 2% [*w/v*] for PET and PLGA, respectively) to the solution. Then, 1 mL of the prepared solvent/non-solvent system was transferred to the scaffolds and incubated with agitation for 1 h before adding a large excess of the non-solvent (4 mL of distilled water). When excess water was

flushed through the scaffolds to substitute the solvent-water mixture, the swollen PLGA or PET surface collapsed. This collapse entrapped the poly ($PEGMA_{188}$) polymer on the scaffold surface in a manner analogous to a previously reported protocol [287, 288].

### 2.3.3.iv Co-electrospinning of poly ($PEGMA_{188}$) and PLGA or PET polymers

#### 2.3.3.iv.a Preparation of the co-polymer solutions

Different polymer solution concentrations were prepared consisting of poly ($PEGMA_{188}$) with recycled PET polymer (1% poly ($PEGMA_{188}$): 10% PET and 2% poly ($PEGMA_{188}$): 30% PET [*w/v*]) in a mixture of 3 mL of TFA/3 mL of DCM. PLGA was also dissolved in 6 mL of DCM, then poly ($PEGMA_{188}$) was added to the mixture, resulting in solutions of different polymer ratios (18.5% PLGA: 5% poly ($PEGMA_{188}$), 18.5% PLGA: 1.2% poly ($PEGMA_{188}$), 18.5% PLGA: 1% poly ($PEGMA_{188}$) and 20% PLGA: 1% poly ($PEGMA_{188}$) [*w/v*]). The mixtures were stirred at RT for different lengths of time (10 min, 4 h and 24 h) until a clear solution was achieved.

#### 2.3.3.iv.b Co-electrospinning of co-polymer solutions

The co-electrospinning process had the same experimental setup as described in section 2.3.1.ii; however, detailed co-electrospinning parameters for each co-polymer solution are presented in Figure 2.16 and Figure 2.17.

### 2.3.4 Scaffold characterisation

#### 2.3.4.i Scanning electron microscopy (SEM)

For SEM analysis, segments of the scaffolds were mounted on aluminium SEM stubs via a carbon self-adhesive disc (Agar Scientific). Samples were gold sputter coated for 4 minutes and analysed on a JEOL SM 1100 SEM. The accelerating voltages used were in the range of 10–30 kV, and the working distances ranged from approximately 15 to 35 cm. The fibre diameters were measured by taking perpendicular measurements of the fibres on the SEM images. Fibre diameters were measured from the images taken from 5 fields of view of each scaffold; a total of 20 measurements from each SEM image were recorded (100 in total for each scaffold analysed) using the SEM-associated SMiles Image processing software.

#### 2.3.4.ii Water contact angle measurements (WCA)

WCA analysis was used to measure the wettability of the poly ($PEGMA_{188}$)-modified scaffolds and PLGA or PET controls. The static WCAs of the scaffolds were determined from sessile WCA measurements taken using distilled water and a CAM 200 sessile drop video capture apparatus. The water drop was gently placed onto the sample surface using a syringe and 10 images were taken at 1 second intervals. Three scaffolds of each scaffold batch and polymer composition were used per treatment; the experiment was repeated three times at 22°C. Readings were taken at five different 1 $cm^2$ areas on the electrospun scaffolds (total scaffold area = 6 $cm^2$), as shown in Figure 2.3, and then the average and standard deviation were calculated.

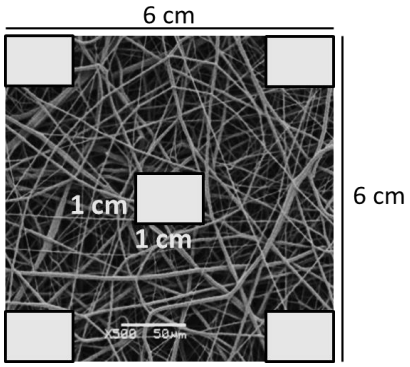



**Figure 2.3:** Schematic representing the five different areas of the same electrospun scaffolds used for WCA measurements.

### 2.3.4.iii Proton nuclear magnetic resonance ($^1$H NMR)

PET, PET-poly ($PEGMA_{188}$), PLGA and PLGA-poly ($PEGMA_{188}$) scaffolds were all prepared for $^1$H NMR by dissolving 10 mg of the scaffolds in 600 µL of chloroform-d. Samples containing PET were dissolved in a mixture of 300 µL of TFA/300 µL of chloroform-d; then samples were analysed using a 400 Bruker MHz NMR spectrometer at 399.8 MHz (1H). $^1$H NMR for PLGA (400 MHz, $CDCl_3$): δ 1.6 (br s, 3H, $CH\mathit{CH_3}$), 4.8 (br m, 2H, $CH_2O$) and 5.2 (br m, 1H, $C\mathit{H}CH_3$). $^1$H NMR for PET (400 MHz, $CDCl_3$): δ 4.8 (br s, 4H, 2 $CH_2$) and 8.1 (br s, 4H, $CH_{aromatic}$).

### 2.3.5 Statistical analysis

Data were expressed as the mean ± standard deviation (SD) or mean ± standard error of the mean (SEM); n refers to the number of experiments. The statistical analysis was carried out in triplicate for a minimum of n = 3 experiments. To analyse significant differences between different treatment groups, one-way ANOVA multiple comparison tests were performed using the Prism 6 software (GraphPad, San Diego CA). Significant differences were determined at $p \leq 0.05$. Statistical significance was set at non-significant (ns) for $p > 0.05$, significant (*) for $p \leq 0.05$, very significant (**) for $p \leq 0.01$, highly significant (***) for $p \leq 0.001$ and very highly significant (****) for $p \leq 0.0001$.

## 2.4 Results and discussion

### 2.4.1 Electrospun scaffold characterization

#### 2.4.1.i Fibre diameter and beads in the electrospun scaffolds

In this study, PLGA (PLA 75: PGA 25; biodegradable) and PET (recycled; non-biodegradable) polyesters were chosen as the main components of the electrospun scaffolds due to their widespread use in such scaffolds in tissue engineering and biomedical applications [103]. In order to obtain bead-free electrospun fibres, different concentrations of PLGA and PET polymer solutions were prepared. From the SEM analysis in Figure 2.4, round and large beads were observed in the PLGA electrospun fibres prepared with 17% (*w/v*) PLGA polymer solution. Furthermore, a non-uniform fibre distribution was observed with an average fibre diameter of 2.2 ± 1.1 µm. When the PLGA polymer solution concentration increased to 17.5% (*w/v*), the morphology of the beads started to change from round to spindle-like shapes, and the fibres present had an average fibre diameter of 2.8 ± 1.1 µm. A polymer solution concentration of 18.5% (*w/v*) resulted in bead-less and uniform fibres, with an average diameter of 3 ± 0.8 µm. However, with further increases in the polymer solution concentrations to 20% and 23% (*w/v*), beads with a spindle-like shape appeared in the scaffolds, but were fewer in number compared with those prepared with lower polymer solution concentrations. The average fibre diameters observed for the 20% and 23% (*w/v*) PLGA scaffolds were 4.0 ± 1.2 µm and 4.6 ± 0.9 µm, respectively. As a result, the 18.5% *(w/v)* PLGA polymer solution was chosen for further studies, because it resulted in PLGA scaffolds with uniform fibres (indicated by the low SD) and no beading.

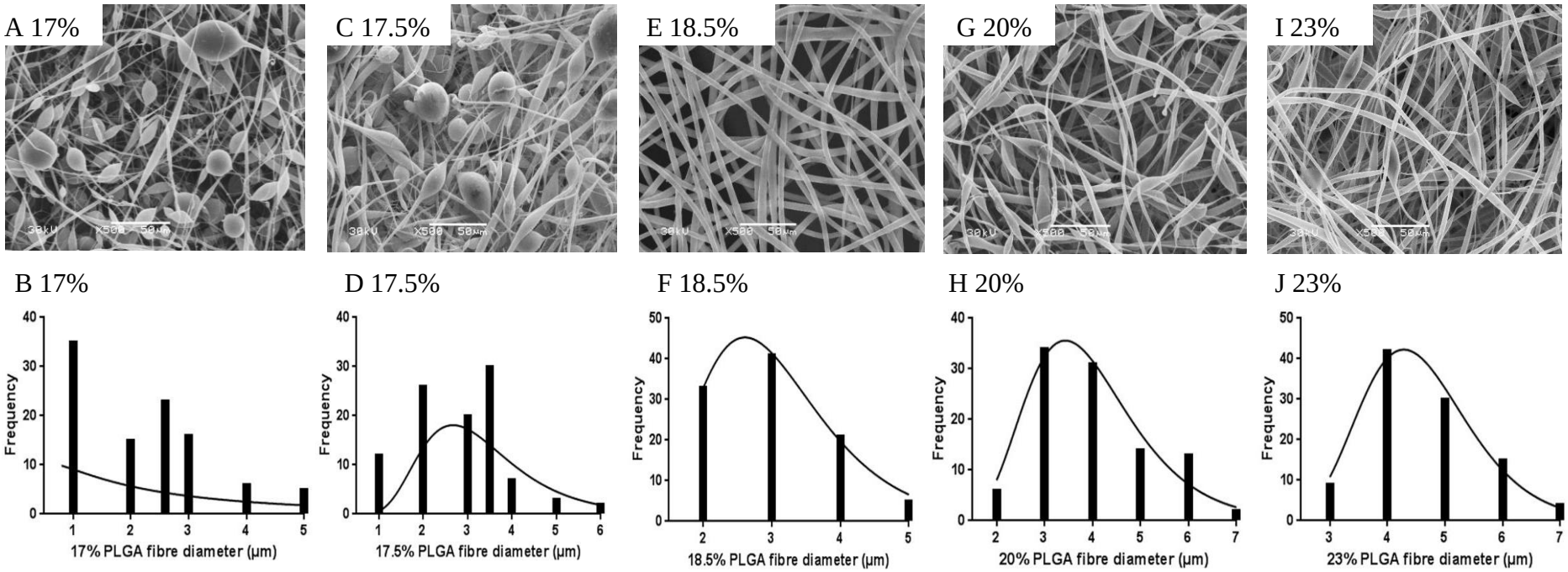



**Figure 2.4:** Representative SEM images and histogram charts of PLGA fibres showing the surface morphology at magnification powers of x500, and frequency of fibre diameter (µm), of five different polymer solution concentrations A-B) 17%, C-D) 17.5%, E-F) 18.5%, G-H) 20% and I-J) 23% (*w/v*). For histogram charts 20 measurements from each SEM image were recorded (100 in total), n = 5, n represent the number of replicates were taken from one batch of each scaffolds.

The SEM analysis of the fibre scaffolds fabricated from recycled PET (sourced from drinks bottles; Figure 2.5) at a concentration of 10% *(w/v)* demonstrated the presence of one or two beads in the scaffolds, but with uniform fibre distributions and an average fibre diameter of 294.6 ± 86.8 nm. By increasing the polymer solution concentration to 30% *(w/v)*, the resultant scaffolds were uniform and bead-free, with an average fibre diameter of 836.2 ± 172.7 nm. As a result, 30% *(w/v)* of recycled PET polymer solution was chosen for further studies, because it resulted in bead-less PET scaffolds with higher nano-range fibre diameters, which are more favourable for cell culture studies. Many cell culture studies have been conducted using higher nano-range (> 300 nm) electrospun fibres, which supported cell attachment, proliferation, differentiation and spread [186, 289, 290].

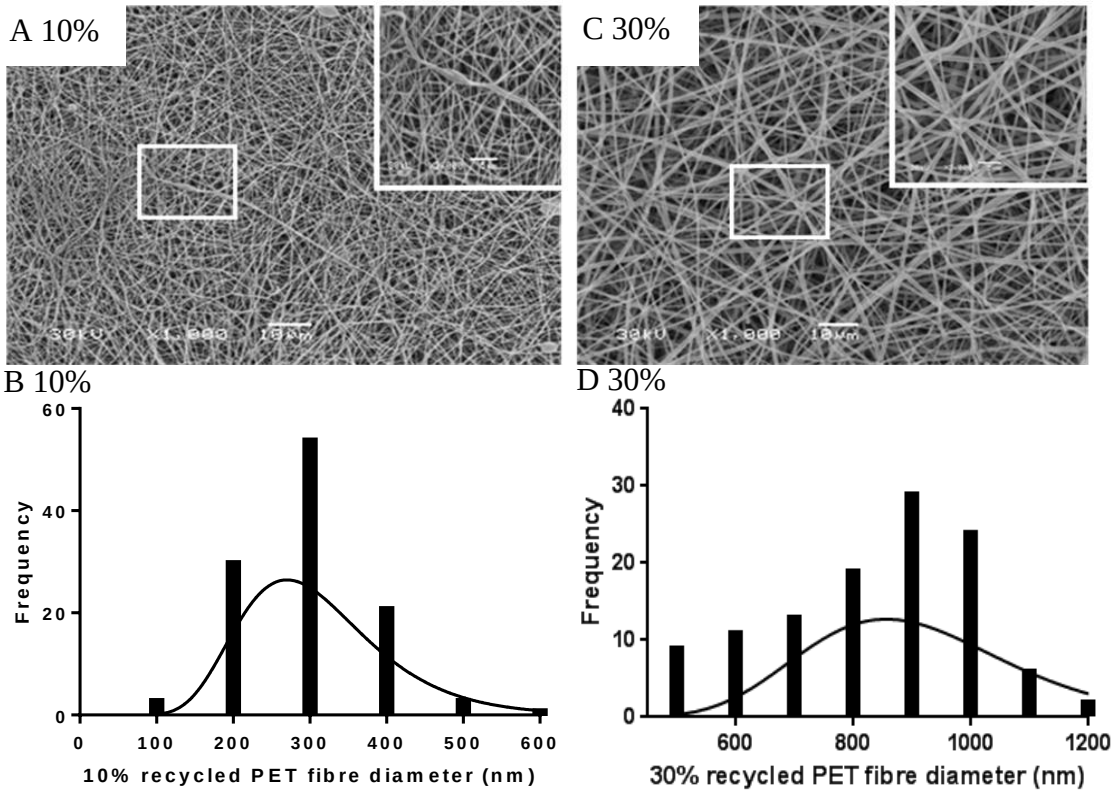



**Figure 2.5:** Representative SEM images and histogram charts of recycled PET fibres showing the surface morphology at two magnification powers of x1000 and x3000, and frequency of fibre diameter (nm), of two different polymer solution concentrations A-B) 10%, C-D) 30% (*w/v*). For histogram charts 20 measurements from each SEM image were recorded (100 in total), n = 5, n represents the number of replicates were taken from one batch of each scaffolds.

To conclude from the SEM images, higher polymer solution concentrations resulted in scaffolds with higher fibre diameters, more uniform fibres and with fewer beads. Therefore, polymer solutions of 18.5% (*w/v*) and 30% (*w/v*) were chosen for PLGA and PET, respectively.

Bead formation within electrospun fibres has frequently been observed [291, 292], and adversely affect the reproducibility of the electrospinning system and the evenness of the resultant fibres. The existence of beads in fibres also may render their utilization for cell culture [293]. The beads appear as irregular round or spindle shapes in the

electrospun fibrous mat [294, 295]. There are a number of factors affecting the presence of the beads such as the choice of solvent, polymer solution viscosity, concentration, surface tension and charge density [296]. The choice of the solvent used for electrospinning can contribute to the reduction in the size and numbers of the beads. The solvent should not be too volatile such that it evaporates quickly and solidifies the Taylor cone, nor should it be non-volatile, which would lead to the production of wet beaded fibres [158].

Bead formation is also attributed to an insufficient stretch of the filaments during the whipping of the polymer jet, due to a low charge density. Therefore, increasing the polymer solution conductivity can reduce bead formation. For example, the addition of a small amount of a cationic surfactant such as dodecyltrimethylammonium bromide (DTAB) in a polystyrene polymer solution improves the net charge density and enhances the whipping instability. The jet stretches under stronger charge repulsion at a higher speed, resulting in exhaustion of the bead structure [297].

Following the recommendations of previous studies, TFA and DCM were chosen as solvents for PET, and DCM as the solvent for PLGA [149, 252, 263, 298]. Additionally, fewer beads were obtained via the use of solutions with higher concentrations of PET and PLGA as, it has been reported that higher polymer solution concentrations resulted in the formation of uniform fibres without beads [298]. That could be explained by relating to solution viscosity; when the polymer concentration is low, then the viscosity of the solution is also low, therefore the process changes to electrospraying the polymer solution instead of electrospinning and resulted with beads in the electrospinning mat [173, 175]. Furthermore, the jet from low viscosity

solutions breaks up into droplets due to the lower amount of polymer and, hence, this results in a lower molecular entanglement density than that which is needed to form a stable jet [298].

Veleirinho *et al.* showed that the spinnable concentration of PET solution in TFA/DCM solvents is 10% (*w/v*) and above, as PET concentrations of less than 10% (*w/v*) resulted in droplet formation and electrospraying, while at higher concentrations of 30% (*w/v*) uniform and bead-less fibres were formed [298]. Therefore, in this study a 10% (*w/v*) PET polymer solution concentration was chosen as a starting point for PET electrospinning, which was subsequently increased to 30% (*w/v*) to obtain bead-less uniform fibres. Zhao *et al.* demonstrated a similar concept of polymer solution concentration effect on bead formation, as when lower concentrations of PLGA polymer solution were prepared, higher numbers of beads were observed in the scaffolds [299]. Another polymer solution parameter that could also contribute to bead formation in the scaffolds and is related to polymer solution concentration is the surface tension of the polymer solution. Low polymer solution concentrations lead to a low surface tension and surface area, resulting in the breakdown of the polymer jet to form droplets and beads in the fibres [175, 300].

Moreover, the working distance between the syringe and the collecting surface also has effects on bead formation, as it needs to be large enough to avoid the creation of sparks between the electrodes, and for the solvent to evaporate in time for the fibres to form [252]. Therefore, a distance of 15 cm was used in this study, which was sufficient for PLGA and PET fibre formation. Different values of working distances between the spinneret and collecting plate to obtain fibre-based scaffolds of PLGA and

PET have been reported in the literature, and ranged between 10 to 20 cm [130, 298, 299, 301]. A study showed that reducing the 35 cm gap between the highly charged needle and the grounded target by only 5 cm resulted in bead formation in the polystyrene electrospun mat [302].

The electrospun fibre diameter is considered as an important factor in tissue engineering applications as it can influence cell proliferation, differentiation and migration [114]. Furthermore, it affects the porosity and biocompatibility of the scaffolds [169]. Therefore, electrospun PLGA and PET fibre diameters were analysed as shown in Figure 2.4 and Figure 2.5. The polymer solution concentration [303], viscosity [42], working distance [158], applied voltage [176], conductivity and flow rate [304] can all influence the size of electrospun fibre diameter. As a general observation, electrospun PET scaffolds possessed fibre diameters in the nano-range (294.6 ± 86.8 nm) when a 10% (*w/v*) polymer solution concentration was used. However, by increasing the polymer concentration to 30% (*w/v*), the average fibre diameter increased to 836.2 ± 172.7 nm, with the appearance of fibres in the micron range (1 µm - 1.2 µm). Veleirinho *et al*. demonstrated a similar trend of increasing PET electrospun fibre diameter with increasing polymer solution concentration, whereby increases in average PET fibre diameters of 209 nm, 374 nm and 625 nm were obtained when higher polymer solution concentrations of 10%, 20% and 30% (*w/v*) were used, respectively [298]. Electrospun PLGA scaffolds consisted of fibres with diameters in the micro-metre range (2.2 ± 1.1 µm, 2.8 ± 1.1 µm, 3 ± 0.8 µm, 4.0 ± 1.2 µm and 4.6 ± 0.9 µm) as higher polymer solution concentrations were used (17, 17.5, 18.5, 20 and 23% [*w/v*], respectively). Zhao *et al*. showed that lower PLGA polymer concentrations of 0.15 g/mL resulted in scaffolds with fibre diameters

between 100 nm and 200 nm. While, increasing the PLGA solution concentration to 0.3 g/mL resulted in the distribution of fibre diameters in the range of 400 to 1000 nm [299]. This phenomenon can be attributed to the higher polymer solution concentration, which leads to an increase in the viscosity and elasticity of the solution. Therefore, during electrospinning, the polymer is less stretched, which results in larger fibres [168].

The difference between PLGA and PET fibre diameters was also likely to have been the result of differences in polymer solution viscosities and the molecular weights of the polymers, which necessitated the use of different flow rates for the PLGA and PET solutions. The prepared PLGA polymer solution was highly viscous and needed a higher flow rate of 4 mL/h to eject the polymer solution from the needle, in combination with a higher voltage of 19 kV. In contrast, the PET polymer solution was spinnable at a lower flow rate of 0.5 mL/h, with a lower voltage of 14 kV. Some studies have reported that an increased flow rate led to an increase in the fibre diameter due to the inability of the fibres to dry completely before reaching the collector plate [195]. Moreover, Zong *et al*. demonstrated that high flow rates increase the polymer solution available for electrospinning, resulting in increased fibre diameters [168, 169]. On the other hand, it has been reported that the applied voltage effect is limited to polymer jet initiation and elongation, and not on fibre diameter [159].

#### 2.4.1.ii Surface wettability of the scaffolds

WCA measurements were conducted to analyse the surface wettability of the electrospun fibrous scaffolds [305]. Scaffolds were hydrophobic, with average

measurements of 134 ± 0.74° for the PLGA scaffolds and 111 ± 6.9° for PET scaffolds, as shown in Figure 2.6. These values are in agreement with the literature, as hydrophobicity was determined by WCA measurement for PLGA electrospun scaffolds with a mean of 111.97 ± 2.59° [306] and in another study with a mean of 105.5 ± 5.2° [307]. WCA measurements were also conducted for PET electrospun fibres with a mean value of 95°, which indicates the hydrophobicity of the surface [308]

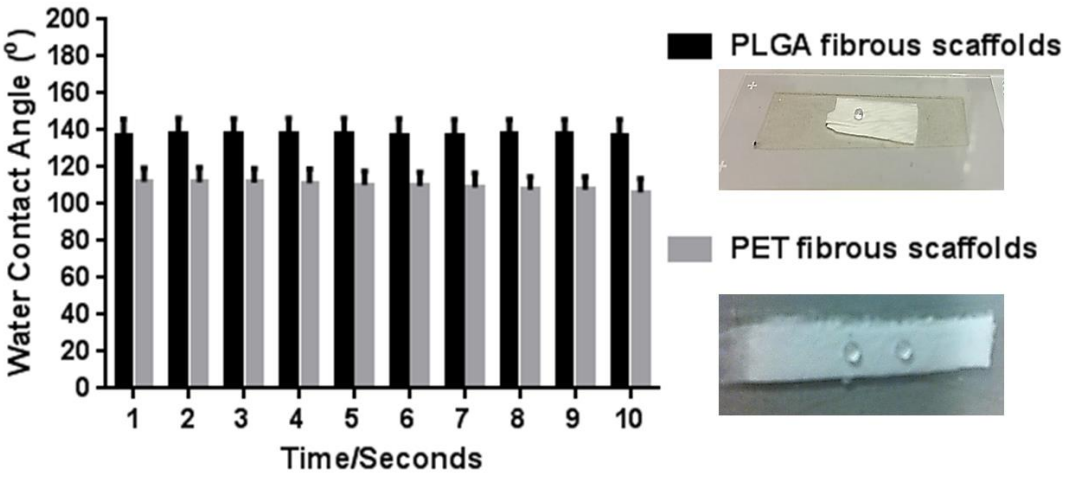



**Figure 2.6:** WCA measurements for PLGA and PET scaffolds. The error bars represent the mean with standard deviation (SD), n = 3, n represents the number of replicates that were taken from one batch of each scaffold type.

**Table 2-1:** A summary table of electrospinning parameters for PLGA and PET polymers and fibre characterizations

| PLGA concentration (*w/v* %) | Solvent (mL) | Collector distance (cm) | Voltage (kV) | Flow rate (mL/h) | Needle gauge | Fibre morphology | Diameter (mean ±SD) µm | WCA (mean ±SD) (°) |
|---|---|---|---|---|---|---|---|---|
| 17 | DCM | 15 | 19 | 4 | 18 | Round, large beads | 2.2 ± 1.1 | 134 ± 0.74 Hydrophobic surface |
| 17.5 | DCM | 15 | 19 | 4 | 18 | Spindle-like beads | 2.8 ± 1.1 | |
| 18.5 | DCM | 15 | 19 | 4 | 18 | Bead-less | 3.0 ± 0.8 | |
| 20 | DCM | 15 | 19 | 4 | 18 | Few beads | 4.0 ± 1.2 | |
| 23 | DCM | 15 | 19 | 4 | 18 | Few beads | 4.6 ± 0.9 | |
| PET concentration (*w/v* %) | Solvent (1:1) (mL) | Collector distance (cm) | Voltage (kV) | Flow rate (mL/h) | Needle gauge | Fibre morphology | Diameter (mean ±SD) nm | WCA (mean ±SD) (°) |
| 10 | DCM/TFA | 15 | 14 | 0.5 | 18 | Few beads | 294.6 ± 86.8 | 111 ± 6.9 Hydrophobic surface |
| 30 | DCM/TFA | 15 | 15 | 0.5 | 18 | Bead-less | 836.2 ± 172.7 | |

### 2.4.2 Scaffold surface modification by poly ($PEGMA_{188}$)

To create a thermo-responsive fibre based scaffold, surface modification by poly ($PEGMA_{188}$) was explored. Poly ($PEGMA_{188}$) (shown in Figure 2.7 A) was synthesized in-house and characterized by gel permeation chromatography (Figure 2.7 C), which indicated a molar mass of 50.8 kDa ($M_w$ (GPC) = 50.8 kDa, Đ = 1.8). Analysis of the $^{1}H$ NMR and $^{13}C$ NMR spectra in Figure 2.8 A and B, showed that poly ($PEGMA_{188}$) was successfully prepared, with no peaks between (5.8 ppm and 6.1 ppm) in $^{1}H$ NMR spectra or (100 ppm and 150 ppm) in $^{13}C$ NMR spectra of the monomer vinyl group (-CH=$CH_2$) observed (Figure 2.7 B). This indicated the complete removal of the unreacted monomer by the 2-butanone /hexane precipitation method.

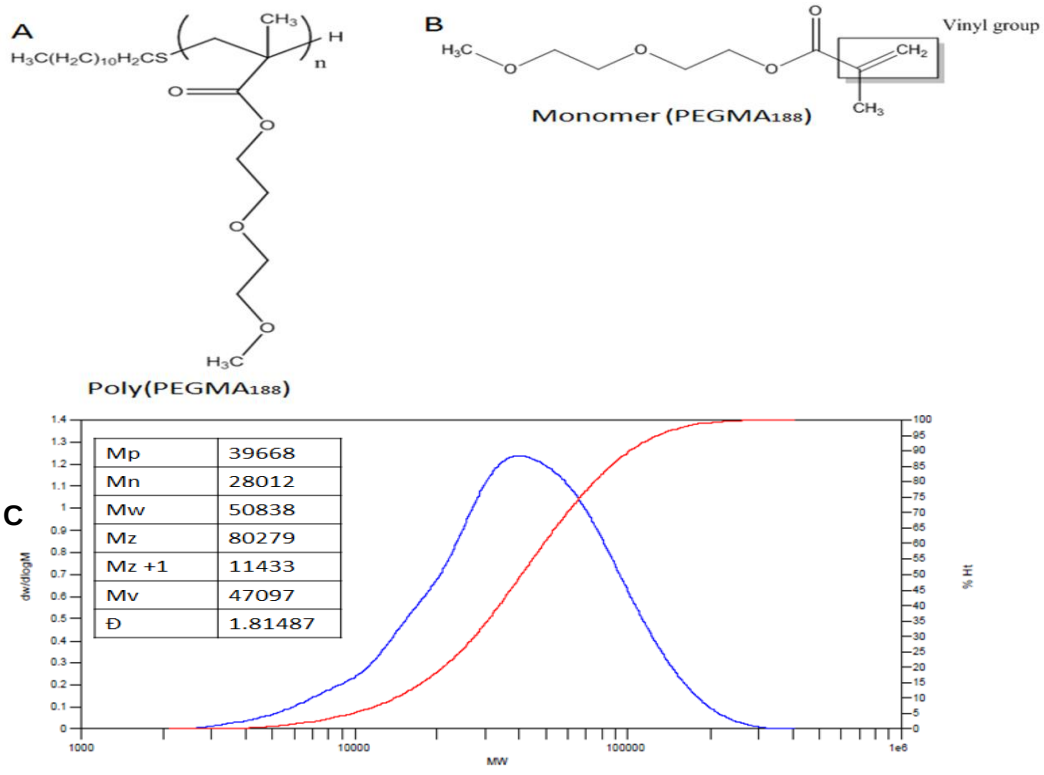



**Figure 2.7:** Image showing the molecular structure of A) Poly ($PEGMA_{188}$) and B) Di (ethylene glycol) methyl ether methacrylate ($PEGMA_{188}$) monomer with the vinyl group highlighted (box). In C) GPC chromatogram showing the molar mass distribution of poly ($PEGMA_{188}$).

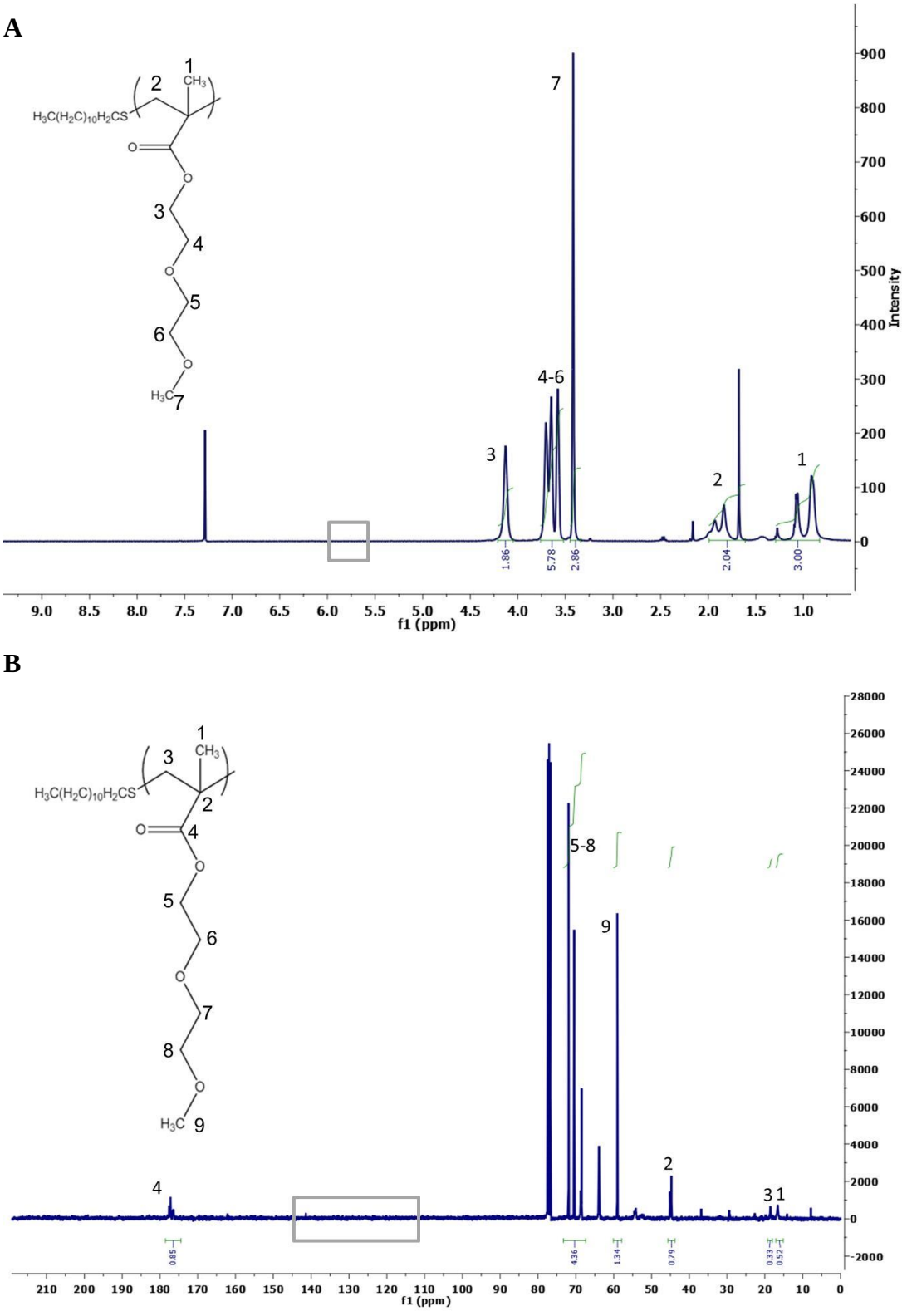



**Figure 2.8:** Images showing A) $^{1}$H NMR and B) $^{13}$C NMR of poly (PEGMA$_{188}$), and the highlighted box indicating the purity of the polymer from any remaining PEGMA$_{188}$ monomer.

The transition temperature (i.e. cloud point, the onset of which corresponds to the first opaqueness that appears in the solution [309]) of poly ($PEGMA_{188}$) was determined by heating 1% (*w/v*) poly ($PEGMA_{188}$) in distilled water. The transparency of the solution changed at temperatures above 26°C to a turbid (opaque) solution, as shown in Figure 2.9. This showed that at a temperature of 26°C, the thermo-responsive poly ($PEGMA_{188}$) chain collapsed from a coil to a globule conformation and phase separated from the aqueous solution. The UV/Vis spectrophotometry results presented in Figure 2.9 indicated that the cloud point of 1% (*w/v*) poly ($PEGMA_{188}$) was between 22.5°C and 25.2°C for five different batches of synthesized poly ($PEGMA_{188}$) polymer, with an average cloud point of 23.6°C.

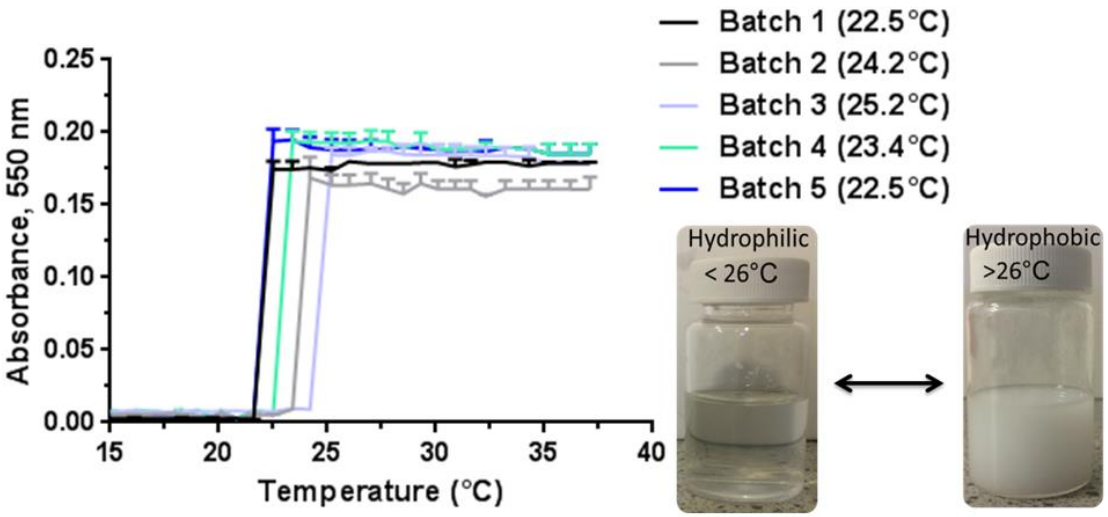



**Figure 2.9:** Cloud point analysis of poly ($PEGMA_{188}$) polymer, assessed by UV-VIS at 550 nm over controlled change in the temperature at rate of 1°C / minute. The error bars represent the mean with SD, n = 2, n represent the number of replicates were taken from each batch. Insert images, showing the LCST for poly ($PEGMA_{188}$) polymer solution by changing the environment temperature above and below 26°C.

The transition temperature of PEG methacrylate polymers (PEGMA) is dependent upon the length of the PEG-side chain (ethylene oxide [EO] units: $CH_2CH_2O$). For

example, polymers possessing an intermediate length of EO units (i.e. 2 ≥ EO < 10) are weakly hydrophilic and present a LCST in water of 26°C or 52°C for 2 and 3 EO units, respectively [310]. However, ethylene glycol methacrylate polymers with slightly longer side chains of 8 to 9 units are very hydrophilic and have higher LCSTs up to 90°C [310]. Therefore, the di (ethylene glycol) methyl ether methacrylate-based polymer is very promising for biomedical applications, since it is principally composed of a biocompatible oligo- (ethylene glycol) segment, and has a reported LCST of ~26°C, which makes it suitable for cell culture studies [249]. As a result, the thermo-responsive poly ($PEGMA_{188}$) polymer was chosen for this study. The measured cloud points (average 23.6°C) of the synthesised poly ($PEGMA_{188}$) in this project are in agreement with the literature (27°C [311], 15–25°C [312] and 26°C [194]).

**Table 2-2:** A summary table of poly ($PEGMA_{188}$) synthesis and characterization

| **Synthesis of thermo-responsive poly ($PEGMA_{188}$) and characterization** | |
|---|---|
| GPC | $M_w$ (GPC) = 50.8 kDa, Đ = 1.8 |
| Cloud point | 23.6°C |
| $^{1}$H NMR (5 peaks) | $^{1}$H NMR (400 MHz, $CDCl_3$): δ 0.9 (br s, 3H, $CH_{3\ backbone}$), 1.9 (br s, 2H, $CH_{2\ backbone}$), 3.4 (br s, 3H, $OCH_3$), 3.6 (br m, 6H, $OCH_2$), 4.2 (br s, 2H, $COOCH_2$). |
| $^{13}$C NMR (6 peaks) | $^{13}$C NMR (400 MHz, $CDCl_3$): δ 17 ($CH_{3\ backbone}$), 20 ($CH_{2\ backbone}$), 46 ($C_{backbone}$), 60 ($OCH_3$), 72 (OCH2), 178 (COOCH2). |

### 2.4.2.i Surface adsorption of poly ($PEGMA_{188}$) onto the 18.5% *(w/v)* PLGA and 30% *(w/v)* recycled PET scaffold surface

Surface adsorption is considered to be the simplest method for the modification of tissue engineering scaffolds, and electrospun fibres in particular. This is due to the extremely high surface area to volume ratio of electrospun fibres, resulting in a higher loading amount per unit mass than any other scaffold type [200]. Generally, electrostatic interactions, hydrogen bonding, hydrophobic interactions, and van der Waals interactions can be used as a driving force for surface adsorption [313]. Therefore, the first method attempted in this project in order to render the electrospun scaffolds thermo-responsive was the incorporation of poly ($PEGMA_{188}$) onto the surface of the electrospun PLGA and PET fibres.

As a general observation from the SEM images of both PLGA and PET scaffolds in Figure 2.10, all the samples were covered partially or almost completely with the poly ($PEGMA_{188}$) layer. As the treatment time increased and/or the poly ($PEGMA_{188}$) concentration increased, more morphological changes in the scaffolds' surfaces (loss of fibre morphology) and difficulties with their handling were evident. It was not possible to carry out an SEM analysis of PET and PLGA scaffolds treated with 5% *(w/v)* poly ($PEGMA_{188}$) for 24 h and 7% *(w/v)* poly ($PEGMA_{188}$) for 1 h, 5 h, 12 h and 24 h. This was due to the high viscosity of the poly ($PEGMA_{188}$) solution creating a strong adhesive layer between the well plate and the scaffolds, which led to scaffold breakage upon handling.

PET and PLGA scaffolds treated with 3% *(w/v)* poly ($PEGMA_{188}$) for 12 hrs and 24 hrs and 5% *(w/v)* poly ($PEGMA_{188}$) for 1 h, 5 h and 12 h all exhibited morphological

changes. PET scaffolds treated with 5% *(w/v)* poly ($PEGMA_{188}$) at 12 h also exhibited clear surface changes while pulling out the scaffolds from the well plate (causing stretching). To conclude, the treatment of scaffolds with 3% *(w/v)* poly ($PEGMA_{188}$) for 1 h and 5 h time periods were chosen for the physical adsorption method, due to their ability to maintain the fibre morphology and subsequent ease of handling.

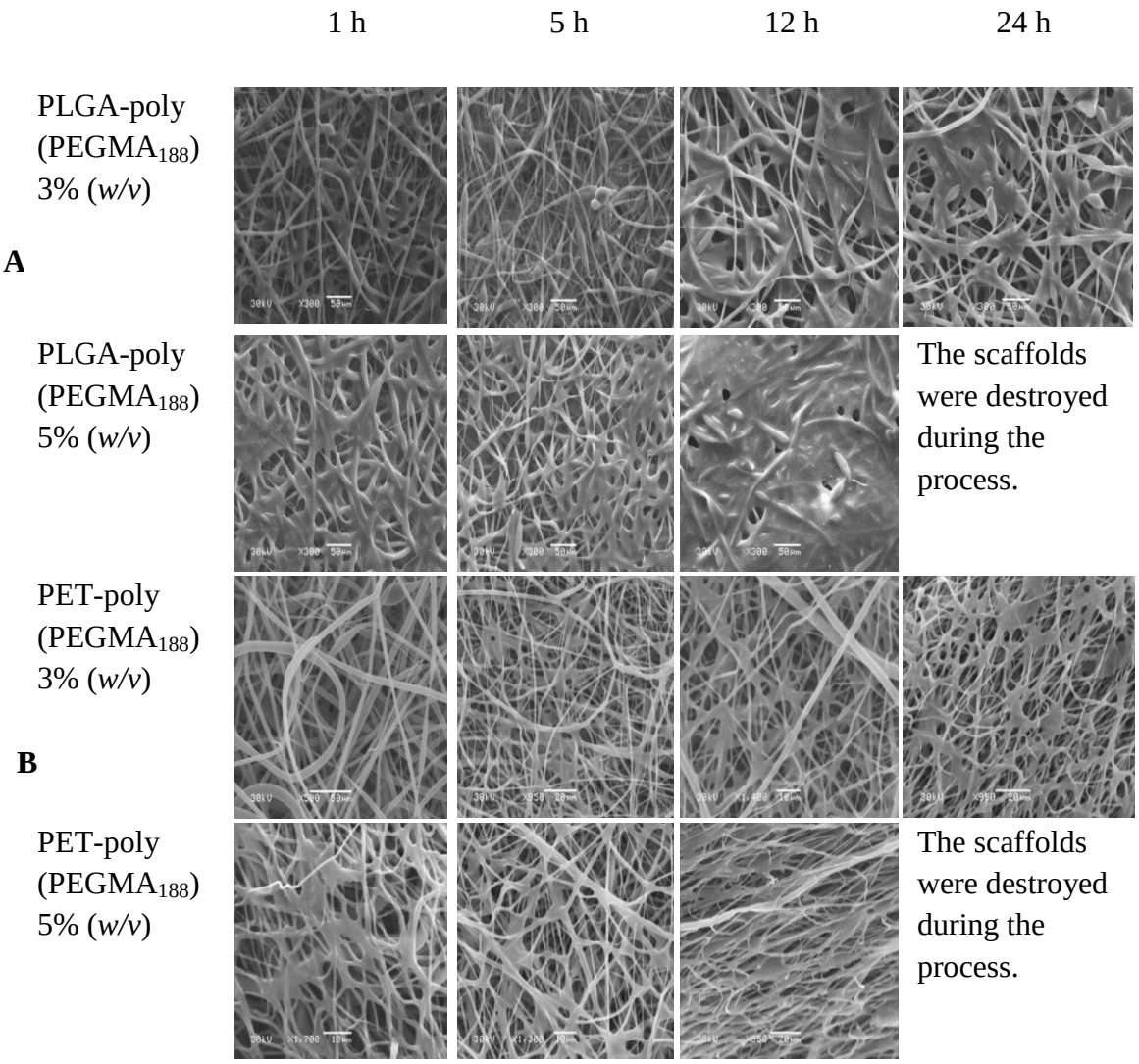



**Figure 2.10:** Representative SEM images showing surface adsorption of two different concentrations 3% and 5% (*w/v*) of poly ($PEGMA_{188}$) onto A) PLGA and B) PET scaffolds at different time periods 1 h, 5 h, 12 h and 24 h.

To ensure that the poly ($PEGMA_{188}$) remained on the scaffold surface after adsorption, WCA measurements were conducted before and after washing the poly ($PEGMA_{188}$)-treated scaffolds with distilled water. From the WCA analysis shown in Figure 2.11, it can be concluded that the physical adsorption of 3% (*w/v*) poly ($PEGMA_{188}$) to all PET and PLGA samples was achieved, as seen by the change in WCA measurements. Untreated PLGA and PET fibres had hydrophobic surfaces with average readings of $138 \pm 0.74°$ and $111 \pm 6.9°$, respectively, whereas, the treated PLGA and PET surfaces were hydrophilic with WCA measurements of less than 90° and less than 60°, respectively. Furthermore, fast ingress of the water droplets into the treated surfaces was observed at RT (22°C). The adsorption of poly ($PEGMA_{188}$) onto the scaffold surface may be attributed to the hydrophobic component of the backbone and the C12 alkanethioether chain end, which were expected to adsorb favourably onto the relatively hydrophobic PLGA and PET fibres. This would result in exposure of the hydrophilic oligoethylene glycol side-chains, which extend from the surface into aqueous solutions, hence, rendering the surface of the modified PLGA and PET scaffolds hydrophilic [200, 251]. Even after washing the treated fibres with distilled water (three times, each for 5 minutes), the hydrophilicity of the surface did not change, suggesting the retention of poly ($PEGMA_{188}$) on the surface.

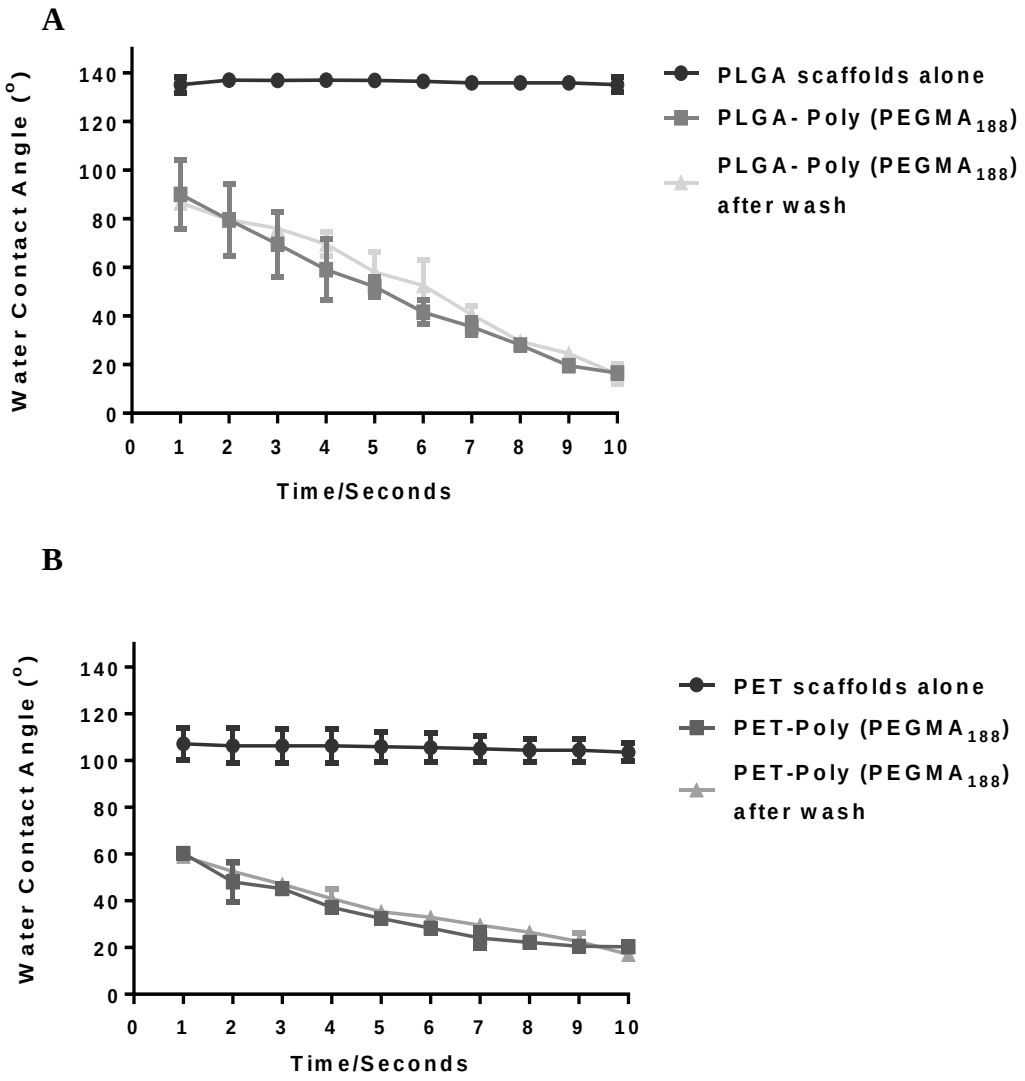



**Figure 2.11:** Change in hydrophobicity of the scaffolds after the addition of thermo-responsive poly ($PEGMA_{188}$) by surface adsorption, indicated by water contact angle measurements, before and after washing with distilled water A) PLGA and B) PET over 10 seconds time period. The error bars represent the mean ± SD; experiments were conducted three times for each scaffold type. (n = 9 total, three scaffolds from three different batches).

### 2.4.2.ii Hydrolysis modification of the PLGA and PET scaffolds surface by NaOH treatment

NaOH surface modification of PLGA and PET scaffolds was conducted simultaneously to induce surface hydrolysis (roughness) without affecting fibre integrity [131, 136, 163]. This was used as a way to increase the presence of the poly ($PEGMA_{188}$) on the surface, allowing the use of lower concentrations, which is preferential due to the viscous nature of poly ($PEGMA_{188}$), as demonstrated above. There are two main hypotheses that support the use of this method. The first involves inducing surface hydrolysis of PLGA and PET fibres, resulting in free hydroxyl and carboxyl functional groups that may contribute to poly ($PEGMA_{188}$) attachment. The second involves increasing the surface roughness (grooves on the fibre surface) for poly ($PEGMA_{188}$) entrapment.

Treatment of the scaffolds started with 10% (*w/v*) NaOH, as this concentration has been previously reported in the literature as the most appropriate concentration for fibre-based scaffold treatment [200, 314]. Moreover, in other studies, it has been reported that exposure times of less than 8 h did not affect the fibres' surfaces [165, 250]. However, in this study, all PET and PLGA scaffolds exposed to 1% –10% *(w/v)* NaOH for 20 minutes to 4 h were very fragile and broke while handling; hence, these scaffolds and treatment regimens were eliminated from the study. Reducing the concentration to 0.5% *(w/v)* and 1% *(w/v)* NaOH, and reducing the exposure times to 5–10 minutes was explored in order to generate the desired surface roughness of the scaffolds, without affecting the scaffold integrity.

The SEM images in Figure 2.12, showed that homogenous hydrolysis of PLGA and PET electrospun fibres occurred as a result of treatment with these NaOH concentrations for the above exposure times, with surface hydrolysis evident as small grooves on the surfaces of individual fibres, without eliciting their breakage. Similar results were observed by Hadjizadeh *et al.* with a similar change in PET fibre morphology (fabricated by the melt blowing process) after NaOH treatment in that study, the fibres were also evaluated using SEM and pores were apparent on the surface of individual fibres [315]. Moreover, PLGA fibres, fabricated using chloroform with heat treatment, were soaked in 1 N NaOH for 10 minutes, with the resultant scaffolds showing increased pores and pore diameters, which were twice those of the non-treated variety [316].

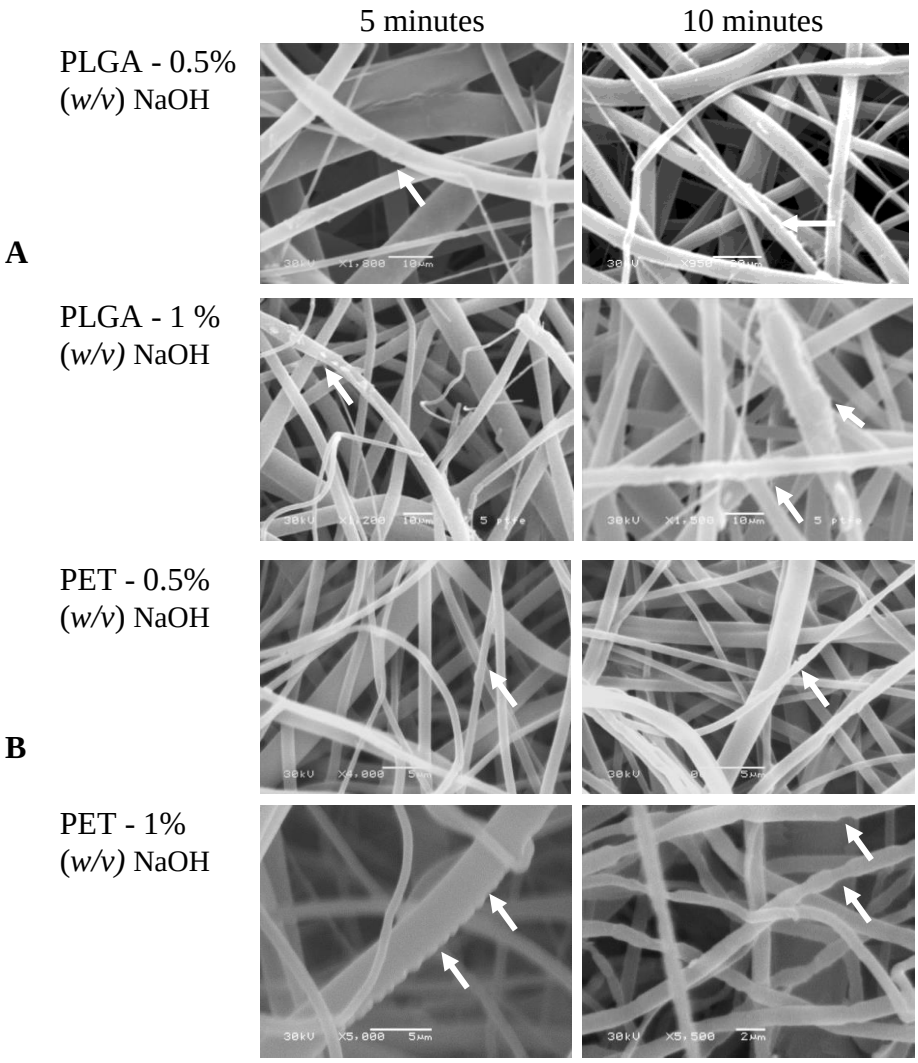



**Figure 2.12:** Representative SEM images show the hydrolysis effect of NaOH treatment on A) PLGA and B) PET scaffolds with 0.5% and 1% (*w/v*) NaOH concentrations at different time periods (5 minutes and 10 minutes). The arrows are representing the surface hydrolysis as small grooves on individual fibre's surface.

The WCA measurements displayed in Figure 2.13 illustrated the hydrophobicity of the PLGA and PET surfaces, with an average WCA of 134 ± 0.74° for the PLGA scaffolds and 111 ± 6.9° for the PET scaffolds. Upon exposure to 0.5% (*w/v*) NaOH for 10 minutes, a more hydrophilic surface ensued, as illustrated by the fast decreasing WCA measurements over ten seconds. As in previous studies, these changes were attributed to the breakdown of ester bonds in the polymer backbones and the

generation of new free hydroxyl and carboxyl groups exposed at the surface [316-318]. Techniques used in previous studies, such as the treatment of non-woven PET fibres with NaOH, rendered the fibre surface more hydrophilic, thereby facilitating the attachment and spreading of human astrocyte cells when compared with non-treated fibres [319]. In the current study, NaOH treatment increased the hydrophilicity of the scaffolds, but this method was not taken further due to its detrimental effects on the integrity of the fibres.

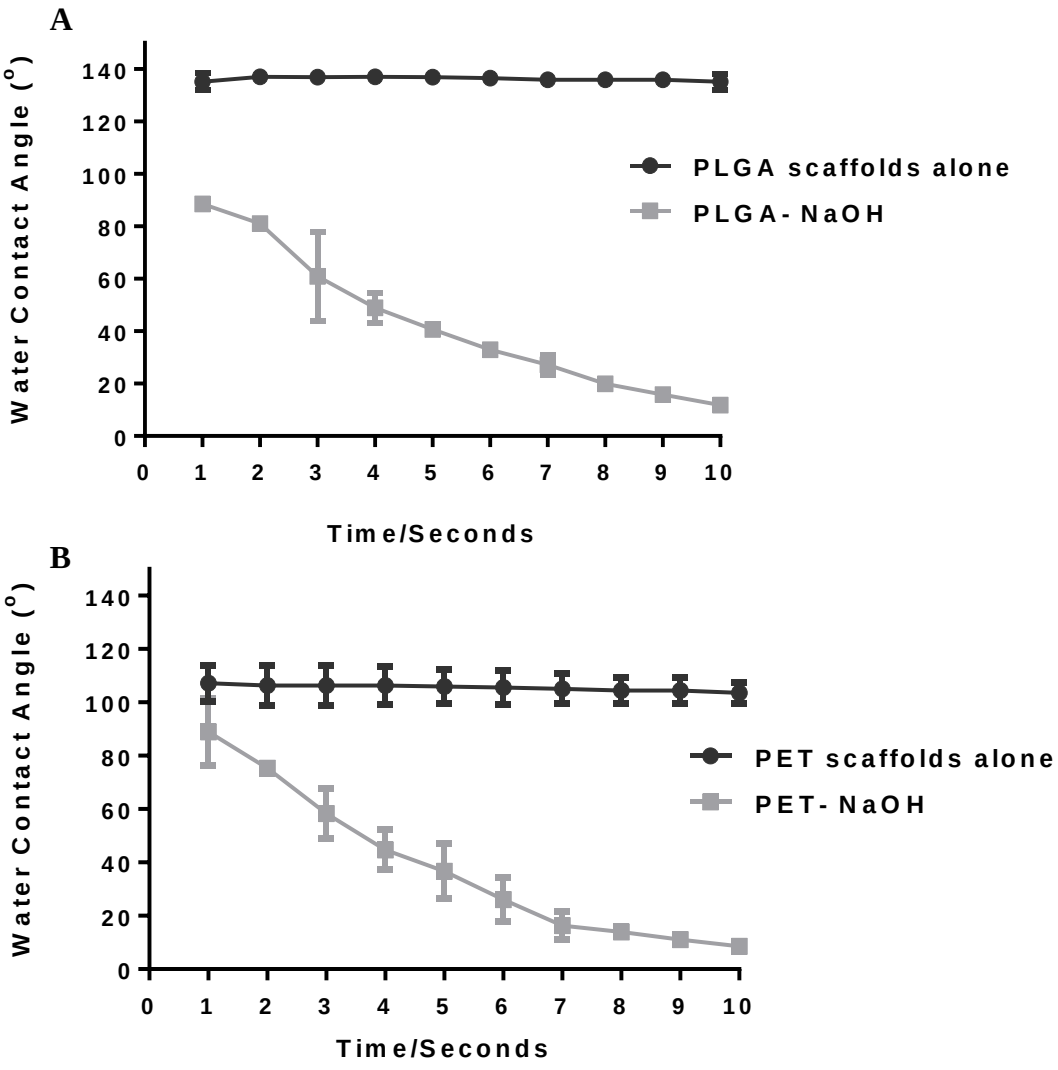



**Figure 2.13:** Change in hydrophobicity over 10 seconds time period, of PLGA and PET scaffolds respectively before and after treatment with 0.5% (*w/v*) NaOH for 10 minutes. The error bars represent the mean ± SD, experiment were conducted three times for each scaffolds (n = 9 total, three scaffolds from three different batches).

### 2.4.2.iii Surface entrapment of poly ($PEGMA_{188}$) polymer into PLGA and PET scaffolds by solvent swelling

Acetone was chosen as a solvent for swelling the PET scaffolds [320-323], and trifluoroethanol (TFE) for the PLGA scaffolds [324, 325]. The aim was to explore the method of swelling the surface of the fibres, and then entrapping the thermo-responsive poly ($PEGMA_{188}$) in the scaffolds. In this study, all PET and PLGA scaffolds following exposure to 5% (*w/v*) acetone or TFE, respectively, for 10 minutes to 3 h were completely dissolved. Furthermore, all PET and PLGA scaffolds exposed to 0.5% and 1% (*w/v*) acetone or TFE, respectively, for 10 minutes to 2 h, exhibited no changes in fibre swelling; hence, these scaffolds/methods were eliminated from the study.

Following the exposure of PLGA and PET scaffolds to 2% *(w/v)* TFE and 2% *(w/v)* acetone for 1 h, respectively, there was an increase in fibre diameter, without an effect on the fibre integrity. From the SEM images shown in Figure 2.14, the average diameter of the 18.5% *(w/v)* PLGA scaffolds increased from 3 ± 0.8 µm to 6.2 ± 2.5 µm after treatment. Following a similar pattern, the average diameter of the recycled 30% *(w/v)* PET scaffolds increased from 836.2 ± 172.7 nm to 3.5 ± 1.4 µm.

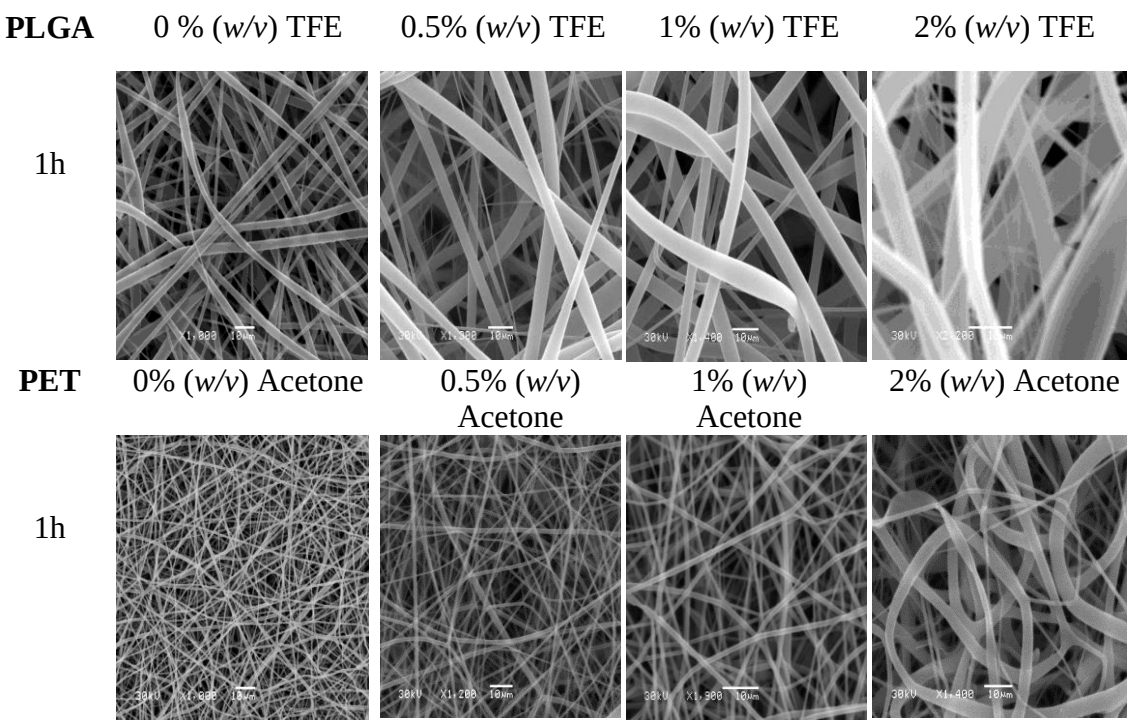



**Figure 2.14:** Representative SEM images of 18.5% (*w/v*) PLGA and recycled 30% (*w/v*) PET scaffolds treated with different concentrations of TFE and acetone as swelling solvents respectively for 1h.

Poly ($PEGMA_{188}$) polymer was added to the swollen scaffolds, followed by the addition of non-solvent, distilled water. This resulted in fibre shrinkage and a decrease in the fibre diameters to their original values, with averages of 1.08 ± 0.2 µm for PET and 2.4 ± 0.5 µm for PLGA, respectively, as shown in Figure 2.15.

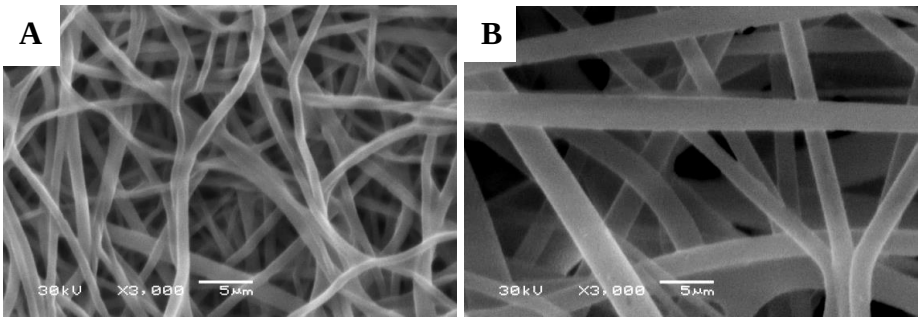



**Figure 2.15:** SEM shows the decrease in fibres diameters of A) PET and B) PLGA, after addition of non-solvent (distilled water) to the treated scaffolds (poly ($PEGMA_{188}$) present in the swelling solvents).

A previous study analysed the entrapment of PEG, using TFE as a swelling solvent, on the surface of PLA disks via X-ray photo spectroscopy (XPS), resulted in the entrapment of PEG onto the surface of PLA disks [325]. In another study, poly (L-lysine) (PLL) coupled with the cell adhesion peptide sequence GRGDS (PLL-GRGDS) was entrapped within alginate fibres by exposing the alginate fibres to a $NaCl/CaCl_2$ mixture solution to induce swelling [287]. In this study, this method was not taken further due to the number of steps involved and the risk of cytotoxicity from the residual solvent.

### 2.4.2.iv Co-electrospinning of poly ($PEGMA_{188}$) and PLGA or PET polymers in a single step

Co-electrospinning of poly ($PEGMA_{188}$) with PLGA and PET was considered as a new approach to create thermo-responsive scaffolds within a single step rather than using post-electrospinning methods. Concentrations of 18.5% *(w/v)* PLGA and 30% *(w/v)* recycled PET were chosen to start the co-electrospinning of PLGA and PET with poly ($PEGMA_{188}$) polymer, as these concentrations resulted in uniform fibres (as presented in section 2.4.1.i).

An appropriate time for the polymer to dissolve in the solvent is an important factor in the fabrication of bead-less fibres [326]. Ten minutes was sufficient for poly ($PEGMA_{188}$), along with PLGA to dissolve in DCM, resulting in a clear solution. However, the SEM images presented in Figure 2.16 illustrated that the resultant scaffolds contained large beads. Extending the dissolution time to 24 h eliminated beading. Co-electrospinning the two polymers using a flow rate of 1mL/h resulted in no fibres being present in the sample. However, by increasing the flow rate to 4 mL/h,

fibres started to appear on the collector plate; it is likely that this was related to the viscosity of the solution. It has been reported that the flow rate needs to be sufficiently high enough to overcome the viscosity and surface tension of the polymer solution in order to form and maintain jet elongation from the spinneret [327]. Additionally, increasing the PLGA concentration from 18.5% to 20% *(w/v)* resulted in bead free and uniform fibres.

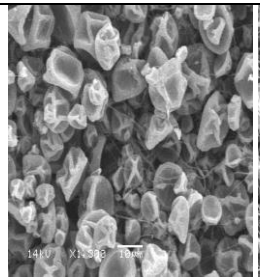
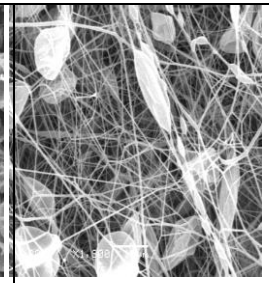
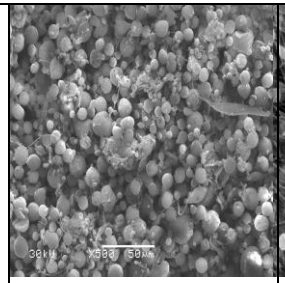
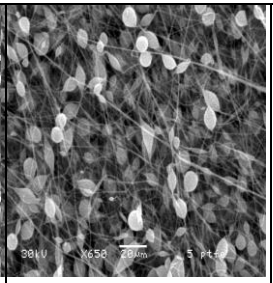
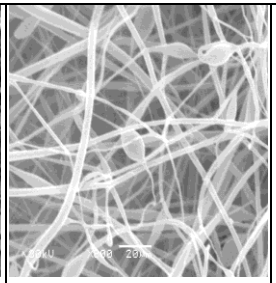
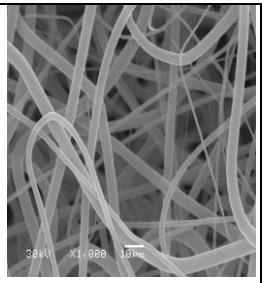
| SEM Images |  |  |  |  |  |  |
|---|---|---|---|---|---|---|
| Poly ($PEGMA_{188}$) concentration (*w/v* %) | 5 | 5 | **1.2** | 1.2 | **1** | 1 |
| PLGA concentration (*w/v* %) | 18.5 | 18.5 | 18.5 | 18.5 | 18.5 | **20** |
| Flow rate (mL/h) | 1 | **4** | 1 | **4** | 4 | 4 |
| Dissolving time | 10 minutes | 10 minutes | **4 h** | **24 h** | 24 h | 24 h |
| Collector distance (cm) | 15 | 15 | 15 | 15 | 15 | 15 |
| Voltage (kV) | 19 | 19 | 19 | 19 | 19 | 19 |

**Figure 2.16:** SEM images representing the co-electrospun fibrous scaffolds of poly ($PEGMA_{188}$) with PLGA polymer and co-electrospinning parameters for each SEM Image, with the changeable parameters highlighted in blue.

SEM images of co-electrospun PET with poly ($PEGMA_{188}$) are shown in Figure 2.17 and indicated that increasing the concentration of recycled PET from 10% to 30% *(w/v)* and the poly ($PEGMA_{188}$) polymer concentration from 1% to 2% *(w/v)* resulted in scaffolds with less beads and more uniform fibres. As reported in the literature, increasing the polymer solution concentration leads to a reduction in beading in the resultant materials [292]. Also, more uniform fibres were achieved when a flow rate of 4 mL/h was used.

To conclude, 20% (*w/v*) PLGA with 1% (*w/v*) poly ($PEGMA_{188}$) and 30% (*w/v*) recycled PET with 2% (*w/v*) poly ($PEGMA_{188}$) electrospun scaffolds were chosen as candidates for further cell culture experimentation.

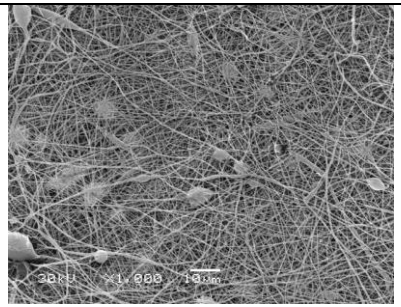
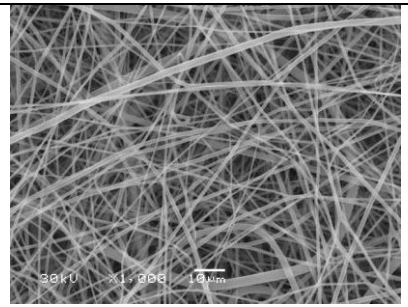
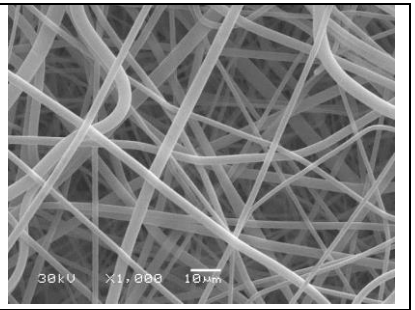
| SEM Images |  |  |  |
|---|---|---|---|
| Poly ($PEGMA_{188}$) concentration (*w/v* %) | 1 | 1 | **2** |
| PET concentration (*w/v* %) | 10 | **30** | 30 |
| Flow rate (mL/h) | 1 | 1 | **4** |
| Dissolving time (h) | 24 | 24 | 24 |
| Collector distance (cm) | 15 | 15 | 15 |
| Voltage (kV) | 14 | 14 | **19** |

**Figure 2.17:** SEM images representing the co-electrospun fibrous scaffolds of poly ($PEGMA_{188}$) with PET polymer and co-electrospinning parameters for each SEM Image, with the changeable parameters highlighted in blue.

$^{1}$H NMR analysis was conducted to confirm the presence of poly ($PEGMA_{188}$) in the electrospun scaffolds, as shown in Figure 2.18 (B) and Figure 2.19 (B). $^{1}$H NMR of PLGA with poly ($PEGMA_{188}$) and PET with poly ($PEGMA_{188}$) showed resonances between 3.5 ppm and 4.3 ppm, which correspond to poly ($PEGMA_{188}$) side chain. While $^{1}$H NMR analysis of PLGA and PET scaffolds alone in Figure 2.18 (A) and Figure 2.19 (A) showed no resonances between 3.5 ppm and 4.3 ppm. This confirms the presence of poly ($PEGMA_{188}$) in the electrospun scaffolds when co-electrospun with either PLGA or PET. As a result, PLGA-poly ($PEGMA_{188}$) and PET-poly ($PEGMA_{188}$) scaffolds were chosen as candidates for further cell culture studies (with scaffolds fabricated from PLGA and PET alone used as a control), as described in the next Chapter of this thesis.

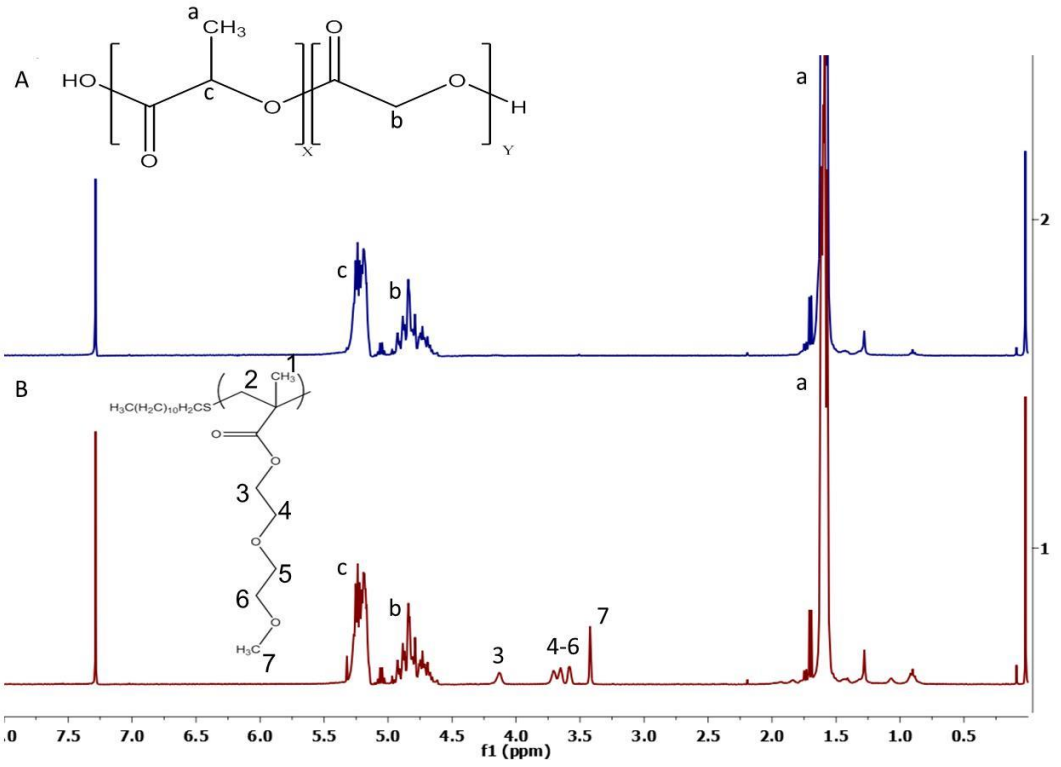



**Figure 2.18:** $^{1}$H NMR of A) electrospun poly (lactic-co-glycolic acid) (PLGA) scaffolds and B) blend electrospun PLGA with poly ($PEGMA_{188}$) scaffolds.

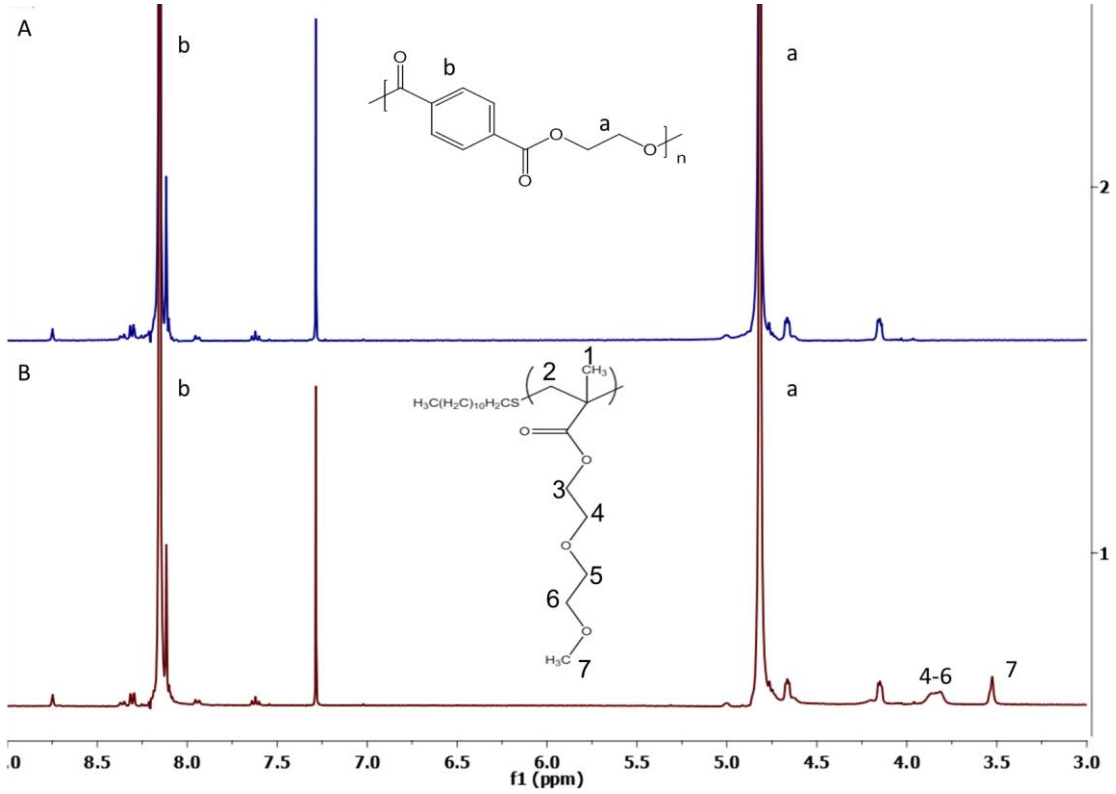



**Figure 2.19:** $^{1}$H NMR of A) electrospun for poly (ethylene terephthalate) (PET) scaffolds and B) blend electrospun for PET with poly ($PEGMA_{188}$) scaffolds.

**Table 2-3** A summary table of creating thermo-responsive scaffolds

| **Incorporation of the thermo-responsive poly ($PEGMA_{188}$) polymer into electrospun PLGA and PET scaffolds** | | | | |
|---|---|---|---|---|
| **Incorporation methods** | **Surface adsorption** | **NaOH hydrolysis** | **Surface entrapment** | **Co-electrospinning** |
| **WCA** | Change from $138 \pm 0.74^{o}$ (PLGA) and $111 \pm 6.9^{o}$ (PET) to less than $90^{o}$ and less than $60^{o}$ respectively | Change from $138 \pm 0.74^{o}$ (PLGA) and $111 \pm 6.9^{o}$ (PET) to hydrophilic surface with fast decreasing in WCA | - | Chapter 3 |
| **NMR** | - | - | - | Peaks between 3.5 ppm and 4.3 ppm corresponding to poly ($PEGMA_{188}$) side chain |
| **Fibre morphology (SEM)** | Fibre surface covered with thermo-responsive polymer | Change in fibres surface (small grooves) | Swelling and de-swelling of the fibres with no negative effects | Bead-less fibres were obtained |
| **Presence of poly ($PEGMA_{188}$) polymer confirmed by** | WCA (hydrophilic surface) | - | - | NMR |
| **Results** | Rejected | Rejected | Rejected | Accepted |
| **Reasons** | Multiple steps process<br>Fragile fibres<br>Difficult handling | Multiple steps process<br>Fragile fibres | Multiple steps process<br>Many solvents required | One step process<br>Fibre morphology maintained<br>Thermo-responsive polymer present |

## 2.5 Conclusions

In the last few decades many 2D thermo-responsive treated surfaces have been used as a cell culture surface to generate healthy cells suitable for clinical application without the need for enzymatic detachment [328]. However, 2D thermo-responsive surfaces do not represent the 3D environment of the human body, which is known to influence cell behaviour, phenotype and growth [329]. The main aim of this work was to create for the first time a 3D thermo-responsive electrospun fibre based scaffold using PLGA and PET polymers with poly ($PEGMA_{188}$) as a thermo-responsive component.

The data presented have illustrated that electrospinning was successfully used to produce bead-less, nano-range PET fibres and micro-range PLGA fibre-based scaffolds. Moreover, a successful single step co-electrospinning of poly ($PEGMA_{188}$) with PET and PLGA was studied for the first time, and resulted in bead-less electrospun mats with confirmation of thermo-responsive polymer presence by NMR studies.

Other methods explored illustrated that surface adsorption produced a covering of poly ($PEGMA_{188}$) on the scaffold's surface. The hydrophobicity of the scaffolds changed and the hydrophilic nature of the scaffold was successfully maintained even after washing. However, due to the high viscosity of poly ($PEGMA_{188}$) and difficulties in the handling of treated scaffolds, the usefulness of these thermo-responsive fibres from further applications was limited, and so this method was not pursued.

NaOH treatment was explored simultaneously as a means to improve surface deposition of poly ($PEGMA_{188}$). Following treatment, PET and PLGA scaffolds showed a reduction in hydrophobicity and roughness of the scaffold surface, but the process was detrimental to the integrity of the fibres and so this method was not taken further.

Surface entrapment of the poly ($PEGMA_{188}$) within the PET and PLGA scaffolds showed an enlargement in the fibre diameters upon addition of acetone and TFE solvents respectively, illustrating swelling and subsequent shrinkage upon addition of the non-solvent (water) into the system. However, further studies need to be conducted to ensure the presence of poly ($PEGMA_{188}$) in the scaffolds.

The next Chapter (Chapter 3) will focus more on the co-electrospinning method of creating thermo-responsive fibres developed here. Additional surface characterization of co-electrospun PET-poly ($PEGMA_{188}$) and PLGA-poly ($PEGMA_{188}$) was performed by SEM, NMR, WCA measurements and XPS. Also, these temperature sensitive scaffolds were used to explore mammalian cell adhesion, proliferation and passage of red fluorescent protein (RFP) expressing 3T3 fibroblast cells.

# Chapter 3. Development of a novel thermo-responsive electrospun scaffold and initial mammalian cell response

## 3.1 Introduction

Many cell types with the potential for use in therapeutic applications require *in vitro* expansion and differentiation in environments that mimic the ECM in the human body. However, the application of these cells within a clinical setting depends not only on the ability to control their differentiation, but also on materials that can support the appropriate culture systems for the safe expansion of the relevant/desired cell populations. Normally, cells are cultured for a certain period of time and once they have reached confluency, they are harvested from the cell-culture substrate in a process called passaging. The efficient recovery of cells from the culture substrate is an essential process for their further utility, which can be accomplished by the use of a cell scraper in order to physically remove them from the culture substrate. However, cell scraping has been shown to affect the cell surface integrity, which has an impact on cell viability [330]. This was illustrated in a study, where the viability of V-79 cells was just 70%, and their plasma membranes were mechanically damaged after being scraped with a rubber policeman, when compared with 91% and 85% viability for cells harvested via trypsinization and citrate buffer treatment, respectively [330]. Alternatively, EDTA and proteolytic enzymes, e.g. trypsin, pronase or collagenase, are commonly used to fully recover the adherent cells from culture substrates as a single cell suspension [331]. Trypsin-EDTA treatment is considered to be the most effective procedure for the recovery of individual cell populations [332]. However, it disrupts the cell-substratum and cell-cell

interactions, thereby, causing the destruction of cell membrane proteins, such as ion channels and growth factor receptors [1]. It has been reported that the permeability and integrity of baby-hamster kidney cells (BHK 2I-C 13) were affected when they were harvested from glass using trypsin-EDTA. The cells lost 10.4% of their cellular RNA and 11.4% of their cellular DNA, which is consistent with the lysis of about 11% of the cells [333]. Moreover, long-term enzymatic passaging is associated with higher cell mortality and causes injury to mammalian cells internally via the degradation of polyribosomes [205, 334]. In line with these findings, it has recently been shown that trypsin altered the cell proteome through enzymatically cleaving some of the cell surface markers [335]. For example, 36 proteins were differentially expressed in cervical adenocarcinoma HeLa cells treated with trypsin. Proteins that are known to regulate cell metabolism, growth regulation, mitochondrial electron transportation and cell adhesion, such as heat shock protein 60 (HSP-60) and calcium-binding mitochondrial carrier protein (SCaMC-1), were down-regulated. However, proteins that regulate cell apoptosis, such as voltage-dependent anion-selective channel protein 1 and 2 (VDAC1 and VDAC2) were up-regulated after trypsin treatment [335]. Another study showed that both the percentage and expression of HLA-I and CD105 cell surface markers of human amniotic epithelial cells (hAECs) were down-regulated after enzymatic digestion [336].

There is, therefore, a pressing need to develop new cell-culture systems that avoid the use of digesting enzymes for the efficient removal of the cultured cells from the surface, and to maintain cell integrity for further clinical applications. Besides reducing the risk of cell damage, the occurrence of cell contamination after exposure

to animal products in culture (e.g. trypsin derived from egg white) can also be reduced [337]. An alternative approach is to synthesise a surface with mutable properties, which can lead to cell detachment by other physical processes, e.g. temperature. On these surfaces, cells can be cultured at temperatures above the LCST of the single thermo-responsive polymer chain (hydrophobic surface) and then harvested by lowering the culture temperature below the LCST (hydrophilic surface), without the use of digestive enzymes or chelating agents [338]. Okano *et al.* have extensively developed this concept using thermo-responsive PNIPAAm-based polymer surfaces for cell culture. For example, bovine hepatocytes (HCs) and bovine aortic endothelial cells (ECs) attached, spread and proliferated on PNIPAAm-coated tissue culture polystyrene (TCPS) surfaces to the same extent as TCPS dishes at 37°C. However, below 32°C (the LCST of the thermo-responsive polymer, PNIPAAm), the dish surface became hydrophilic, leading to the formation of a hydration layer between the dish surface and the cultured cells, which resulted in cell detachment from the PNIPAAm-grafted surface. In these experiments, cells were harvested as intact cell sheets along with their deposited ECM, and cell surface proteins, such as ion channels, growth factor receptors and cell-to-cell junction proteins, remained intact [231, 338, 339]. The recovery of rat HCs and ECs co-cultured on patterned dual thermo-responsive surfaces comprising PNIPAAm and n-butyl methacrylate (BMA) was achieved after reducing the culture temperature to 20°C [340]. Another study utilized PNIPAAm-brush surfaces with different layer thicknesses on polystyrene substrates that were prepared by surface-initiated atom transfer radical polymerization (ATRP). These brush surfaces exhibited a higher hydrophilicity with an increase in the PNIPAAm layer thickness; furthermore, they

allowed the spontaneous detachment of confluent EC monolayers as contiguous cell sheets after reducing the culture temperature [341].

Recently, surfaces grafted with poly ($MEO_2MA$-co-OEGMA) have been shown to successfully support mouse embryonic stem cell (mESC) adhesion and proliferation above the polymer's LCST, in addition to cell detachment from the 2D culture surface by decreasing the temperature below the LCST. Importantly, these cells were viable, maintained a stem cell-like morphology and proliferated in a similar manner to those cultured on control surfaces [205]. Another study showed the same trend of results using thermo-gelling particles of polycaprolactone (PCL) and a thermo-responsive polymer, poly (polyethylene glycol methacrylate ethyl ether), poly (PEGMA-$EE_{246}$), as a 3D cell culture platform for NIH 3T3 fibroblasts [251]. Poly (OEGMA-co-$MEO_2MA$)-modified gold surfaces have also been used as a switchable culture surface, as demonstrated using L929 mouse fibroblasts, where cell detachment and harvesting occurred upon decreasing the environmental temperature to 23°C [226, 342]. A recent study demonstrated the use of poly ($MEO_2MA$) with magnetic colloidal gels as a responsive 3D scaffold for 3T3 fibroblast and human mesenchymal stem cell (hMSC) culture. This system allowed the attachment and spread of cells at 37°C, and then their recovery after reducing the culture temperature to below 26°C [343, 344].

While there is now an extensive amount of literature on the use of thermo-responsive polymer surfaces (2D) for cell culture, very few studies have been conducted using 3D electrospun culture systems. Only a few reports have been published on thermo-responsive electrospun fibrous scaffolds (3D) for biological studies [253-255]. A

recent study showed that cells adhered and proliferated on cross-linked electrospun poly (ethylene glycol) methacrylate (PEGMA) and polyurethane (PU) fibre-based scaffolds, with a low cell death rate, indicating that PEGMA/PU scaffolds were highly biocompatible non-cytotoxic. However, there were no further studies regarding the thermal detachment of the cells from such scaffolds [228]. Another study used hydrogel-based nano-fibre mats based on thermo-responsive multiblock poly (ester urethane) containing PEG, poly (propylene glycol) (PPG), and PCL segments that were fabricated by electrospinning. Cell culture studies on these nano-fibre mats were carried out using human dermal fibroblasts, and a healthy cell morphology was observed with excellent cell adhesion when compared with pure PCL nano-fibres, but with no further thermal cell detachment from the fibre mats [345]. A few other studies showed the thermo-responsive properties of electrospun fibres via WCA measurements, but no cell culture data was included. For example, core-sheath electrospun nano-fibres are created using a coaxial spinneret connected with two syringes. Two different polymers can be spun at the same time, with one polymer forming the sheath, and the other forming the core of the electrospun fibres. Core-sheath electrospun nano-fibres have been produced from PNIPAAm and PCL showed that wettability of all the scaffolds displayed evident changes from hydrophilic (WCA∼5°) to hydrophobic (WCA∼120°) with the temperature changes from 20°C to 40°C [346]. Another study of nano-fibres prepared with PNIPAAm and poly (2-acrylamido-2-methylpropanesulfonic acid) using a single-spinneret electrospinning technique were developed for the controlled release of nifedipine (NIF) in response to temperature. These scaffolds also showed change in surface

wettability from hydrophilic (WCA~0°) to hydrophobic (WCA~109°) with the temperature changes from 20°C to 40°C [347].

In the previous chapter (Chapter 2), different techniques were investigated to create thermo-responsive fibre-based scaffolds, either pre- or post-electrospinning. However, the blend electrospinning (co-electrospinning) method was chosen due to its ability to achieve bead-less fibres and the presence of thermo-responsive polymer in the scaffolds was confirmed. In this chapter (Chapter 3), the work included the detailed characterisation of the co-electrospinning method in addition to initial mammalian cell culture on thermo-responsive co-electrospun fibres, without the use of digesting enzymes as shown in Figure 3.1.

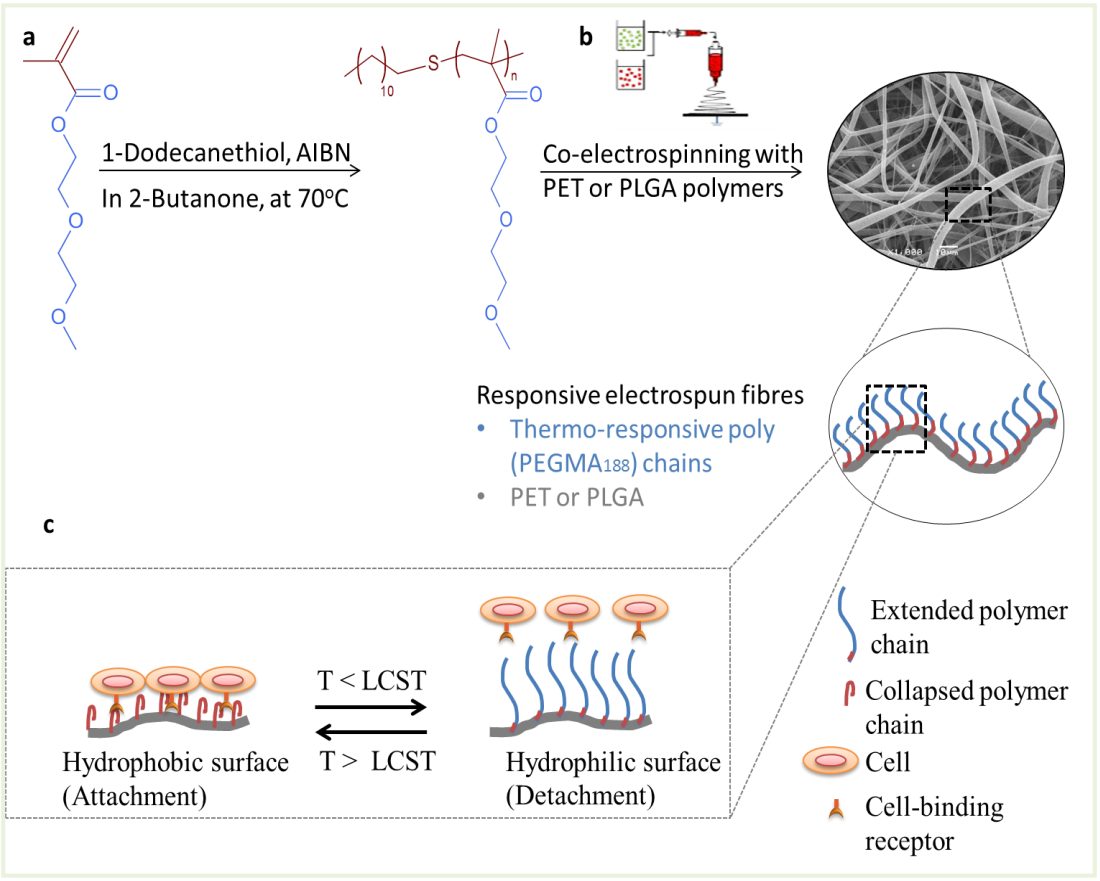



**Figure 3.1:** A schematic of the thermo-responsive 3D scaffolds synthesis route. a) Synthesis of the thermo-responsive polymer; 1-dodecanethiol chain transfer agent was used in the free radical polymerization of 2-(2-methoxyethoxy) ethyl methacrylate ($MEO_2MA$) monomers to make thermo-responsive poly ($PEGMA_{188}$) polymer. b) Co-electrospinning of synthesised poly ($PEGMA_{188}$) with PET or PLGA polymers. Insert image modified from [348] c) Application of responsive scaffolds for cell culture; cell attachment (above LCST) and detachment (below LCST) to/from thermo-responsive co-electrospun fibres. Thermo-responsive polymer chains at temperatures below the LCST are shown as chain extended, forming a 'cell-resistant' surface, whereas collapse of the polymer chain above the LCST results in a surface more favourable for cell attachment. Note: cells, polymer chains and fibres were shown out of scale.

## 3.2 Aims and objectives

The main aim of this chapter was to study the effect of different concentrations of the thermo-responsive polymer, poly ($PEGMA_{188}$), on co-electrospun (blend-electrospun) fibres prepared with PLGA and PET polymers. This was then followed by cell culture and passage on these scaffolds using red fluorescent protein (RFP)-expressing 3T3 fibroblast cells as a model cell type.

The aims of this chapter were achieved though the following objectives:

- To co-electrospun six different concentrations (0, 2, 4, 6, 8 and 10% [*w/v*]) of thermo-responsive polymer poly ($PEGMA_{188}$) with 18.5% *(w/v)* PLGA and 30% *(w/v)* recycled PET (concentrations based on data presented in 0).
- To characterize the surface and confirm the thermo-responsive nature of these synthesised scaffolds by SEM, WCA, $^{1}H$ NMR, and XPS.
- To culture 3T3 fibroblast cells on electrospun scaffolds and TCPS for five days.
- To evaluate cell attachment, viability, proliferation and detachment (i.e. a cell culture cycle of cell proliferation followed by passaging) by changing the culture temperature above and below the LCST without the use of digesting enzymes over one passage.

## 3.3 Materials and methods

### 3.3.1 Synthesis of the thermo-responsive poly ($PEGMA_{188}$)

The thermo-responsive polymer, poly ($PEGMA_{188}$), was synthesised by free radical polymerization and characterized as described in 0, section 2.3.2.

### 3.3.2 Preparation of the co-polymer poly ($PEGMA_{188}$)-PLGA and poly ($PEGMA_{188}$)-PET solutions

PLGA polymer was dissolved in 6 mL of DCM. Poly ($PEGMA_{188}$) was then added to the mixture to generate a range of different concentrations (18.5% PLGA: 0% poly ($PEGMA_{188}$), 18.5% PLGA: 2% poly ($PEGMA_{188}$), 18.5% PLGA: 4% poly ($PEGMA_{188}$), 18.5% PLGA: 6% poly ($PEGMA_{188}$), 18.5% PLGA: 8% poly ($PEGMA_{188}$) and 18.5% PLGA: 10% poly ($PEGMA_{188}$) [*w/v*]). The same concentrations of poly ($PEGMA_{188}$) were prepared with 30% *(w/v)* recycled PET polymer, in a mixture of 3 mL of TFA/3 mL of DCM. The mixtures were stirred at RT for 24 h to ensure their complete solvation. Three different batches were prepared for each concentration on different days.

### 3.3.3 Blend electrospinning (co-electrospinning)

The co-electrospinning process was described in Chapter 2, section 2.3.3.iv; however, the co-electrospinning parameters used for PLGA-poly ($PEGMA_{188}$) and PET-poly ($PEGMA_{188}$) are detailed in Table 3-1.

**Table 3-1:** Co-electrospinning parameters of PLGA-poly ($PEGMA_{188}$) and PET-poly ($PEGMA_{188}$)

| Spinning volume | Flow rate | Working distance | Voltage |
|---|---|---|---|
| 6 mL | 4 mL/h | 15 cm | 19 KV |

### 3.3.4 Surface characterization of the thermo-responsive scaffolds

#### 3.3.4.i Scanning electron microscopy (SEM)

Samples preparation for SEM analysis is described in Chapter 2, section 2.3.4.i. The fibre diameters were measured by taking perpendicular measurements of the fibres on the SEM images. The fibre diameters were measured from images taken from 5 fields of view for each scaffold; a total of 20 measurements from each SEM image were recorded (100 in total for each scaffold analysed) using the SEM-associated SMiles Image processing software.

#### 3.3.4.ii Water contact angle measurements (WCA)

WCA analysis was used to determine the surface properties of the co-electrospun poly ($PEGMA_{188}$)-PLGA, poly ($PEGMA_{188}$)-PET, PLGA and PET scaffolds. The static WCAs of the scaffolds were determined from sessile WCA measurements taken using distilled water and a CAM 200 sessile drop video capture apparatus at RT (20°C). The water drop was then gently placed onto the sample surface using a syringe and 20 images were taken at 1 second intervals. Readings were taken at five

different positions, each with an area of 1 $cm^2$, from the resultant 6 $cm^2$ electrospun scaffolds; the average and standard deviation were calculated.

### 3.3.4.iii Proton nuclear magnetic resonance ($^1$H NMR)

$^1$H NMR spectra were recorded on a Bruker 400 spectrometer at 399.8 MHz ($^1$H) in $CDCl_3$. All chemical shifts are reported in ppm relative to TMS. The MestReNova software was used to process the data. Samples (10 mg) of PLGA scaffolds and scaffolds prepared with PLGA containing different concentrations of poly ($PEGMA_{188}$) were cut and dissolved in 600 µL of chloroform-d. Samples (10 mg) of PET scaffolds and scaffolds prepared with PET containing different concentrations of poly ($PEGMA_{188}$) were cut and dissolved in 300 µL of chloroform-d and 300 µl of TFA. $^1$H NMR for PLGA (400 MHz, $CDCl_3$): δ 1.6 (br s, 3H, CH*$CH_3$*), 4.8 (br m, 2H, $CH_2O$) and 5.2 (br m, 1H, C*H*$CH_3$). $^1$H NMR for PET (400 MHz, $CDCl_3$): δ 4.8 (br s, 4H, 2 $CH_2$) and 8.1 (br s, 4H, $CH_{aromatic}$). $^1$H NMR for poly ($PEGMA_{188}$) (400 MHz, $CDCl_3$): δ 0.9 (br s, 3H, $CH_{3\ backbone}$), 1.9 (br s, 2H, $CH_{2\ backbone}$), 3.4 (br s, 3H, $OCH_3$), 3.6 (br m, 6H, $OCH_2$) and 4.2 (br s, 2H, $COOCH_2$).

### 3.3.4.iv X-ray photoelectron spectroscopy (XPS).

The surface chemistry of PLGA, PLGA-2% poly ($PEGMA_{188}$), PLGA-10% poly ($PEGMA_{188}$), PET, PET-2% poly ($PEGMA_{188}$) and PET-10% poly ($PEGMA_{188}$) scaffolds were analysed using the Kratos Axis Ultra XPS instrument with a monochromated Al $K_\alpha$ X-ray source (1486.6 eV) operated at a 10 mA emission current and 12 kV anode potential. The spectrometer was operated in the fixed analyser transmission mode, with pass energy of 80 eV for wide scans and 20 eV for

high-resolution scans. All samples were analysed at seven positions with an analysis area of approximately 300 × 700 μm defined by the slot aperture. Survey scans were acquired for 20 minutes each and high-resolution scans for up to 10 minutes, depending on the signal to noise observed. The survey scans and high-resolution scans had a step size of 0.5 eV and 0.1 eV, respectively. Samples were inserted into an airlock and the chamber was evacuated for approximately 16 h before the transfer of the samples into the main ultrahigh-vacuum chamber. Electrons emitted from the top surface were taken through an electrostatic/magnetic lens system (hybrid lens) and a hemispherical analyser, with electron detection and counting achieved with a delay line detector (DLD). The pressure in the analysis chamber was maintained at 3 × $10^{-9}$ Torr or less throughout the experiment. The high-resolution scans were charge corrected to the aliphatic component of the C1s core level (285.0 eV) for chemical state assignment. The areas were quantified to compare the amounts of each element present using the CasaXPS software version 2.3.16 with empirically modified sensitivity factors provided by the manufacturer.

### 3.3.5 Maintenance and passage of red fluorescent protein (RFP)-expressing 3T3 fibroblast cells

All cell-culture manipulations were performed using aseptic procedures in a Class II microbiology safety cabinet. The RFP-expressing 3T3 fibroblast cells (NIH 3T3 cells; a gift from Dr. James Dixon, Nottingham, UK) [349], and the start and end of the experimental period was between passages 62–72. Cells were cultured in Dulbecco's modified Eagle's medium (DMEM; 500 mL, Gibco [Invitrogen™, LTD]) supplemented with 10% (*v/v*) foetal calf serum (FCS, 50 mL), 100 units/mL penicillin, 100 μg/mL streptomycin (Sigma-Aldrich Poole, UK) and non-essential

amino acids solution (5 mL; Sigma-Aldrich, UK; 3T3 media). They were maintained in T75 flasks in a humidified incubator at 37°C and with 5% $CO_2$ in air. When the cells reached 70–80% confluency, they were passaged by rinsing them once with phosphate-buffered saline (PBS) and after aspirating the PBS they were incubated with 3 mL of 0.255% *(w/v)* trypsin and 2 mM EDTA for 3 minutes, followed by the addition of 7 mL of 3T3 media to stop the activity of trypsin. The cells were collected by centrifugation at 200 *xg* using a Sigma Laboratory centrifuge 2–16 K (Scientific Laboratory Supplies, UK) for 5 minutes. The cell pellet was re-dispersed in 1 mL of fresh media.

### 3.3.6 Scaffold sterilization and seeding

Fibrous scaffolds were cut into discs (areas = 1 $cm^2$) using a trephine (stainless steel cylinders with a diameter of 1 cm) and placed in sterile non-tissue-culture-treated 6 well plates. Each scaffold was sterilized with UV radiation for 20 minutes on each side, and then incubated at 37°C with 2 mL of PBS containing 100 μg/mL of gentamicin/amphotericin (AB/AM), (10 mL of PBS: 100 μL of AB/AM) for 24 h. The scaffolds were then washed with warm PBS and pre-incubated in 3T3 media, as described in, section 3.3.5 for 24 h. The 3T3 cells were seeded on scaffolds at a density of $1 \times 10^5$ cells/mL and cultured for five days at 37°C in 5% $CO_2$ in air. (n = 9 total, three scaffolds of each polymer, from three different batches).

### 3.3.7 Cell response to culture on the thermo-responsive scaffolds

#### 3.3.7.i Assessing cell viability using the AlamarBlue® (AB) assay

The AB assay is an indirect measure of cells' metabolic activity and is used to confer cell viability. Figure 3.2, illustrates the concept of the AB assay. Resazurin is the active ingredient of the AB reagent and is a non-toxic, cell-permeable compound that is stable in culture medium, which allows the continuous measurement of cell proliferation *in vitro* [350]. It is blue in colour and virtually non-fluorescent. Upon entering metabolically active cells, resazurin is reduced to resorufin, a compound that is red in colour and highly fluorescent. Healthy living cells maintain a reducing state within their cytosol. This "reducing potential" of the cells converts the AB reagent into a detectable fluorescent (or absorbent) product. Therefore, cell viability is proportional to the fluorescence intensity/absorbance or colour of the media surrounding the cells [350]. A working AB solution of 10% (*v/v*) was prepared by diluting 1 mL of AB stock solution (Invitrogen) in 9 mL of Hanks Balanced Salts Solution (HBSS) without phenol red and serum (Sigma), followed by filter sterilisation through a 0.2 µm filter. The assay was carried out for 90 minutes, then the fluorescence intensity was measured at 560 nm (excitation) and 590 nm (emission) using a plate reader (TECAN, infinite ® M200, Männedrof, Switzerland).

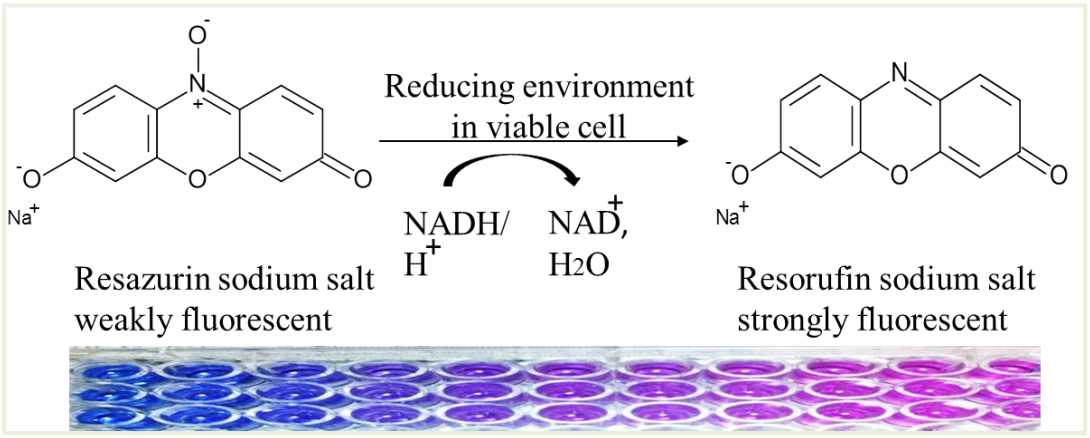



**Figure 3.2:** AlamarBlue® assay principle, modified from [351]

The cultured 3T3 cell viability experiments were conducted for five days, with fresh solution prepared on each day of the assay, as described in Figure 3.3. At day 0, the AB assay was conducted after 6 h of seeding the scaffolds. Scaffolds were transferred to a new 6 non-tissue-culture well plate and washed 3 times with warm, sterile PBS to remove any unattached cells. Two millilitres of the AB solution was added to each scaffold well before incubation at 37°C in 5% $CO_2$ for 90 minutes. After incubation, 200 µL of the AB working solution was transferred to a 96 well plate. The plate was then wrapped in foil until the fluorescence measurements were carried out. Scaffolds were washed 3 times with warm PBS then returned to the same cell culture media and incubated at 37°C in 5% $CO_2$ until the next day. Detachment at day 2 was carried out by lowering the temperature to 17°C for 10 minutes for both the test (thermo-responsive PLGA or PET) and control (PLGA and PET alone) scaffolds. Cell numbers were calculated using the equation obtained from a 3T3 fibroblast calibration curve. (n = 9 total, three scaffolds from three different batches. Three independent experiments were carried out with three technical replicates in each experiment).

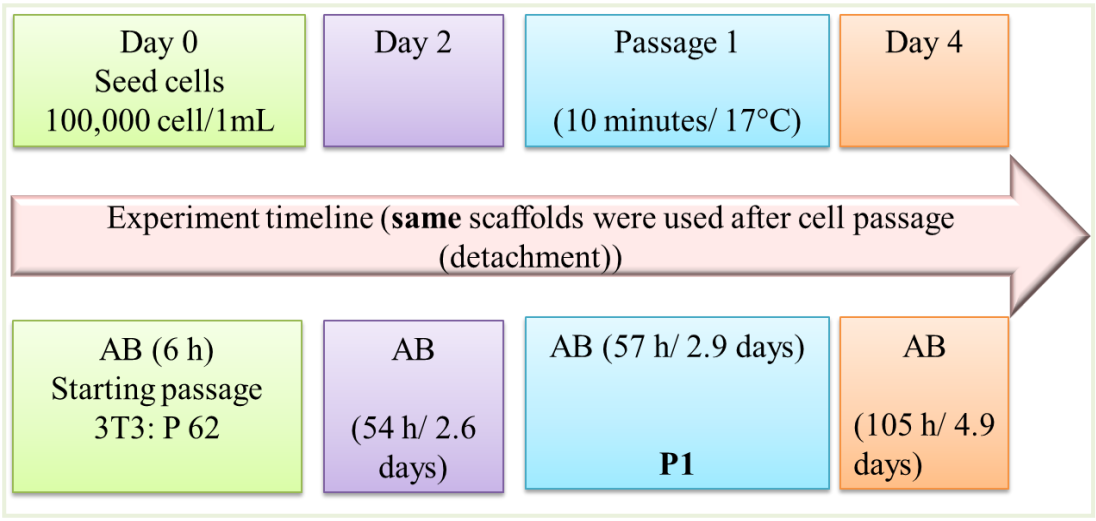



**Figure 3.3:** Schematic representing the AB experiment timeline for cultured 3T3 fibroblast cells

### 3.3.7.ii Cell imaging and image analysis

RFP-expressing 3T3 fibroblast cells adhesion, proliferation and detachment were analysed using a Nikon Eclipse TS 100 inverted microscope using green fluorescence at an excitation wavelength of 558 nm and emission of 583 nm; images were taken using a DS-L3 Nikon capture unit (20x objectives). The thermo-responsive surface properties were determined by changing the environmental temperature above and below the LCST of the poly ($PEGMA_{188}$) polymer (37°C and 17°C, alternatively) in order to allow cell attachment, detachment and reattachment to the same scaffold.

### 3.3.7.iii Cell fixation and preparation for SEM

The cell morphology and spreading were examined using SEM. Prior to SEM, the medium in the 6 well plates was removed and the cultivated cell scaffolds were washed for 5 minutes with PBS three times. The cells were fixed with 2.5%

glutaraldehyde (500 mL, TAAB UK) for 24 h at 4°C. The glutaraldehyde was removed and the scaffolds were washed with PBS three times, each for 15 minutes. Further fixation in 1% (*v/v*) osmium tetroxide (100 mL, TAAB, UK) for 1 h was carried out; the samples were then washed with $dH_2O$ three times, each for 15 minutes. Samples were dehydrated through a graded series of ethanol with concentrations of 25, 50, 70, 90, 95, and 100% (*v/v*), each for 10 minutes. Finally, the samples were chemically dried in hexamethyldisilazne (HMDS; 100 mL, Sigma) for 10 minutes, then air-dried for 24 h. Cell-scaffold constructs were then mounted onto aluminium holders and sputter-coated with gold for 4 minutes before analysing them on a JEOL SM 1100 SEM. The accelerating voltages used were in the range of 10–30 kV and the working distances ranged from approximately 15 to 35 cm.

### 3.3.8 Statistical analysis

Data were expressed as the mean ± standard deviation (SD). Statistical analyses were performed using the two-way ANOVA test with multiple comparisons using the software package Prism (GraphPad Prism6, San Diego CA). Significant differences were determined at $p \leq 0.05$. Statistical significance was set as non-significant (ns) for $p > 0.05$, significant (*) for $p \leq 0.05$, very significant (**) for $p \leq 0.01$, highly significant (***) for $p \leq 0.001$ and very highly significant (****) for $p \leq 0.0001$.

## 3.4 Results and discussion

The ultimate objective of this study was to further develop electrospun thermo-responsive fibre-based scaffolds and to illustrate their potential as a cell culture substrate for enzyme-free passaging. To achieve this, different concentrations of the thermo-responsive poly ($PEGMA_{188}$) were used, and their effect on fibres' morphology, wettability and composition were examined. Additionally, fibroblast 3T3 cells were used as an exemplar mammalian cell type for initial cell expansion and passaging on these co-electrospun scaffolds.

### 3.4.1 Preparation and characterisation of thermo-responsive co-electrospun scaffolds

Blend-electrospinning was used to create thermo-responsive scaffolds as it is an easy and effective one-step approach to modulate the composition, as well as the properties, of the resultant materials [352]. Concentrations of 18.5% (*w/v*) PLGA and 30% (*w/v*) PET polymers were chosen based on the previous work conducted in Chapter 2, section 2.4.1.i. Additionally, the same electrospinning parameters were used; including a flow rate of 4 mL/h, an applied voltage of 19 kV and a working distance of 15 cm; due to the uniformity and bead-less electrospun fibres that were achievable with these settings.

Co-electrospinning of poly ($PEGMA_{188}$) with PLGA or PET can be considered a new approach for the creation of thermo-responsive scaffolds in a single-step method rather than carrying out post-electrospinning modifications. Different concentrations of the thermo-responsive poly ($PEGMA_{188}$) (0, 2, 4, 6, 8 and 10% [*w/v*]) were added

to 18.5% PLGA (*w/v*) and 30% PET (*w/v*) polymer solutions for co-electrospinning. The SEM analysis of the resultant co-electrospun fibres in comparison with the control PLGA fibres alone is shown in Figure 3.4, illustrated the formation of bead-less co-electrospun fibres. Furthermore, a uniform fibre distribution with an average fibre diameters of 3.6 ± 0.42 µm, 3.8 ± 0.45 µm, 5.5 ± 0.7 µm, 5.8 ± 0.75 µm and 6.1 ± 0.72 µm, for the 18.5% (*w/v*) PLGA blended with different concentrations of poly ($PEGMA_{188}$) (2, 4, 6, 8 and 10% [*w/v*], respectively) were observed. The addition of the thermo-responsive polymer did not affect the fibre morphology or bead formation in the scaffolds. However, the fibre diameters of the co-electrospun scaffolds increased significantly with the increase in the thermo-responsive polymer concentration. Co-electrospun scaffolds from higher poly ($PEGMA_{188}$) concentrations (6, 8, and 10%, [*w/v*]), resulted with higher average fibre diameters which were very highly significant ($p \leq 0.0001$), compared with the average fibre diameter of PLGA alone of 3 ± 0.8 µm. While co-electrospun scaffolds from lower poly ($PEGMA_{188}$) concentrations (2 and 4%, [*w/v*]), resulted with higher average fibre diameters which were very significant ($p \leq 0.01$), compared with the average fibre diameter of PLGA alone.

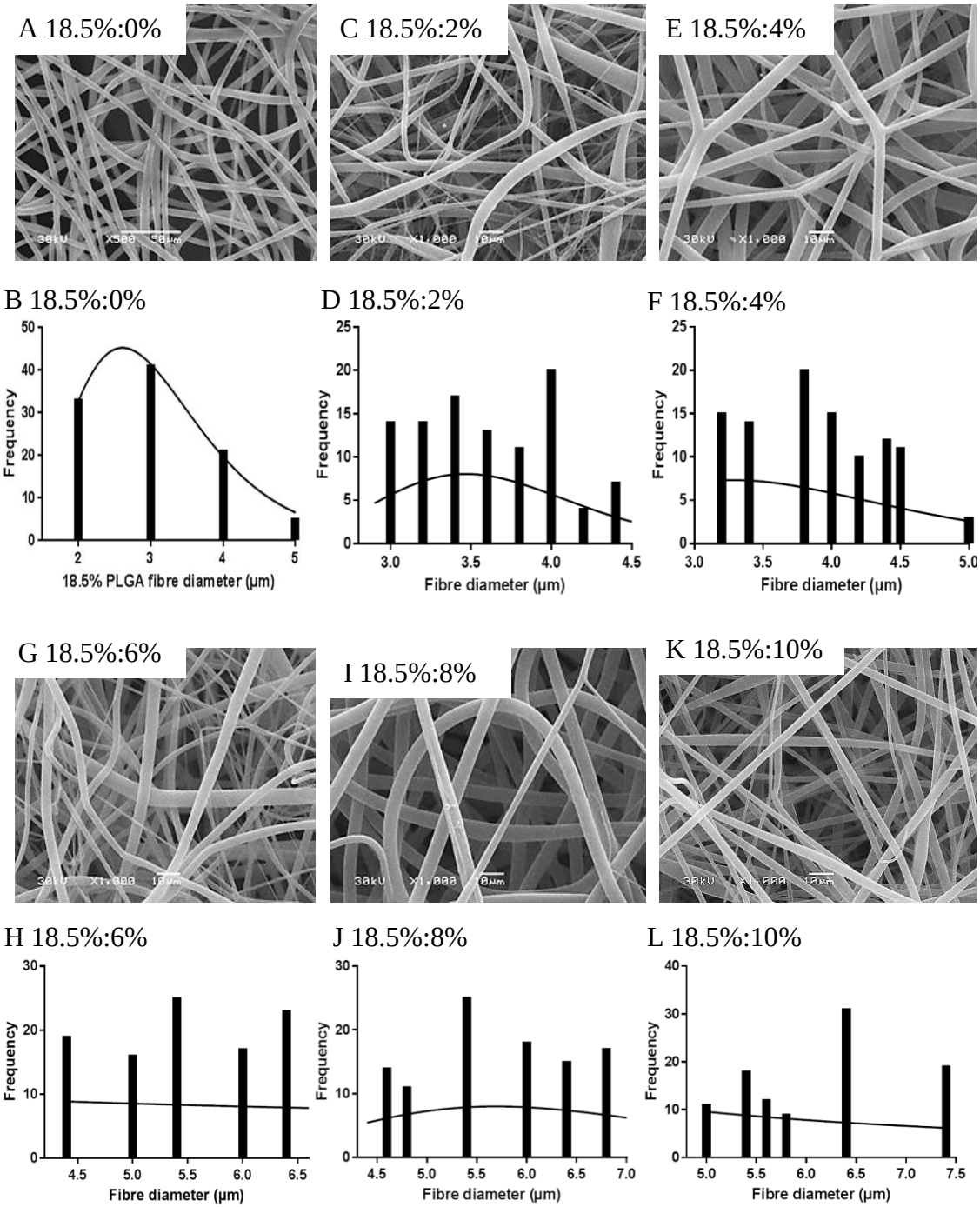



**Figure 3.4:** Representative SEM images and histogram charts of co-electrospun PLGA-poly ($PEGMA_{188}$) fibres showing the surface morphology at magnification powers of x1000, and frequency of fibre diameter (µm), of six different polymer solution concentrations ratios A-B) 18.5%: 0% (*w/v*), C-D) 18.5%: 2% (*w/v*), E-F) 18.5%: 4% (*w/v*), G-H) 18.5%: 6% (*w/v*), I-J) 18.5%: 8% (*w/v*) and k-L) 18.5%: 10% (*w/v*). For histogram charts 20 measurements from each SEM image were recorded (100 in total), n = 5, n represent the number of replicates were taken from one batch of each scaffolds. Scale bars = 10 µm except image A) = 50 µm.

The SEM analysis of the resultant co-electrospun fibres in comparison with the control PET fibres alone is shown in Figure 3.5, illustrated the formation of bead-less co-electrospun fibres. Furthermore, a uniform fibre distribution with an average fibre diameters of 838.9 ± 195 nm, 877 ± 195 nm, 955 ± 182 nm, 1067 ± 179 nm and 1304 ± 339 nm, for 30% (*w/v*) PET blended with different concentration of poly ($PEGMA_{188}$), (2, 4, 6, 8 and 10% [*w/v*], respectively) were observed. Fibre diameters of the co-electrospun scaffolds increased significantly with the increase in the thermo-responsive polymer concentration in the solution. PET-co-electrospun scaffolds from higher poly ($PEGMA_{188}$) concentrations (6, 8, and 10%, [*w/v*]), resulted with higher average fibre diameters which were very highly significant ($p \leq 0.0001$), compared with the average fibre diameter of PET alone of 836.2 ± 172.7 nm. While co-electrospun scaffolds from lower poly ($PEGMA_{188}$) concentrations (2 and 4%, [*w/v*]), resulted with average fibre diameters which were not significantly different ($p > 0.05$) from that with PET alone.

To conclude, from the SEM images and fibre diameter analysis in Figure 3.4 and Figure 3.5 , co-electrospun scaffolds made of PLGA or PET, with 2% and 4% (*w/v*) concentrations of poly ($PEGMA_{188}$) were considered to be chosen for future cell-culture studies as they rendered beadless, uniform fibres with fibre diameters close to the control PLGA or PET fibre diameters. The higher poly ($PEGMA_{188}$) concentrations in the blend PLGA-poly ($PEGMA_{188}$) solution resulted in higher fibre diameters of up to 6.1 µm, which is significantly ($p \leq 0.0001$), greater than the 3 µm diameter when PLGA was used alone. A similar trend was observed with PET, as higher poly ($PEGMA_{188}$) concentrations in the blend PET-poly ($PEGMA_{188}$) solution resulted in higher fibre diameters of up to 1304 nm, which is also significantly ($p \leq$

0.0001), a lot higher than when PET was used alone (836.2 nm). Due to the similar fibre diameters and morphology resulting from the addition of the chosen concentrations of poly ($PEGMA_{188}$), any differences in the cell response between the blended and control scaffolds can be related to the effect of the thermo-responsive polymer rather than the fibre diameters or morphology.

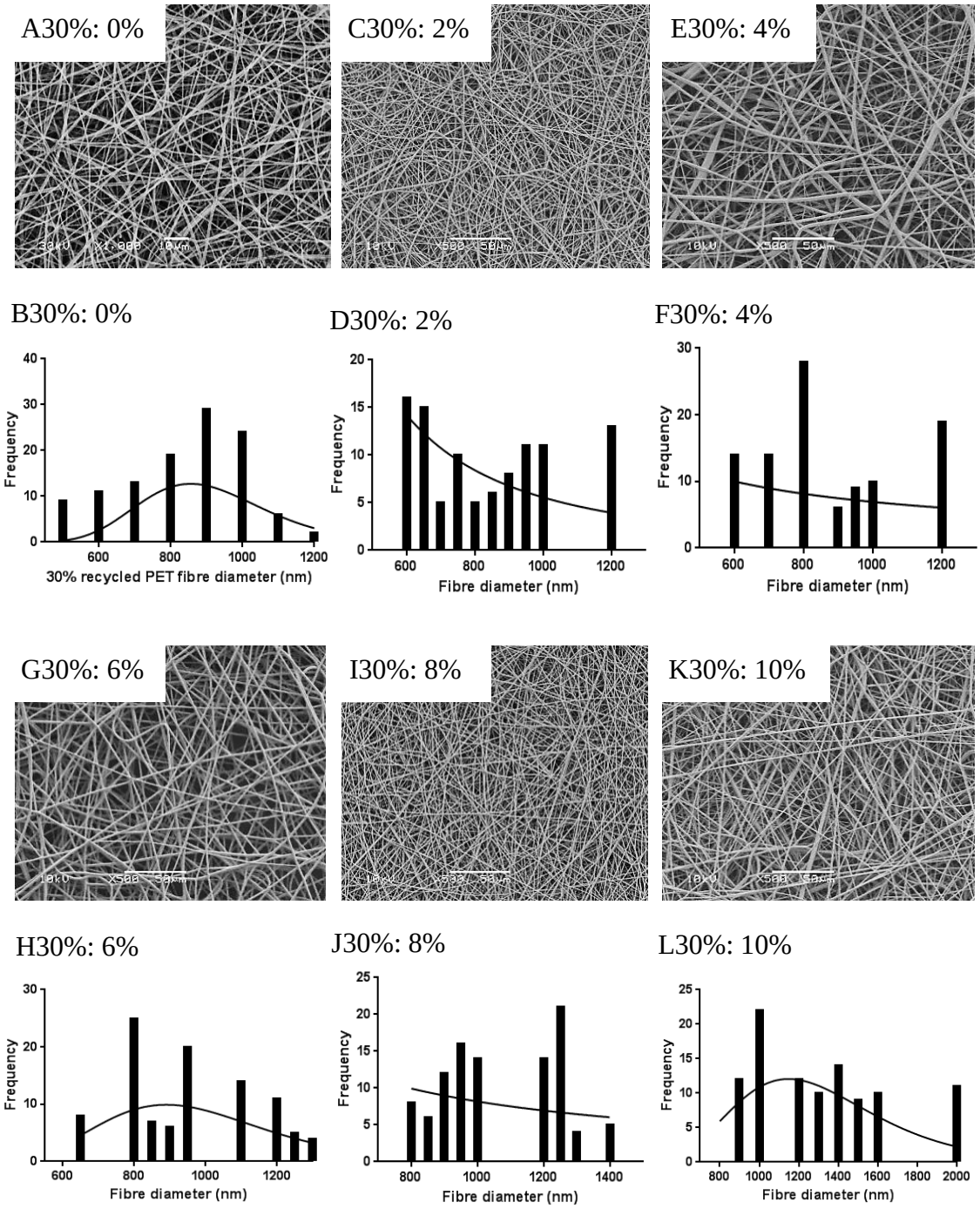



**Figure 3.5:** Representative SEM images and histogram charts of co-electrospun PET-poly ($PEGMA_{188}$) fibres showing the surface morphology at magnification powers of x500, and frequency of fibre diameter (nm), of six different polymer solution concentrations ratios A-B) 30%: 0% (*w/v*), C-D) 30%: 2% (*w/v*), E-F) 30%: 4% (*w/v*), G-H) 30%: 6% (*w/v*), I-J) 30%: 8% (*w/v*) and k-L) 30%: 10% (*w/v*). For histogram charts 20 measurements from each SEM image were recorded (100 in total), n = 5, n represent the number of replicates were taken from one batch of each scaffolds. Scale bars = 50 µm.

The absence of beads has been proven to influence cell adhesion and growth on electrospun scaffolds. A recent study showed that the lowest NIH 3T3 fibroblast cell adhesion and minimal growth kinetics were observed on beaded electrospun PCL scaffolds, despite having the lowest average fibre diameter of 117 nm, in comparison with uniform bead-less fibres [293]. Moreover, beads have an influence on the scaffold loading characteristics, it has been reported that the formation of beads among blend PNIPAAm/PEO fibres reduced the length to diameter ratio of the fibres and, thus, was detrimental to the scaffold's vitamin B12 loading [353].

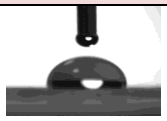
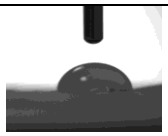
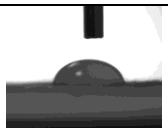
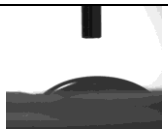
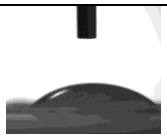
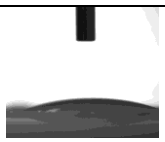
Bead-less fibres were obtained through varying different electrospinning parameters such as the polymer solution concentration, flow rate and working distance, which were described in detail in the previous chapter. Briefly, higher polymer concentrations, which influence the viscosity of the solution and droplet surface tension, generated uniform bead-less fibres with higher fibre diameters [173, 175, 354]. It was reported that when an aqueous silk solution was electrospun, no fibres were formed because the viscosity and surface tension of the solution were not high enough to maintain a stable drop at the end of the capillary tip. However, with the addition of PEO to the solution, a stable drop at the end of the capillary tip was achieved. Moreover, a slight increase in the silk concentration from 6.3 to 7.2% (*w/v*) in the blend silk/PEO polymer solution resulted in a slight increase in the average fibre diameter from 700 to 740 nm [355].

Furthermore, concentration of 18.5% PLGA and 30% PET with different poly ($PEGMA_{188}$) concentrations were co-electrospun at a high flow rate of 4 mL/h, which produced fibres on the collecting plate in accordance with prior reports

regarding appropriate flow rates and solution viscosities [327]. Moreover, as the concentration, or equivalently, the viscosity increases, a higher electrical force of 19 kV was required to overcome both the surface tension and the viscoelastic force required to stretch the fibres. A study showed that an increase in the threshold voltage from 4.3 to 5.6 kV was required when the concentration of a polyurethaneurea copolymer solution was increased from 3.8 to 12.8% (*w/v*) in order to obtain fibres on the collecting sheet. Another study that described the electrospinning of a collagen/PEO blend showed that an increase in the collagen weight ratios from 1:1 to 3:1 necessitated an increase in voltage from 22 to 23.5 kV, respectively [356]. Additionally, a distance of 15 cm between the syringe and the collecting surface was great enough for the solvent to evaporate in time for the fibres to form. Many studies have been conducted using a working distance of between 10 and 20 cm; by increasing the distance, thinner and bead-less fibres were obtained [252, 295].

Confirmation of the presence of poly ($PEGMA_{188}$) in the co-electrospun scaffolds was provided via WCA measurements, $^{1}H$ NMR and XPS. The wettability changes in the resultant electrospun scaffolds were investigated using WCA measurements, as shown in Table. 3-2. At 20°C, the average wettability of the PLGA and PET scaffolds alone was low ($\theta = 131 \pm 9.6°$ and $105 \pm 4.7°$ respectively), indicating a hydrophobic surface. As apparent from Table. 3-2, co-electrospinning of the amphiphilic polymer with PLGA or PET led to increases in the scaffolds' wettability with increasing poly ($PEGMA_{188}$) concentration. These values are in good agreement with data in the literature for similar polymers [200, 205, 251, 357-359].

**Table. 3-2** WCA measurements (θw), of co-electrospun scaffolds surfaces. Data shown for each surface are the mean of five independent measurements ± standard deviation.

| Poly ($PEGMA_{188}$) | PLGA($\theta_w$) | PET($\theta_w$) | Water droplet on (PLGA) scaffolds surface |
|---|---|---|---|
| **0%** | 131 ± 9.6° | 105 ± 4.7° |  |
| **2%** | 87.5 ± 3.1° | 96.9 ±13.5° |  |
| **4%** | 74.9 ± 12.9° | 73.7 ± 11.9° |  |
| **6%** | 71.8 ± 9.1° | 71.3 ± 34.8° |  |
| **8%** | 57.6 ± 28.2° | 46.1 ± 8.6° |  |
| **10%** | 43.5 ± 9.8° | 42.2 ± 9.2° |  |

However, some of the co-electrospun scaffold samples showed differences in their wettability behaviour, as shown in Figure 3.6. This was investigated further and it was found that some areas of the PLGA-8% poly ($PEGMA_{188}$) scaffolds yielded low WCA measurements (θ = 36°, 34° and 44°), indicating hydrophilicity. However,

other areas displayed higher WCA measurements that were indicative of hydrophobicity (θ = 105° and 60°). Similar data were obtained from the PET-6% poly ($PEGMA_{188}$) scaffolds, where some areas were hydrophilic, with WCA measurements of 80.3°, 37° and 32.5°; whereas, other areas were hydrophobic, with WCA measurements of 104.5° and 102°. It is postulated that this was most likely due to a heterogeneous distribution of the poly ($PEGMA_{188}$) on the fibre surface during the electrospinning process. This is, perhaps, due to the electrospinning process itself, or the small diameters of the fibres, which limits hydrophobic/hydrophilic partitioning.

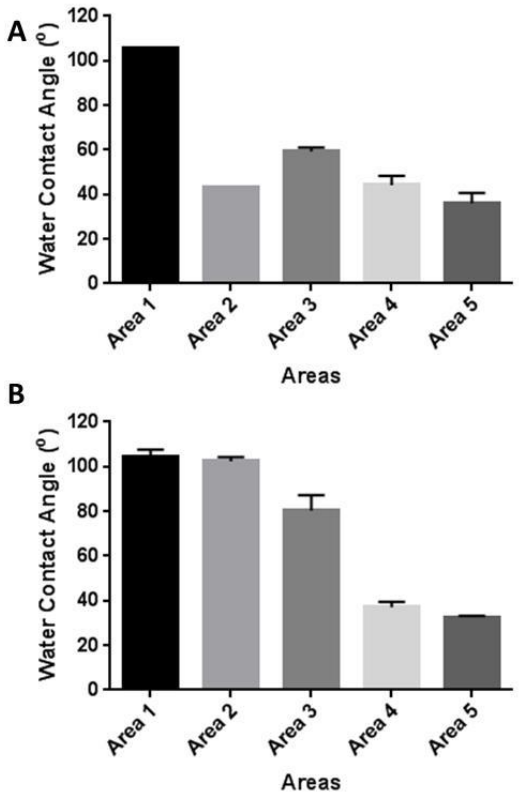



**Figure 3.6:** Differences in wettability represented by measuring the WCA of five different areas of the same co-electrospun scaffold A) 18.5% PLGA-8% poly ($PEGMA_{188}$) and B) 30% PET-6% poly ($PEGMA_{188}$) (*w/v*). The error bars represent the mean of 20 measurements in that area with standard deviation; the experiment was conducted two times for each scaffold type (n=2 batches).

Surface wettability is considered an important factor associated with substrate engineering for cell-culture applications as it influence cell attachment and their subsequent recovery from the substrate surface [360]. It is proven that NIH 3T3 fibroblast cell attachment, spreading and cytoskeletal organization were significantly greater on hydrophilic glass surfaces modified with oxidized thiol or quaternary amine groups, when compared to hydrophobic glass surfaces modified with methyl groups. Among the hydrophilic surfaces, different surface wettability characteristics influenced cell attachment, but not cell area, shape or cytoskeletal organization. Moderately hydrophilic surfaces with WCA measurements of 20° to 40° promoted the highest levels of cell attachment [361]. Another study showed that fibronectin-receptor-rich focal adhesion and the formation of actin stress fibres by human fibroblasts, in addition to their proliferation rate, were higher on hydrophilic surfaces of glass or aminopropylsilane (WCA = 25°) when compared with hydrophobic surfaces of polylacetate, silicon and octadecylsilane (WCA = 111°) [362].
Modifications in the surface wettability of electrospun fibres have also been studied, with the results showing that an increase in fibre hydrophilicity led to an increase in cell attachment and proliferation. A recent study showed that composite PCL/gelatin (70:30) nano-fibrous scaffolds with a WCA of 32 ± 8° enhanced the differentiation and proliferation of nerve stem cells (C17.2 cells) when compared to PCL nano-fibrous scaffolds with a WCA of 118 ± 6°. Furthermore, the scaffolds acted as a positive cue to support neurite outgrowth [363].

To conclude, the WCA measurements show that the incorporation of poly ($PEGMA_{188}$) in the PLGA or PET polymer solutions rendered the scaffold surfaces hydrophilic, despite the concentrations that were used. However, PLGA and PET

solutions co-electrospun with a 2% (*w/v*) poly ($PEGMA_{188}$) solution, resulted in surfaces that were closer to being hydrophobic, rather than hydrophilic, with WCA measurements of 87.5 ± 3.1° and 96.9 ± 13.5°, respectively. Moreover, solutions containing higher concentrations of poly ($PEGMA_{188}$), such as 6% or 8% (*w/v*), rendered heterogeneous surfaces. Therefore, solutions containing 4% poly ($PEGMA_{188}$) were considered to be chosen for the cell-culture studies due to their moderate surface hydrophilicity with less heterogeneous distribution (indicated by a low standard deviation).

$^{1}H$ NMR analysis of the dissolved co-electrospun fibres was also conducted to confirm the presence of the thermo-responsive polymer. Irrespective of the concentration of poly ($PEGMA_{188}$) used in the initial electrospinning solution (2, 4, 6, 8 and 10% [*w/v*]), peaks attributable to poly ($PEGMA_{188}$) were observed between 3.4 - 4.3 ppm as shown in Figure 3.7 A and B for co-electrospun PLGA and PET, respectively.

Moreover, the molar ratio between PET or PLGA with poly ($PEGMA_{188}$) in the co-electrospun scaffolds were calculated as shown in Table 3-3. This conducted by assigning a diagnostic peaks of PLGA and PET, which is in this case, protons of CH group of lactic acid (1 proton) at 5.2 ppm and of the benzene ring (4 protons) at 8.1 ppm, respectively, as 1. Then integrate the diagnostic peak of poly ($PEGMA_{188}$), which was the protons of methyl group at around 3.4 ppm and then divide the integration of protons of methyl by 3. Data presented in Table 3-3, showed an overall increase in poly ($PEGMA_{188}$) ratio in co-electrospun scaffolds with increase in the polymer concentration. However, some of co-electrospun scaffolds such as

PLGA co-electrospun with 6% (*w/v*) poly ($PEGMA_{188}$) concentration showed lower molar ratio than the PLGA co-electrospun with 4%, which indicate heterogeneities and uneven coating.

**Table 3-3:** Molar ratio (Mole) of PLGA or PET with poly ($PEGMA_{188}$) in co-electrospun scaffolds

| **Poly ($PEGMA_{188}$)** | **(Poly ($PEGMA_{188}$): PLGA)** | **(Poly ($PEGMA_{188}$): PET)** |
|---|---|---|
| **2%** | (0.08 : 1) | (0.05 : 1) |
| **4%** | (0.16 : 1) | (0.05 : 1) |
| **6%** | (0.09 : 1) | (0.07 : 1) |
| **8%** | (0.16 : 1) | (0.19 : 1) |
| **10%** | (0.11 : 1) | (0.21 : 1) |

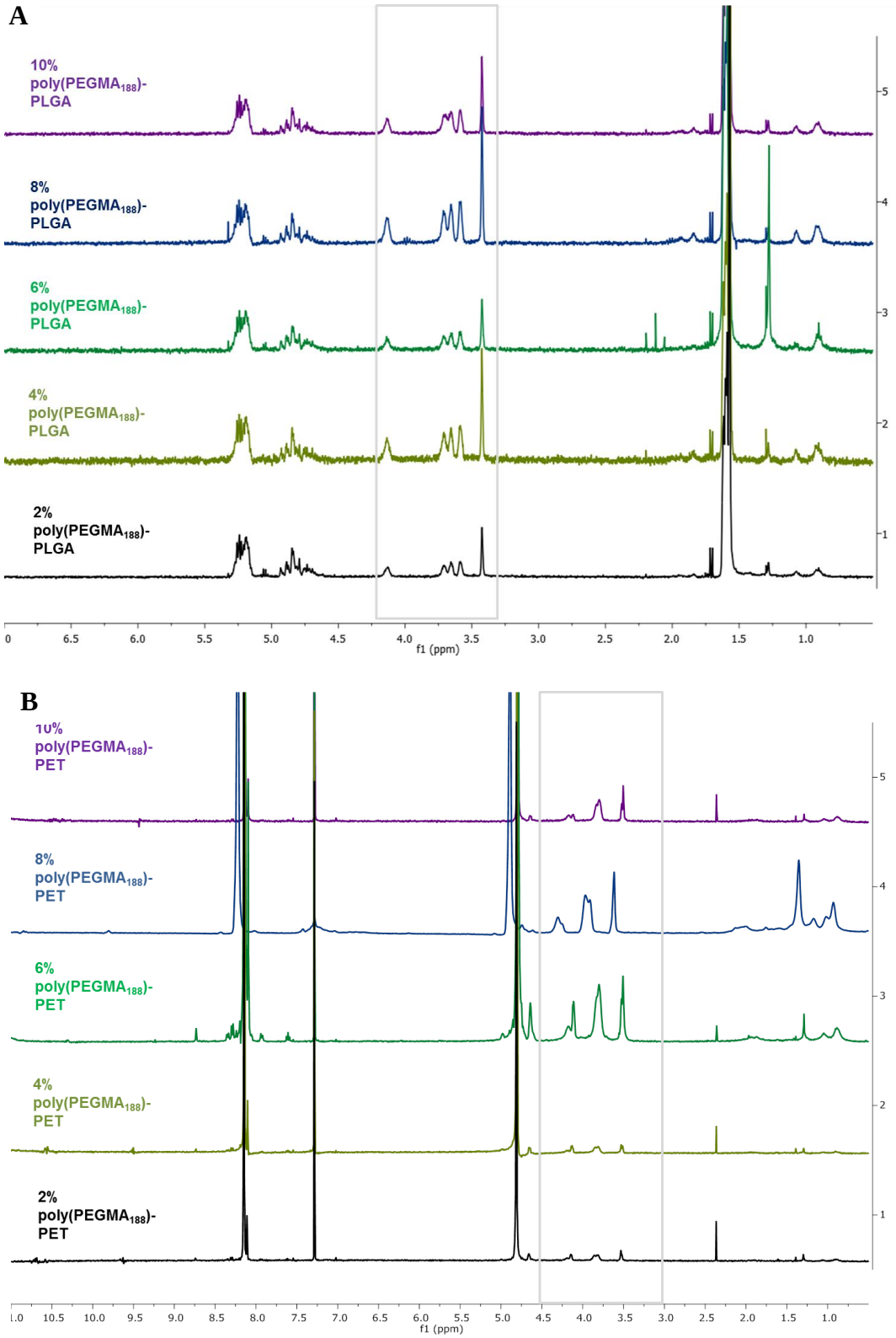



**Figure 3.7:** $^{1}$H NMR of A) PLGA scaffolds, B) PET scaffolds co-spun with different poly ($PEGMA_{188}$) concentrations of (2, 4, 6, 8 and 10% [*w/v*]), and the highlighted box indicating the presence of poly ($PEGMA_{188}$) polymer in the blend-electrospun scaffolds.

The surface chemical compositions of the PLGA, PLGA-poly ($PEGMA_{188}$), PET, and PET-poly ($PEGMA_{188}$) scaffolds were analysed using XPS. The predominant elements detected were carbon and oxygen, with no silicon signal (silicon signal; could result due to the tape used to fix scaffolds on glass slide). The XPS analysis of the carbon peaks showed three peaks which corresponded to the three binding states of carbon in PLGA (1 C-C bonded carbons at 285 eV, 2 C-O bonded carbons at 286.5 eV and 2 O-C=O bonded carbons at 288 eV) and three peaks of PET (6 C-C bonded carbons at 285 eV, 2 C-O bonded carbons at 286.5 eV and 2 O-C=O bonded carbons at 288 eV) as shown in Figure 3.8. Moreover, six peaks for co-electrospun PLGA or PET with poly ($PEGMA_{188}$), three peaks assigned to PLGA or PET and three absorptions assigned to poly ($PEGMA_{188}$) (3 C-C bonded carbons at 285 eV, 5 C-O bonded carbons at 286.5 eV and 1 O-C=O bonded carbons at 288 eV).

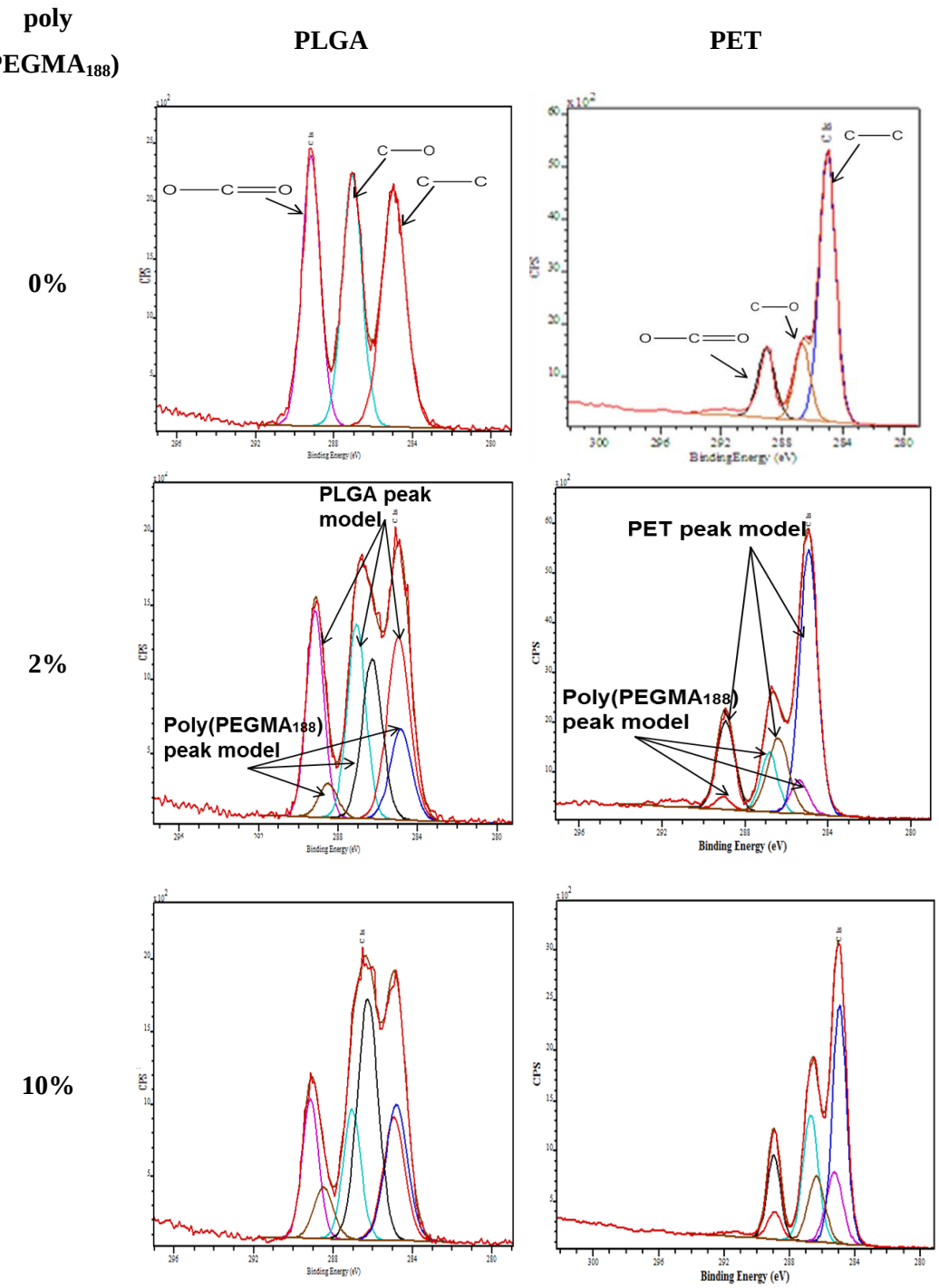



**Figure 3.8:** XPS C1s-peak of electrospun scaffolds of 18.5% PLGA and 30% PET, co-electrospun with different concentrations of poly ($PEGMA_{188}$), 0 %, 2% and 10% (*w/v*). Typical PLGA, PET and poly ($PEGMA_{188}$) carbon peaks are visible.

The assignments of the high-resolution spectra are shown in Figure 3.8, which provide qualitative confirmation of the presence of poly ($PEGMA_{188}$) in the scaffolds. Samples spun from PLGA-10% poly ($PEGMA_{188}$) yielded greater peak areas for poly ($PEGMA_{188}$) than fibres spun from PLGA-2% poly ($PEGMA_{188}$), which was in line with expectations [364]. However, the recorded intensity in Table 3-4, of a carbon band assigned to poly ($PEGMA_{188}$) in co-spun scaffolds from 10% poly ($PEGMA_{188}$) resulted in an average carbon percentage of (56 ± 16.2%) which was not significantly different ($p > 0.05$), from that of the average carbon percentage of co-spun scaffolds from 2% poly ($PEGMA_{188}$) (32 ± 4.3%). Similar results were observed with co-electrospun PET-2% poly ($PEGMA_{188}$) and PET-10% poly ($PEGMA_{188}$), with an average carbon percentage of 23 ± 3.5% and 39 ± 5.9%, respectively. This suggests that fibres spun with the higher poly ($PEGMA_{188}$) concentrations formed heterogeneous, patchy layers at or near the surface of the fibres. These findings may be related to the smaller fibre diameter that limits uniform polymer distribution on the fibre surface. Another reason could be related to the effect of the high voltage that was applied during the electrospinning process, which could separate both components in the blend solution. As the polymers were physically mixed in the solution, they may be easier to separate than chemically formulated co-polymers, which could result in the heterogeneous distribution of polymer over the scaffolds' surface.

**Table 3-4:** Carbon ratio of poly ($PEGMA_{188}$), PLGA and PET polymers in PLGA, PET and their co-electrospun with 2% and 10% (*w/v*) poly ($PEGMA_{188}$) scaffolds determined by XPS. SD represents seven different areas of each scaffold.

| Scaffolds | C1s of poly ($PEGMA_{188}$) | C1s of PLGA | C1s of PET |
|---|---|---|---|
| PLGA scaffolds | 0 ± 0% | 100 ± 0% | - |
| PLGA-2% poly ($PEGMA_{188}$) scaffolds | 32 ± 4.3% | 68 ± 4.3% | - |
| PLGA-10% poly ($PEGMA_{188}$) | 56 ± 16.2% | 44 ± 16.2% | - |
| PET scaffolds | 0 ± 0% | - | 100 ± 0% |
| PET-2% poly ($PEGMA_{188}$) scaffolds | 23 ± 3.5% | - | 77 ± 3.5% |
| PET-10% poly ($PEGMA_{188}$) | 39 ± 5.9% | - | 61 ± 5.9% |

Similar observations were reported by Hyoung *et al.* when XPS was used to estimate the surface composition of electrospun scaffolds prepared with silk in hexafluoro-2-propanol, in addition to blend co-electrospun silk/PEO in water. The N1s/C1s and O1s/C1s ratios of the silk scaffolds were 0.33 and 0.44, respectively. In the case of the silk/PEO mats, the N1s/C1s ratio decreased to 0.17 at minimum, and the O1s/C1s ratio increased to 0.49 at maximum. Since silk is relatively hydrophobic, a lower silk content on the fibre surface was expected when it was electrospun in water. However, this was not the case, perhaps due to the blend-electrospinning process or the small diameters of the fibres that limited hydrophobic/hydrophilic partitioning on the fibre surface [355]. Another study showed a similar

heterogeneous distribution of PEG/bovine serum albumin (BSA) in PCL scaffolds using the blend-electrospinning technique. In contrast, a homogeneous distribution of PEG/BSA in PCL was achieved using the co-axial electrospinning technique [365].

To conclude, the XPS data showed that there was no significant difference ($p > 0.05$) between the co-electrospun scaffolds' surfaces when higher or lower poly ($PEGMA_{188}$) concentrations (10% or 2%, respectively) were used. Therefore, from the SEM, WCA, $^{1}H$ NMR and XPS data that are summarized in Table 3-5, lower thermo-responsive polymer concentration of 4% (*w/v*) was mostly to be chosen for cell culture studies.

**Table 3-5:** A summary tables of characterisation of thermo-responsive scaffolds of 18.5% (*w/v*) PLGA and 30% (*w/v*) PET co-electrospun with poly ($PEGMA_{188}$).

| Poly ($PEGMA_{188}$) (*w/v* %) | Fibre morphology | Diameter (mean ±SD) | | WCA (mean ±SD) (°) | | XPS C1s ratio (%) | | $^1$H NMR | |
|---|---|---|---|---|---|---|---|---|---|
| | | PLGA (µm) | PET (nm) | PLGA | PET | PLGA | PET | PLGA | PET |
| 0 | Bead-less and uniform distribution | 3 ± 0.8 | 836.2 ± 172.7 | 131 ± 9.6 | 105 ± 4.7 | 100 ± 0/ 0 ± 0 | 100 ± 0/ 0 ± 0 | Presence of thermo-responsive polymer between 3.4 - 4.3 ppm. | |
| 2 | | 3.6 ± 0.42 | 838.9 ± 195 | 87.5 ± 3.1 | 96.9 ±13.5 Hydrophobic | 68 ± 4.3/ 32 ± 4.3 | 77 ± 3.5/ 23 ± 3.5 | | |
| 4 | | 3.8 ± 0.45 | 877 ± 195 | 74.9 ± 12.9 | 73.7± 11.9 | - | - | | Increase poly ($PEGMA_{188}$) ratio by increasing the polymer concentration |
| 6 | | 5.5 ± 0.7 | 955 ± 182 | 71.8 ± 9.1 | 71.3 ± 34.8 Heterogeneous | - | - | Heterogeneous | |
| 8 | | 5.8 ± 0.75 | 1067 ± 179 | 57.6 ± 28.2 Heterogeneous | 46.1 ± 8.6 | - | - | | |
| 10 | | 6.1 ± 0.72 | 1304 ± 339 | 43.5 ± 9.8 | 42.2 ± 9.2 | 44 ± 16.2/ 56 ± 16.2 Heterogeneous | 61 ± 5.9/ 39 ± 5.9 Heterogeneous | | |

### 3.4.2 Application of the thermo-responsive scaffolds to 3T3 fibroblast cell culture

This experiment aimed to evaluate the biocompatibility and thermo-responsive properties of the co-electrospun scaffolds. To investigate the effect of the incorporation of different concentrations of poly ($PEGMA_{188}$) (2, 4, 6, 8, and 10%, [*w/v*]) within the scaffolds, the initial cell adhesion, viability and proliferation were determined. In order to do this, 3T3 fibroblasts were cultured on all these scaffold types, including PLGA and PET scaffolds alone as a control. Cell attachment and detachment were observed by changing the culture environment temperature from 37°C to 17°C.

The fluorescence microscope images in Figure 3.9 and Figure 3.10 show the attachment and proliferation of the 3T3 fibroblast cells on the scaffolds comprising PLGA and PET alone, in addition to the polymers blended with different concentrations of poly ($PEGMA_{188}$). Following their culture at 37°C, cells appeared to adhere and spread on the scaffolds over the first two days of culture, indicating the biocompatibility of the scaffolds. Following culture for 2 days, cells detached from all scaffolds containing poly ($PEGMA_{188}$) once incubated at 17°C (passage 1). Cells were transferred to the same scaffold and allowed to attach again, which can be observed after 4 days in culture. In the control samples containing 0% poly ($PEGMA_{188}$), no cell detachment after decreasing the culture temperature was observed.

The biocompatibility of these scaffolds is related to the use of PLGA, PET and the PEG-based poly ($PEGMA_{188}$) polymer, which are all approved by the FDA for human

use [121, 122, 127-129]. Electrospun PLGA scaffolds have been widely reported in the literature as a 3D carrier for many cell culture types [301, 366], including stem-cell culture and differentiation, e.g. hMSC differentiation into chondrogenic and osteogenic cells was observed after an incubation time of 2 weeks on PLGA nano-fibres [367]. This was the case for PET-based electrospun scaffolds, as they were found to support the attachment and proliferation of different cell types, e.g. endothelial cells (ECs) [130], SH-SY5Y neuroblastoma cells [368] and rat MSCs [369].

Okano *et al.* described the mechanism of cell detachment from thermo-responsive substrates [231, 370, 371]. In this study, the detachment is also thought to be controlled via the surface hydration of the temperature-responsive electrospun scaffolds as the temperature is decreased from 37°C to 17°C. This surface hydration can be explained in relation to the thermo-responsive polymer chain extension and contraction that accompanies the change in temperature. Increasing the culture temperature above the polymer's LCST, collapses the poly ($PEGMA_{188}$) chains, generating a strong hydrophobic surface that is supportive of cell attachment. Below its LCST, poly ($PEGMA_{188}$) is water soluble, with an amphiphilic character due to its hydrophobic methacrylate backbone and hydrophilic pendant PEG side chains. The electrospun scaffold becomes hydrophilic; this leads to the formation of a hydration layer between the scaffold fibre surface and the cultured cells, which results in cell detachment from the thermo-responsive scaffolds. The hydrophilicity of the same surface can be reversed by increasing the temperature above the LCST, which results in dehydration of the poly ($PEGMA_{188}$) chains, leading to their collapse. A similar concept was utilised for the attachment and subsequent recovery of mESCs, from 2D

surfaces grafted with poly ($MEO_2MA$-co-OEGMA) after reducing the culture temperature to 20°C [205]. PNIPAAm thermo-responsive surfaces have also been extensively used for the enzyme-free culture of different cell types [219, 372]. For example, human keratinocytes proliferated and formed a multilayer on a PNIPAAm-grafted surface at 37°C. By reducing the culture temperature to 20°C, the multi-layered keratinocyte sheets were able to detach from the grafted surfaces without the need for enzymatic treatment [206]. Bovine carotid artery ECs were also cultured on PNIPAAm-grafted TCPS and proliferated to form confluent cell monolayers. The cell monolayers were harvested as single cell sheets via a temperature decrease from 37°C to 20°C [373]. Such cell sheet detachment was related to the hydration of the PNIPAAm-grafted surfaces as the chains were in an expanded conformation below the LCST of 32°C. However, cell attachment ensued when the surface dehydrated and the PNIPAAm chains formed a collapsed conformation above the LCST [339].

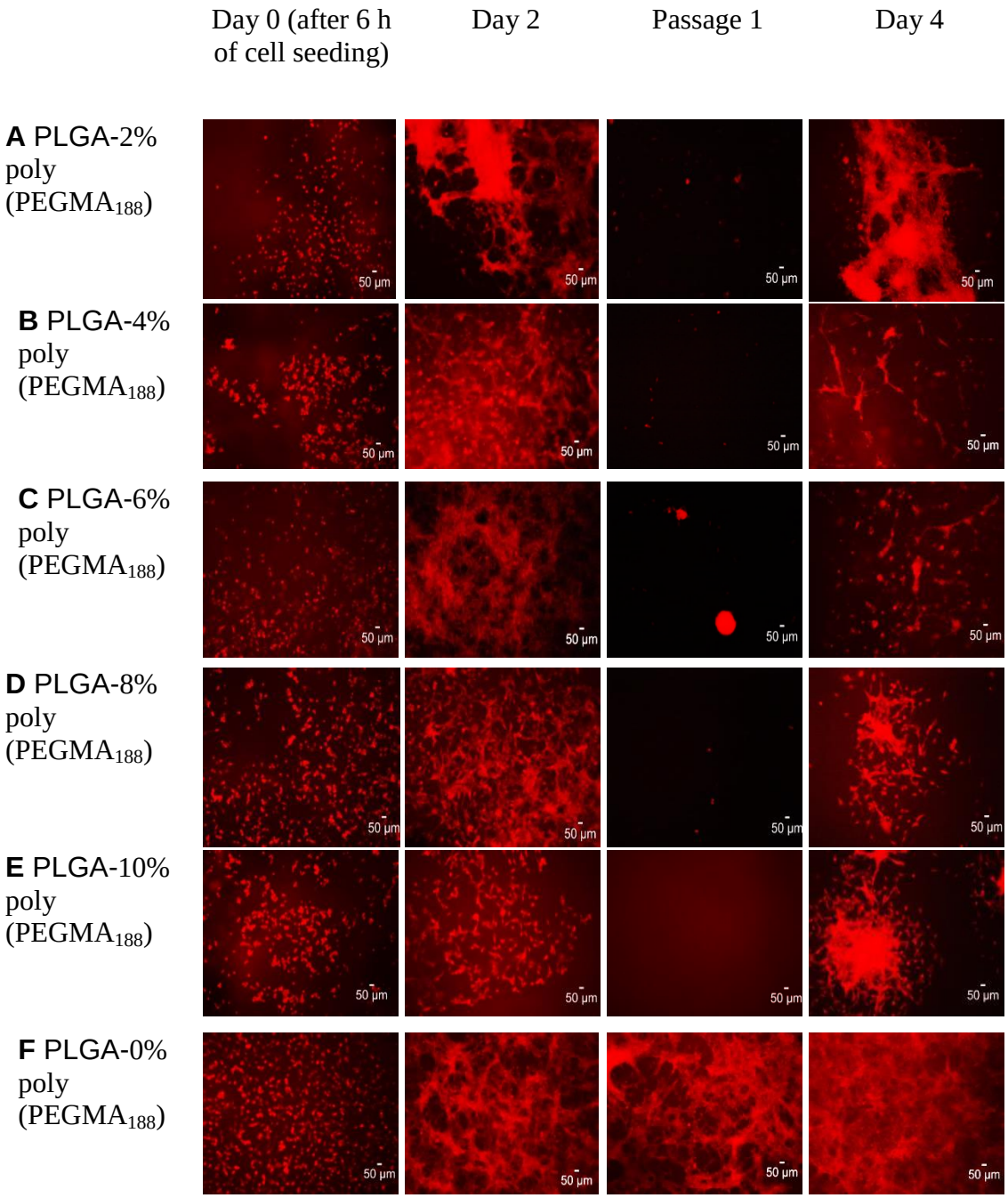



**Figure 3.9:** Representative fluorescence microscopy images showing 3T3 cells attachment to co-spun scaffolds of 18.5% PLGA with different concentration of poly ($PEGMA_{188}$); A) 2% B) 4%, C) 6%, D) 8%, E) 10% and F) 0% (*w/v*) after 6 h at varying temperature/time regimes. In day 0 and day 2 cells were allowed to attach to the surfaces at 37°C, whereas, cell detachment took place over 10 minutes at 17°C (passage 1). In day 4, re-attachment of cells occurred at 37°C on the same scaffolds. Scale bars = 50 µm.

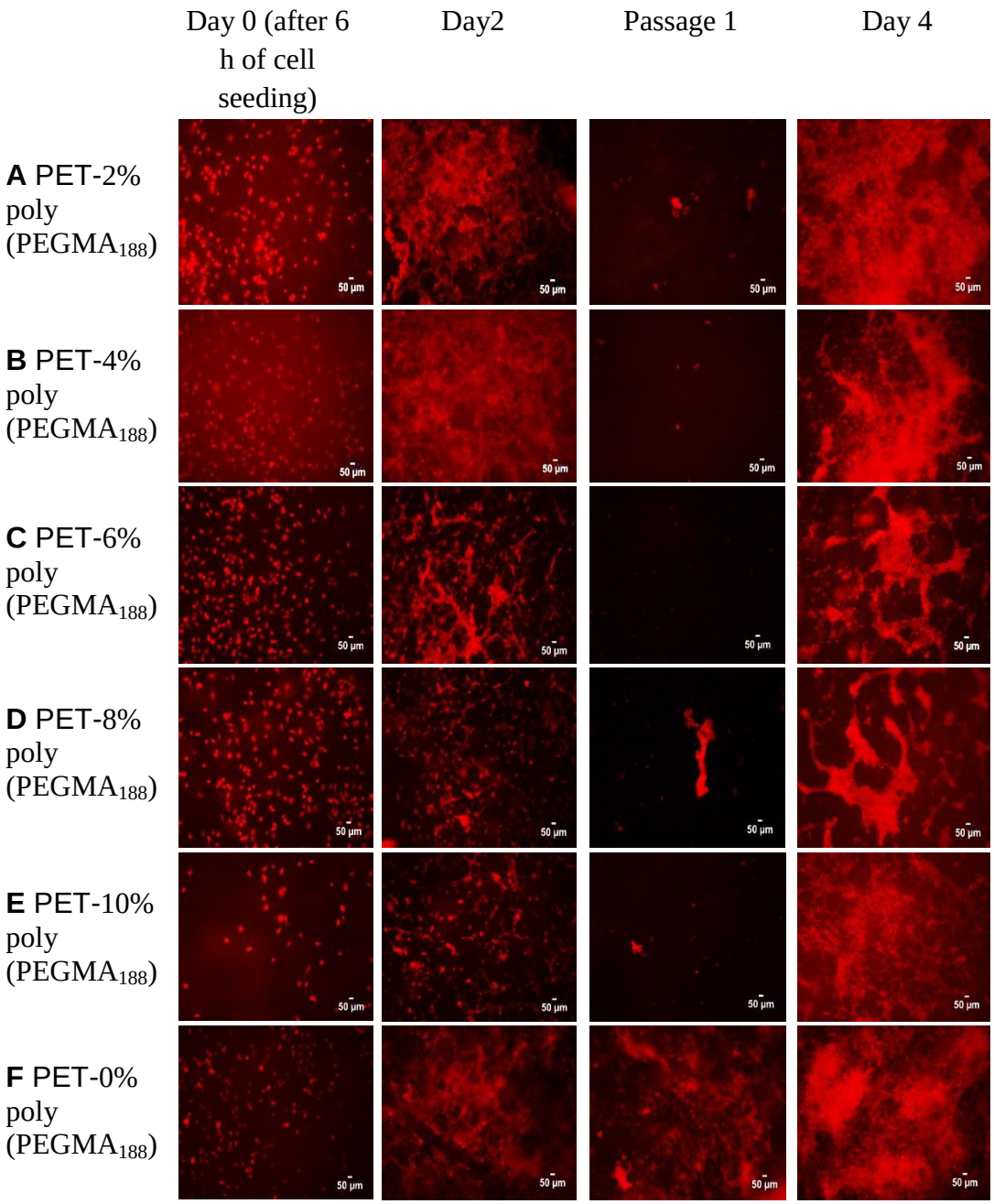



**Figure 3.10:** Representative fluorescence microscopy images showing 3T3 cells attachment to co-spun scaffolds of 30% PET with different concentration of poly ($PEGMA_{188}$); A) 2% B) 4%, C) 6%, D) 8%, E) 10% and F) 0% (*w/v*) after 6 h at varying temperature/time regimes. In day 0 and day 2 cells were allowed to attach to the surfaces at 37°C, whereas, cell detachment took place over 10 minutes at 17°C (passage 1). In day 4, re-attachment of cells occurred at 37°C on the same scaffolds. Scale bars = 50 µm.

The SEM images in Figure 3.11 showed the presence of 3T3 fibroblast cells on the fibres' surfaces 6 hours after cell seeding. One day after seeding, more 3T3 cells attached and spread on both the thermo-responsive and non-thermo-responsive PLGA scaffolds. The cell spreading on the scaffolds increased with the increasing culture time. After reducing the culture temperature to 17°C, the thermo-responsive PLGA scaffolds showed no attached cells on the surface (passage 1). In contrast, cells were present on the non-thermo-responsive electrospun PLGA scaffold's surface. This indicates that cell detachment occurred due to the presence of poly ($PEGMA_{188}$) polymer in the fibres, not due to the effect of the change in culture temperature on the cells. After 4 days of culture, the cells almost completely covered the surface of the PLGA scaffolds and showed larger spreading areas. Moreover, cells re-attached to the same PLGA thermo-responsive scaffolds, which indicates the usefulness of these co-electrospun scaffolds for supporting cell re-attachment.

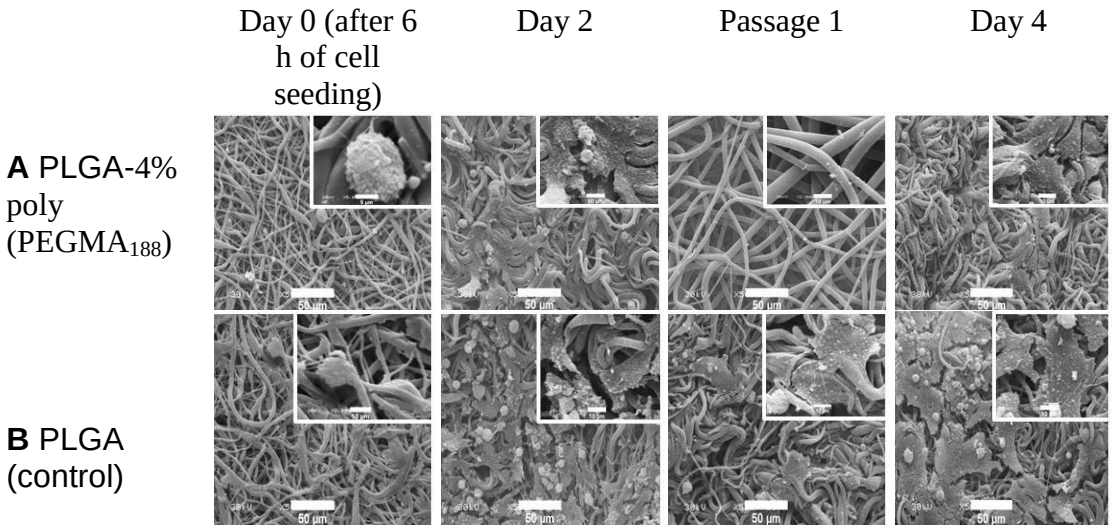



**Figure 3.11:** Representative SEM images showing 3T3 cells attachment to A) PLGA-4% poly ($PEGMA_{188}$) and B) PLGA scaffolds (control) surfaces after 6 h at varying temperature/time regimes. In day 0 and day 2 cells were allowed to attach to the surfaces at 37°C, whereas, cell detachment took place over 10 minutes at 17°C (passage 1). In day 4, re-attachment of cells occurred at 37°C. Scale bars = 50 µm. The inset images show a higher magnification view of the 3T3 cells on the scaffolds, scale bars 10 = µm.

The AB assay, was conducted to quantify the biocompatibility and thermo-responsive behaviour of co-electrospun scaffolds via detecting the change in cell numbers while changing the culture temperature over 5 days.

The outcome of the AB assay is presented in Figure 3.12 A, where differences in the cell number were reported in relation to the change in culture days. At 37°C, a significant increase in the cell number up to 100,000 cells from day 0 to day 2 was occurred, for both control and poly ($PEGMA_{188}$) containing scaffolds ($p \leq 0.0001$). At 17°C a significant decrease in cell number (~ 135,000) was observed for poly ($PEGMA_{188}$) containing scaffolds (passage 1). While no significant decrease in the cell numbers was observed at 17°C for PLGA scaffolds (control) ($p > 0.05$). A significant subsequent increase in the cell numbers was then noted on day 4, with up to 200,000 cells present on scaffolds containing (2, 4, 6 and 8% [*w/v*]) poly ($PEGMA_{188}$), and increases of 120,000 cells present on scaffolds spun from 10% (*w/v*) poly ($PEGMA_{188}$) solutions from day 2 detachment ($p \leq 0.0001$). Further AB assays were conducted with seeded PET and PET-poly ($PEGMA_{188}$) scaffolds. In each case, the attachment profiles of the cells were similar to those of the PLGA fibres as shown in Figure 3.12 B.

Differences in the cell number were reported in relation to the different poly ($PEGMA_{188}$) concentrations were also investigated on each day of culture. At day 0, no significant difference in the 3T3 fibroblast cell number was observed between the PLGA and co-electrospun PLGA-2% and 4% (*w/v*) poly ($PEGMA_{188}$) scaffolds. However, there was a significantly lower cell number on co-electrospun PLGA-6%, 8% and 10% (*w/v*) poly ($PEGMA_{188}$) than on PLGA scaffolds, which may be due to

the higher amount of poly ($PEGMA_{188}$), which could interfered the cell adhesion. Therefore, at day 2 the comparison was made between the 2% and 4% poly ($PEGMA_{188}$)-containing co-electrospun scaffolds, which showed no significant differences. Additionally, a comparison between the 6%, 8% and 10% (*w/v*) poly ($PEGMA_{188}$)-containing co-electrospun scaffolds showed a significant decrease in cell number ($p \leq 0.0001$) on the scaffolds containing 10% poly ($PEGMA_{188}$) when compared with the 6% and 8% (*w/v*) concentrations. At day 4, no significant difference was observed between the 2% and 4% (*w/v*) poly ($PEGMA_{188}$)-containing co-electrospun scaffolds. However, there were significant decreases in cell numbers ($p \leq 0.0001$) on the 10% (*w/v*) poly ($PEGMA_{188}$)-containing scaffolds compared to when 6% or 8% concentrations were used.

For the PET scaffolds, at day 0, no significant difference in 3T3 fibroblast cell numbers was observed between all the PET scaffolds. However, by day 2, significant decreases in the cell numbers ($p \leq 0.0001$) were observed on the co-electrospun scaffolds comprising PET with 8% and 10% (*w/v*) poly ($PEGMA_{188}$) when compared with the other scaffolds. Moreover, at passage 1, a significant difference in the cell numbers ($p \leq 0.001$) was observed between the lower concentrations and the 8% and 10% co-electrospun scaffolds, which is related to the initial lower cell number on day 2. On day 4, there was a significant increase in the cell numbers on scaffolds containing lower concentrations of poly ($PEGMA_{188}$), when compared with those containing higher concentrations of the polymer (8% or 10% [*w/v*]).

These differences between the cell numbers in relation to the poly ($PEGMA_{188}$) concentration may be related to the patchy surfaces when higher concentrations of

poly ($PEGMA_{188}$), 8% or 10%, were used. These cell-culture results were in agreement with the previous surface characterization of these scaffolds based on WCA measurements, XPS and $^{1}H$ MR in section 3.4.1.

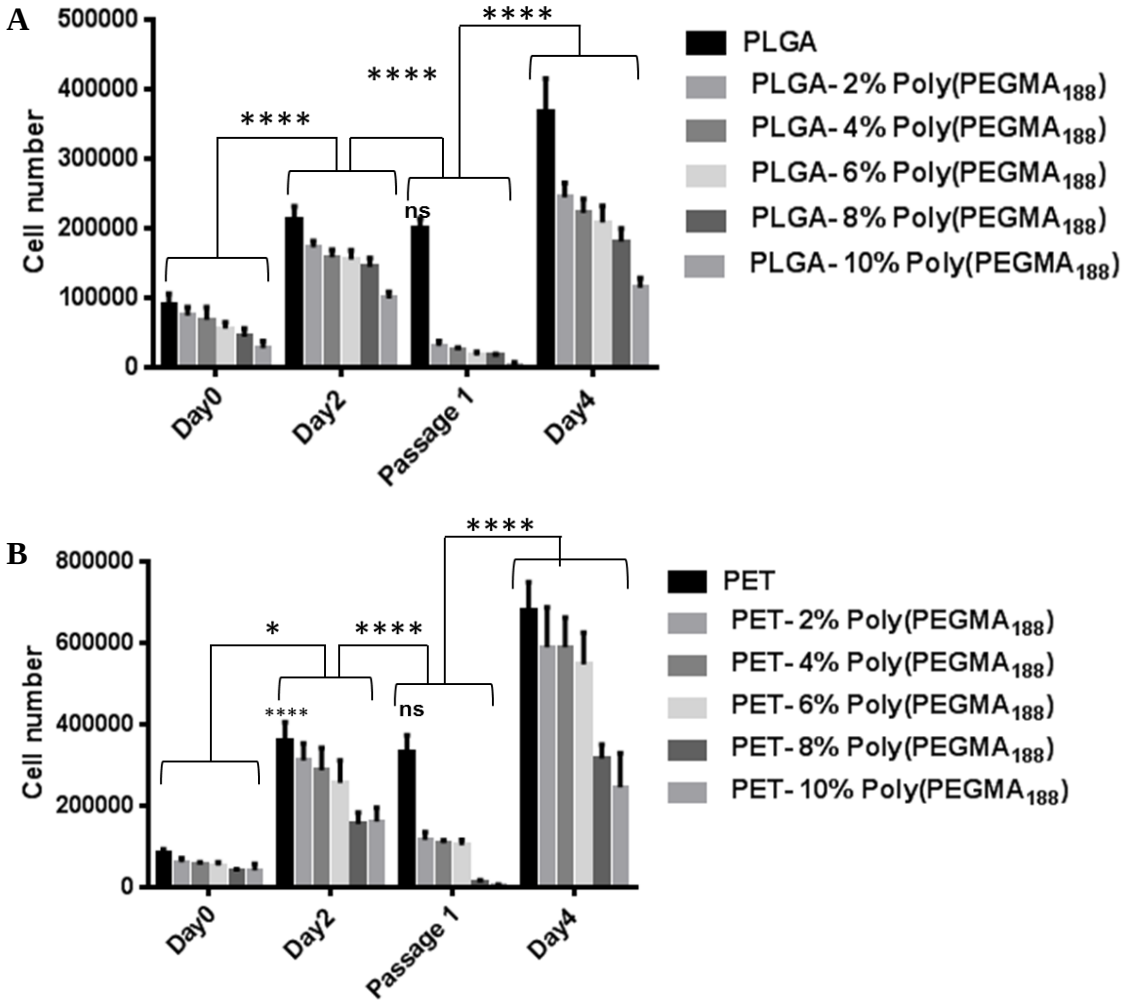



**Figure 3.12:** AB assay representing the change in cell number over the initial culture time (up to 6 h - 54 h /day 0 - day 2). Following detachment (10 minutes at 17°C / passage 1 (56 hrs)) and subsequent re-attachment (48 h at 37°C/ day 4) of 3T3 cells, on A) PLGA scaffolds and B) PET scaffolds, with different concentrations of poly ($PEGMA_{188}$). Error bars represent mean ± SD; n = 9. Statistical significance, Day 0 versus Day 2, Day 2 versus passage 1 and passage 1 versus Day 4: (ns) $p > 0.05$, (*) $P \leq 0.05$ and (****) $p \leq 0.0001$, (Two-way ANOVA).

To conclude, after application of different thermos-responsive scaffolds to 3T3 fibroblast cell culture, all scaffolds have supported cell adherence, growth and cells were recovered through a simple decrease in temperature (17°C for 10 minutes)

without the use of enzymes. However, polymer blends including 4% (*w/v*) poly ($PEGMA_{188}$) concentration will be used for further cell culture and passage studies based on the results in this chapter.

## 3.5 Conclusions

The main purpose of this chapter was to study the effect of different concentrations of the thermo-responsive polymer, poly ($PEGMA_{188}$), when used in a blend to generate electrospun fibre-based scaffolds, on the fibre morphology, fibre-surface wettability and scaffolds composition. In addition, preliminary cell culture and passage experiments confirmed the effect of the different concentrations of poly ($PEGMA_{188}$) on cell behaviour using 3T3 fibroblasts as an exemplar mammalian cell type.

The data presented demonstrates that blend-electrospinning is a promising way to create a stimuli-responsive surface with the potential for application in controllable cell culture. Different concentrations of the thermo-responsive polymer material, poly ($PEGMA_{188}$), were co-electrospun with PLGA and PET polymers. The resulting fibres with thermo-responsive surfaces were characterized using SEM, XPS, $^{1}H$ NMR and WCA measurements. These smart scaffolds were able to support 3T3 fibroblast cell adhesion and proliferation at 37°C. Furthermore, it was possible to detach the cells from the scaffolds by decreasing the temperature to 17°C, without the use of enzymes. Importantly, these cells were viable and proliferated in a similar manner to those cultured on control surfaces (PLGA or PET scaffolds). This is the first time that 3T3 fibroblast cells have been cultured and passaged on thermo-responsive co-electrospun fibres. In addition, this is the first time that poly ($PEGMA_{188}$) has been used to create thermo-responsive fibre-based scaffolds using electrospinning. This

indicates that these scaffolds show promise as a new generation of 3D culture materials for enzyme-free cell culture and passage, suitable for generating mammalian cell populations.

The next chapter (Chapter 4) will investigate the use of this thermo-responsive system for prolonged 3T3 fibroblast cell expansion and passaging experiments. Additionally, this culture system will also be used to culture and passage different cell lines, e.g. human colon carcinoma epithelial cells (Caco2) and immortalized hMSCs (ihMSCs), in order to confirm that the phenomenon is not cell-line specific.

# Chapter 4. Evaluation of thermo-responsive co-electrospun scaffolds for human colon adenocarcinoma cells (Caco2), immortalized human mesenchymal stem cells (ihMSCs) and prolonged passaging of mouse 3T3 fibroblasts

## 4.1 Introduction

Conventional cell passaging requires the use of a proteolytic enzyme, e.g. trypsin, in order to digest the cell membrane proteins, most importantly integrins, which are responsible for cell-cell and cell-substrate interactions. This process can affect cell adhesion to further substrates and also the cell quality after passaging. As the interest in cell therapy for regenerative purposes grows, there is a pressing need to develop alternative culture environments that do not require the use of enzymes in order to limit cell damage and prevent the risk of contamination. Synthetic 'smart' biomaterials, in which the bio-adhesive properties of the surface can be changed by altering environmental factors, such as temperature, without the need for proteolytic enzyme treatment, are therefore, of interest. The applications of this technology encompass different cell types, such as keratinocytes [206], limbal stem cells [374], oral mucosal epithelial cells [375, 376] and many others.

The use of 2D thermo-responsive surfaces has been previously described and used in different mammalian cell culture and for their prolonged passage in order to avoid the deteriorated effect of trypsin treatment upon cultured cells [203]. Okano and co-workers have pioneered the use of the thermo-responsive PNIPAAm-based polymers as switchable surfaces for cell attachment and detachment [338, 377]. Following on

from the Okano study, further cell-sheet engineering methods have been proposed, whereby cultured bovine aortic endothelial cells were harvested as intact sheets, along with their deposited fibronectin matrix, from PNIPAAm-grafted TCPS surfaces [231, 378]. These two-dimensional cell-sheet layers can be used for tissue engineering applications as they can be directly transplanted to tissue beds, or even layered to construct 3D tissue-like structures. For example, four neonatal rat cardiomyocyte sheets that were detached from PNIPAAm-grafted surfaces were overlaid in order to construct cardiac grafts that were then transplanted into the subcutaneous tissues of nude rats. Three weeks after transplantation, surface electrograms originating from transplanted grafts were detected and spontaneous beating was observed macroscopically [241]. Another study showed the utilization of limbal stem cells or autologous oral mucosal epithelial cells harvested as cell sheets from PNIPAAm-grafted surfaces for the treatment of rabbit bilateral corneal stem cell deficiency. The clinical results showed that the corneal surface remained clear, with significantly improved visual acuity for more than 1 year after the corneal epithelial cell-sheet transplantation [374, 375]. Moreover, autologous oral mucosal epithelial cell sheets obtained from thermo-responsive PNIPAAm-grafted surfaces enhanced the treatment of dog oesophageal ulcerations and reduced the host inflammatory responses with no stenosis [379].

Poly ($MEO_2MA$-co-OEGMA) 2D responsive surfaces have also been used for cell culture and passage experiments. Mouse embryonic stem cells (mESCs) were seeded on these surfaces following the adsorption of fibronectin, and subsequent passaging experiments were performed over 10 passage cycles. These thermo-responsive

polymer/fibronectin surfaces were found to be suitable for mESC culture without promoting differentiation during the early stages of culture [205].

To conclude, it has been proven that 2D stimuli responsive surfaces can be used for different cell types and prolonged cell passage applications in cell-sheet engineering. However, it has not been shown that 3D electrospun thermo-responsive scaffolds can be used for the culturing and passaging of individual cell populations. Therefore, the previous chapters described the development of a thermo-responsive scaffold as a result of co-electrospinning poly ($PEGMA_{188}$) with either PLGA or PET. The initial experiments then illustrated the concept using an exemplar mammalian cell type, murine 3T3 fibroblasts.

## 4.2 Aims and objectives

The main aim of this chapter was to investigate the prolonged culture and passaging of the murine 3T3 fibroblasts (differentiated cell type) over 10 passages, without the usage of digestive enzyme. Moreover, to demonstrate that the phenomenon is not cell-line specific, human Caco2 cells (carcinoma cell type) and ihMSC (stem cell type) were also used.

The aim of this chapter was achieved though the following objectives:

- To culture 3T3 fibroblast cells and passage them from the thermo-responsive scaffolds by lowering the culture temperature alone (when compared with TCPS surfaces using trypsin/EDTA treatment as a control) for a total of 10 passages (Figure 4.1 A).

- To determine the cell yield after the thermal detachment of cultured 3T3 fibroblast cells from the thermo-responsive scaffolds when compared with enzymatic detachment from TCPS.
- To culture and passage ihMSCs and Caco2 cells independently on the thermo-responsive scaffolds for a total of two passages on same scaffolds (Figure 4.1 B).
- To evaluate cell attachment, viability and detachment by changing the culture temperature above and below the LCST, without the usae of proteolytic enzymes throughout the experiments.

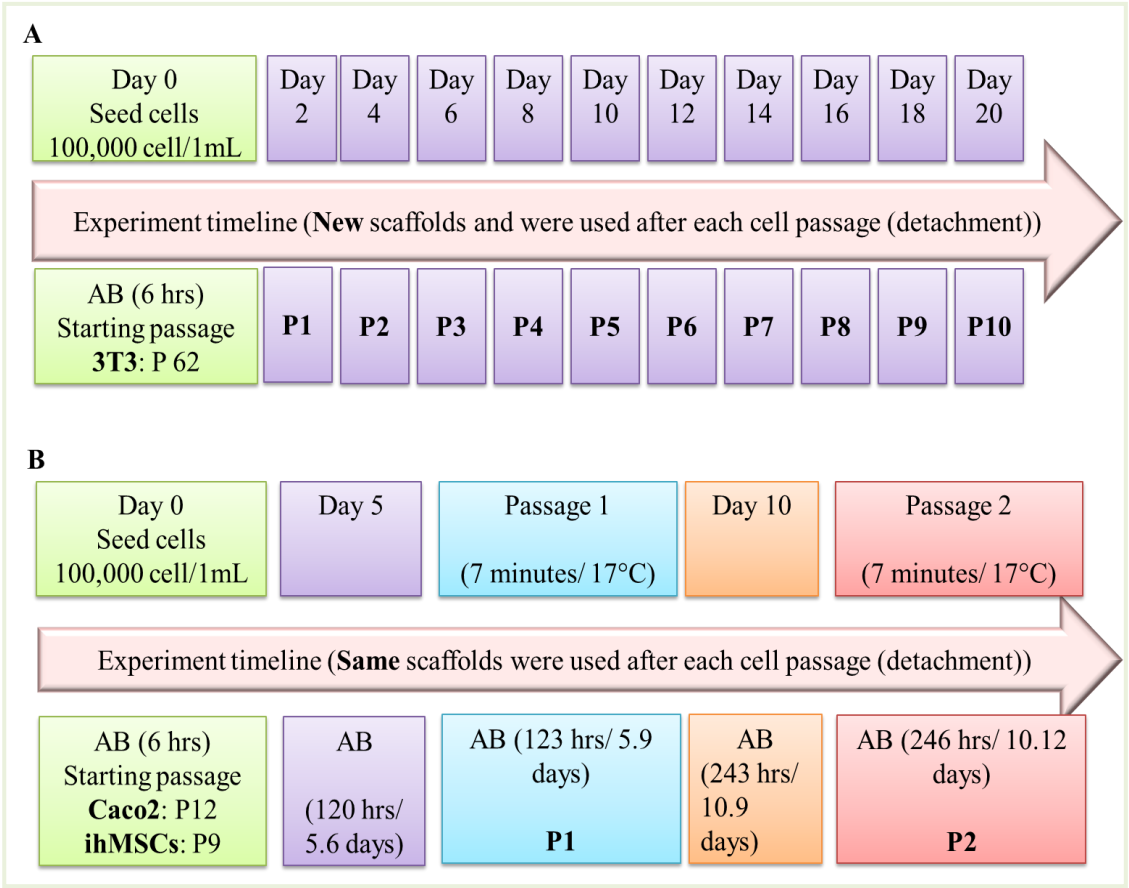



**Figure 4.1:** Schematic representing the passaging experiment timeline for cultured A) 3T3 fibroblast cells over ten passages on new co-electrospun thermo-responsive scaffolds each passage and B) Caco2 or ihMSCs over two passages on same co-electrospun thermo-responsive scaffold each passage.

## 4.3 Materials and methods

### 4.3.1 Preparation of the co-polymer 18.5% PLGA-4% poly ($PEGMA_{188}$) and 30% PET-4% poly ($PEGMA_{188}$) (*w/v*) solutions and co-electrospinning

Polymer solutions were freshly prepared and co-electrospun as described in Chapter 3, sections 3.3.2 and 3.3.3. Experiments in this chapter were conducted on co-electrospun fibrous scaffolds prepared with PLGA and PET containing 4% (*w/v*) poly ($PEGMA_{188}$).

### 4.3.2 Maintenance and passage of 3T3 fibroblast cells, ihMSCs and Caco2 cells

All cell-culture manipulations were performed using aseptic procedures in a Class II microbiology safety cabinet.

- RFP-expressing mouse 3T3 fibroblast cells [349] (NIH 3T3 cells; a gift from Dr. James Dixon, Nottingham, UK).
- Green fluorescent protein (GFP)-expressing primary ihMSCs cells were immortalized in-house following the method developed by Takeshi Okamoto, *et al*. [380] (Primary ihMSCs cells; a gift from Dr. James Dixon, Nottingham, UK).
- Human colon adenocarcinoma Caco2 cells (derived from a cancer of the colon; a gift from Prof Mohammad Ilyas, Clinical Pathology Laboratory, Queens Medical Centre, Nottingham, UK).

All the cell types were cultured in DMEM (500 mL, Gibco [InvitrogenTM, LTD]) supplemented with 10% (*v/v*) FCS (50 mL), 100 units/mL penicillin, 100 μg/mL streptomycin (Sigma-Aldrich, UK), 1% (*v/v*) non-essential amino acids solution (5

mL; Sigma-Aldrich, UK) and 1% (*v/v*) L-glutamine (5 mL; Sigma-Aldrich, UK). They were maintained in T75 flasks in a humidified incubator at 37°C in 5% $CO_2$ in air. When the cells reached 70–80% confluency, they were passaged by rinsing them once with PBS, followed by incubation with 3 mL of a mixture of 0.255% *(w/v)* trypsin and 2 mM EDTA for 3 minutes. This was then followed by the addition of 7 mL of serum-containing media to stop the activity of trypsin. The cells were collected by centrifugation at 200 *xg* using a Sigma Laboratory centrifuge 2–16 K (Scientific Laboratory Supplies, UK) for 5 minutes. The cell pellet was re-dispersed in 1 mL of fresh culture media.

### 4.3.3 Scaffold sterilization and seeding

Fibrous scaffolds were cut into discs (areas = 1 $cm^2$) using a trephine (stainless steel cylinders with 1 cm diameter) and placed in sterile 6 non-tissue-culture-treated well plates, as described in Chapter 3, section 3.3.6. The 3T3 cells were seeded at a density of $1 \times 10^6$ cells/mL and $1 \times 10^5$ cells/mL for cell yield and prolonged passage experiments, respectively. Primary ihMSCs and Caco2 cells were seeded at a density of $1 \times 10^5$ cells/mL and cultured at 37°C in 5% $CO_2$ in air. (n = 9 total, three scaffolds from three different batches. Three independent experiments were carried out with three technical replicates in each experiment).

### 4.3.4 Determination of 3T3 mouse fibroblast cell attachment and detachment

3T3 fibroblasts were maintained and passaged on TCPS, as described in section 04.3.2. Cells were grown to 80% confluency and removed from the TCPS culture surface using trypsin. Cells were pelleted by centrifugation; they were then washed and re-suspended in culture medium (section 4.3.2). The cells were plated onto

thermo-responsive PLGA or PET scaffolds and TCPS (control), and then cultured at 37°C in 5% $CO_2$ in air. The medium was changed the day after seeding the cells. Detachment studies were carried out by lowering the culture temperature from 37°C to 17°C for 7 minutes and with gentle agitation in 5% $CO_2$ in air.

**For the cell-yield experiment**, the the start and end of the experimental period was between passages 62–63, and the cells were seeded at a density of $1 \times 10^6$ cells/mL. The detachment study was carried out after 6 h in order to eliminate excessive cell proliferation from the cell number calculations.

**For the prolonged passage experiment**, the the start and end of the experimental period was between passages 62–72 and the cells were seeded at a density of $1 \times 10^5$ cells/mL. The detachment study was carried out after 48 h (every two days for 10 passages, total of 20 days) on new (1 $cm^2$) co-electrospun PLGA-poly ($PEGMA_{188}$) and PET-poly ($PEGMA_{188}$) scaffolds for each passage; 12 well TCPS was used as the control, where cells were detached using trypsin/EDTA treatment. Cells detached from the scaffolds were gently pipetted for 5 to 10 minutes in order to ensure a single-cell suspension was obtained. Cells were counted after each passage using a Neubauer haemocytometer chamber under a light microscope (10 × objective). The population doublings (PDs) at each passage were calculated using the following formula:

$$PD = \log_{10} (\text{total cell counts/cells seeded}) / \log_{10} 2$$

where the initial cell number seeded was $1 \times 10^5$ cells/mL. Proliferation rates were calculated as the cumulative population doublings (CPD) as a function of time (n = 9

total, three scaffolds from three different batches. Three independent experiments were carried out with three technical replicates in each experiment).

### 4.3.5 Determination of ihMSC and Caco2 cell attachment and detachment

The ihMSCs and Caco2 cells were maintained and passaged on TCPS as described in section 4.3.2. The start of the experimental period and end was between passage 9–11 for hMSCs and 12–14 for Caco2 cells. Cells were grown to 80% confluency and removed from the TCPS culture surface using trypsin. Cells were pelleted by centrifugation; they were then washed and re-suspended in culture media as described in section 4.3.2. The cells were plated onto 1 $cm^2$ co-electrospun thermo-responsive PLGA and PET scaffolds and non-thermo-responsive PLGA or PET scaffolds (control) at a density of $1 \times 10^5$ cells/mL in a total of 1 mL of medium at 37°C in 5% $CO_2$ in air. The medium was changed the day after seeding the cells. Detachment studies were carried out following 120 h (every five days for two passages on the same scaffolds, total of 10 days) of culture, where the temperature was lowered from 37°C to 17°C for 7 minutes in 5% $CO_2$ in air.

Cells were detached from the scaffolds and were gently pipetted for 5–10 minutes to ensure a single-cell suspension was obtained. Cells were counted after each passage using a Neubauer haemocytometer chamber under a light microscope (10× objective). ihMSCs and Caco2 cell viability was measured using the AB assay (cell viability test) described in Chapter 3, section 3.3.7.i (n = 9 total, three scaffolds from three different batches. Three independent experiments were carried out with three technical replicates in each experiment).

### 4.3.6 Cell imaging and image analysis

Cell adhesion, proliferation and detachment were analysed under a Nikon Eclipse TS 100 microscope using green fluorescence at an excitation wavelength of 558 nm and emission of 583 nm for RFP-expressing 3T3 cells. The blue fluorescence was used for GFP-expressing ihMCSs at an excitation wavelength of 490 and emission of 516 nm. Images were taken with a DS-L3 Nikon capture unit. The thermo-responsive surface properties were determined by changing the environmental temperature above and below the LCST of the poly ($PEGMA_{188}$) polymer (37°C and 17°C, alternatively) to allow cell attachment, detachment and reattachment to the same scaffold.

#### 4.3.6.i Cell fixation and preparation for SEM

Cell fixation and the subsequent SEM imaging of the electrospun scaffolds are described in Chapter 3, section 3.3.7.iii.

### 4.3.7 Statistical analysis

Data were expressed as the mean ± standard deviation (SD). Statistical analyses were performed using the two-way ANOVA test with multiple comparisons performed using the Prism 6 software (GraphPad, San Diego CA). Significant differences were determined at $p \leq 0.05$. Statistical significance was set at non-significant (ns) for $p > 0.05$, significant (*) for $p \leq 0.05$, very significant (**) for $p \leq 0.01$, highly significant (***) for $p \leq 0.001$ and very highly significant (****) for $p \leq 0.0001$.

## 4.4 Results and discussion

In the previous chapter (Chapter 3), the biocompatibility of co-electrospun thermo-responsive scaffolds was proven via their ability to support NIH 3T3-fibroblast cell adhesion, proliferation and detachment. In this chapter, the main focus was to utilize this system for prolonged NIH 3T3 fibroblast cell culture and passage experiments. Additionally, this system was tested with different mammalian cell types such as ihMSCs (stem) and Caco2 (carcinoma) cells.

In order to determine the efficiency of NIH 3T3 fibroblast cell detachment from the thermo-responsive system, a yield experiment was conducted on 18.5% PLGA-4% poly ($PEGMA_{188}$) and 30% recycled PET-4% poly ($PEGMA_{188}$) (*w/v*) scaffolds when compared with TCPS (control). Scaffolds and TCPS were seeded with $1 \times 10^6$ cells/ 1 mL and cultured for 6 h at 37°C in 5% $CO_2$ in air in order to limit the cell proliferation contributing to cell number. In general, after reducing the culture temperature to 17°C for 7 minutes, an average of $8 \times 10^5 \pm 0.8 \times 10^5$ cells/mL detached from the 18.5% PLGA-4% poly ($PEGMA_{188}$) scaffold and $7 \times 10^5 \pm 0.4 \times 10^5$ cells/mL detached from 30% recycled PET-4% poly ($PEGMA_{188}$) scaffolds, compared with an average of $9.2 \times 10^5 \pm 0.3 \times 10^5$ cells/mL that detached from TCPS, as shown in Figure 4.2. The cell yields obtained from the temperature treatment of responsive PLGA and PET were 80 ± 8% and 70 ± 4%, respectively; of the original cultured cells when compared with 92 ± 3% harvested using trypsin/EDTA treatment from TCPS. These results indicate that either not all of the cultured cells detached from the co-electrospun thermo-responsive scaffolds, or that not all were retrieved from the culture environment. Incomplete detachment of cultured 3T3 fibroblast cells may be related to the uneven distribution

of the thermo-responsive polymer in the co-electrospun scaffolds. Another reason is that cells could be entrapped within the scaffold matrix, which may contribute to the yield differences between scaffolds and TCPS.

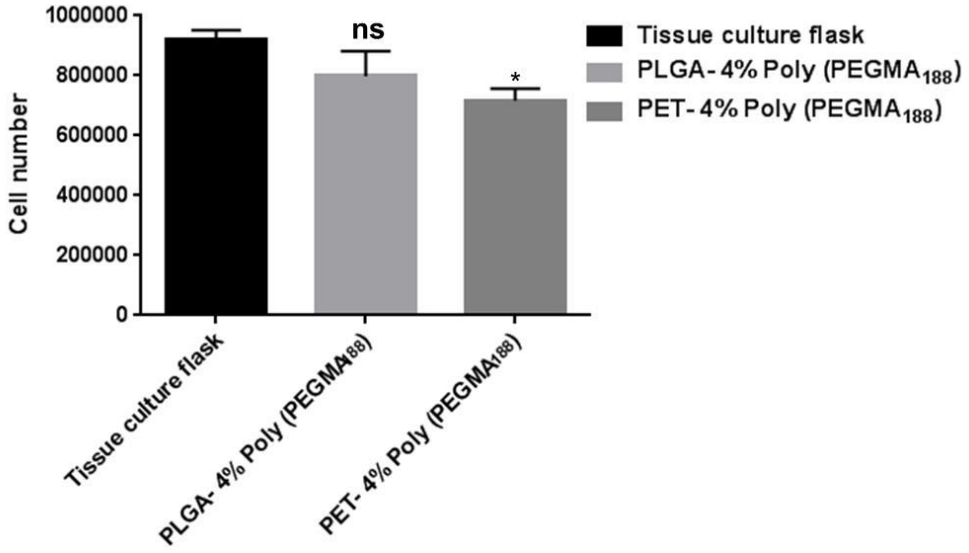



**Figure 4.2:** The 3T3 cell detachment using trypsin/EDTA from tissue culture flask and temperature from thermo-responsive co-electrospun 18.5% PLGA-4% poly ($PEGMA_{188}$) and 30% recycled PET-4% poly ($PEGMA_{188}$) scaffolds (*w/v*) after 6 h in cell culture. Error bars represent mean ± SD; (n = 9, three scaffolds from three different batches). Statistical significance versus tissue culture flask: (ns) $p > 0.05$ and (*) $p \leq 0.05$, (one-way ANOVA).

To date, there have been no reported cell detachment studies conducted on 3D thermo-responsive electrospun scaffolds, which highlights the novelty of this work. However, temperature-responsive 2D surfaces grafted from PNIPAAm polymer have been extensively used for cell attachment and detachment [338, 339, 373, 381]. Recently, poly ($MEO_2MA$-co-OEGMA)-grafted surfaces have been used for enzyme-free cell culture studies. One study showed that a grafted surface of poly ($MEO_2MA$-co-OEGMA) was able to support 3T3 fibroblast adhesion at 37°C, over a culture period of 96 h. This was then followed by subsequent cell recovery when the culture

temperature was lowered to 20°C, i.e. below the LCST of the copolymer brushes. Most of the 3T3 fibroblast cell detachment was achieved by gentle agitation of the substrate in order to release the cells [205, 226]. In comparison, surfaces treated with the PNIPAAm homo-polymer supported neither the adhesion nor proliferation of 3T3 fibroblasts, which was improved by surface modification with collagen [382], while 3T3 fibroblasts adhered, proliferated and spread on poly ($MEO_2MA$-co-OEGMA) surfaces only [226].

A recent study demonstrated the thermal release of hepatocyte cells from 3D non-woven scaffolds fabricated using needle-punching technology from poly (propylene) (PP), PET and nylon that had been later grafted with PNIPAAm. A comparison of the thermal release versus trypsin treatment of the cells growing on scaffolds revealed a similar efficiency in the cell release from the scaffolds. Fewer cells were released after 2 h at 20°C than the total number that were estimated to be growing on the scaffold using AB, which indicates that neither trypsin nor thermal release is fully effective in releasing all the cells. Moreover, fluorescence microscopy confirmed that not all the cells were released from these thermo-responsive scaffolds. The cells that remained on the scaffolds may either be trypsin-resistant due to the 3D nature of the cell clusters, or they may be entrapped in the non-woven fibre network. The uneven grafting of PNIPAAm may also be responsible for cells remaining on the scaffolds [90].

Similar findings were observed using a 2D poly (N-isopropylacrylamide-co-2-carboxyisopropylacrylamide), poly (NIPAAm-co-CIPAAm), copolymer grafted onto TCPS dishes, which permitted the immobilization of RGDS (Arg-Gly-Asp-Ser) cell

adhesion peptides. Human umbilical vein endothelial cells adhered and spread at 37°C. When the culture temperature was reduced to 20°C, cell detachment occurred due to the hydrated grafted copolymer chains dissociating the immobilized RGDS from cell integrins. However, not all the cells detached from the substrate, but detachment improved when the concentration of soluble RGDS increased at 20°C [383]. Another study showed that the thermal detachment of L929 fibroblasts from thermo-responsive (PNIPAAm-PEG-thiol)-grafted gold substrates was enhanced by the use of laminar flow in a microfluidic device. This external force was used to apply defined shear forces to the cells in order to facilitate their detachment, in combination with an increased detachment time from 10 minutes to 35 minutes at 25°C [384].

In this chapter, the 3D thermo-responsive system was utilized for the passaging of individual 3T3 fibroblast cell populations over 10 consecutive thermal passages. To achieve this, 3T3 fibroblast cells were cultured on co-electrospun thermo-responsive poly ($PEGMA_{188}$) with PLGA or PET scaffolds and compared with TCPS (control). Cell attachment and detachment was conducted by changing the environmental temperature from 37°C to 17°C in the case of the thermo-responsive scaffolds, and using trypsin/EDTA treatment with TCPS. The passaging of 3T3 fibroblasts using trypsin/EDTA dissociated the TCPS-adhered cells, which resulted in a cell suspension. However, cultures passaged using temperature as the detachment factor produced clumps of cells, as shown in Figure 4.3, which were then dissociated using gentle pipetting to ensure a single cell suspension was obtained. Similar results were obtained using 2D thermo-responsive glass surfaces grafted with poly ($MEO_2MA$-co-OEGMA) [205, 226], PNIPAAm-PEG-grafted porous membranes [377] or thin films grafted with copolymers of poly (N,N-diethylacrylamide) (PDEAAm) or PNIPAAm

with PEG [381]. On these surfaces, the cells detached as intact sheets or clumps, this indicates that the cell-cell interactions remained intact while harvesting the cells from the substrates. However, with trypsin/EDTA treatment, dissociation of these interactions occurred, which resulted in a single cell suspension [1, 205, 226, 377, 381].

It has been reported that there is an obvious difference in the detachment behaviour of single cells and cell clusters from thermo-responsive surfaces. The detachment of cells in clusters takes less time and less shear force than single-cell detachment. This is most likely due to the internal tension in the cell clusters, which provides the potential energy that leads to their detachment when the cell-surface contacts are no longer sufficient to maintain stable cell adhesion. In the case of single cells, such energy is not available and, therefore, even the disappearance of all adhesive contacts does not lead to a removal of the cells from their location on the surface. In order to remove individual cells from the surface, an external force is required [384].

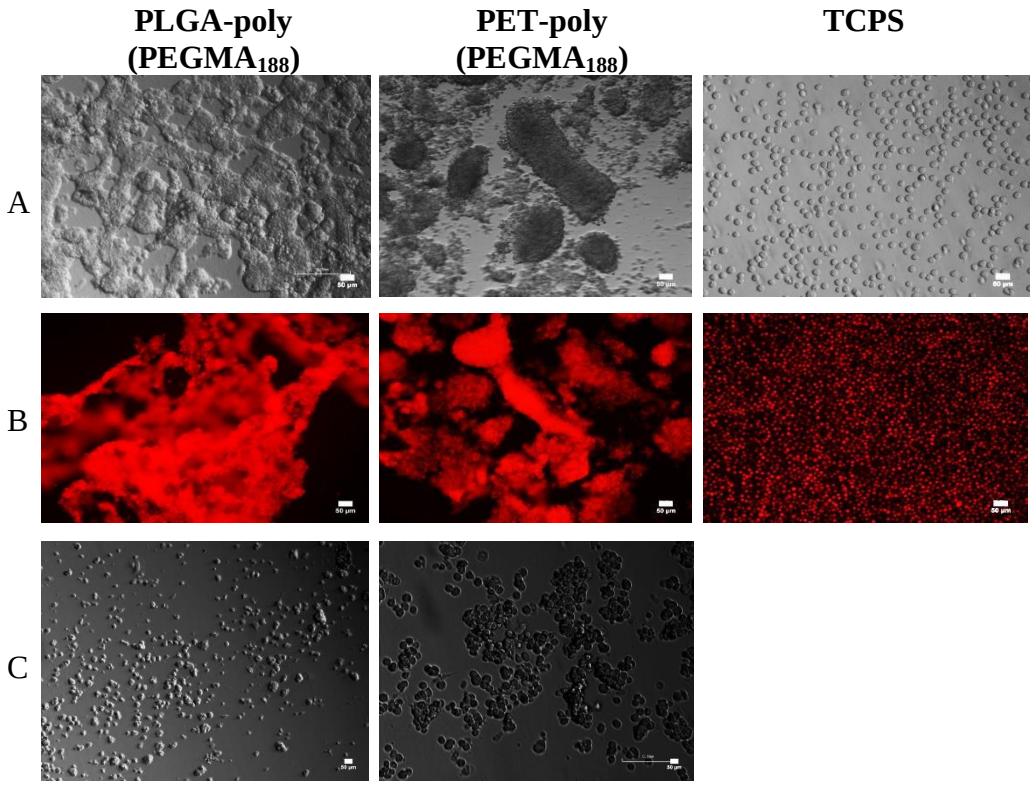



**Figure 4.3:** Representative A) Bright field and B) Fluorescence microscopy images showing 3T3 fibroblast cells after thermal detachment process at 17°C from thermo-responsive scaffolds and enzymatic detachment from TCPS. C) Cell following dissociation using a gentle pipetting for 5-10 minutes, following detachment from the scaffold. Scale bars = 50 µm.

For 3T3 fibroblast cell thermal detachment, an incubation time of 7 minutes at 17°C (with gentle agitation) was enough to detach the cells from the thermo-responsive electrospun scaffolds. This may be related to the high porosity of the co-electrospun scaffolds. The rapid recovery of the cells from thermo-responsive surfaces is considered an important factor for the maintenance of cell biological functions and viability [385]. The incubation time for cell detachment studies at lower culture temperatures may be related to the topography and composition of the substrate; it has been reported that 3T3 fibroblast cell detachment from a 2D poly ($MEO_2MA$-co-OEGMA) glass surface occurred after 1 h of incubation at 20°C [205]. In another study, a 55 minute incubation time at 20°C was required in order to detach bovine

aortic endothelial cells (BAECs) from PNIPAAm-TCPS surfaces. An incubation time of almost 35 minutes at 20°C was required to completely detach BAEC sheets from PIPAAm porous membranes, while only 19 minutes was required to detach BAEC sheets from PIPAAm porous membranes containing 0.5% (*w/v*) PEG. With porous membranes, water molecules had access to the PNIPAAm molecules grafted onto the surfaces from both underneath and peripheral to the attached cell sheet, resulting in the rapid detachment of the cell sheet. Additionally, increasing the surface hydrophilicity via the incorporation of PEG molecules into the PIPAAm porous membrane reduced the time required for cell-sheet recovery [377, 385].

The number of cells harvested from each scaffold and the TCPS were calculated using a haemocytometer at each passage as shown in Figure 4.4 A, No significant difference ($p > 0.05$), was observed in 3T3 cell numbers on PLGA- and PET-containing poly ($PEGMA_{188}$) scaffolds at each time point. However, there was a significant difference ($p \leq 0.0001$), in the cell numbers that detached from TCPS using trypsin enzyme and the number of cells retrieved from thermo-responsive scaffolds, which indicates the incomplete recovery of attached 3T3 cells from the scaffolds.

Population doublings (PDs) were calculated at each passage using the following formula:

$$PD = \log_{l0} (\text{total cell counts/cells seeded}) / \log_{10} 2.$$

The proliferation rates were calculated using the following equation:

Proliferation rate = 'hours in culture' (on TCPS or co-electrospun PLGA or PET with poly ($PEGMA_{188}$))/ cumulative population doublings [CPDs] over 10 passages.

On day 2 and 4 there were no significant differences ($p > 0.05$), in CPDs between the thermal detachment and enzymatic detachment. As the culture time increased there was a significant increase ($p \leq 0.0001$), in CPDs in the cells that underwent enzymatic detachment when compared to those that were subjected to thermal detachment. Analysis of these proliferation rates indicated that the average PD interval for 3T3 fibroblasts on TCPS was 17 ± 0.6 h, whereas on PLGA-poly ($PEGMA_{188}$) and PET-poly ($PEGMA_{188}$) scaffolds it was 24 ± 1.4 h and 21 ± 1.2 h, respectively. This indicates that thermo-responsive co-electrospun scaffolds are bio-adherent materials that support the growth and proliferation of 3T3 fibroblast cells Figure 4.4 B. However, the slight difference in the fibroblasts' PDs may be related to the nature of the 2D surfaces when compared with the 3D surfaces, where cells need an increased time to adjust and proliferate, as all other factors such as the cell number, media type and culture constituents were the same. Other reasons could be related to the presence of the thermo-responsive polymer in the scaffolds, which may also be considered by the cells as a foreign material.

These results were in good agreement with previous work conducted on TCPS and thermo-responsive 2D glass surfaces grafted with thermo-responsive poly ($ME0_2MA$-co-OEGMA) using 3T3 fibroblast cells. Over 10 passages, the proliferation rates were 14 ± 0.16 h and 20 ± 4.8 h, respectively; these differences could be related to the thermo-responsive polymer in the culture [205]. Another study showed the differences in mESC PDs between 3D cultispher-S micro-carriers and 2D TCPS. The PDs for mESCs in 3D and 2D culture were 32 h and 18 h, respectively. However, after three serial passages, the PDs reduced from 32 h to 21 h for the 3D culture, which is very similar to the PD of the 2D culture. These results indicate that cells

need more time to adapt to a 3D environment than on a 2D culture [386]. Additionally, Sarber *et al*, showed a significant increase in cell growth, proliferation and the DNA synthesis rate of fibroblasts cultured on 2D TCPS when compared with fibroblasts cultured on 3D collagen lattices. These differences were interpreted in relation to the cell cycle, where cells could have entered a rest period or several cell differentiation stages upon culturing on the 3D environment that mimics the cell cycle *in vivo* [387].

Differences in PDs may also be related to the type of medium or constituents used. A study reported that slower PD rates for human umbilical cord perivascular cells (HUCPVCs) were observed when they were cultured in DMEM when compared with a-MEM medium [388]. Another study showed a higher proliferation rate for MSCs in medium containing 20% serum in comparison with media containing 5%, 10% or 15% serum [389].

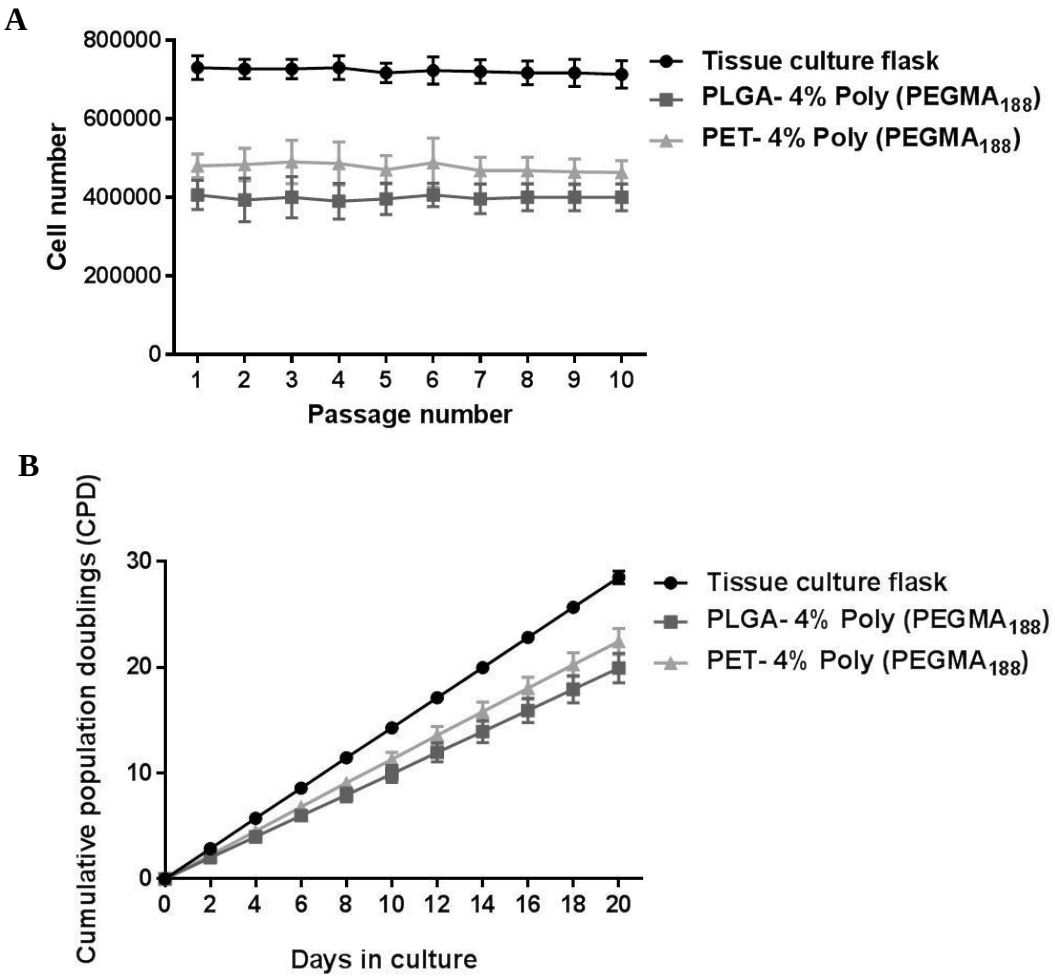



**Figure 4.4:** Graphs showing A) 3T3 fibroblast cell number and B) growth curve for 3T3 fibroblasts, which they were serially passaged, over 10 passages, using trypsin and temperature from TCPS or co-electrospun scaffolds containing poly ($PEGMA_{188}$) respectively. Error bars represent mean ± SD; (n = 9, three scaffolds from three different batches). Statistical significance versus tissue culture flask: (ns) $p > 0.05$ and (****) $p \leq 0.0001$, (two -way ANOVA).

After the detailed application of the thermo-responsive scaffolds with mouse 3T3 fibroblast cell culture, other cell types, e.g. Caco2 and ihMSCs, were chosen to prove that the thermo-responsive co-electrospun system could support the attachment, proliferation and detachment of different mammalian cell types. Human mesenchymal stem cells were chosen due to their importance in tissue regeneration and cell therapy. They are multipotent stromal cells that can differentiate into several cell types such as osteoblast (bone cells), chondrocytes (cartilage cells), myocytes (muscle cells) and

adipocytes (fat cells) [390, 391]. A human colon adenocarcinoma cell line has been widely used as an experimental model in many clinical studies, e.g. intestinal drug absorption. This is due to their capacity to differentiate and display specialised small intestinal cell functions such as the secretion of intestinal enzymes and retention of the ability to transport vitamins, ions and glucose [392, 393].

Caco2 and ihMSCs cells were cultured on the thermo-responsive co-electrospun scaffolds and on PLGA and PET scaffolds alone (control) for 10 days at 37°C. Two thermal passages were conducted at 17°C on day 5 and day 10. The AB assay was used to determine the change in cell viability over 10 days of cell culture.

The fluorescence microscopy images in Figure 4.5 showed the attachment and proliferation of the ihMSCs cells on the PLGA and PET scaffolds alone, or their co-electrospun with poly ($PEGMA_{188}$) at 37°C on days 5 and 10, indicating the ability of these scaffolds to support cell adhesion and spreading, as seen previously with 3T3 fibroblasts. Detachment of the cells at 17°C from all the scaffolds containing poly ($PEGMA_{188}$) was observed at the 'day 5 detachment' and 'day 10 detachment' time points, while scaffolds containing 0% poly ($PEGMA_{188}$) (control), showed no cell detachment after decreasing the culture temperature. The SEM images in Figure 4.6 supported these findings as at 17°C, ihMSCs and Caco2 cells were not present on the thermo-responsive scaffolds; whereas, cells could be seen on the PLGA or PET scaffolds alone. Moreover, there were different cellular spread patterns between PLGA and PET scaffolds. Cells on PET scaffolds proliferated mainly on the surface, while cells on PLGA scaffolds proliferated between the PLGA fibres. This is related to the fibrous diameters and porosity; the PET scaffolds used were in the range of

0.877 ± 0.195 µm, whereas, the PLGA scaffolds were in the range of 3.8 ± 0.45 µm. The same results were observed from the SEM images of rat hippocampus-derived adult neural stem cells (rNSCs) cultured on laminin-coated electrospun polyethersulfone (PES) fibre meshes. They revealed that cells stretched multi-directionally to cover the underlying 283 nm fibres, but extended along a single fibre axis on the larger 1.452 µm fibres [289].

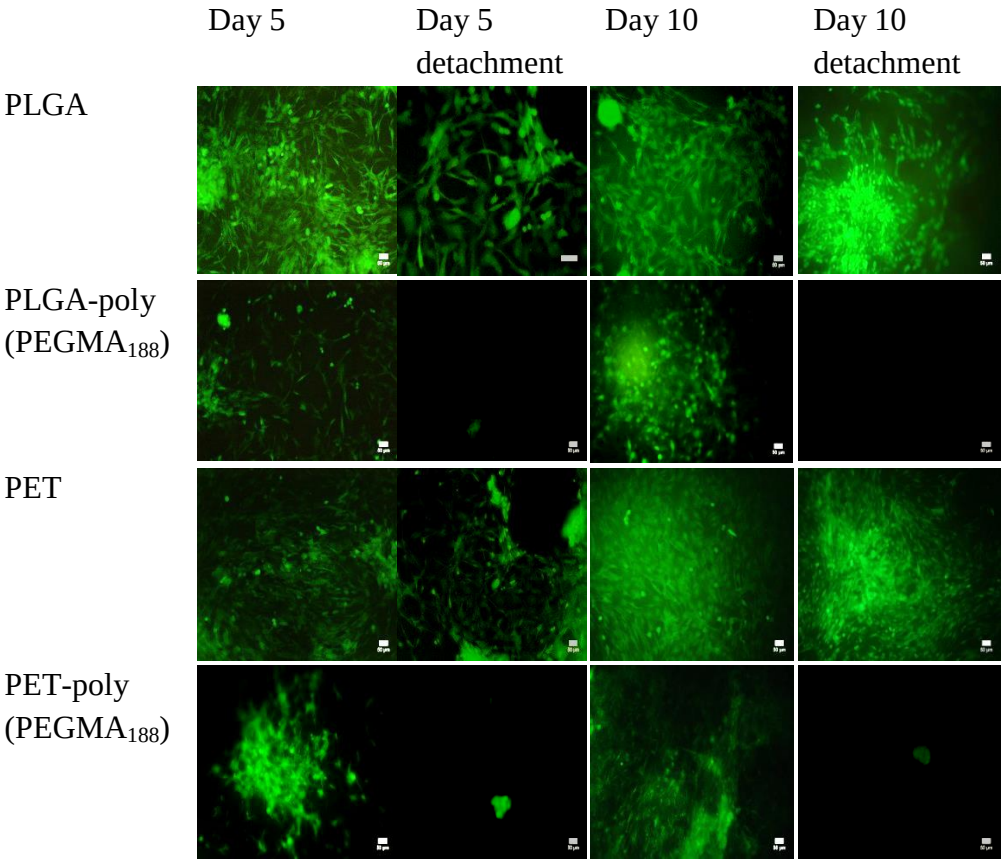



**Figure 4.5:** Representative fluorescence microscopy showing ihMSCs cell attachment to PLGA, PLGA-4% poly ($PEGMA_{188}$), PET and PET-4% poly ($PEGMA_{188}$) scaffolds for 5 days at 37°C. In day 5 detachment, cell detachment took place over 7 minutes at 17°C on scaffolds containing thermo-responsive polymer only. Cells were allowed to reattach to the same scaffolds by returning the culture plate to the incubator at 37°C. The cells were cultured for a further 10 days when they were detached again from the scaffold by reducing the temperature to 17°C again, illustrating the reversible nature of the thermo-responsive polymer. Scale bars = 50 µm.

The integrity of the scaffolds after 10 days of ihMSC or Caco2 cell culture, in addition to cell attachment and detachment were investigated by analysing the SEM images, as shown in Figure 4.6. These scaffolds remained intact during their 10 days in cell culture, with the maintenance of their fibre morphology.

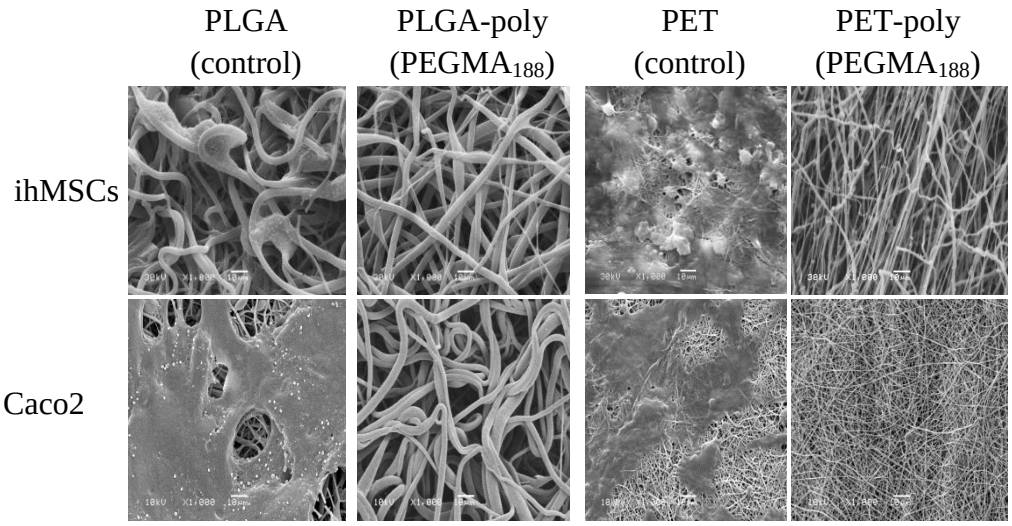



**Figure 4.6:** Representative scanning electron microscope images showing ihMSCs and Caco2 cell detachment over 7 minutes at 17°C from PLGA-4% poly ($PEGMA_{188}$) and PET-4% poly ($PEGMA_{188}$) scaffolds after ten days in cell culture. While, cells remained attached on PLGA and PET scaffolds (control). Scale bars = 10 µm.

The AB assay was conducted in order to quantify the biocompatibility and thermo-responsive behaviour of co-electrospun scaffolds. The ihMSCs and Caco2 cells were cultured independently on thermo-responsive scaffolds over a 10 days period and the AB assay was conducted during the culture and following cell detachment from the scaffold. The fluorescence intensity is considered as an indirect proportional indicator of viable cells in the culture.

As a general outcome from the AB assay shown in Figure 4.7 A and B, a significant increase in the fluorescence intensity was observed from day 0 to day 5 at 37°C. This indicated that both cell types proliferated on both the control and poly ($PEGMA_{188}$)-

containing scaffolds. Following incubation at 17°C, a significant decrease in the fluorescence intensity ($p \leq 0.0001$) was observed, indicating detachment of the cells from the poly ($PEGMA_{188}$)-containing scaffolds only (passage 1). In contrast, the fluorescence intensity of the cells cultured on the PLGA and PET scaffolds alone (control) at day 2 and passage 1 were not significantly different ($p > 0.05$) for both the ihMSCs and Caco2 cells. This illustrates that they remained on the scaffolds regardless of the temperature. A similar trend was observed for both cell types following a further 5 days of culture on the scaffolds. A significant subsequent increase in the fluorescence intensity was noted on day 10 ($p \leq 0.0001$), indicating further cell proliferation and a significant decrease in the fluorescence intensity ($p \leq 0.0001$) at 17°C (passage 2) for cells cultured on PLGA-poly ($PEGMA_{188}$) and PET-poly ($PEGMA_{188}$) scaffolds. No significant decrease in the fluorescence intensity for both ihMSCs and Caco2 cells ($p > 0.05$) was observed following a decrease in the temperature when they were cultured on PLGA and PET scaffolds alone.

In this experiment two passages were conducted at day 5 and day 10 for both ihMSCs and Caco2 cell cultures. The cells were then reseeded onto the same electrospun scaffolds, indicating that these thermo-responsive scaffolds were re-usable, and that the thermo-responsive polymer did not dissociate from the fibrous scaffolds during culture. In comparison, 2D surfaces grafted with thermo-responsive polymers were freshly prepared after each passage, which was due to the risk of the polymer washing off the surface [205].

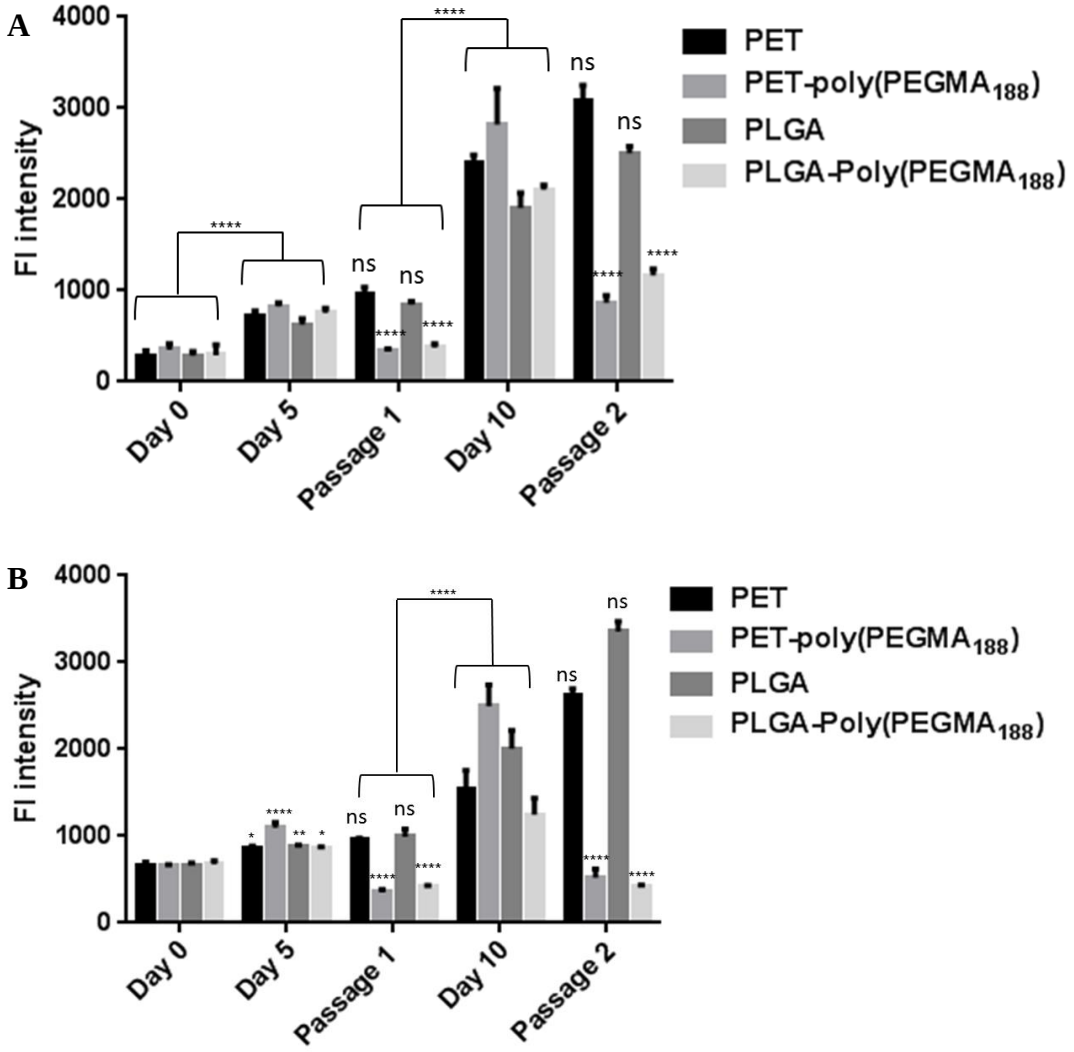



**Figure 4.7:** Alamar blue assay representing the change in cell fluorescence intensity over the initial culture time (up to 6 h - 126 h /day 0 - day 5), following detachment (7 minutes at 17°C/ passage 1) and subsequent re-attachment and culture (246 h at 37°C/ day 10), following detachment (7 minutes at 17°C/ passage 2) of A) ihMSCs and B) Caco2 cells on PLGA, PLGA-poly ($PEGMA_{188}$), PET and PET-poly ($PEGMA_{188}$) scaffolds. Error bars represent mean ± SD; (n = 9, three scaffolds from three different batches). Statistical significance, Day 0 versus Day 5, Day 5 versus passage 1, passage 1versus Day 10 and Day 10 versus passage 2: (ns) $p > 0.05$, (*) $p \leq 0.05$, (**) $p \leq 0.01$, (***) $p \leq 0.001$ and (****) $p \leq 0.0001$, (Two-way ANOVA).

To conclude, these responsive scaffolds were able to support Caco2 and ihMSC cell attachment, proliferation and then their subsequent recovery from the scaffolds, without affecting their viability.

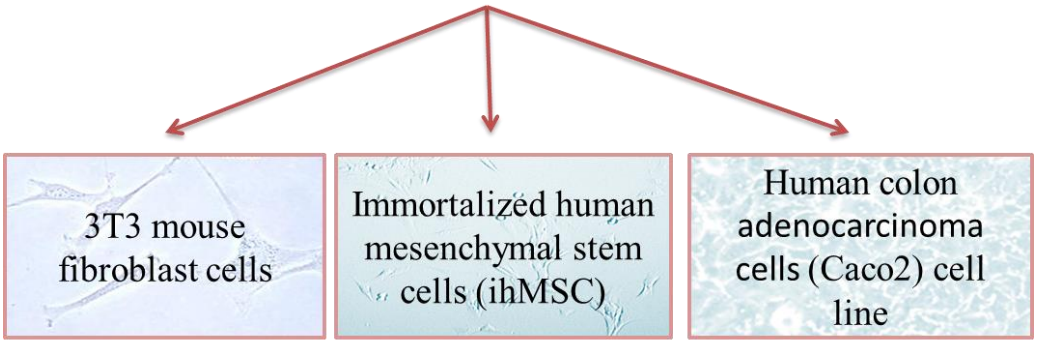
## 4.5 Conclusions

The main purpose of this chapter was to utilise the thermo-responsive co-electrospun scaffolds to passage single cell populations and test this system on different cell types.

The data presented demonstrates that blend-electrospun scaffolds prepared from PLGA and PET with 4% (*w/v*) of the thermo-responsive polymer, poly ($PEGMA_{188}$), were able to support 3T3-fibroblast cell culture and passage over 10 consecutive passages, without the use of digestive enzymes. In addition, these smart scaffolds were able to support ihMSCs and Caco2 cell adhesion and proliferation at 37°C. Furthermore, it was possible to detach these cells from the scaffolds by decreasing the environmental temperature to 17°C over 7 minutes for two passages on the same thermo-responsive scaffolds. Importantly, these cells were viable and proliferated in a similar manner to those cultured on control surfaces (PLGA or PET scaffolds). To conclude, the suitability of thermo-responsive co-electrospun fibrous scaffolds as a substitute for conventional cell culture methods, with a number of different cell types, is reported here for the first time. They were able to support cell attachment, growth and detachment in appropriate numbers, without any negative effects on the viability, proliferation and adhesion potential of the cultured cells. This indicates that these synthetic biomaterials could play a significant role in meeting the demands for the development of well-defined 3D culture systems for the derivation and maintenance of cultured cells.

**Table 4-1: A summary of the experimental work of Chapter 4**

Application of co-electrospun thermo-responsive 18.5% PLGA-4% poly ($PEGMA_{188}$) and 30% PET-4% poly ($PEGMA_{188}$) (*w/v*) scaffolds




| | |
|---|---|
| Cell attachment | At 37°C |
| Cell detachment | At 17°C |
| Recovery time | 7 minutes |
| Cell yield experiment for 3T3 fibroblast cells | PLGA-poly ($PEGMA_{188}$) 80 ± 8%.<br><br>PET-poly ($PEGMA_{188}$) 70 ± 4%.<br><br>TCPS 92 ± 3%. |
| Alamar Blue assay for ihMSCs and Caco2 cells | Viable and proliferating cells indicated by increasing fluorescence intensity over cell culture time. |

Since these scaffolds supported the growth and proliferation of NIH 3T3 fibroblasts, ihMSCs and Caco2 cells these thermo-responsive scaffolds were proposed for the investigation for the culture of a therapeutically relevant stem cell type, primary human corneal stromal stem cells ($hCSSC_S$). In addition, the next chapter (Chapter 5) describes the effect of extended culture on these scaffolds with repeated thermal passage on cell phenotype and cell surface markers.

# Chapter 5. Extended culture and passage of primary human corneal stromal stem cells (hCSSCs) on thermo-responsive co-electrospun scaffolds

## 5.1 Introduction

The cornea is a tough connective tissue that provides two-thirds of the refractive power required to focus light on the retina (Figure 5.1). Approximately 90% of the corneal thickness is the stroma which is a collagenous mesenchymal tissue composed of multiple lamellae of tightly packed parallel collagen fibrils, and their small uniform diameter is essential in rendering the tissue transparent [394, 395]. The keratocytes are the major cellular component of the human corneal stroma. They are typically described as quiescent [396, 397] and are responsible for maintaining the transparency of the cornea via the synthesis of collagens and proteoglycans; they also secrete collagenase and other enzymes that degrade the old stromal matrix [398-402]. Additionally, it has been proposed that the keratocytes provide structural stability for the maintenance of the interlamellar organization, which contributes to maintaining corneal transparency [403]. Corneal blindness is a condition affecting more than 10 million individuals worldwide [404]. Scarring of the cornea can result as a response to surgery, trauma or viral and bacterial infections (keratitis) [405-407]. Currently, surgical replacement of the stroma is the only successful approach for restoring vision in scarred corneas. However, chronic donor shortages, tissue quality issues and complications with immune rejection have led scientists to develop regenerative-medicine strategies targeting the cornea. These

new treatments include the use of stem-cell therapies for the treatment of ocular surface disorders [408].

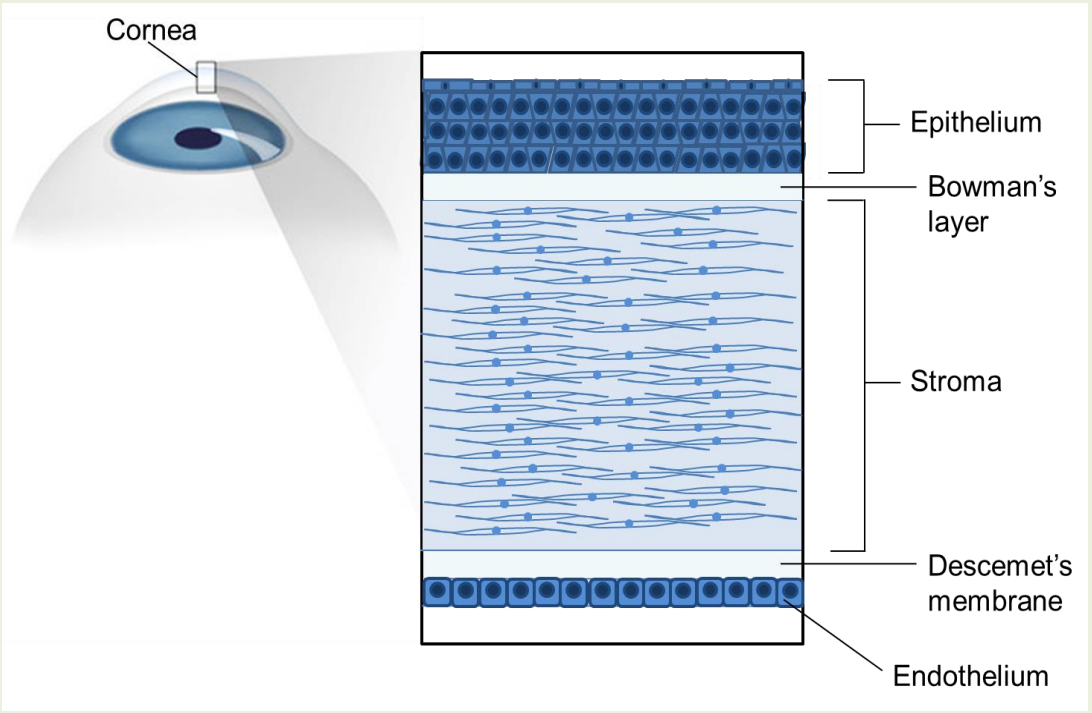



**Figure 5.1:** Corneal structure, modified from [409].

During stromal wound healing, the quiescent keratocyte is activated and dedifferentiated into its repair phenotype, the corneal fibroblast [410, 411], which migrates to the wound area and produces new stromal matrix. During the wound repair process, some corneal fibroblasts can transform into myofibroblasts [412], which possess contractile activity that helps to reduce the wound area, and can be identified by the expression of smooth muscle α-actin (α-SMA). This process can lead to scar formation and the loss of corneal transparency, hence, blindness [413, 414]. *Ex vivo* studies showed that primary keratocytes also differentiate into their active form and take on a fibroblastic phenotype when cultured on 2D tissue culture polystyrene [415-419].

Markers traditionally used to identify the keratocyte phenotype include aldehyde dehydrogenase (ALDH), keratocan, CD133 and CD34 [420-424]. *In vitro,* keratocytes extracted from the limbus (a distinctive border or edge located at the junction between the sclera and cornea of the eye, Figure 5.2), display the characteristics of multipotent mesenchymal stromal cells (MSC) after several passages [425, 426]. The extracted human corneal stromal stem cells (hCSSCs) express MSC cell-surface markers such as CD29, CD73, CD90 and CD105, and possess the ability to differentiate down to osteogenic, chondrogenic and adipogenic lineages *in vitro* [417, 427]. Therefore, it has been hypothesized that the limbal keratocyte is an MSC progenitor found in the corneal stroma [417, 428]. A specific population of hCSSCs, which can be identified by side population isolation, has also been described and is believed to be a keratocyte progenitor [429]. hCSSCs are localized in the anterior limbal stroma and their function is to support the potency of corneal epithelial stem cells in their unique limbal niche [430]. The ability of hCSSCs to adopt a keratocyte function was most striking *in vivo*. When injected into mouse corneal stroma, hCSSCs expressed human keratocyte messenger RNA (mRNA) and protein, replacing mouse extracellular matrix with human matrix components [418]. These injected cells remained viable for many months, apparently having become permanently quiescent keratocytes [418]. These results suggest that the keratocyte represents the default lineage for hCSSCs. The implication of such a hypothesis is that some aspect of their limbal microenvironment maintains the stem/progenitor character of hCSSCs *in vivo*; however, if they enter the stroma, the hCSSCs become keratocytes.

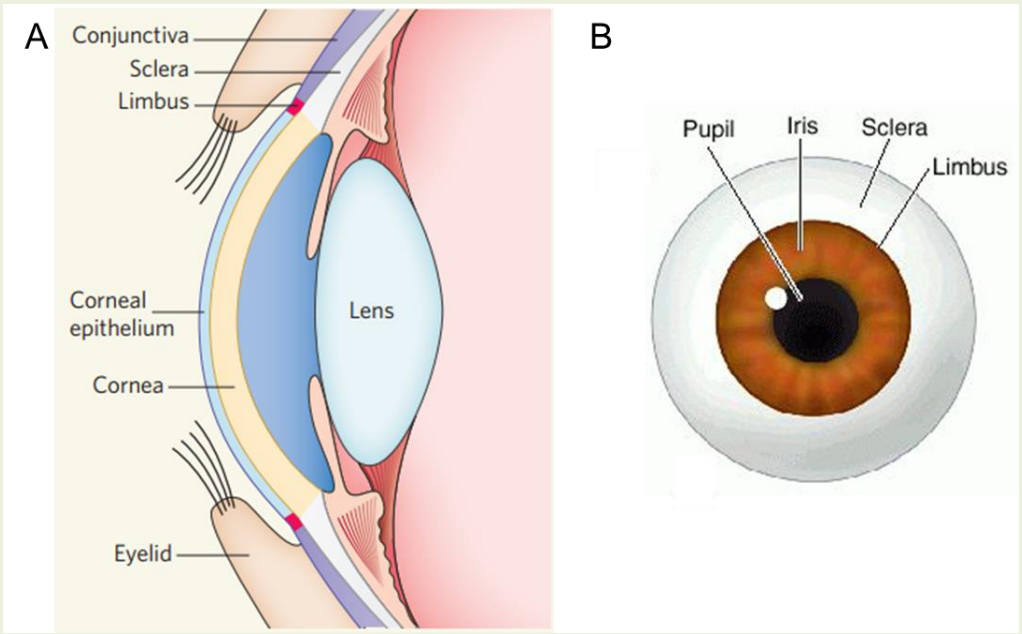



**Figure 5.2:** Schematic diagram of human eye showing limbus cornea in A) horizontal section and B) anterior section, taken from [431].

Unlike keratocytes, hCSSCs can undergo extensive expansion *in vitro*, without the loss of their ability to adopt a keratocyte phenotype [408]. However, little information is available regarding the role of hCSSCs *in vivo* for stromal wound healing or regeneration. *In vitro*, hCSSCs reproduce the highly organized connective tissue of the stroma, demonstrating the potential use of these cells in tissue bioengineering [432]. It has been reported that the direct introduction of hCSSCs into the corneal stroma generated transparent tissue in a mouse model of corneal opacity [432]. Additionally, hCSSCs injected into mice corneas did not elicit immune rejection over an extended period of time [433]. Therefore, utilisation of hCSSCs appear to offer an opportunity to develop cell- and tissue-based therapies to treat corneal blindness [408]. However, their ultimate application within a clinical setting is not only dependent on the ability to control their differentiation, but also to develop optimal culture systems for the safe expansion of cell populations, whilst maintaining them in their undifferentiated state.

In this chapter, 3D thermo-responsive co-electrospun scaffolds were explored for hCSSC expansion *in vitro*. Temperature-responsive surfaces have been used in differentiated mammalian cell culture to avoid the deleterious effects of trypsin/EDTA treatment upon cells [231, 338, 339, 381, 382]. Thermo-responsive surfaces also been used for corneal surface reconstruction in rabbits, where human or rabbit limbal stem cells were co-cultured with mitomycin C-treated 3T3 feeder layers on a 2D thermo-responsive surface. Corneal epithelial sheet constructs were recovered after reducing the culture temperature to 20°C, then transplanted to rabbit corneal stroma, where they adhered rapidly without the need for sutures [374]. Moreover, previous work has shown that 3D environments can promote the reversion of activated corneal stromal cells to a quiescent keratocyte phenotype [434]. However, difficulties in using enzymatic digestion to extract cells from 3D culture led the group at the University of Nottingham to develop thermo-responsive 3D scaffolds for longer term culture and passaging of clinically relevant mammalian cell types, which formed the ultimate motivation for this thesis.

In Chapter 2, the synthesis of poly ($PEGMA_{188}$) by free radical polymerization and its co-electrospinning with PET or PLGA polymers were described. Detailed characterization and preliminary cell culture with 3T3 fibroblast cells were then described in Chapter 3. These substrates were used to culture ihMSCs and Caco2 cells, on which they attached, spread, proliferated and detached, as described in Chapter 4. Thereafter, the application of these surfaces for controllable attachment/detachment of hCSSCs as a potential method to manipulate these cells in culture, without the use of enzymes and whilst maintaining their keratocyte phenotype, was investigated in this final chapter.

## 5.2 Aims and objectives

The main aim of this chapter was to use thermo-responsive co-electrospun scaffolds for extended hCSSC culture and passaging (7 passage cycles; from passage 3 to 9) using changes in temperature to detach the cells from the substrate. Cell adhesion, viability and phenotype during this experiment were determined and compared to those of identical cells cultured in conventional 2D culture using enzymatic passaging.

The aim of this chapter was achieved through the following objectives:

- To observe the hCSSC response, i.e. adhesion and confluency, on thermo-responsive PLGA-poly ($PEGMA_{188}$) or PET-poly ($PEGMA_{188}$) scaffolds.
- To test the effect of the presence of the thermo-responsive poly ($PEGMA_{188}$) on hCSSC viability.
- To culture hCSSCs and passage them from the thermo-responsive scaffolds (PET-poly ($PEGMA_{188}$) only) and TCPS surfaces by lowering the culture temperature and using trypsin/EDTA treatment, respectively, for a total of seven passages (new scaffolds and TCPS were used for each passage).
- To explore the effect of extended passaging (thermal and enzymatic) and 3D versus 2D culture on hCSSC phenotype, which was assessed using a quantitative reverse transcriptase real-time polymerase chain reaction (RT-qPCR) and immunocytochemistry at passages 3, 6 and 9.
- To determine the cell proliferation rate after nine thermal and enzymatic passages.

## 5.3 Materials and methods

### 5.3.1 Preparation of the co-polymer 18.5% PLGA-4% poly ($PEGMA_{188}$) and 30% PET-4% poly ($PEGMA_{188}$) (*w/v*) solutions and co-electrospinning

Polymer solutions were freshly prepared and co-electrospun as described in Chapter 3, section 3.3.2 and 3.3.3. Experiments in this chapter were conducted on co-electrospun fibrous scaffolds of PLGA and PET containing 4% (*w/v*) of the thermo-responsive poly ($PEGMA_{188}$).

### 5.3.2 Cell culture media and maintenance for primary human corneal stromal stem cells (hCSSCs)

All cell culture manipulations were performed using aseptic procedures in a Class II microbiology safety cabinet.

Human donor corneal tissue was used with the approval of the local ethics research committee and in accordance with the tenets of the declaration of Helsinki, following consent obtained from the donors and/or their relatives. Corneal tissue was obtained from Manchester or Bristol Eye Banks. The hCSSCs were isolated and gifted by Dr. Laura Sidney, Academic Ophthalmology, Queens Medical Centre, University of Nottingham, UK.

hCSSCs were isolated from corneoscleral rims using a modification of a previously described method [435]. The excess sclera was removed and the epithelium and endothelium were detached by gentle scraping. Stromal tissue was divided into small pieces and digested in 1 mg/mL collagenase Type IA (Sigma Aldrich, Poole, UK) in medium 199 (M199; Sigma Aldrich) supplemented with 20 ng/mL

gentamicin and 0.5 ng/mL amphotericin B (antibiotics) for 7 h at 37°C. Digests were filtered through a 40 μm cell strainer, pelleted and the cells were cultured in medium 199 (M199; 500 mL, Sigma Aldrich) supplemented with 20% (*v/v*) foetal bovine serum (FBS; 100 mL, Sigma Aldrich), 100 units/mL penicillin, 100 μg/mL streptomycin (Sigma-Aldrich Poole, UK) and 1% (*v/v*) L-glutamine (5 mL; Sigma-Aldrich, UK). They were maintained in T75 flasks in a humidified incubator at 37°C and with 5% $CO_2$ in air, with medium changes every 2 days. When the cells reached 70–80% confluency, they were passaged by rinsing them once with PBS. The PBS was then aspirated and they were incubated with 3 mL of TrypLE™ Express dissociation reagent (Gibco, Life Technologies) for 5 minutes, followed by the addition of 7 mL of media to stop the enzymatic activity. The cells were collected by centrifugation at 200 *xg* using a Sigma Laboratory centrifuge 2–16 K (Scientific Laboratory Supplies, UK) for 5 minutes. The cell pellet was re-dispersed in 1 mL of fresh media. Cells were counted after each passage using a Neubauer haemocytometer chamber under a light microscope (10× objective).

### 5.3.3 Scaffold sterilization and seeding

Fibrous scaffold sterilization was described in Chapter 3, section 3.3.6. The scaffolds were pre-incubated for 1 h in hCSSC media. The hCSSCs were seeded at a density of $1 \times 10^5$ cells/mL and cultured at 37°C in 5% $CO_2$ in air.

### 5.3.4 Determination of cell confluence using the Live-Dead™ assay

Corneal stromal stem cell confluency was determined using the Live-Dead™ assay using the Cellstain™ double-staining kit (Sigma Aldrich). The assay solution was prepared by adding 10 μL of solution A (acetoxymethyl ester of calcein, calcein-

AM) and 5 µL of solution B (propidium iodide, PI) to 5 mL of PBS. Calcein-AM is highly lipophilic and cell-membrane permeable. In viable cells, calcein generated from calcein-AM by esterase enzymes was identified by the emission of green fluorescence (excitation 490 nm, emission 515 nm). PI, a nuclei dye, cannot pass through the membrane of viable cells; however, it interacts with the DNA double helix of dead cells, which can be identified by red fluorescence (excitation 535 nm, emission 617 nm). Cell-seeded PET, PET-poly ($PEGMA_{188}$), PLGA, PLGA-poly ($PEGMA_{188}$) scaffolds and TCPS were incubated with 500 µL of the assay solution for 15 minutes at 37°C.

### 5.3.5 Effect of poly ($PEGMA_{188}$) on corneal stromal stem cell viability assessed using the AB assay

The AB assay was used to determine the viability of hCSSCs cultured on scaffolds containing poly ($PEGMA_{188}$) as compared with scaffolds not containing the thermo-responsive polymer. In addition, it was used to observe the detachment of the cells following a change in the culture temperature; this was described in Chapter 3, section 3.3.7.i. Briefly, a 10% (*v/v*) AB solution was prepared by mixing 1 mL of AB stock solution (25 mL, Invitrogen) with 9 mL of HBSS without phenol red and serum (500 mL, Sigma); this solution was then passed through a 0.2 µm filter. The assay was carried out for 90 minutes. The fluorescence intensity was then measured at excitation wavelength of 560 nm and an emission wavelength of 590 nm using a plate reader (TECAN, infinite ® M200) (Männedrof, Switzerland).

The cultured hCSSC viability experiments were conducted for 10 days, with fresh solutions prepared on each day of the assay, as described in Figure 5.3. On day 0,

the AB assay was conducted after 6 hrs of seeding the scaffolds. Scaffolds were transferred to a new 6 non-tissue-culture well plate and washed 3 times with warm, sterile PBS to remove the unattached cells. A 2 mL aliquot of the AB solution was added to each scaffold before incubation at 37°C, 5% $CO_2$ for 90 minutes. After incubation, 200 µL of the AB working solution was transferred to a 96 well plate, which was wrapped in foil until the fluorescence was measured. Scaffolds were washed 3 times with warm PBS then returned to the same cell culture media and incubated at 37°C in 5% $CO_2$ for day 3 and day 5 readings. Detachment on day 5 (passage 1) was carried out by lowering the temperature to 17°C for 7 minutes for both test (thermo-responsive PLGA or PET) and control (PLGA and PET alone) scaffolds. On day 5 post passage, new scaffolds were used and reseeded with $1 \times 10^5$ cells/mL for the AB measurements. Cell detachment was conducted again on the scaffolds (passage 2). (n = 9 total, three scaffolds from three different batches. Three independent experiments were carried out with three technical replicates in each experiment).

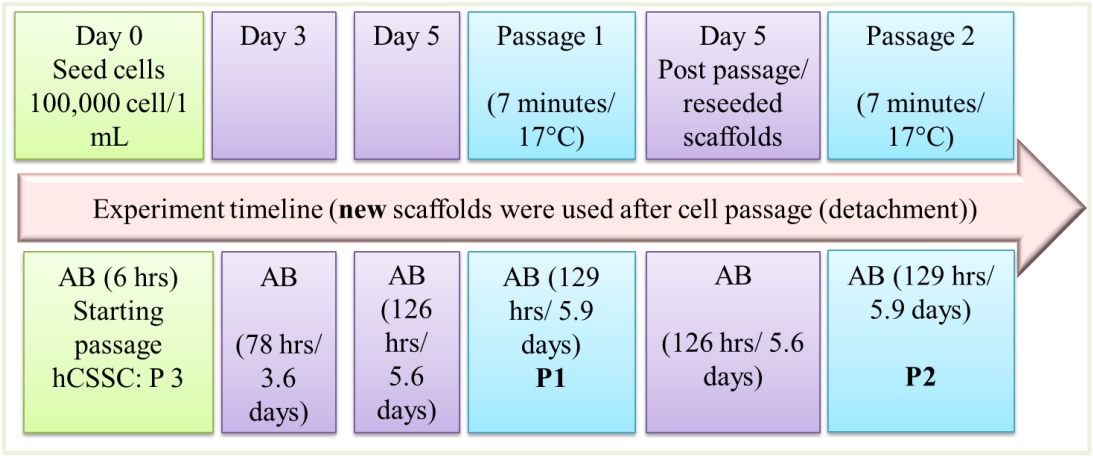



**Figure 5.3:** Schematic representing the AB experiment timeline for cultured hCSSCs

### 5.3.6 Prolonged (seven) thermal and enzymatic passages of corneal stromal stem cells on thermo-responsive PET-poly ($PEGMA_{188}$) scaffolds and TCPS respectively

hCSSCs were maintained and passaged on TCPS as described in section 5.3.2. Three different human donors of primary hCSSCs were used for this experiment; donor 1 E1809, donor 2 E1812 and donor 3 E2208.

The prolonged passage experiments are shown in Figure 5.4, the starting passage number of the cells was 2; cells were grown to 80% confluency and removed from the TCPS culture surface using TrypLE™. Cells were pelleted by centrifugation, washed, and re-suspended in medium as described in 5.3.2. They were then seeded onto 1 $cm^2$ co-electrospun thermo-responsive PET scaffolds and (12 well) TCPS at a density of $10^5$ cells/mL in a total of 1 mL of medium, then cultured at 37°C in 5% $CO_2$ in air. The medium was changed the day after seeding the cells. Thermal detachment studies from PET-poly ($PEGMA_{188}$) scaffolds were carried out following 120 h (every five days for seven passages on new scaffolds for each passage; total of 35 days) of culture, where the temperature was lowered from 37°C to 17°C for 7 minutes in 5% $CO_2$ in air. Enzymatic detachment of the cells from TCPS was carried via TrypLE™ treatment at 37°C for 5 minutes in 5% $CO_2$ in air.

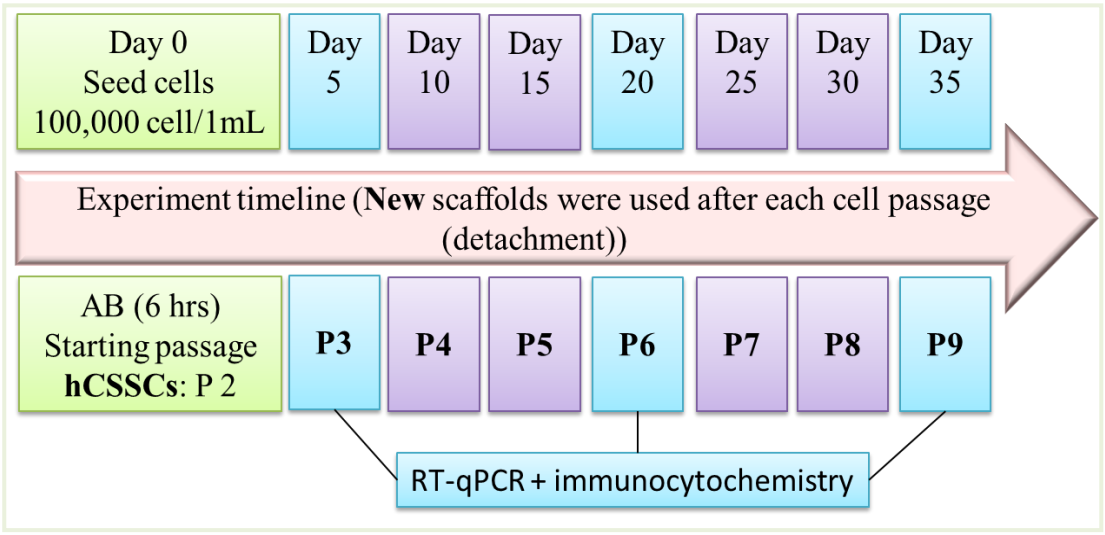



**Figure 5.4:** Schematic representing the prolonged seven thermal passages experiment timeline for cultured hCSSCs

Cells detached from the scaffolds were gently pipetted for 5–10 minutes, to ensure a single-cell suspension was obtained. Cells were counted after each passage using a Neubauer haemocytometer chamber under a light microscope (10× objective). Population doublings (PDs) at each passage were calculated using the following formula:

$$PDs = [\log_{10} (\text{total cell counts/cells seeded}) / \log_{10} 2]$$

where the initial cell number seeded was $1 \times 10^5$ cells/mL. Proliferation rates were calculated as the cumulative population doublings (CPD) as a function of time. (n = 9 total, three scaffolds from three different batches. Three independent experiments were carried out with three technical replicates in each experiment).

### 5.3.7 RNA extraction and quantitative reverse transcription-polymerase chain reaction (RT-qPCR)

Total RNA was extracted from hCSSCs cultured on both thermo-responsive PET- or PLGA-poly (PEGMA$_{188}$) scaffolds (3 samples) and TCPS surfaces (3 samples) using the RNeasy Mini Kit (Qiagen) following the manufacturer's instructions. Samples from the non-thermo-responsive scaffolds (PET and PLGA) were chopped into small pieces using a scalpel then treated with the mixture. In brief, each sample was treated with 350 µL of a mixture of RLT buffer/mercaptoethanol (1 mL: 10 µL) and homogenized using QIAshredder columns (Qiagen, Manchester, UK). The RNA was subsequently quantified using a Nanodrop ND-l 000 spectrophotometer using the associated software ND-l 000 3.3.

#### 5.3.7.i Reverse transcription (RT)

A total of 300 ng of total RNA for each sample was reversed transcribed into single stranded cDNA using Superscript III reverse transcriptase (Life Technologies) with random hexamer primers, according to the manufacturer's instructions. The RNA/primer mixture (10 µL) was prepared as shown in Table 5-1 and incubated at 65°C for 5 minutes to denature the RNA, which was subsequently incubated on ice for 1 minute. The cDNA Synthesis Mix (10 µL) was prepared and mixed with each RNA/primer mixture. An RT cycle at 25°C for 10 minutes was used, followed by 50°C for 50 minutes, followed by incubation at 85°C for 5 minutes to inactivate the transcriptor reverse transcriptase enzyme. One microlitre of RNase H was added to each sample and incubated at 37°C for 20 minutes. The cDNA product was stored at -20°C until further use in the PCR reaction.

**Table 5-1:** Reverse transcription mixture volumes used for both cells collected from the thermo-responsive scaffolds and TCPS surfaces.

| RNA/primer mixture | |
|---|---|
| Component | Amount |
| RNA | n µL |
| 50 ng/µL Random hexamers | 1 µL |
| 10 mM dNTP mix | 1 µL |
| DEPC-treated water | To 10 µL |
| Total 10 µL | |

| cDNA Synthesis Mix | |
|---|---|
| Component | Amount/sample |
| 10 X RT buffer | 2 µL |
| 25 mM $MgCl_2$ | 4 µL |
| 0.1 M DTT | 2 µL |
| 40 U/ µL RNaseOUT™ | 1 µL |
| 200 U/ µL SuperScript lll RT | 1 µL |

### 5.3.7.ii Polymerase chain reaction (PCR)

PCR reactions were conducted using the prepared cDNA (2 µL) with inventoried Taqman assays (Applied Biosystems, Life Technologies) to detect glyceraldehyde 3-phosphate dehydrogenase (*GAPDH*; Hs99999905_m1), *CD34* (Hs00990732_m1), *THY1* (*CD90*; Hs00174816_m1), *ACTA2* (Hs00426835_g1) and *ALDH3A1* (Hs00964880_m1). Amplification was performed on an Mx3005P multicolour 96-well PCR system (Stratagene, Agilent Technologies, Stockport, UK). Table 5-2 showed the mixture volumes for the PCR reaction; the mixtures were cycled under the following conditions: 50°C for 2 minutes for one cycle (initial denaturation), one cycle at 95°C for 10 minutes (de-naturing), then 50 cycles at 95°C for 15 seconds (annealing) and 60°C for 1 minute (extension). RT-qPCR reactions were analysed using the Real Time PCR Miner algorithm [436] which calculates the efficiency and threshold cycle. All experimental values were normalised to readings of the endogenous reference gene, *GAPDH*.

**Table 5-2:** Polymerase chain reaction mixture volumes used for both cells collected from the thermo-responsive scaffolds and TCPS surfaces.

| PCR | |
|---|---|
| Component | Amount/sample |
| cDNA | 2 µL |
| Taqman gene expression assays (x5) | 1 µL |
| Taqman gene expression master mix | 10 µL |
| Hypure molecular biology grade water | 7 µL |

### 5.3.8 Immunofluorescent staining for CD34 and alpha-smooth muscle actin (α-SMA)

Cells on the thermo-responsive PET-poly ($PEGMA_{188}$) scaffolds and TCPS surfaces were fixed in a 4% (*w/v*) solution of buffered paraformaldehyde (Sigma Aldrich) for 10 minutes for immunocytochemistry. After washing the samples three times in PBS, cells were permeabilised, where appropriate, in 100% (*v/v*) methanol (Sigma Aldrich) for 10 minutes with subsequent washing in PBS. Blocking of non-specific protein binding was performed for 1 hour at RT in PBS with 1% (*v/v*) bovine serum albumin (BSA, Sigma Aldrich), 0.3 M glycine (Sigma Aldrich) and 3% (*v/v*) donkey serum (Sigma Aldrich). The Samples were incubated with primary antibodies Table 5-3, at 4°C overnight (mouse monoclonal antibodies) diluted in 1% *(v/v)* BSA in PBS (CD34, 1:200 and α-SMA, 1:200). After washing the samples with PBS, they were incubated with secondary antibodies (Alexa Fluor 488 donkey anti-mouse IgG, diluted in 1% *(v/v)* BSA in PBS [1:300]) for 1 h at RT. Samples were counterstained with 1 mg/mL propidium iodide (PI) for 10 minutes at RT in the dark. The PI was removed and the samples were washed 3 times with PBS, each for 5 minutes. Samples were mounted in fluorescence mounting medium (Dako, Ely, UK) before imaging. Images were analysed under a Nikon Eclipse TS 100 microscope using blue and green fluorescence at excitation and emission wavelengths of (490 nm and 516 nm) and (558 nm and 583 nm), respectively. Images were captured with a DS-L3 Nikon capture unit.

**Table 5-3:** Details of antibodies used in immunocytochemistry

| Antigen | Clone | Source (Catalogue #) | Host | Conjugate |
|---|---|---|---|---|
| α-SMA | 1A4 | LSBio (LS-C210475) | Mouse | - |
| CD34 | QBEND10 | Sigma (SAB4700736) | Mouse | - |
| Mouse IgG | Polyclonal | Life Technologies (A-21202) | Donkey | Alexa Fluor-488 |

### 5.3.9 Statistical analysis

Data were expressed as the mean ± standard deviation (SD). Statistical analyses were performed using the Prism 6 software (GraphPad, San Diego CA). Two groups were compared using unpaired Student's t-tests, and multiple groups were compared using one-way ANOVA with a post hoc Dunnett's test multiple comparison. Significant differences were determined at $p \leq 0.05$. Statistical significance was set at non-significant (ns) for $p > 0.05$, significant (*) for $p \leq 0.05$, very significant (**) for $p \leq 0.01$, highly significant (***) for $p \leq 0.001$ and very highly significant (****) for $p \leq 0.0001$

## 5.4 Results and discussion

The ultimate objective of this study was to utilise thermo-responsive co-electrospun scaffolds for the extended cell culture and passaging of primary human cells with therapeutic relevance. In this chapter, detailed cell culture and passage experiments were performed using hCSSCs. In a previous study, these cells were cultured on non-thermo-responsive 3D electrospun PLGA scaffolds, and the desired keratocyte "inactivated'' phenotype was maintained [434]. However, extracting the cultured cells from the scaffolds without using trypsin was the main obstacle to further detailed cell analysis. To use the hCSSCs as part of regenerative cellular therapies, cells would need to be expanded in large quantities, whilst maintaining a quiescent phenotype. Therefore, in this chapter the thermo-responsive system was utilised for hCSSC culture, expansion and passage. Furthermore, the stromal keratocyte phenotype was examined at different passages intervals.

Initial studies involved the culture of hCSSCs on PET, PET-poly ($PEGMA_{188}$), PLGA, PLGA-poly ($PEGMA_{188}$) scaffolds and TCPS surfaces at 37°C for seven days to confirm cell confluency and the biocompatibility of the scaffolds. Therefore, Calcein-AM/PI stain was used to observe cell attachment, pattern of growth, spreading and confluency on the scaffolds and TCPS (control).

As a general observation from the fluorescence microscope images in Figure 5.5, hCSSCs were viable, as indicated by the green fluorescence, without any dead cells evident (lack of red fluorescence) during the seven days of cell culture. Additionally, the attachment and proliferation of hCSSCs on scaffolds and TCPS at 37°C confirmed the biocompatibility of the electrospun scaffolds, and that the

inclusion of the thermo-responsive polymer was not detrimental to the cells. Moreover, cells covered almost the whole scaffold area by day 6 of the culture (90–100% confluence). The attachment pattern of the cells was also observed; on PET-containing scaffolds there was a high degree of cell-cell contact, while on PLGA scaffolds the cells were more spread out between the electrospun fibres. However, the dendritic morphology of the hCSSCs was maintained on both scaffold types. Differences in the attachment pattern of the cells are likely to be related to the differences between PET and PLGA fibre diameters, as PET scaffold fibre diameters were in the nano-metre range (877 ± 195 nm), while PLGA scaffold fibre diameters were in the micron range (3.8 ± 0.45 μm). Cell morphology and proliferation were highly influenced by the electrospun fibre diameter and uniformity. A study by Schindler *et al.*, investigated the ability of a nano-fibre matrix to promote *in-vivo*-like organization and morphologies of different types of cultured cells [437]. It has been reported that human skin fibroblasts cultured on PLGA electrospun scaffolds with fibre diameters of less than 1 μm were well spread with an elongated morphology, in comparison with cells that exhibited a more rounded morphology when cultured on higher fibre diameters of 6 μm [438]. Another study demonstrated that gelatin nano-fibres promoted Schwann cell (SC) adhesion, spreading, actin cytoskeleton organization and an increase in the proliferation rate. However, both the migration rate and motility were greater in cells cultured on micro-fibres [289]. Human umbilical vein endothelial cells (HUVECs) also displayed differences in their spreading and proliferation rates when cultured on biodegradable poly (l-lactide-co-ε-caprolactone) (PLCL) scaffolds, where cells adhered well and proliferated on the smaller electrospun fibres with diameters of 0.3 μm and 1.2 μm,

compared with reduced cell adhesion, restricted cell spreading and no signs of proliferation when they were cultured on electrospun fibres with larger diameters (7.0 μm) [439]. It has been demonstrated that human astrocyte cells cultured on micro-structured PLGA scaffolds could span over distances greater than four times their average length within a 3D space [440]. Electrospun PLGA (50:50) fibrous membranes (3 μm in diameter) were prepared by electrospinning and layer-by-layer photocuring micro-fabrication approaches as an artificial limbal stem cell niche. Primary rabbit limbal fibroblasts (RLF) were seeded on these membranes and showed the typical elongated morphology of fibroblasts when stained with phalloidin–TRITC; furthermore, the cells were viable after 8 days in culture. Additionally, primary rabbit limbal epithelial cells (RLE) were seeded later and their attachment to the PLGA scaffolds was observed using SEM [441]. Another study showed that increased keratocyte cell density was observed, with the presence of rough endoplasmic reticulum and fibril clusters, when cultured on fibre with average fibre diameters of (38.1 ± 7.4 nm). This could be related to the similarity level to the fibre diameter of the native corneal stroma (30.1 ± 2.5 nm) [442]. ECs cultured on silk nano-fibres formed a differentiated and interconnected endothelial monolayer, with higher expression level of integrin-β1, compared with cells grown on micro-fibres. In addition, single nano-fibres were recognised by the integrin-receptor mechanism, supporting the formation of focal adhesion at the interface of ECs and nano-fibrous matrix [443]. To conclude, both nano-PET and micro-PLGA electrospun fibres are promising synthetic electrospun scaffolds that can support hCSSC adhesion, spreading and proliferation. Culture media constituents and respective concentrations can also influence the cell morphology, proliferation and

phenotype. These were discussed by Sidney *et al.* when hCSSCs were cultured in seven different media types for 5 days at passage 2 using gelatin-coated glass 2D surfaces. Cells aligned spontaneously and cell numbers were higher when cells were cultured in M199 medium containing 20% FBS and endothelial growth medium (EGM), when compared with cells cultured in DMEM, MethoCult, serum-free keratinocyte medium (K-SFM) and StemPro-34 [444]. Therefore, M199 medium supplemented with 20% FBS was chosen for hCSSC culture in this study.

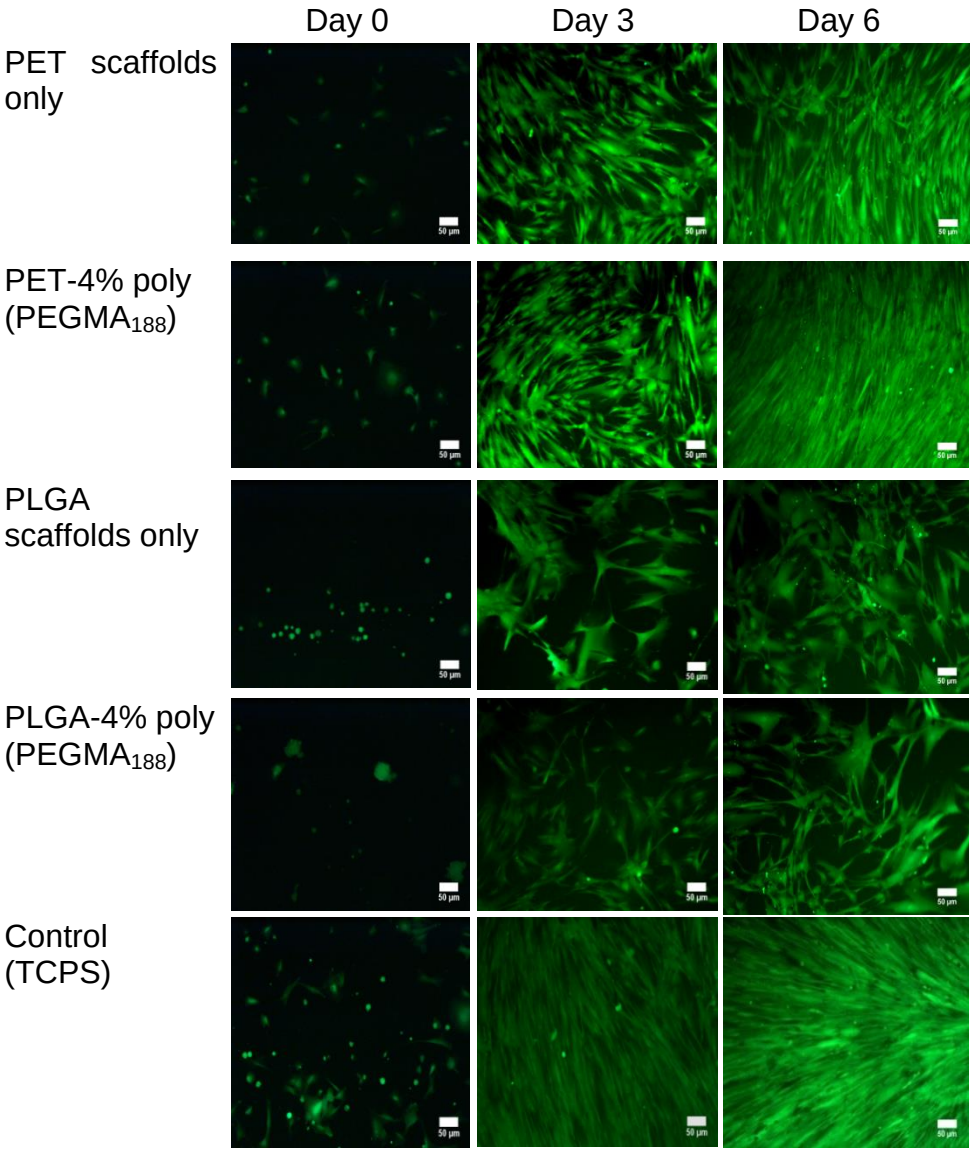



**Figure 5.5:** Representative fluorescence microscopy images showing hCSSCs attachment, proliferation and confluency using live-dead assay on PET, PET-4% poly ($PEGMA_{188}$), PLGA, PLGA-4% poly ($PEGMA_{188}$) (*w/v*) and control (TCPS) over six days of cell culture at 37°C. In day 0, cells were round in shape after 6 h of attachment. In day 3 and day 6, cells adopted a more spread morphology. Scale bars = 50 µm.

Studies of hCSSC detachment from PET-poly ($PEGMA_{188}$) and PLGA-poly ($PEGMA_{188}$) scaffolds confirmed the detachment of the cells from the scaffolds after reducing the temperature to 17°C (below the LCST of the thermo-responsive poly

($PEGMA_{188}$)) for 7 minutes (Figure 5.6). Detachment of hCSSCs after six days in culture resulted in cell sheets.

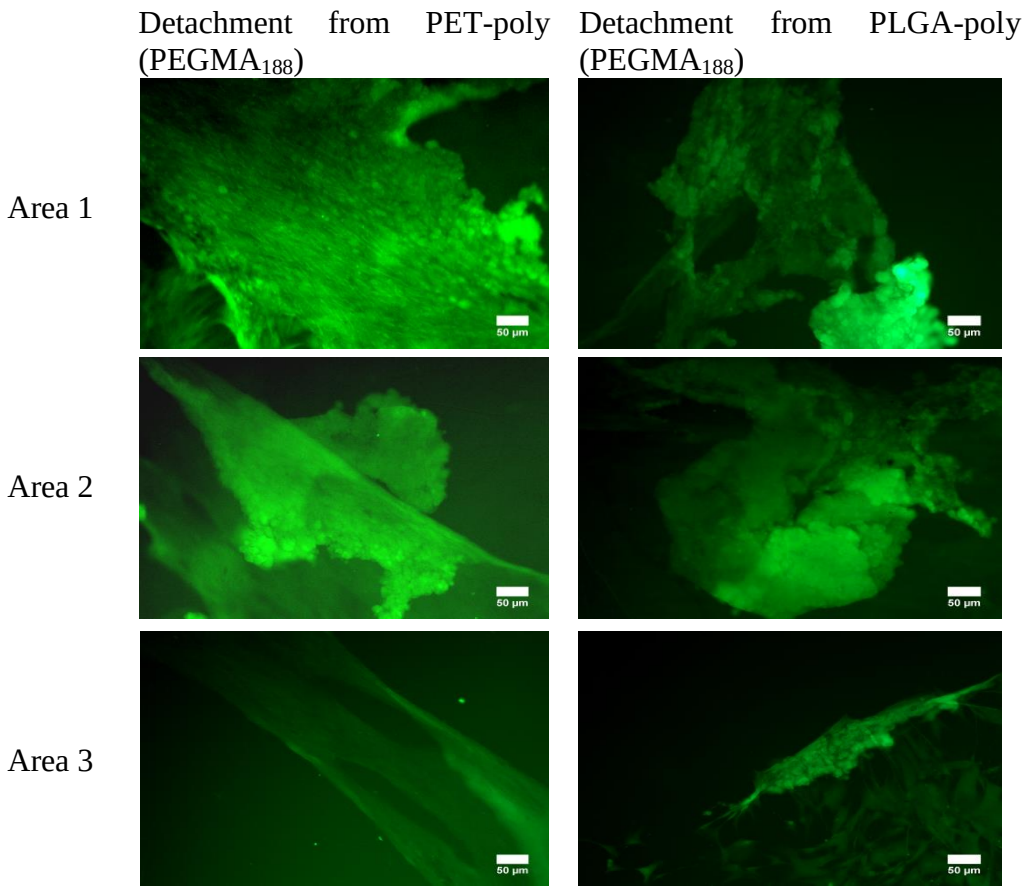



**Figure 5.6:** Representative fluorescence microscopy images showing hCSSCs detachment after six days of culture from PET-4% poly ($PEGMA_{188}$) and PLGA-4% poly ($PEGMA_{188}$) (*w/v*) in the culture media after reducing the culture temperature to 17°C for 7 minutes. Images were taken on three different areas in the well plate. Scale bars = 50 µm.

The AB assay was conducted to evaluate the viability of the cultured hCSSCs over five days in culture. As a general outcome from the AB assay shown in Figure 5.7 (A and B), a significant increase in the cell fluorescence intensity ($p \leq 0.0001$) was observed from day 0 to day 3 and from day 3 to day 5 at 37°C on all electrospun scaffolds and on TCPS. These results indicate that hCSSCs were viable over the five days in culture and that the scaffolds were biocompatible, as they supported the

growth and proliferation of cells in a similar way to cells cultured on TCPS. Additionally, there was no negative effect of the thermo-responsive poly ($PEGMA_{188}$) on the cell viability when compared with non-thermo-responsive scaffolds (PLGA and PET scaffolds alone).

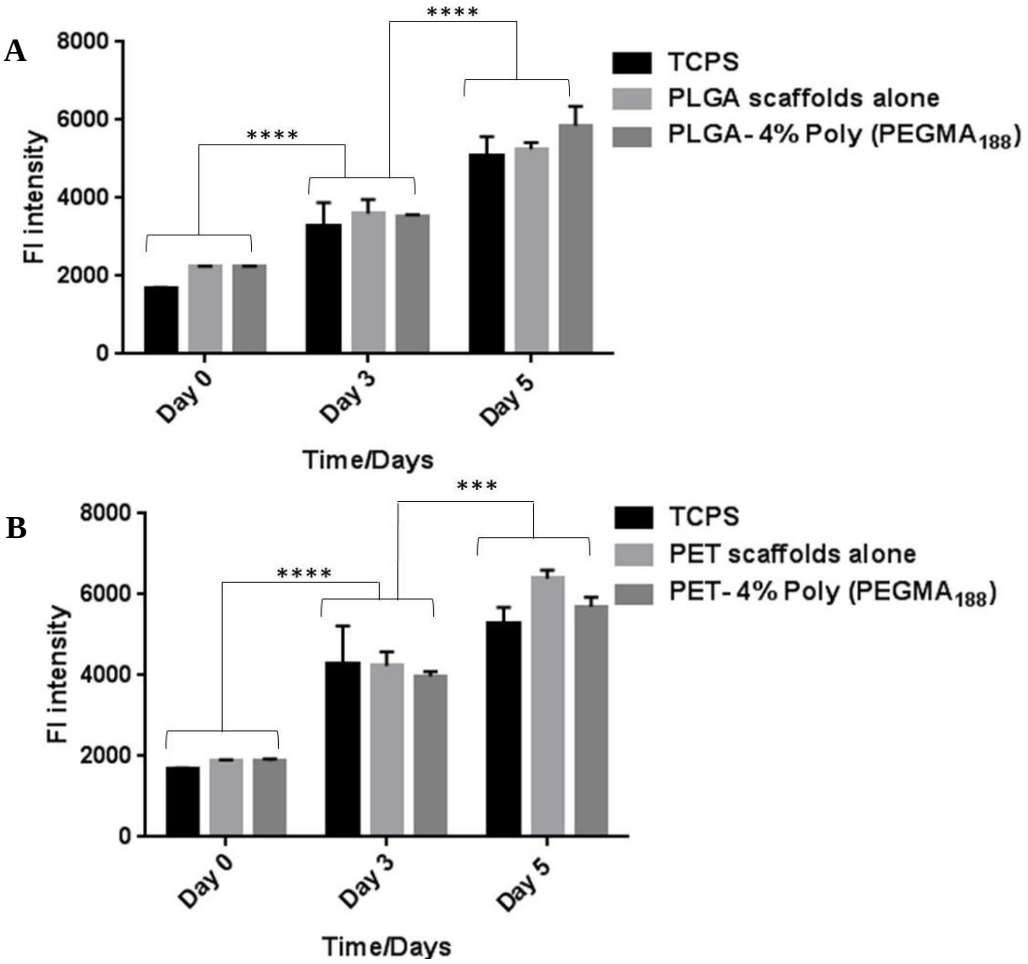



**Figure 5.7:** Alamar blue assay representing the significant change in fluorescence intensity of hCSSCs over the culture time (up to 6 h – 78h – 126 h /Day 0 – Day3 – Day 5) at 37°C on A) TCPS, PLGA and PLGA-poly ($PEGMA_{188}$) and B) TCPS, PET, PET-poly ($PEGMA_{188}$). Error bars represent mean ± SD; n = 9. Statistical significance, Day 0 versus Day 3 and Day 3 versus Day 5: (***) $p \leq 0.001$ and (****) $p \leq 0.0001$, (Two-way ANOVA).

The AB assay was also conducted to determine the thermo-responsive behaviour of the co-electrospun scaffolds by detecting the change in cell fluorescence intensity

while changing the culture temperature, periodically, over a total of 10 days in culture (2 passages every 5 days/ using new scaffolds at each passage). As shown in Figure 5.8 (A and B), at 17°C, there was a significant decrease in the cells fluorescence intensity ($p \leq 0.0001$) at passage 1 and passage 2 for poly ($PEGMA_{188}$)-containing scaffolds, while the fluorescence intensity of cells on PLGA scaffolds, PET scaffolds and TCPS at day 5 and passage 1, or at day 5 post passage and passage 2 were not significantly different ($p > 0.05$). To conclude, cells detached from the thermo-responsive PLGA-poly ($PEGMA_{188}$) and PET-poly ($PEGMA_{188}$) co-electrospun scaffolds after reducing the culture temperature from 37°C to 17°C, while no cell detachment occurred from TCPS and PET or PLGA scaffolds.

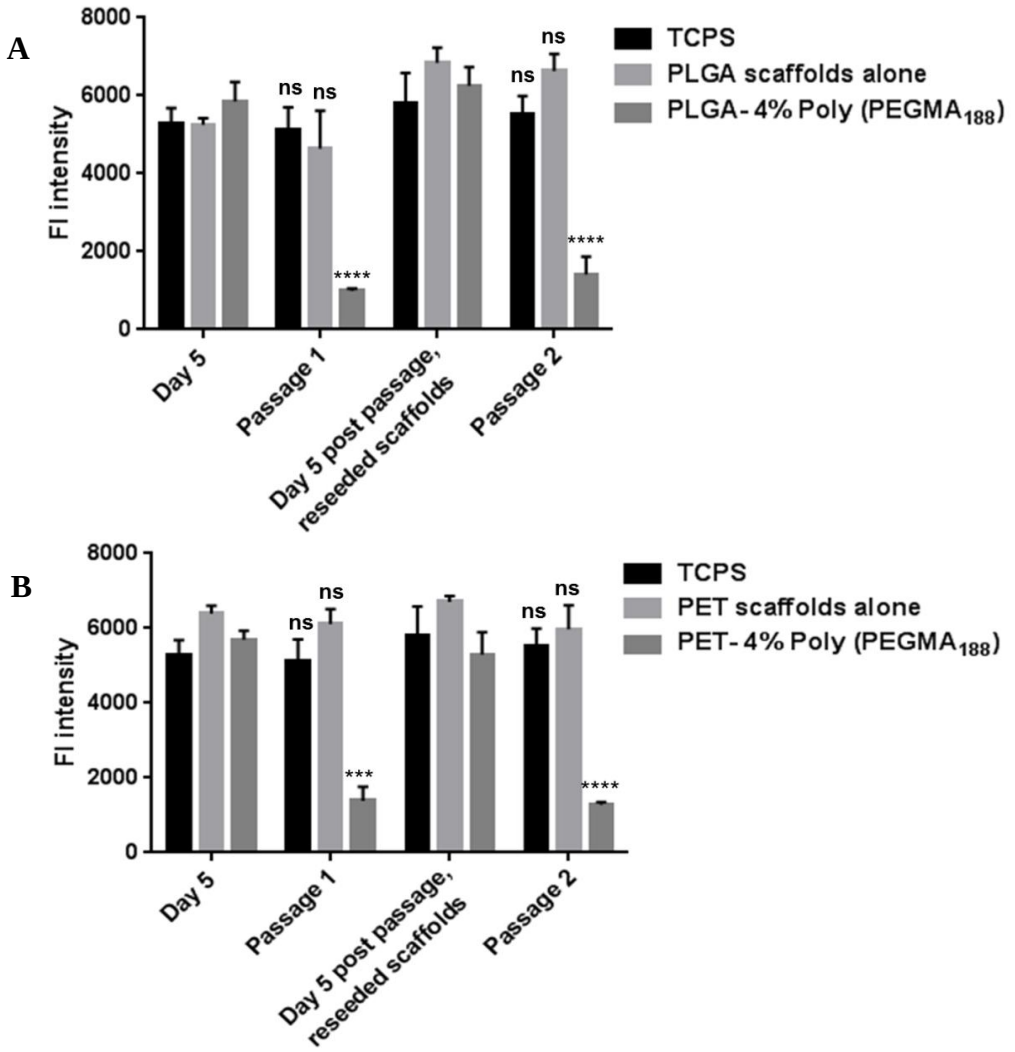



**Figure 5.8:** Alamar blue assay representing the change in fluorescence intensity in response to change of hCSSCs culture temperature. After five days of cell culture (126 h / Day 5 and Day 5 post passage, reseeded scaffolds), detachment occurred (for 7 minutes at 17°C/ passage 1 and passage 2) on A) TCPS, PLGA and PLGA-poly ($PEGMA_{188}$) and B) TCPS, PET, PET-poly ($PEGMA_{188}$). Error bars represent mean ± SD; n = 9. Statistical significance, Day 5 versus passage 1 and Day 5 post passage, reseeded scaffolds versus passage 2: (ns) $p > 0.05$, (***) $p \leq 0.001$ and (****) $p \leq 0.0001$, (Two-way ANOVA).

Having confirmed that hCSSCs were viable and proliferated on the scaffolds, subsequent experiments focussed on phenotyping the cells following culture. RT-qPCR was performed on hCSSCs seeded onto PLGA, PLGA-poly ($PEGMA_{188}$), PET, PET-poly ($PEGMA_{188}$) and TCPS at passage 3 to determine relative differences in mRNA levels of the quiescent stem cell markers *CD34* and *ALDH3A1*, and the activated/myofibroblast markers *THY1* (gene name for CD90) and *ACTA2*

(gene name for α-SMA). All experimental values were normalised to readings of the endogenous reference gene glyceraldehyde phosphate dehydrogenase (*GAPDH*), a stable gene expressed in all the cells.

As shown in Figure 5.9 and Figure 5.10, there were no significant differences ($p > 0.05$), in the mRNA levels of *CD34*, *ALDH3A1*, *THY1* and *ACTA2* in cells cultured on either the thermo-responsive (PLGA-poly ($PEGMA_{188}$) or PET-poly ($PEGMA_{188}$)) scaffolds, when compared with the non-thermo-responsive electrospun (PLGA and PET) scaffolds. This indicates that the thermo-responsive poly ($PEGMA_{188}$) did not influence the cultured hCSSC phenotype. In addition, the effect of different surface topographies, the 2D TCPS and 3D electrospun scaffolds, on the hCSSC phenotype was examined. Data presented in Figure 5.9 and Figure 5.10 showed that the mRNA levels of *CD34* and *ALDH3A1* were significantly higher ($P \leq 0.05$), when cells were cultured on all of the 3D electrospun scaffolds, when compared with those cultured on 2D TCPS with the complete absence of *CD34* expression in cells cultured on TCPS at passage 3. *CD34* is a well-established cell-surface glycoprotein marker for quiescent keratocytes *in vivo* [421, 422, 445] and it has been linked to the stem-cell properties of hCSSCs and other potentially related cell types [446, 447]. *CD34* was also reported to be expressed in human MSCs as they differentiated into keratocytes after transplantation to the corneas of mice [448]. The function of *CD34* expression in keratocytes has not yet been elucidated, although it has been speculated that *CD34* plays roles in the regulation of differentiation, adhesion and quiescence [421, 447]. *ALDH3A1* is also considered as a keratocyte stromal cell marker. During stromal injury transformation from a normal ‘in-active’ to a ‘active’ repair phenotype, the differentiation into a corneal

fibroblast and myofibroblast phenotype is accompanied by a loss in the expression of corneal crystallins *(ALDH3A1)*, which is associated with the loss of corneal transparency [423]. For *ACTA2* (α-SMA), mRNA levels were significantly lower ($P \leq 0.05$), when cells were cultured on all electrospun scaffolds, when compared with those cultured on TCPS. *ACTA2* is a myofibroblast indicator (scar tissue forming cells). When corneal injury occurs, the transformation of keratocytes to an activated myofibroblast phenotype ensues, and it is these cells that exhibit the development of a contractile apparatus. This is composed of intracellular F-actin microfilament bundles (stress fibres) containing α-SMA, α-actin, myosin and the associated surface membrane receptor $\alpha_5\beta_1$-integrin [413, 449]. These features are distinct from the quiescent keratocyte phenotype, which appears as a homogenous cell population composed of broad, flat, interconnected stellate cells with a contractile protein localized to the cortex, but not organised into stress fibres [450, 451]. For *THY1* (CD90) there were no significant differences ($p > 0.05$), in mRNA levels between cells cultured on all electrospun scaffolds when compared with those cultured on TCPS. *THY1* is associated with multipotent MSCs, which possess the ability to differentiate into osteogenic, chondrogenic and adipogenic lineages *in vitro* [417, 427]. Moreover, *THY1* has been shown to play a significant role in stromal wound healing and provides an *in vitro* surface marker to distinguish between quiescent keratocytes and its activated repair fibroblast phenotype [452].

Three dimensional substrates have been extensively shown to influence cell phenotype as many cell types, when isolated from tissues and placed into planar cell culture, become progressively flatter, divide aberrantly and lose their differentiated phenotype [71, 453, 454]. Culturing cells in a 3D environment, rather than in 2D,

can guide the differentiation of the cells back to their original form. For example, the encapsulation of dedifferentiated chondrocytes in an agarose gel was shown to restore their physiological phenotype, including cell shape and the expression of cartilaginous markers [455]. Similarly, mammary epithelial cells embedded in a 3D environment of floating collagen membranes in medium containing insulin, hydrocortisone and prolactin were shown to halt uncontrolled division, assemble into acinar structures and establish a *de novo* basement membrane [456]. Another study showed that corneal stromal cells cultured on 3D collagen–chondroitin sulphate foam populated the scaffold and produced a newly synthesised ECM. Moreover, immunohistochemistry studies showed the absence of α-SMA, which indicates that these cells had not differentiated into myofibroblasts when cultured in the 3D environment [457]. Additionally, mouse ESCs cultured on 3D, highly porous, tantalum-based scaffolds (Cytomatrix™) showed a significantly higher hematopoietic differentiation efficiency than those cultured under conventional 2D tissue culture conditions [458].

To conclude, the synthesized 3D electrospun thermo-responsive and non-thermo-responsive scaffolds were able to support hCSSC growth and proliferation. They also promoted the expression of a quiescent keratocyte phenotype, as indicated by the increased expression of the keratocyte markers, *CD34* and *ALDH3A1*, and decreased expression of the myofibroblast marker, *ACTA2*, when compared with cells cultured on 2D TCPS.

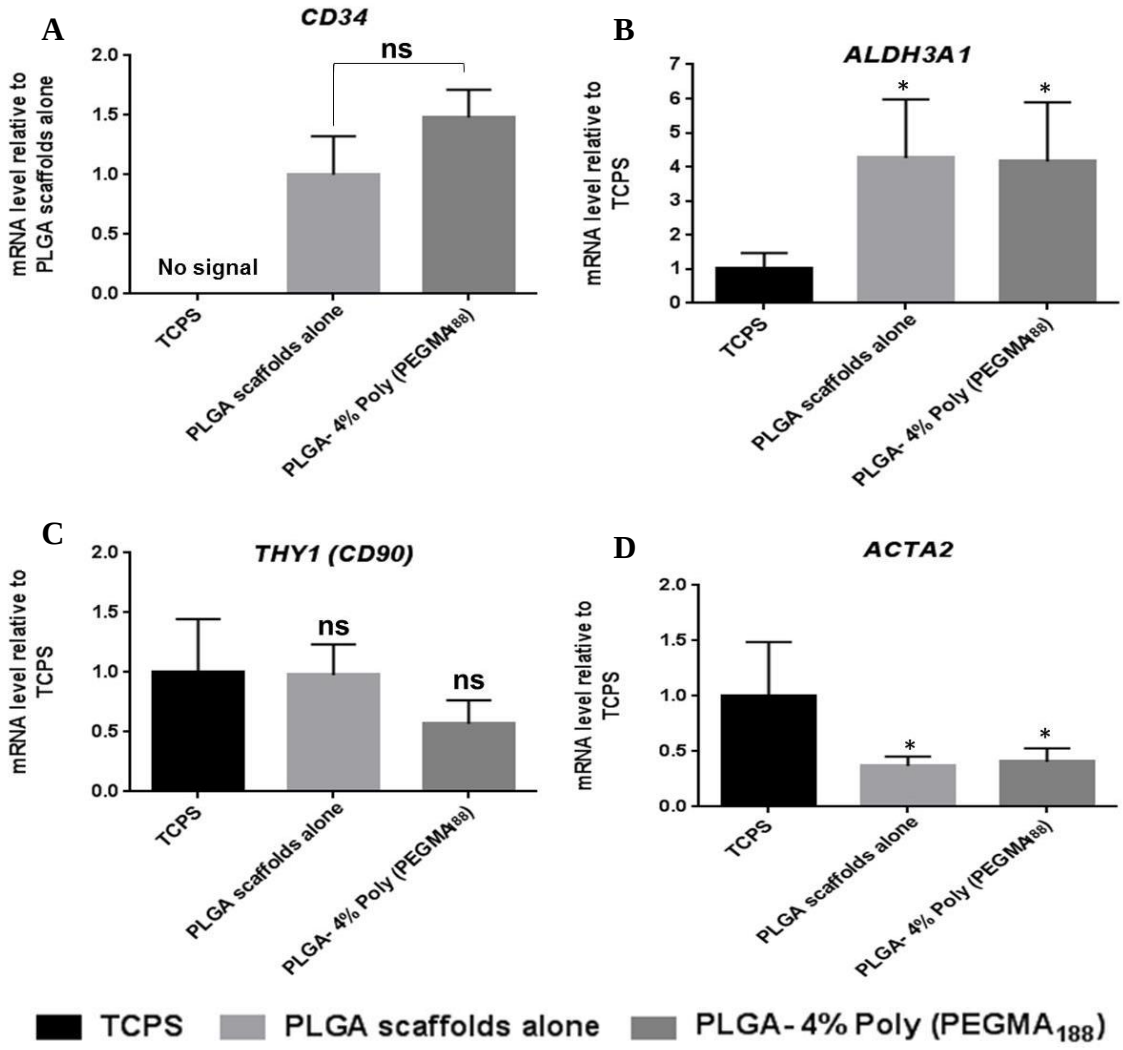



**Figure 5.9:** Comparative effects of culture environment (TCPS, PLGA scaffolds alone and PLGA-4% poly ($PEGMA_{188}$)) and thermo-responsive polymer on gene expression of hCSSCs at passage 3. Relative levels of mRNA were determined by means of RT-qPCR for the following genes: (A) *CD34*, (B) *ALDH3A1*, (C) *THY1* and (D) *ACTA2*. Expression of each target gene is normalized to *GAPDH* (housekeeping gene) and represented relative to mRNA expression in TCPS. Data are shown as mean ± standard error of the mean of three independent experiments (n = 3), each with two replicates, one donor. Statistical significance versus TCPS: (ns) $p > 0.05$, (*) $P \leq 0.05$ (one-way ANOVA).

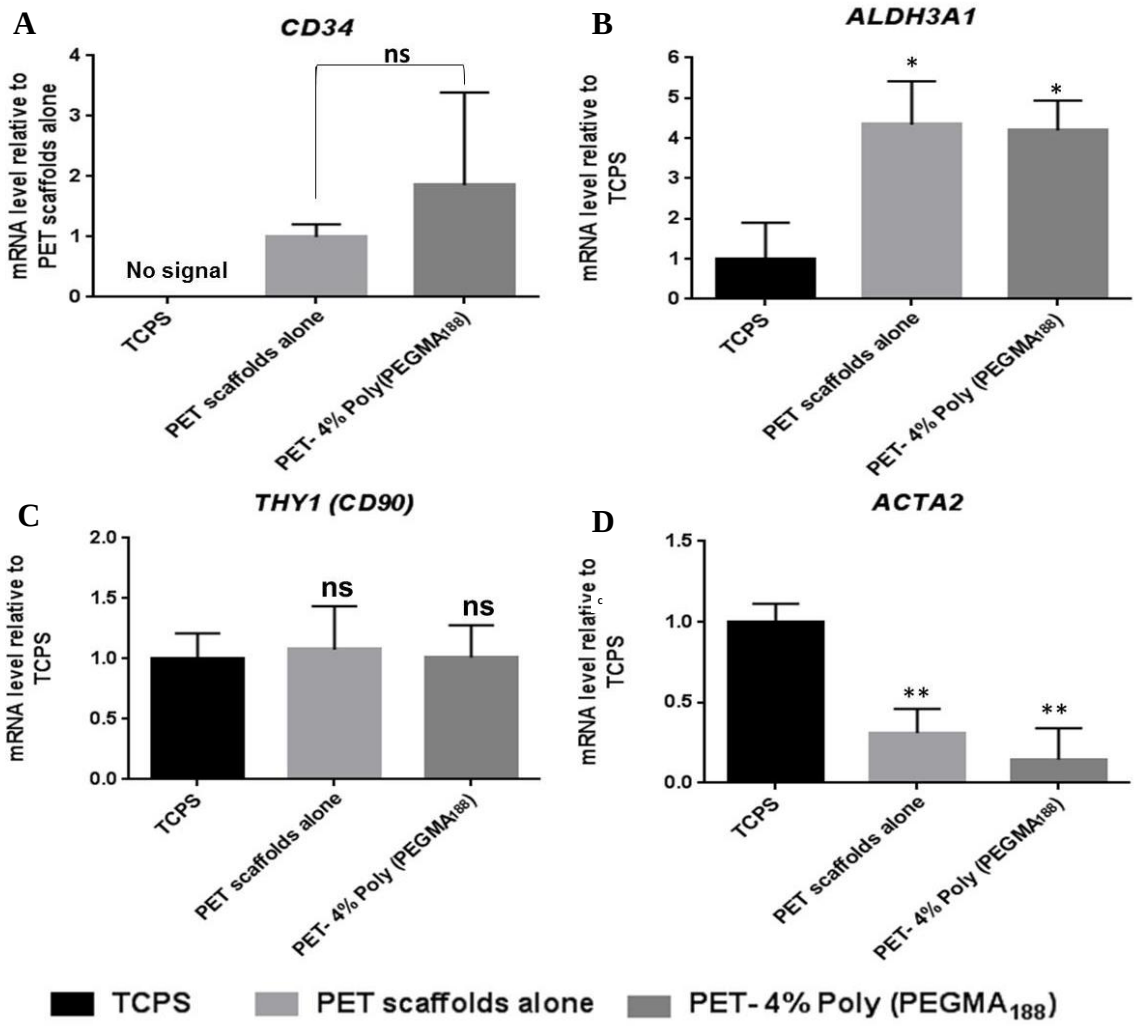



**Figure 5.10:** Comparative effects of culture environment (TCPS, PET scaffolds alone and PET-4% poly ($PEGMA_{188}$)) and thermo-responsive polymer on gene expression of hCSSCs at passage 3. Relative levels of mRNA were determined by means of RT-qPCR for the following genes: (A) *CD34*, (B) *ALDH3A1*, (C) *THY1* and (D) *ACTA2*. Expression of each target gene is normalized to *GAPDH* (housekeeping gene) and represented relative to mRNA expression in TCPS. Data are shown as mean ± SEM of three independent experiments (n = 3), each with two replicates, one donor. Statistical significance versus TCPS: (ns) $p > 0.05$, (*) $P \leq 0.05$, (**) $P \leq 0.01$ (one-way ANOVA).

Thermo-responsive scaffolds made of PET blended with poly ($PEGMA_{188}$) were chosen as the candidate scaffold for prolonged hCSSC passage experiments. Co-electrospun scaffolds made from PET maintained their size when immersed in culture media (M199) for 6 h when compared with PLGA-poly ($PEGMA_{188}$) scaffolds, where shrinkage of the co-electrospun scaffolds occurred after 6 h in the

same cell culture medium by almost 35% (from 1 cm to 0.65 cm), as shown in Figure 5.11. During electrospinning, the polymer solution is subjected to a high electric field. This process results in a high degree of alignment and orientation of polymer chains in the fibre assembly, but it also induces inner stress within the scaffolds. When immersed in liquid at a temperature higher than 35°C, macromolecular chains can rapidly relax, which undesirably causes dimensional shrinkage of the PLGA fibrous assembly [459]. It has been reported that PLGA electrospun scaffolds shrink by almost 80% when immersed in cell culture medium at 37°C for 2 h [460]. Dimensional shrinkage and distortion of the electrospun scaffolds restrict the initial adhesion of cells and infiltration into the scaffold structures [461]. It has been reported that shrinkage can be reduced by up to 53% with the use of a copper grid as the collector, in order to obtain nest-like nano-fibrous PLGA scaffolds and prevent the fibres from contracting into the centre part. Cell crown plastic rings or polypropylene rings have also been used to constrain the scaffolds to their original size. However, the culture medium level must be carefully maintained to ensure that cells on the scaffold are covered with culture medium at all times, which is a time-consuming task [459, 462]. The use of recycled PET polymer for this study was a cost-effective choice in comparison to using commercial PLGA polymer. Moreover, PET is a non-biodegradable polymer and the electrospun scaffolds are robust during cell culture [168], while PLGA is a biodegradable polymer with acidic by-products, which may affect viability of cultured cells [463]. Another reason for choosing PET scaffolds over those fabricated from PLGA is that the diameters of co-electrospun thermo-responsive PET scaffolds are in the nano range, whereas the diameters of PLGA responsive scaffolds are in the micro range. Many studies preferred the use of nano scale fibres over micro scale for tissue

engineering and regenerative medicine applications [329] as cell attachment, proliferation, signalling, cell-cell interactions and cell-matrix interactions were promoted on nano scale fibres when compared with those in the micron range [453, 464]. Therefore, to fulfil the main aim of this work, which was to create supportive thermo-responsive scaffolds for *in vitro* cell culture studies, thermo-responsive PET scaffolds were chosen for prolonged *in vitro* hCSSC culture and passage studies.

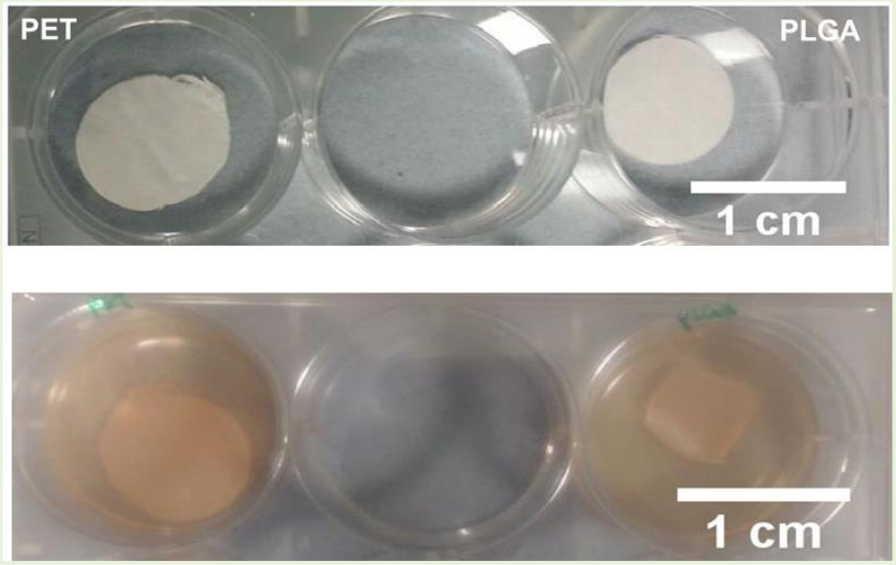



**Figure 5.11:** Images showing the effect of culture media on thermo-responsive PET and PLGA co-electrospun scaffolds after 6 h of incubation in cell culture media at 37$^{o}$C**.** Scale bars = 1 cm.

For prolonged culture and passage experiments, hCSSCs were seeded at passage 2 on TCPS (2D) and on PET-poly ($PEGMA_{188}$) scaffolds (3D) and cultured for a total of 35 days. During this period, the cells were passaged seven times using either thermal (3D scaffolds) or enzymatic (2D TCPS) methods. RT-qPCR, was performed on hCSSCs at passages 3, 6 and 9 to determine relative differences in mRNA levels of *CD34*, *ALDH3A1*, *THY1* and *ACTA2*. All experimental values were normalised to readings of the endogenous reference gene *GAPDH*. Cells from three different human donors were used for this study, with cells from each donor cultured on both

3D and 2D substrates. The key aim of this prolonged cell culture and passage experiment was to confirm that extended culture of these cells on the scaffolds, in a similar manner as for conventional 2D culture, was possible. An additional aim was to assess the effect of the extended 3D culture in comparison with 2D TCPS on the gene expression of corneal stromal stem cells.

As shown in Figure 5.12, a clear difference in mRNA levels was seen in cells cultured on 2D surfaces when compared with those cultured on 3D scaffolds. *CD34* and *ALDH3A* mRNA expression levels were significantly higher ($P \leq 0.05$ and $P \leq 0.01$, respectively) in cells cultured on 3D thermo-responsive electrospun scaffolds than in cells cultured on 2D TCPS for all passages (3, 6 and 9) and for all three donors used. *CD34* gene expression was detected in cells from two donors only at passage 6 and 9 when cultured on 2D surfaces, in comparison with 3D scaffolds where *CD34* gene expression was maintained in all donors. These results indicate that the quiescent keratocyte phenotype was maintained on PET-poly ($PEGMA_{188}$) scaffolds over 35 days of cell culture. For the *THY1 (*CD90*)* MSC/fibroblast marker, there were no significant differences ($p > 0.05$), in mRNA levels between cells cultured on 3D scaffolds and 2D TCPS over all passages. For the myofibroblast marker, *ACTA2*, there was a significant decrease in gene expression when cells were cultured on 3D scaffolds when compared with 2D TCPS at passage 6 and 9 ($p \leq 0.01$ and $p \leq 0.001$, respectively), with no significant difference ($p > 0.05$) observed at passage 3.

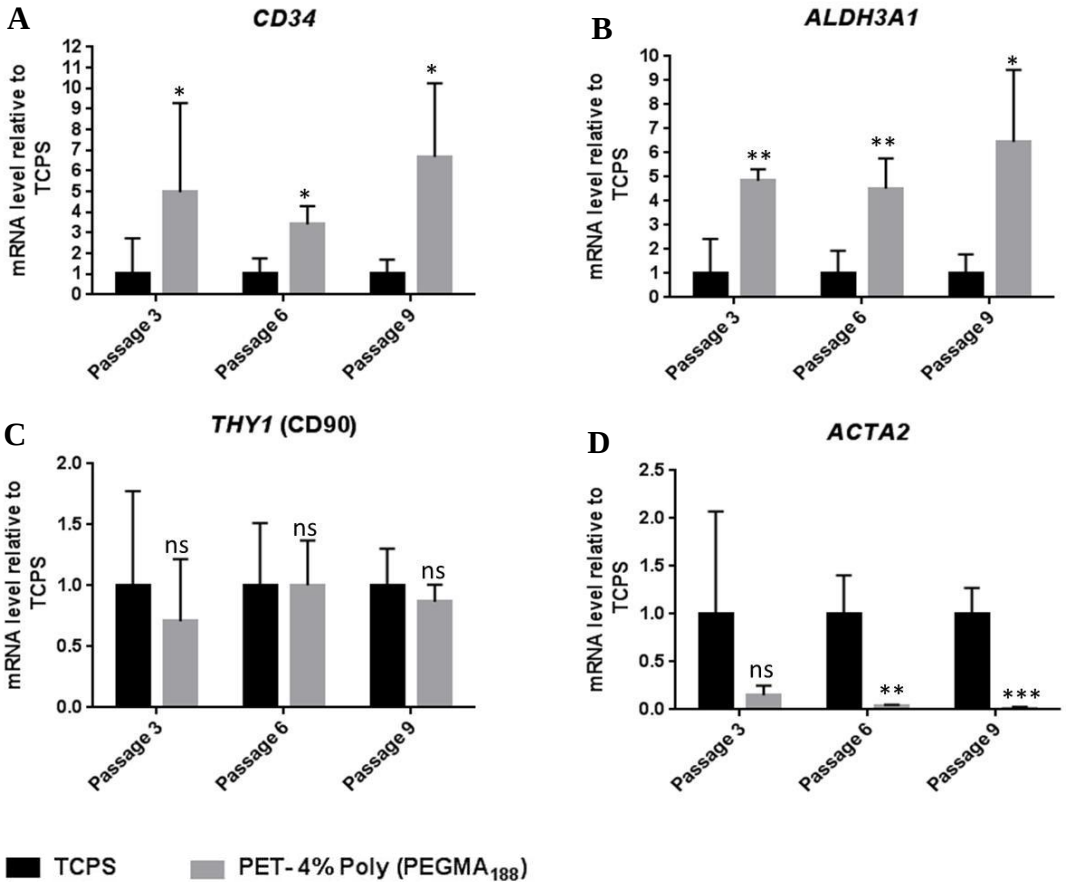



**Figure 5.12:** Comparative effects of culture environment TCPS and PET-4% poly ($PEGMA_{188}$) on gene expression of hCSSCs at different thermal (3D scaffold) and enzymatic (2D TCPS) passages of 3, 6 and 9. Relative levels of mRNA were determined by means of RT-qPCR for the following genes: (A) *CD34*, (B) *ALDH3A1*, (C) *THY1* and (D) *ACTA2*. Expression of each target gene is normalized to *GAPDH* (housekeeping gene) and represented relative to mRNA expression in TCPS of each passage. Data are shown as mean ± SEM of three independent experiments (n = 3), each with two replicates. Statistical significance versus TCPS: (ns) $p > 0.05$, (*) $P \leq 0.05$, (**) $P \leq 0.01$, (***) $P \leq 0.001$ (Student's t-test). Note: after passage 3, *CD34* gene expression of TCPS is equal to n = 2 for passage 6 and passage 9.

Data for the prolonged culture experiment of hCSSCs on 2D TCPS and 3D scaffolds were also presented relative to TCPS at passage 3 to explore the change in phenotypic marker expression with increasing the passage number. As shown in Figure 5.13, *CD34* and *ALDH3A1* mRNA levels were significantly decreased ($p \leq 0.05$ and $p \leq 0.0001$, respectively) from passage 3 to passage 6 and 9, with no

significant difference ($p > 0.05$), between passage 6 and 9 in cells cultured on both 2D TCPS and 3D electrospun scaffolds, suggesting that the overall population of cells expressing these markers reduces over time. However, *CD34* expression was lost in one of hCSSC donors cultured on TCPS after passage 3. These results are overall in agreement with the literature. A recent study showed that *CD34* gene expression was observed in early extracted corneal stromal cells, then lost at higher passages (passage 4) when cultured on 2D surfaces [445]. Another study of corneal stromal cells cultured on 2D surfaces and maintained over nine passages, showed that *CD34* gene expression was negative after passage 3 [435]. Reduction or loss of *ALDH3A1* gene expression was observed after 3 passages in repair phenotype human keratocytes (fibroblast and myofibroblast) cultured on 2D surfaces, when compared with normal human keratocytes [423]. For *THY1* (CD90), mRNA levels were significantly higher ($p \leq 0.0001$), at passage 9 than earlier cell passages. It has been reported that, *THY1* expression in corneal stromal cells cultured on 2D surfaces was lower in early passage cells (passage 0) compared with those of a higher passage (passage 4) [445]. Similar findings were observed with an increase in *THY1* (CD90) expression after passage 3 when corneal stromal cells were cultured on 2D surfaces and maintained over nine passages [435]. *THY1* (CD90) expression is considered an undesirable cell marker as it is rarely present in a healthy cornea, and is associated with an activated keratocyte phenotype [452]. However, it is expressed by cells throughout this *in vitro* study regardless of the culture environment, and the expression was not lost during their 2D culture in the Ophthalmology laboratory at Nottingham [444]. For *ACTA2,* mRNA levels were significantly decreased ($p \leq 0.05$), from passage 3 to passage 6 and from passage 6 to passage 9 in cells cultured

on both 2D TCPS and 3D scaffolds. The downregulation of *ACTA2* over different passages was considered as a promising finding as *ACTA2* gene expression is related to the undesirable activated corneal myofibroblast and this phenomenon has not been previously reported in the literature.

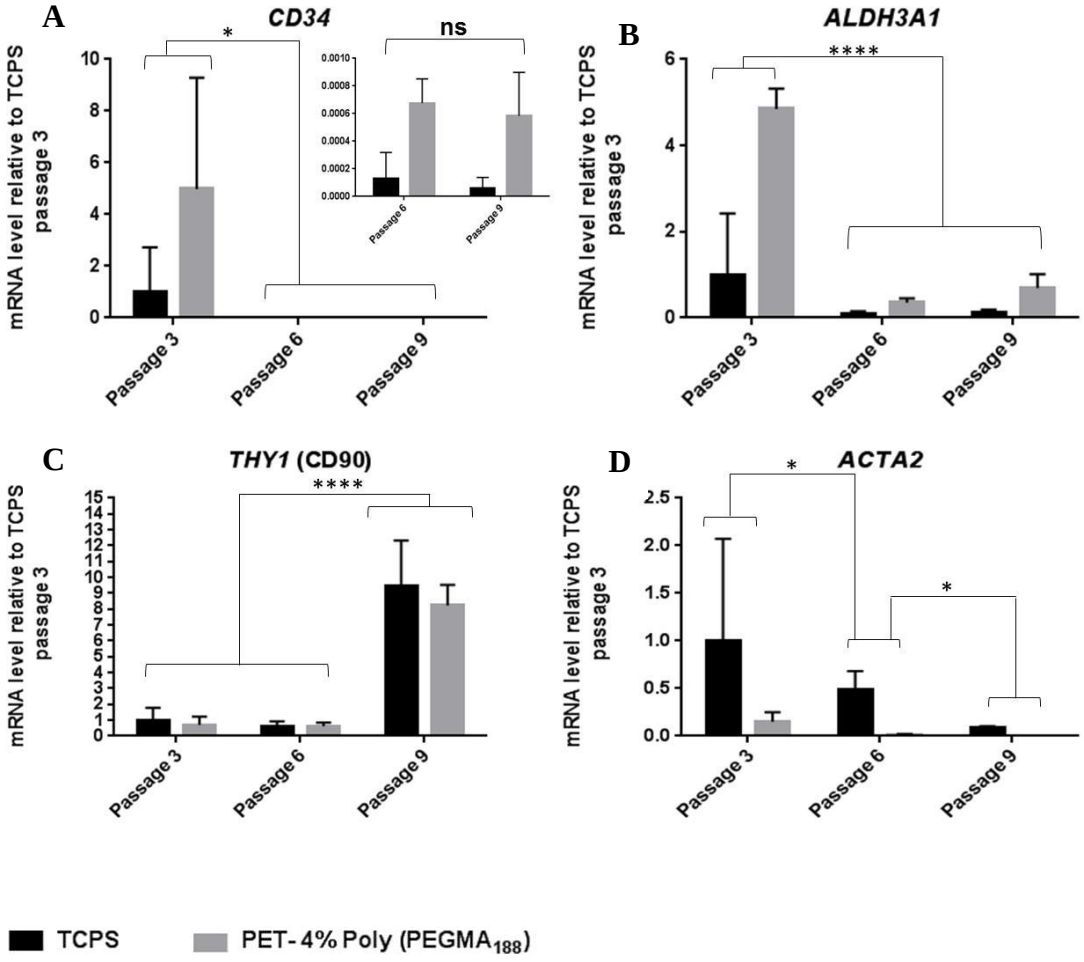



**Figure 5.13:** Comparative effects of increasing passage number on gene expression of hCSSCs culture on TCPS and PET-4% poly ($PEGMA_{188}$) at different thermal (3D scaffold) and enzymatic (2D TCPS) passages of 3, 6 and 9. Relative levels of mRNA were determined by means of RT-qPCR for the following genes: (A) *CD34*, (B) *ALDH3A1*, (C) *THY1* and (D) *ACTA2*. Expression of each target gene is normalized to *GAPDH* (housekeeping gene) and represented relative to mRNA expression in TCPS of passage 3. Data are shown as mean ± SEM of three independent experiments (n = 3), each with two replicates. Statistical significance versus TCPS at passage 3: (ns) for $p > 0.05$, (*) $P \leq 0.05$, (****) $P \leq 0.0001$ (one-way ANOVA). Note: after passage 3, *CD34* gene expression of TCPS is equal to n = 2 for passage 6 and passage 9.

In addition to substrate type (2D or 3D), the culture medium has a significant influence on the phenotype and differentiation capacity of corneal stromal cells [435]. A recent study illustrated the effect of seven different medium types on mRNA levels and protein expression of hCSSCs cultured on 2D glass surfaces at passage 2 [444]. In another study using corneal stromal cells, the cells were cultured on 2D surfaces in two different media, DMEM-based keratocyte medium supplemented with 10% FBS and M199-based medium supplemented with 20% FBS. The cells were then analysed using flow cytometry for the expression of *CD34* over nine consecutive passages. Cells cultured in M199 retained the quiescent keratocyte marker *CD34* over several passages, but this was absent in cells cultured in DMEM [435]. Traditionally, keratocytes have been cultured in DMEM supplemented with 10% FBS [425, 465, 466]; however, this has been shown to produce sub-optimal culture conditions for keratocytes and causes a rapid loss of the *CD34* marker [427]. Attempts to differentiate the cells back to a keratocyte phenotype was evident by the regain of *CD34* expression, after it was lost at passage 4 when mesenchymal culture medium was used [445]. Culture in medium containing serum of varying concentrations also influences the hCSSC phenotype [444]. Serum has advantages as it provides a source of attachment and growth factors, allowing the proliferation and rapid expansion of the cells. However, FBS is considered as an undefined biological product, which varies from batch to batch, and can trigger the spontaneous differentiation of cells [467]. The presence of serum in the culture medium or growth factors, such as transforming growth factor-beta 1 (TGF-β1), were reported to induce a fibroblastic or myofibroblastic phenotype, along with protein markers such as α-SMA [468, 469] and CD90 [470], combined

with the loss of keratocytes markers [411, 415]. Culture in low-serum media has been reported to preserve the keratocyte phenotype, while promoting proliferation; however, cells exhibited much lower proliferation rates [471]. When hCSSCs were placed in a serum-free medium supplemented with insulin and ascorbate, they upregulated the expression of keratocyte-specific markers [472]. Stem cell medium (SCM) has also been used for hCSSC culture due to its ability to promote markers associated with progenitor cells and pluripotency. SCM does not contain FBS, but instead uses knockout serum replacement (KSR), which is chemically defined and contains a mix of amino acids, vitamins, antioxidants, trace elements, insulin, transferrin and lipid-rich albumin. KSR has been identified as the ingredient with the greatest involvement in the regulation of pluripotency [473]. SCM contains the recombinant protein fibroblast growth factor (b-FGF), which is associated with differentiation into the keratocyte phenotype [467]. Several other groups reported the retention of keratocyte and stem cell phenotypes when culturing in DMEM/F12 [474, 475] or DMEM/MCDB-201[472, 476] rather than DMEM, which was proven to cause a rapid loss of several markers, including CD105 and the keratocyte marker, CD34 [466]. In this study, the observed change in the gene expression profiles of the hCSSCs on the 2D and 3D culture substrates were obtained using 20% serum (highly proliferative media); due to this, the changes reported were related to the substrate type used (2D TCPS and 3D thermo-responsive scaffolds). Therefore, it would be appropriate for future work to assess the keratocyte phenotype when the cells are cultured on the 3D scaffolds using a low-serum-containing and chemically defined medium.

Immunocytochemistry was conducted in parallel with RT-qPCR for hCSSCs at passages 3, 6 and 9 on TCPS and PET-poly ($PEGMA_{188}$) to identify the protein expression of key markers associated with keratocytes (CD34) [420-422, 477] and corneal myofibroblasts (α-SMA) [478, 479]. As shown in Figure 5.14, the results of the RT-qPCR were reflected in the protein immunocytochemistry studies. CD34 positive stain was seen in all cells at all passages when cultured on the thermo-responsive 3D scaffolds, while this expression was lost after passage 3 when cells were cultured on 2D TCPS. The myofibroblast protein, α-SMA, is visible in individual cells cultured on TCPS at all passages, but not on the 3D electrospun scaffolds. Similar results were reported in another study where CD34 staining was not observed when cells were cultured on 2D surfaces, but the expression of α-SMA was detected [444, 477].

To conclude, from the prolonged culture and passaging experiments, hCSSCs cultured on 3D thermo-responsive electrospun scaffolds promoted the expression of *CD34* and *ALDH3A1* keratocyte markers (quiescent phenotype). This was accompanied by a significant reduction in the myofibroblastic marker, *ACTA2* (activated phenotype), and with the expression of the MSC/fibroblast marker, CD90, on both scaffolds and TCPS.

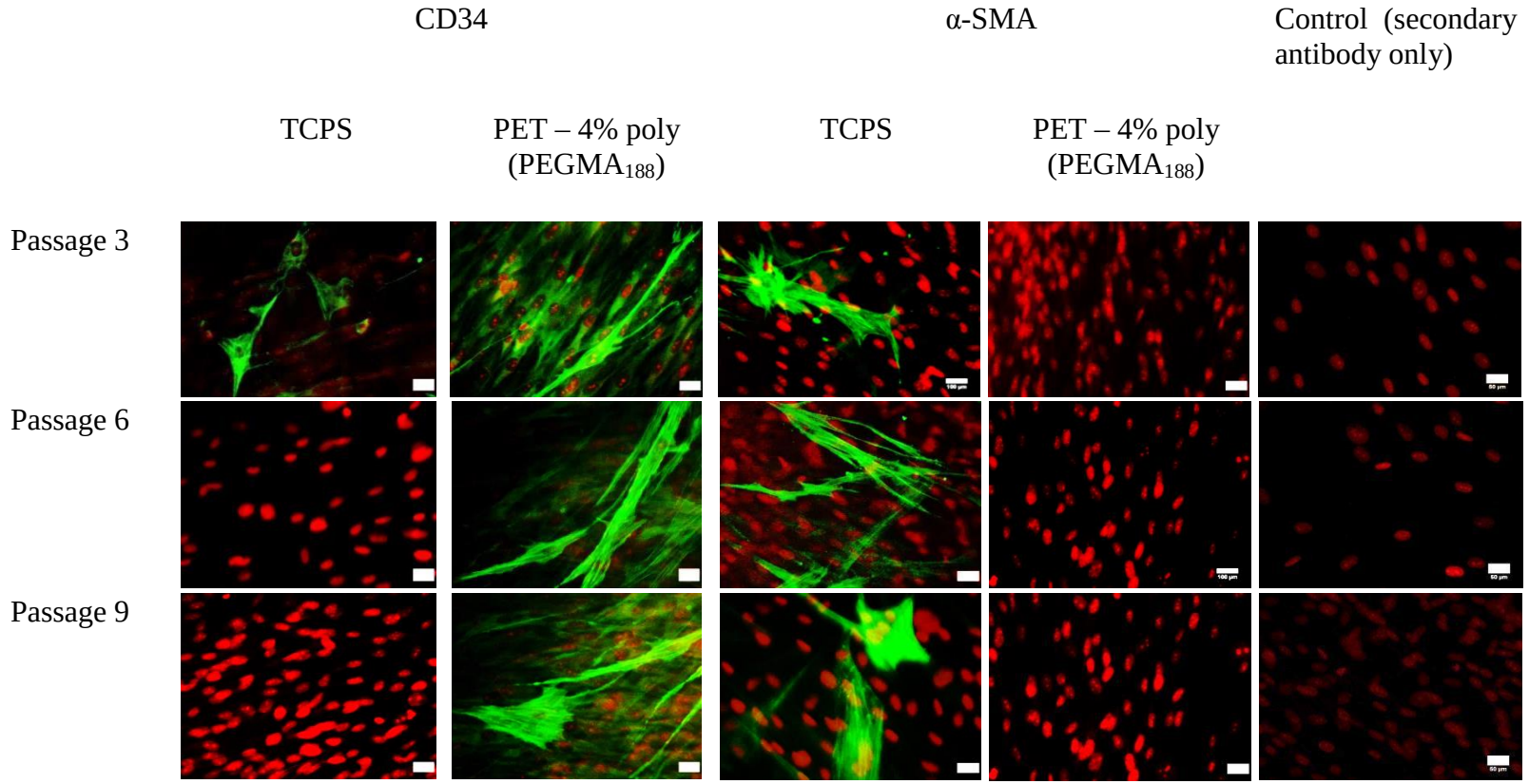



**Figure 5.14:** Representative fluorescence microscopy images showing the effects of culture environment of TCPS and PET-4% poly ($PEGMA_{188}$) scaffolds on keratocyte and myofibroblast markers of hCSSCs. Immunocytochemistry was performed for CD34 (green) and **α-**SMA (green) after five days in cell culture at passages 3, 6 and 9 from one donor. Negative control images (secondary antibody only) of donkey anti-mouse immunoglobulin (Ig)G Alexa Fluor-488. All images shown with PI counterstain (red), scale bar = 50 μm.

Cells harvested from thermo-responsive PET-poly ($PEGMA_{188}$) scaffolds and TCPS via reducing the culture temperature or trypsin digestion, respectively, were counted using a haemocytometer at each passage (total of nine passages), as shown in Figure 5.15 A. Significant differences ($p \leq 0.05$), in hCSSC cell numbers between the thermo-responsive scaffolds and TCPS were observed at passages 1 and 3 only, which suggests the incomplete recovery of attached hCSSCs cells from the scaffolds. However, at passages 2, 4, 5, 6, 7, 8 and 9 there was no significant difference ($p > 0.05$) between cell numbers harvested from TCPS when compared with thermal detachment from the 3D scaffolds.

Population doublings (PDs) were calculated at each passage using the following formula:

$$PD = [\log_{10} (\text{total cell counts/cells seeded}) / \log_{10} 2]$$

Proliferation rates were calculated by hours in culture (on TCPS or co-electrospun PET-poly ($PEGMA_{188}$))/ cumulative population doublings (CPDs) over 9 passages.

An analysis of these proliferation rates is shown in Figure 5.15 B, The average PD interval for hCSSCs on TCPS was 2.8 ± 0.75 days and on PET-poly ($PEGMA_{188}$) it was 3.6 ± 1.2 days. No significant difference ($p > 0.05$), in the CPDs was observed up to 20 days in culture, but there were significant differences in the CDPs observed on days 25 and 30 ($p \leq 0.01$), day 35 ($p \leq 0.001$) and days 40 and 45 ($p \leq 0.0001$) in culture between the scaffolds and TCPS. This indicates that the thermo-responsive

co-electrospun scaffolds supported the growth and proliferation of the hCSSCs in a similar way to the 2D TCPS.

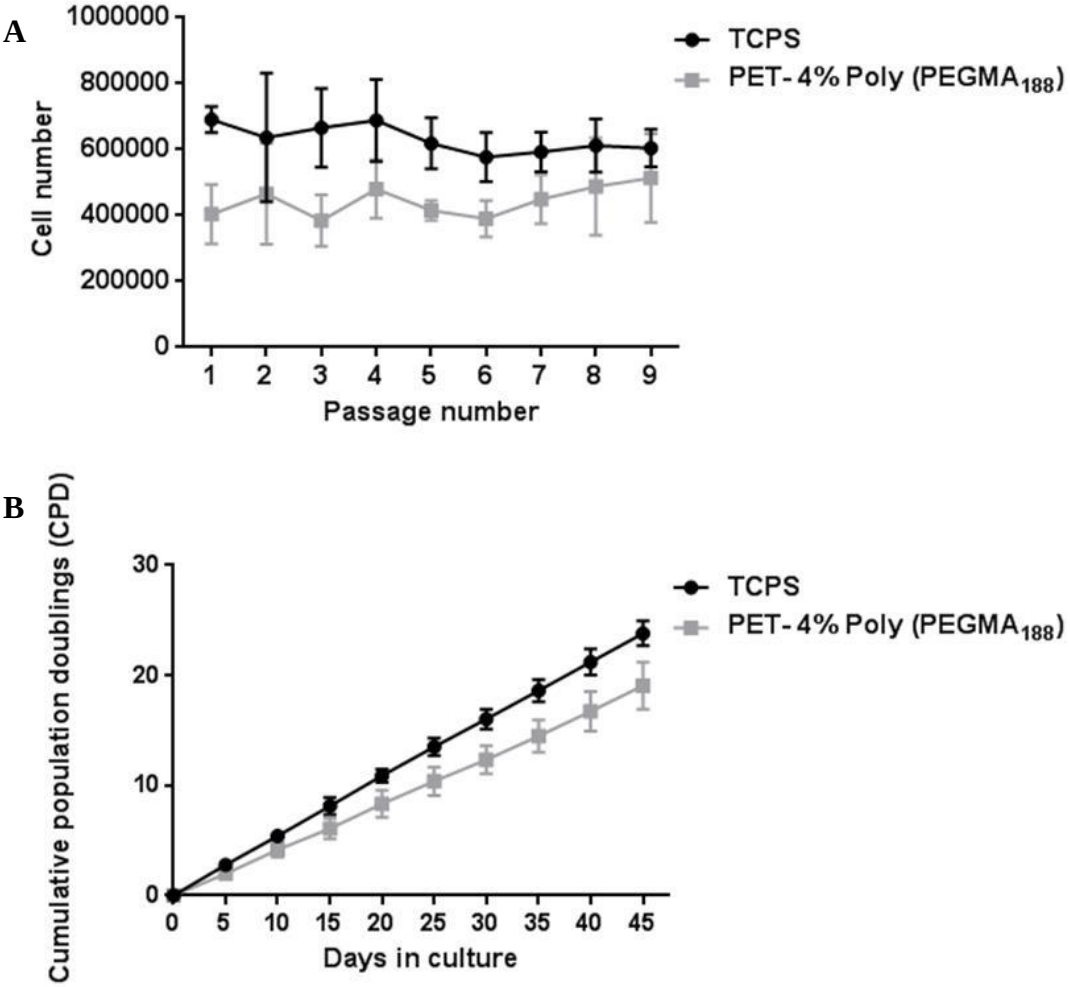
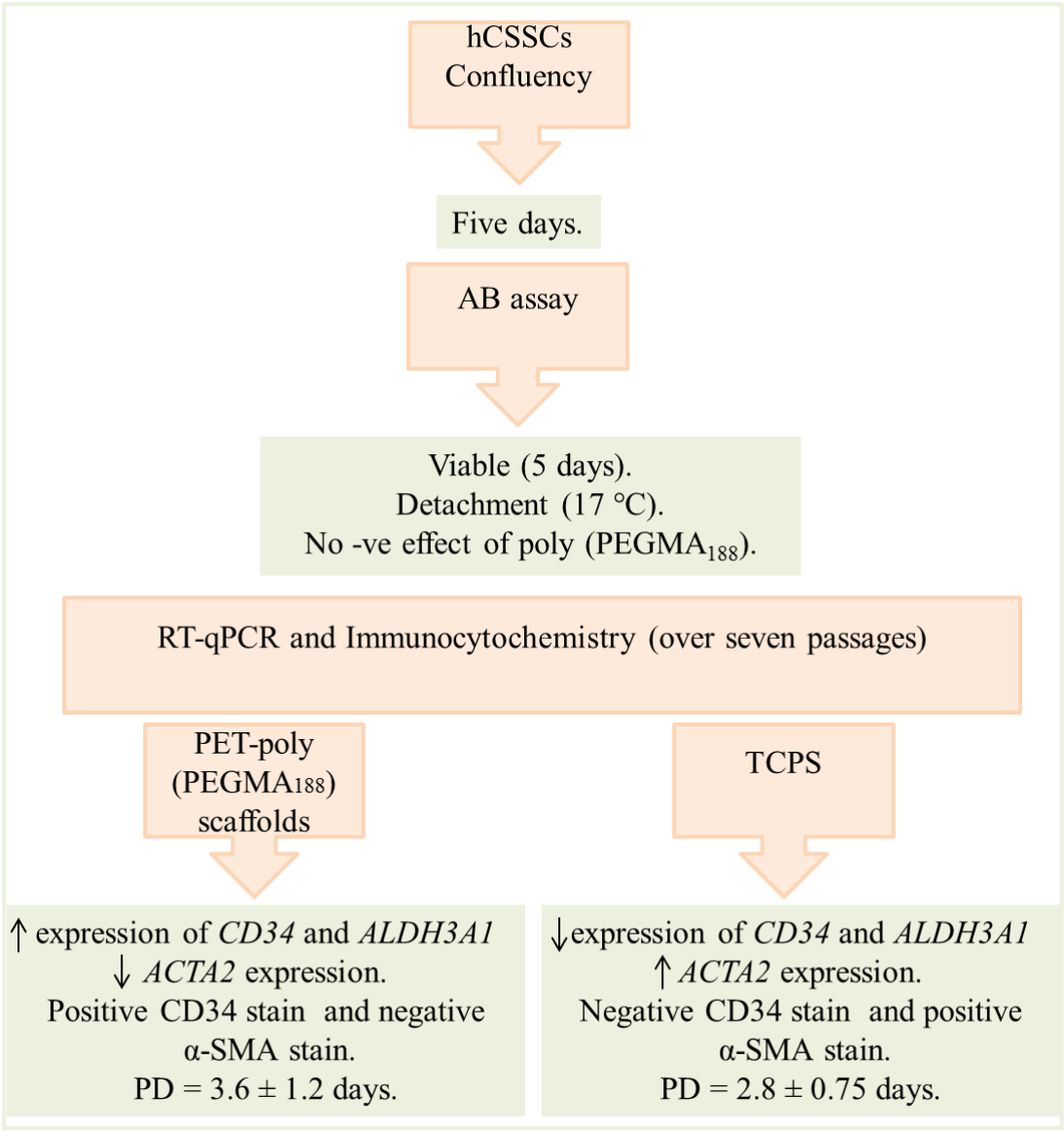



**Figure 5.15:** Graphs showing A) hCSSCs number and B) growth curve for hCSSCs, which they were serially passaged, over 9 passages, using trypsin and temperature from TCPS or co-electrospun scaffolds containing poly ($PEGMA_{188}$) respectively. Data are shown as mean ± standard error of the mean of three independent experiments (n = 3). Statistical significance versus TCPS: (ns) $p > 0.05$, (*) $P \leq 0.05$, (**) $p \leq 0.01$, (***) $p \leq 0.001$, (****) $P \leq 0.0001$ (two-way ANOVA).

## 5.5 Conclusions

Human corneal stromal stem cells have been proposed for tissue regeneration and cell-based therapies in order to treat corneal diseases. However, they are known for their differentiation into an undesirable activated fibroblast or myofibroblast phenotype when extracted and cultured on 2D surfaces. The maintenance of quiescent hCSSCs is an important step for their further use in clinical applications or scientific research. In order to achieve this, hCSSCs were cultured on 3D thermo-responsive electrospun scaffolds. Cells were not affected by the thermo-responsive polymer, poly ($PEGMA_{188}$), as the cells were viable and proliferated in a similar manner to those cultured on the TCPS. Furthermore, culture of the cells on the 3D scaffolds promoted the quiescent keratocyte phenotype, with increased expression of the keratocyte markers, *CD34* and *ALDH3A1,* and decreased expression of the myofibroblast marker, *ACTA2,* when compared to 2D culture flasks. However, *CD34* and *ALDH3A1,* expression were decreased after passage 3, suggesting that the overall population of cells expressing this marker reduces over time. Immunocytochemistry was conducted and resulted with a positive CD34, and negative α-SMA stain at all passages, on 3D scaffolds in comparison with the 2D culture. Moreover, these thermo-responsive 3D scaffolds, supported the culture and detachment of hCSSCs without enzymes. This culture system has the potential to provide high numbers of a desirable cell phenotype for the regeneration of the ocular surface in cases of disease or trauma.

**Table 5-4:** A summary of the experimental finding of Chapter 5



# Chapter 6. General discussion, conclusions and future works

Severely injured or damaged organs are normally replaced via organ or tissue transplantation. However, difficulties associated with organ shortages, the tissue or organ quality and immune system complications after transplantation have led scientists to apply regenerative medicine to the repair, replacement or regeneration of the function of the injured tissues [2, 11]. The maintenance and expansion of mammalian cells is an important step prior to their further use in regenerative medicine applications. Traditionally, cells are usually maintained on 2D culture substrates such as TCPS. In addition, cells are usually sub-cultured when they reach confluency using trypsin/EDTA or a cell scraper to physically remove them from the culture substrate. However, both of these passaging methods are disadvantageous as they can dramatically affect the quality of the cells [1, 205, 330, 333, 334, 336].

Synthetic 'responsive' polymeric surfaces, on which the bio-adhesive properties of the surface can be switched by environmental factors or external controls, e.g. temperature, have been paid considerable attention due to their potential applications in cell culture [385], drug delivery systems [480] and sensors [481]. These responsive biomaterials have been widely used as a tuneable artificial ECM for different cell types, including endothelial cells [328], hepatocytes [214], cardiomyocytes [241] and hMSCs [233]. On these surfaces, cells can be cultured at temperatures above the LCST of the thermo-responsive polymer (hydrophobic surface), and then harvested by lowering the culture temperature below the LCST (hydrophilic surface), without the use of digestive enzymes or chelating agents [338]. The Okano group has extensively studied the use of thermo-responsive

PNIPAAm as a 2D surface mediator of biopolymers or cell culture due to its ability to undergo a sharp coil-globule transition in water at 32°C [203, 231, 338-341].

A three-dimensional culture environment for mammalian cells is considered an important factor for the replication of the ECM found in native 3D tissues. Additionally, various complicated biological mechanisms, such as stem cell differentiation [83] and tissue morphogenesis [84], are known to differ from those of *in vivo* organs or tissues [19]. Moreover, the large surface area provided by the 3D substrates results in more biding sites and a higher loading capacity than on the 2D substrates. As a result, many methods have been conducted to develop a 3D growth environment that mimics the original tissue as closely as possible [85-88]. One of these methods involves fabricating 3D polymeric scaffolds using the electrospinning technique. The resultant electrospun fibres have controlled morphology, porosity and composition, with nano- or micro-range diameters [164, 245, 252]. These electrospun scaffolds have been used widely in tissue engineering, cell culture, wound dressing, sensors, clothing and filtration devices [164].

Despite the wide use of the electrospinning technique and its application with many different natural or synthetic polymers [164], there are limited reports describing the electrospinning of thermo-responsive polymers and the creation of responsive electrospun fibres [253-258]. Additionally, very few studies have reported the fabrication of thermo-responsive electrospun scaffolds for biological applications [228, 345], with none illustrating their use for the thermal detachment of mammalian cells.

Therefore, the aim of this research project was to fabricate environment-responsive (to temperature) scaffolds using electrospinning for extended mammalian cell culture and passage. Two polyesters were used in this study, PLGA (bio-degradable) and PET (non-biodegradable), in order to demonstrate that the phenomenon is not polymer specific. These polymers have a fundamental application in tissue engineering and regenerative medicine [176, 200, 259, 301]. An exemplar cell type, 3T3 fibroblasts (differentiated cell type), was used to investigate the thermo-responsive behaviour and biocompatibility of the scaffolds. Then ihMSCs (stem cell type) and Caco2 (carcinoma cell type) cells were used to demonstrate that the phenomenon is not cell-line specific. hCSSCs (primary human stem cell type) were also used to illustrate the effect of extended cell culture and (seven) thermal passages on the cell phenotype. Such a culture system could eliminate the need to detach cells from the culture surface using proteolytic enzymes (trypsin). PEG-based polymers were proposed to fabricate switchable surfaces for mammalian cell culture because they are water soluble, non-toxic, non-immunogenic and FDA-approved [205, 226, 249]. Additionally, they possess a reversible phase transition, unlike PNIPAAm-based polymers, which possess a strong H-bond donor in their molecular structure [248]. This makes switchable PEG-based substrates intended for cell-culture applications more desirable. This is particularly the case where the process of cell attachment onto the hydrophobic surface (above the LCST), and the subsequent detachment of cells from the hydrophilic surface (below the LCST) is continuous and unhindered by irreversible hydration [248].

Chapter 2 described the electrospinning and characterization of PET and PLGA fibre-based scaffolds. Bead-less fibres with nano- and micro-range diameters were

prepared from PET and PLGA, respectively. This was achieved by altering various electrospinning parameters such as the polymer solution concentration, voltage and flow rate. The surface wettability of these scaffolds was also determined by WCA measurements, with a mean of 134 ± 0.74° for PLGA and 111 ± 6.9° for PET scaffolds. After that, poly ($PEGMA_{188}$) polymer was synthesized by free radical polymerization following a published method [251]. $^{1}H$ NMR and $^{13}C$ NMR were conducted in order to confirm the successful preparation and purification of poly ($PEGMA_{188}$). The synthesized polymer showed LCST properties when the solution transparency changed from clear to turbid at 26°C. Spectrophotometry was used to determine the LCST of poly ($PEGMA_{188}$), which was found to be between 22.5°C and 25.2°C; this is in agreement with the literature [194, 311, 312]. Different methods were investigated for the incorporation of the thermo-responsive polymer in the PET and PLGA electrospun matrix, either during the electrospinning process or as a post-electrospinning modification. Post-electrospinning methods for thermo-responsive polymer incorporation within the fibres included surface adsorption, NaOH surface treatment and surface entrapment. The SEM data showed that surface adsorption produced a covering of poly ($PEGMA_{188}$) on the scaffold's surface. Additionally, the surface wettability of PLGA and PET scaffolds was measured via the WCA after surface adsorption, demonstrating hydrophilic surfaces of less than 90° and less than 60°, respectively. The hydrophilic nature of the treated scaffold was successfully maintained even after washing them with distilled water, which indicates the presence of poly ($PEGMA_{188}$) on the scaffolds' surface. However, due to the high viscosity of poly ($PEGMA_{188}$) and difficulties in the handling of treated scaffolds, the usefulness of these thermo-responsive fibres in further applications

was limited; therefore, this method was not pursued. NaOH surface hydrolysis was explored in order to induce homogenous surface hydrolysis without affecting the fibre integrity [131, 136, 163], as a means of improving the surface deposition of the poly ($PEGMA_{188}$). Following NaOH treatment, the surface hydrophobicity of PET and PLGA scaffolds was reduced. Although the desired grooves on the scaffold surface were created, the process was detrimental to the integrity of the fibres and so this method was not taken further. Post-electrospinning surface entrapment of the poly ($PEGMA_{188}$) within the PET and PLGA scaffolds resulted in an enlargement in the fibre diameters upon addition of acetone [320-323] and TFE [324, 325] solvents, respectively, illustrating the swelling and subsequent shrinkage upon addition of the non-solvent, water, into the system. However, further studies need to be conducted in order to ensure the presence of poly ($PEGMA_{188}$) in the scaffolds. Finally, a single-step method in which the poly ($PEGMA_{188}$) was mixed with either the PET or PLGA polymer solutions before co-electrospinning (blend-electrospinning) was conducted. Many polymer mixtures have been successfully co-electrospun using this method for drug-delivery or cell-culture applications [277-279]. For example, PNIPAAm was co-electrospun with PEO and used as a thermo-responsive drug carrier system for vitamin B12 [277]. Moreover blend-electrospinning was used to incorporate different materials in the polymer solution, such as the co-electrospinning of basic fibroblast growth factor (bFGF) with PLGA polymer for MSC culture [482]. Therefore, after trying different electrospinning parameters, bead-less electrospun mats were formulated and the presence of the thermo-responsive polymer was confirmed via $^{1}H$ NMR studies. As a result, co-

electrospinning was the method of choice for further characterization and cell-culture studies.

The thermo-responsive nature of the synthesised 3D fibrous scaffolds and their suitability for mammalian cell culture was tested for the first time in Chapter 3. Firstly, different concentrations of the thermo-responsive polymer were co-electrospun with PLGA and PET polyesters to create thermo-responsive fibrous mats. Additionally, the effect of different concentrations of poly ($PEGMA_{188}$) (2, 4, 6, 8 and 10% [*w/v*]) on the co-electrospun fibres was studied. The co-electrospun scaffolds were characterized by SEM, which confirmed the production of uniform and bead-less fibres. Co-electrospun fibres prepared with lower concentrations (2 and 4% [*w/v*]) resulted in fibres with average diameters of 3.6 ± 0.42 µm and 3.8 ± 0.45 µm, respectively, which were similar to the control PLGA (3 ± 0.8 µm) scaffolds alone. Similar findings were observed when PET was co-electrospun with 2 and 4% (*w/v*) poly ($PEGMA_{188}$), which resulted in fibres with average diameters of 838.9 ± 195 nm and 877 ± 195 nm, respectively, when compared to PET fibres alone (836.2 ± 172.7 nm). Higher poly ($PEGMA_{188}$) concentrations in the co-electrospun scaffolds resulted in fibres with higher diameters. The surface wettability is considered an important factor for cell adhesion and the subsequent cell recovery from the culture surface [360-362]. Therefore, WCA measurements at 20°C were conducted on co-electrospun fibres, which illustrated a change in the hydrophobic nature of the PLGA and PET fibres to a more hydrophilic surface. With increasing amphiphilic poly ($PEGMA_{188}$) concentrations, a change in the WCA from 87.5 ± 3.1° to 43.5 ± 9.8° was observed when 2% and 10% poly ($PEGMA_{188}$) concentrations were used, respectively. These values were in good agreement with

the literature [200, 205, 251, 357-359]; however, some co-electrospun scaffolds made from higher poly ($PEGMA_{188}$) concentrations exhibited a heterogeneous surface with hydrophilic and hydrophobic areas across the scaffolds. Moreover, PLGA and PET solutions co-electrospun with a 2% (*w/v*) poly ($PEGMA_{188}$) solution, resulted in fibres with surfaces that were closer to being hydrophobic, rather than hydrophilic, with WCA measurements of 87.5 ± 3.1° and 96.9 ± 13.5°, respectively. XPS and $^{1}$H-NMR analysis were conducted to investigate the elemental composition of these surfaces, in addition to confirming the presence of poly ($PEGMA_{188}$) in the fibres. The molar ration calculations from $^{1}$H NMR, demonstrated an overall increase in poly ($PEGMA_{188}$) ratio in co-electrospun scaffolds with increase in the polymer concentration. However, XPS data showed that PLGA and PET solutions co-electrospun with a higher poly ($PEGMA_{188}$) concentration resulted in fibres with heterogeneous surfaces when compared with those prepared with lower concentrations of 2% (*w/v*). These scaffolds were then used as a 3T3-mouse-fibroblast cell-culture substrate and were able to support their attachment, spreading and proliferation in a similar manner to those cultured on non-thermo-responsive scaffolds. Moreover, the detachment of the cultured cells from these thermo-responsive scaffolds was achieved after reducing the culture temperature to 17°C. However, significant decreases in the cell numbers were recorded on co-electrospun scaffolds with higher poly ($PEGMA_{188}$) concentrations of 8 and 10% (*w/v*), when compared with lower concentrations of 2, 4 and 6% (*w/v*). These cell-culture results were in agreement with the previous surface characterisation of these scaffolds based on the WCA measurements, XPS and $^{1}$H MR. Therefore, a lower concentration of

4% (*w/v*) of poly ($PEGMA_{188}$) in the co-electrospinning solution was chosen for further experiments.

After conducting preliminary cell culture and passaging experiments on the thermo-responsive scaffolds for the first time in Chapter 3, further cell culture and passage experiments were investigated in Chapter 4. In order to determine the efficacy of cell detachment from the thermo-responsive scaffolds, cell yields were determined using 3T3 fibroblasts. The average cell yields obtained from PLGA-4% poly ($PEGMA_{188}$) and PET-4% poly ($PEGMA_{188}$) scaffolds were $8 \times 10^5 \pm 0.8 \times 10^5$ cells/mL and $7 \times 10^5 \pm 0.4 \times 10^5$ cells/mL, respectively, compared to an average cell yield of $9.2 \times 10^5 \pm 0.3 \times 10^5$ cells/mL obtained from TCPS. Future work with regard to the incomplete recovery of the attached cells could be resolved by changing the electrospinning method and the usage of core-sheath electrospun fibres to insure that the thermo-responsive polymer is covering the entire fibre surface. It has been proven that co-axial (core-sheath) electrospinning of PEG with PCL resulted in a uniform protein distribution in the scaffolds when compared with a heterogeneous protein distribution in the blend electrospun scaffolds [365]. Following this, the prolonged culture and passage of 3T3 cells (over 10 passage cycles) was conducted. The thermo-responsive scaffolds were able to support 3T3 cell attachment at 37°C and their detachment at 17°C over 7 minutes; although, cells were retrieved as clumps rather than a single-cell suspension, as from TCPS. However, the dissociation of cell clumps into a single-cell suspension was achievable using gentle pipetting for 5–10 minutes. In Chapter 3, a recovery time of 10 minutes was enough to detach the cells; however, by reducing the recovery time to 7 minutes, it was possible to harvest the cells from the thermo-responsive

scaffolds. Fast cell detachment may be related to the high porosity of the 3D fibrous structure. It has been reported that the detachment of 3T3 fibroblast cells from 2D thermo-responsive surfaces required an incubation period of approximately 1 h at 20°C [205]. In another study, it took BAECs almost 35 minutes to detach from a porous membrane of PNIPAAm, when compared with the longer time of 55 minutes from non-porous PNIPAAm-TCPS surfaces [377, 385]. These scaffolds were then tested with other cell types, including ihMSC and Caco2 cells, in order to illustrate that the thermo-responsive scaffolds can be used for the cell expansion of different mammalian cell types. These experiments showed cell attachment, proliferation and detachment over 10 days in culture for both cell types. These scaffolds had good mechanical strength over the 10 days in culture, as the fibres remained intact and supported two cell passages. Importantly, ihMSCs and Caco2 cells were viable over the time-course of the experiment, as confirmed by the AB assay.

Clinically relevant primary human corneal stromal stem cells (hCSSCs) have been investigated for use in stromal wound healing or regeneration [444, 445, 477, 483]. It has been reported that the direct introduction of hCSSCs into the corneal stroma generated transparent tissue in a mouse model of corneal opacity [432]. Additionally, hCSSCs injected into mice corneas did not elicit immune rejection over an extended period of time [433]. Therefore, the utilisation of hCSSCs appears to offer an opportunity to develop cell- and tissue-based therapies for the treatment of corneal blindness [408]. These cells are believed to be a keratocyte progenitor [429]. However, they undergo fibroblastic and myofibroblastic differentiation when expanded on 2D culture surfaces [408]. Moreover, the reported difficulties in extracting these cells from PLGA electrospun scaffolds [434] have led to the

application of the synthesised thermo-responsive system for hCSSC culture and passage, as described in Chapter 5. Corneal stromal stem cells were cultured in M199 medium supplemented with 20% (*v/v*) serum, as it has been proven that this media supports hCSSC proliferation [444]. Initial studies involved the staining of hCSSCs cultured on scaffolds and TCPS with calcein-AM/PI to confirm the cell confluency on the scaffolds and the scaffolds' biocompatibility. The cells required almost five days to become 70% confluent, and then they were detached at 17°C without the use of trypsin. Importantly, hCSSCs were not affected by the thermo-responsive polymer poly ($PEGMA_{188}$) when they were cultured on the scaffolds; the cells were viable and proliferated in a similar manner to those cultured on the TCPS surfaces. In order to utilise hCSSCs in tissue regeneration and cell-based therapies for the treatment of corneal diseases, the maintenance of a keratocyte phenotype of the hCSSCs is an important step for their further use in clinical applications or scientific research [478, 484]. Therefore, preliminary RT-qPCR using *CD34* or *ALDH3A1* as keratocyte markers, *TYH1* as a MSC/fibroblast marker and *ACTA2* as a myofibroblast marker was carried out to evaluate the effect of the thermo-responsive polymer and the 3D environment on the cell phenotype in comparison with the 2D surface. The data showed that the thermo-responsive poly ($PEGMA_{188}$) did not elicit a negative effect on the cultured cells in comparison with the non-thermo-responsive scaffolds (PLGA and PET alone). Moreover, cell culture on the 3D scaffolds promoted the quiescent keratocyte phenotype, with the increased expression of the *CD34* and *ALDH* markers, and the decreased expression of *ACTA2* markers when compared with 2D culture flasks. Thermo-responsive PET-poly ($PEGMA_{188}$) scaffolds were then chosen for a prolonged (seven thermal and enzymatic cell

passages) passage experiment, due to their nano-range fibre diameter and robustness in the culture medium. The results showed the maintenance of mRNA levels of markers of the keratocyte phenotype over passage 3, 6 and 9, in addition to the reduction of the activated phenotype *ACTA2* gene over passages, which has not been previously reported in the literature. Immunocytochemistry was conducted in parallel with RT-qPCR for hCSSCs at passages 3, 6 and 9 on TCPS and PET-poly ($PEGMA_{188}$) in order to identify the protein expression of key markers associated with keratocytes (CD34) [420-422, 477] and corneal myofibroblasts (α-SMA) [478, 479]. CD34 expression was seen in all cells at all passages when cultured on thermo-responsive 3D scaffolds, while this expression was lost after passage 3 when cells were cultured on 2D TCPS. α-SMA can clearly be seen in individual cells cultured on TCPS at all passages, but not on the 3D electrospun scaffolds. The culture media and its constituents, such as serum, are considered as important factors that trigger the change in protein and gene expression of hCSSCs [444]. Therefore, for short-term future studies, changing the culture medium or reducing the serum in the medium could contribute to more desirable results in combination with the 3D thermo-responsive scaffolds. This is supported by reports of the upregulation of the expression of keratocyte-specific markers when mouse CSSCs were cultured in 2D and placed in a serum-free medium supplemented with insulin and ascorbate [485]. Additionally, the inclusion of more human donors should be considered.

## Future works

Through the work described in this thesis, thermo-responsive co-electrospun fibres, a class of scaffolds not previously explored for cell culture and passage applications,

were introduced into the field. The superiority of these scaffolds lies in the achievable level of control using mild stimuli such as temperature, which eliminates the use of the trypsin enzyme that can have an impact on the quality of the cultured cells [1, 205, 333, 334]. Additionally, these responsive scaffolds were not polymer or cell-type specific. Moreover, they possess 3D structures that mimic the *in vivo* construct for cell culture. This 3D environment is essential for cell signalling, proliferation and phenotype [75].

Attachment of the cultured cells to these co-electrospun scaffolds is an essential event in order to determine the cell morphologies and maintain cell functions [486]. These cell-substrate interactions are mediated by the ECM and their associated proteins [487] and can have a significant impact on biomaterial-based therapies [97]. Therefore, further investigations will be conducted to determine if any ECM was secreted by the cultured cells on the electrospun scaffolds.

One of the imminent important potential applications for these thermo-responsive scaffolds is scalable cell culture for the large-scale production of therapeutic cells. This is due to their low cost, simple design, 3D structure and physical associations. This is a challenging area of research, particularly with regards to stem cells [488]. Therefore, the short-term future work would involve the transfer of the thermo-responsive scaffolds for use in primary hMSC culture and passage. This application will be combined with the utilisation of an IME electrospinning machine for the scalable production of responsive scaffolds.

These scaffolds can also be used for the *in vitro* construction of cell-sheet layers, as they offer an easily built three-dimensional environment for cell culture. These cell

sheet layers can be used for tissue engineering applications and the regeneration of damaged organs or functions [241, 374, 375].

Further modifications to the formulated system would involve the utilisation of fluorescent-tagged poly ($PEGMA_{188}$). This could help to fully understand the distribution pattern of the thermo-responsive polymer across the co-electrospun scaffolds during the blend-electrospinning process. Moreover, attenuated total reflection-Fourier transform infrared spectroscopy (ATR-FTIR) could be useful for detecting the poly ($PEGMA_{188}$) in the scaffolds, as it can analyse from 0.5 to 2 μm below the surface of the scaffolds [265, 489]. Additionally, the inclusion of bioactive compounds could be a modification option and is expected to significantly improve the cellular response and culture within the scaffolds. This can be achieved via the encapsulation of different growth factors within the scaffolds [482].

In conclusion, blend-electrospinning was used for the first time to generate 3D responsive culture system. This system composed of thermo-responsive co-electrospun fibrous, of poly ($PEGMA_{188}$) with PLGA or PET polymers. These fibrous scaffolds were able to support the attachment, proliferation and spread of different mammalian cell types. Moreover, cell recovery was possible by reducing the culture temperature below the LCST of the thermo-responsive polymer. Additionally, this culture system has the potential to provide high numbers of a desirable hCSSC phenotype over seven consecutive passages. Therefore, this indicates that these synthetic biomaterials could play a significant role in meeting the demands for the development of well-defined culture systems for the derivation and maintenance of cultured cells.

# References


1. Phillips, D.R., *Effect of trypsin on the exposed polypeptides and glycoproteins in the human platelet membrane.* Biochemistry, 1972. **11**(24): p. 4582-4588.
2. Polak, D.J.M., *Regenerative medicine: A primer for paediatricians.* Early Human Development, 2009. **85**(11): p. 685-689.
3. Atala, A., *Engineering tissues, organs and cells.* Journal of tissue engineering and regenerative medicine, 2007. **1**(2): p. 83-96.
4. Yannas, I.V., *Facts and theories of induced organ regeneration*, in *Regenerative Medicine I*. 2005, Springer. p. 1-38.
5. Polak, J.M. and A.E. Bishop, *Stem cells and tissue engineering: past, present, and future.* Annals of the New York Academy of Sciences, 2006. **1068**(1): p. 352-366.
6. Kim, K. and G. Evans, *Tissue engineering: the future of stem cells.* Topics in tissue engineering, 2005. **2**: p. 1-21.
7. Fung, Y., *Biomechanical aspects of growth and tissue engineering*, in *Biomechanics*. 1990, Springer. p. 499-546.
8. Cohen, S., et al., *Design of synthetic polymeric structures for cell transplantation and tissue engineering.* Clinical materials, 1993. **13**(1): p. 3-10.
9. Khademhosseini, A., et al., *Microscale technologies for tissue engineering and biology.* Proceedings of the National Academy of Sciences of the United States of America, 2006. **103**(8): p. 2480-2487.
10. Dvir, T., et al., *Nanotechnological strategies for engineering complex tissues.* Nature nanotechnology, 2011. **6**(1): p. 13-22.
11. Atala, A., *Regenerative medicine strategies.* Journal of Pediatric Surgery, 2012. **47**(1): p. 17-28.
12. Rodriguez, A., et al., *Characteristics of cartilage engineered from human pediatric auricular cartilage.* Plast Reconstr Surg, 1999. **103**(4): p. 1111-9.
13. Haycock, J.W., *3D cell culture: a review of current approaches and techniques*, in *3D Cell Culture*. 2011, Springer. p. 1-15.
14. Goss, J.A., et al., *Achievement of insulin independence in three consecutive type-1 diabetic patients via pancreatic islet transplantation using islets isolated at a remote islet isolation center.* Transplantation, 2002. **74**(12): p. 1761-1766.
15. O'Connell, P., *Pancreatic islet xenotransplantation.* Xenotransplantation, 2002. **9**(6): p. 367-71.
16. Groth, C., et al., *Transplantation of porcine fetal pancreas to diabetic patients.* The Lancet, 1994. **344**(8934): p. 1402-1404.
17. Edge, A.S., M.E. Gosse, and J. Dinsmore, *Xenogeneic cell therapy: current progress and future developments in porcine cell transplantation.* Cell transplantation, 1998. **7**(6): p. 525-539.
18. Freemont, A.J. and J. Hoyland, *Lineage plasticity and cell biology of fibrocartilage and hyaline cartilage: its significance in cartilage repair and replacement.* European journal of radiology, 2006. **57**(1): p. 32-36.
19. Redi, C.A., *3D cell culture - Methods and protocols*. 2011. Vol. 55. 2011.
20. Grande, D., et al., *Evaluation of matrix scaffolds for tissue engineering of articular cartilage grafts.* Journal of biomedical materials research, 1997. **34**(2): p. 211-220.
21. Chistiakov, D.A., *Endogenous and exogenous stem cells: a role in lung repair and use in airway tissue engineering and transplantation.* J Biomed Sci, 2010. **17**(1): p. 92.
22. Becker, A.J., E.A. McCulloch, and J.E. Till, *Cytological demonstration of the clonal nature of spleen colonies derived from transplanted mouse marrow cells.* 1963.
23. Alvarez, A., et al., *Stem cell and regenerative medicine.* Current stem cell research & therapy, 2009. **4**(4): p. 287-297.

24. Sykova, E. and S. Forostyak, *Stem cells in regenerative medicine.* Laser therapy, 2013. **22**(2): p. 87.
25. Can, A., *A concise review on the classification and nomenclature of stem cells.* Turk J Hematol, 2008. **25**: p. 57-59.
26. Martin, G.R., *Isolation of a pluripotent cell line from early mouse embryos cultured in medium conditioned by teratocarcinoma stem cells.* Proceedings of the National Academy of Sciences, 1981. **78**(12): p. 7634-7638.
27. Murry, C.E. and G. Keller, *Differentiation of embryonic stem cells to clinically relevant populations: lessons from embryonic development.* Cell, 2008. **132**(4): p. 661-680.
28. Klug, M.G., et al., *Genetically selected cardiomyocytes from differentiating embronic stem cells form stable intracardiac grafts.* Journal of clinical investigation, 1996. **98**(1): p. 216.
29. Kim, J.-H., et al., *Dopamine neurons derived from embryonic stem cells function in an animal model of Parkinson's disease.* Nature, 2002. **418**(6893): p. 50-56.
30. Lindvall, O. and Z. Kokaia, *Stem cells for the treatment of neurological disorders.* Nature, 2006. **441**(7097): p. 1094-1096.
31. McDonald, J.W., et al., *Transplanted embryonic stem cells survive, differentiate and promote recovery in injured rat spinal cord.* Nature medicine, 1999. **5**(12): p. 1410-1412.
32. Leon-Quinto, T., et al., *In vitro directed differentiation of mouse embryonic stem cells into insulin-producing cells.* Diabetologia, 2004. **47**(8): p. 1442-1451.
33. Freed, C.R., et al., *Transplantation of embryonic dopamine neurons for severe Parkinson's disease.* New England Journal of Medicine, 2001. **344**(10): p. 710-719.
34. Herberts, C.A., M. Kwa, and H. Hermsen, *Risk factors in the development of stem cell therapy.* 2011.
35. Takahashi, K. and S. Yamanaka, *Induction of pluripotent stem cells from mouse embryonic and adult fibroblast cultures by defined factors.* cell, 2006. **126**(4): p. 663-676.
36. Soldner, F., et al., *Parkinson's disease patient-derived induced pluripotent stem cells free of viral reprogramming factors.* Cell, 2009. **136**(5): p. 964-977.
37. Yu, J., et al., *Induced pluripotent stem cell lines derived from human somatic cells.* Science, 2007. **318**(5858): p. 1917-1920.
38. Zhang, J., et al., *A human iPSC model of Hutchinson Gilford Progeria reveals vascular smooth muscle and mesenchymal stem cell defects.* Cell stem cell, 2011. **8**(1): p. 31-45.
39. Lee, E. and J. Hui, *The potential of stem cells in orthopaedic surgery.* Journal of Bone & Joint Surgery, British Volume, 2006. **88**(7): p. 841-851.
40. De Coppi, P., et al., *Isolation of amniotic stem cell lines with potential for therapy.* Nature biotechnology, 2007. **25**(1): p. 100-106.
41. Wang, H.S., et al., *Mesenchymal stem cells in the Wharton's jelly of the human umbilical cord.* Stem cells, 2004. **22**(7): p. 1330-1337.
42. Zuk, P.A., et al., *Multilineage cells from human adipose tissue: implications for cell-based therapies.* Tissue engineering, 2001. **7**(2): p. 211-228.
43. Gage, F.H., *Mammalian neural stem cells.* Science, 2000. **287**(5457): p. 1433-1438.
44. Caplan, A.I., *Mesenchymal stem cells.* Journal of orthopaedic research, 1991. **9**(5): p. 641-650.
45. Tropepe, V., et al., *Retinal stem cells in the adult mammalian eye.* Science, 2000. **287**(5460): p. 2032-2036.
46. Toma, J.G., et al., *Isolation of multipotent adult stem cells from the dermis of mammalian skin.* Nature cell biology, 2001. **3**(9): p. 778-784.

47. Bajada, S., et al., *Updates on stem cells and their applications in regenerative medicine.* Journal of tissue engineering and regenerative medicine, 2008. **2**(4): p. 169-183.
48. Rizouli, V. and J. Gribben. *The role of stem cell transplantation in chronic lymphocytic leukemia*. in *Seminars in hematology*. 2004. Elsevier.
49. Jabbour, E., et al., *Stem cell transplantation for chronic lymphocytic leukemia: should not more patients get a transplant?* Bone marrow transplantation, 2004. **34**(4): p. 289-297.
50. Goshima, J., V.M. Goldberg, and A.I. CAPLAN, *The osteogenic potential of culture-expanded rat marrow mesenchymal cells assayed in vivo in calcium phosphate ceramic blocks.* Clinical orthopaedics and related research, 1991. **262**: p. 298-311.
51. Ohgushi, H., V.M. Goldberg, and A.I. Caplan, *Repair of bone defects with marrow cells and porous ceramic: experiments in rats.* Acta Orthopaedica, 1989. **60**(3): p. 334-339.
52. Bruder, S.P., et al., *The Effect of Implants Loaded with Autologous Mesenchymal Stem Cells on the Healing of Canine Segmental Bone Defects*.* The Journal of Bone & Joint Surgery, 1998. **80**(7): p. 985-96.
53. Young, R.G., et al., *Use of mesenchymal stem cells in a collagen matrix for Achilles tendon repair.* Journal of Orthopaedic Research, 1998. **16**(4): p. 406-413.
54. Akiyama, Y., et al., *Remyelination of the spinal cord following intravenous delivery of bone marrow cells.* Glia, 2002. **39**(3): p. 229-236.
55. Makino, S., et al., *Cardiomyocytes can be generated from marrow stromal cells in vitro.* Journal of Clinical Investigation, 1999. **103**(5): p. 697.
56. Orlic, D., et al., *Bone marrow cells regenerate infarcted myocardium.* Nature, 2001. **410**(6829): p. 701-705.
57. Messina, E., et al., *Isolation and expansion of adult cardiac stem cells from human and murine heart.* Circulation research, 2004. **95**(9): p. 911-921.
58. Kanematsu, A., et al., *Induction of smooth muscle cell-like phenotype in marrow-derived cells among regenerating urinary bladder smooth muscle cells.* The American journal of pathology, 2005. **166**(2): p. 565-573.
59. Wakitani, S., et al., *Human autologous culture expanded bone marrow mesenchymal cell transplantation for repair of cartilage defects in osteoarthritic knees.* Osteoarthritis and Cartilage, 2002. **10**(3): p. 199-206.
60. Banas, A., et al., *Adipose tissue-derived mesenchymal stem cells as a source of human hepatocytes.* Hepatology, 2007. **46**(1): p. 219-228.
61. Toma, C., et al., *Human mesenchymal stem cells differentiate to a cardiomyocyte phenotype in the adult murine heart.* Circulation, 2002. **105**(1): p. 93-98.
62. Liechty, K.W., et al., *Human mesenchymal stem cells engraft and demonstrate site-specific differentiation after in utero transplantation in sheep.* Nature medicine, 2000. **6**(11): p. 1282-1286.
63. Bruder, S.P., et al., *Bone regeneration by implantation of purified, culture-expanded human mesenchymal stem cells.* Journal of Orthopaedic Research, 1998. **16**(2): p. 155-162.
64. Van Laar, J. and A. Tyndall, *Adult stem cells in the treatment of autoimmune diseases.* Rheumatology, 2006. **45**(10): p. 1187-1193.
65. Jiang, Y., et al., *Multipotent progenitor cells can be isolated from postnatal murine bone marrow, muscle, and brain.* Experimental hematology, 2002. **30**(8): p. 896-904.
66. Alvarez-Dolado, M., et al., *Fusion of bone-marrow-derived cells with Purkinje neurons, cardiomyocytes and hepatocytes.* nature, 2003. **425**(6961): p. 968-973.
67. Terada, N., et al., *Bone marrow cells adopt the phenotype of other cells by spontaneous cell fusion.* Nature, 2002. **416**(6880): p. 542-545.
68. Vacanti, C.A., et al., *Replacement of an avulsed phalanx with tissue-engineered bone.* New England Journal of Medicine, 2001. **344**(20): p. 1511-1514.

69. Griffith, C.K., et al., *Diffusion limits of an in vitro thick prevascularized tissue.* Tissue engineering, 2005. **11**(1-2): p. 257-266.
70. Birgersdotter, A., R. Sandberg, and I. Ernberg, *Gene expression perturbation in vitro--a growing case for three-dimensional (3D) culture systems.* Semin Cancer Biol, 2005. **15**(5): p. 405-12.
71. Petersen, O.W., et al., *Interaction with basement membrane serves to rapidly distinguish growth and differentiation pattern of normal and malignant human breast epithelial cells.* Proceedings of the National Academy of Sciences, 1992. **89**(19): p. 9064-9068.
72. Moore, K.A. and I.R. Lemischka, *Stem cells and their niches.* Science, 2006. **311**(5769): p. 1880-1885.
73. Cordonnier, T., et al., *3D environment on human mesenchymal stem cells differentiation for bone tissue engineering.* Journal of Materials Science: Materials in Medicine, 2010. **21**(3): p. 981-987.
74. Hwang, N.S., et al., *Effects of Three-Dimensional Culture and Growth Factors on the Chondrogenic Differentiation of Murine Embryonic Stem Cells.* Stem cells, 2006. **24**(2): p. 284-291.
75. Baker, B.M. and C.S. Chen, *Deconstructing the third dimension–how 3D culture microenvironments alter cellular cues.* Journal of cell science, 2012. **125**(13): p. 3015-3024.
76. Mooney, D.J. and H. Vandenburgh, *Cell delivery mechanisms for tissue repair.* Cell stem cell, 2008. **2**(3): p. 205-213.
77. Kim, B.-S. and D.J. Mooney, *Development of biocompatible synthetic extracellular matrices for tissue engineering.* Trends in biotechnology, 1998. **16**(5): p. 224-230.
78. Marler, J.J., et al., *Transplantation of cells in matrices for tissue regeneration.* Advanced drug delivery reviews, 1998. **33**(1): p. 165-182.
79. Frisch, S.M. and R.A. Screaton, *Anoikis mechanisms.* Current opinion in cell biology, 2001. **13**(5): p. 555-562.
80. Lutolf, M.P. and H.M. Blau, *Artificial stem cell niches.* Advanced Materials, 2009. **21**(32-33): p. 3255-3268.
81. Freshney, R.I., *Aseptic Technique*, in *Culture of Animal Cells*. 2010, John Wiley & Sons, Inc. p. 57-70.
82. Zhang, S., X. Zhao, and L. Spirio, *PuraMatrix: Self-assembling peptide nanofiber scaffolds.* Scaffolding in Tissue Engineering, 2005: p. 217-238.
83. Jaiswal, N., et al., *Osteogenic differentiation of purified, culture-expanded human mesenchymal stem cells in vitro.* J Cell Biochem, 1997. **64**(2): p. 295-312.
84. Schnaper, H.W., et al., *Type IV collagenase(s) and TIMPs modulate endothelial cell morphogenesis in vitro.* J Cell Physiol, 1993. **156**(2): p. 235-46.
85. Abbott, A., *Cell culture: biology's new dimension*. Nature. 2003 Aug 21;424(6951):870-2.
86. Langer, R. and D.A. Tirrell, *Designing materials for biology and medicine.* Nature, 2004. **428**(6982): p. 487-92.
87. Lee, J., M.J. Cuddihy, and N.A. Kotov, *Three-dimensional cell culture matrices: state of the art.* Tissue Eng Part B Rev, 2008. **14**(1): p. 61-86.
88. Lavik, E. and R. Langer, *Tissue engineering: current state and perspectives.* Appl Microbiol Biotechnol, 2004. **65**(1): p. 1-8.
89. Ashe, H.L. and J. Briscoe, *The interpretation of morphogen gradients.* Development, 2006. **133**(3): p. 385-394.
90. Rossouw, C.L., et al., *Thermo-responsive non-woven scaffolds for "smart" 3D cell culture.* Biotechnology and Bioengineering, 2012. **109**(8): p. 2147-2158.
91. Gieni, R.S. and M.J. Hendzel, *Mechanotransduction from the ECM to the genome: are the pieces now in place?* Journal of cellular biochemistry, 2008. **104**(6): p. 1964-1987.

92. Bokhari, M., et al., *Culture of HepG2 liver cells on three dimensional polystyrene scaffolds enhances cell structure and function during toxicological challenge.* Journal of anatomy, 2007. **211**(4): p. 567-576.
93. Sun, T., et al., *Culture of skin cells in 3D rather than 2D improves their ability to survive exposure to cytotoxic agents.* Journal of biotechnology, 2006. **122**(3): p. 372-381.
94. Tanaka, H., et al., *Chondrogenic differentiation of murine embryonic stem cells: effects of culture conditions and dexamethasone.* Journal of cellular biochemistry, 2004. **93**(3): p. 454-462.
95. Cukierman, E., et al., *Taking cell-matrix adhesions to the third dimension.* Science Signaling, 2001. **294**(5547): p. 1708.
96. Li, D., Y. Wang, and Y. Xia, *Electrospinning of polymeric and ceramic nanofibers as uniaxially aligned arrays.* Nano letters, 2003. **3**(8): p. 1167-1171.
97. Weaver, V.M., et al., *Reversion of the malignant phenotype of human breast cells in three-dimensional culture and in vivo by integrin blocking antibodies.* The Journal of cell biology, 1997. **137**(1): p. 231-245.
98. Luca, A.C., et al., *Impact of the 3D microenvironment on phenotype, gene expression, and EGFR inhibition of colorectal cancer cell lines.* PLoS One, 2013. **8**(3): p. e59689.
99. Ekert, J.E., et al., *Three-dimensional lung tumor microenvironment modulates therapeutic compound responsiveness in vitro–implication for drug development.* PloS one, 2014. **9**(3): p. e92248.
100. Prestwich, G.D., *Simplifying the extracellular matrix for 3-D cell culture and tissue engineering: A pragmatic approach.* Journal of cellular biochemistry, 2007. **101**(6): p. 1370-1383.
101. Lutolf, M.P., P.M. Gilbert, and H.M. Blau, *Designing materials to direct stem-cell fate.* Nature, 2009. **462**(7272): p. 433-441.
102. Martin, I., D. Wendt, and M. Heberer, *The role of bioreactors in tissue engineering.* TRENDS in Biotechnology, 2004. **22**(2): p. 80-86.
103. Liu, W., S. Thomopoulos, and Y. Xia, *Electrospun nanofibers for regenerative medicine.* Advanced healthcare materials, 2012. **1**(1): p. 10-25.
104. Goldberg, M., R. Langer, and X. Jia, *Nanostructured materials for applications in drug delivery and tissue engineering.* Journal of Biomaterials Science, Polymer Edition, 2007. **18**(3): p. 241-268.
105. Wu, H., et al., *Electrospinning of Fe, Co, and Ni nanofibers: synthesis, assembly, and magnetic properties.* Chemistry of Materials, 2007. **19**(14): p. 3506-3511.
106. Middleton, J.C. and A.J. Tipton, *Synthetic biodegradable polymers as orthopedic devices.* Biomaterials, 2000. **21**(23): p. 2335-2346.
107. Therin, M., et al., *< i> In vivo</i> degradation of massive poly (α-hydroxy acids): Validation of< i> In vitro</i> findings.* Biomaterials, 1992. **13**(9): p. 594-600.
108. Browning, A. and C. Chu, *The effect of annealing treatments on the tensile properties and hydrolytic degradative properties of polyglycolic acid sutures.* Journal of biomedical materials research, 1986. **20**(5): p. 613-632.
109. Salih, V., *Biodegradable scaffolds for tissue engineering.* Cellular response to biomaterials, CRC Press, Boca Raton, 2008: p. 185-211.
110. Lutolf, M. and J. Hubbell, *Synthetic biomaterials as instructive extracellular microenvironments for morphogenesis in tissue engineering.* Nature biotechnology, 2005. **23**(1): p. 47-55.
111. Ratner, B.D. and S.J. Bryant, *Biomaterials: where we have been and where we are going.* Annu. Rev. Biomed. Eng., 2004. **6**: p. 41-75.
112. Li, D., Y. Wang, and Y. Xia, *Electrospinning nanofibers as uniaxially aligned arrays and layer-by-layer stacked films.* Advanced Materials, 2004. **16**(4): p. 361-366.
113. Cen, L., et al., *Collagen tissue engineering: development of novel biomaterials and applications.* Pediatric research, 2008. **63**(5): p. 492-496.

114. Agarwal, S., J.H. Wendorff, and A. Greiner, *Progress in the field of electrospinning for tissue engineering applications.* Advanced Materials, 2009. **21**(32-33): p. 3343-3351.
115. Zhong, S., et al., *An aligned nanofibrous collagen scaffold by electrospinning and its effects on in vitro fibroblast culture.* Journal of Biomedical Materials Research Part A, 2006. **79**(3): p. 456-463.
116. Esposito, A., et al., *Hyaluronic acid based materials for intestine tissue engineering: A morphological and biochemical study of cell-material interaction.* Journal of Materials Science: Materials in Medicine, 2006. **17**(12): p. 1365-1372.
117. Yamamoto, M., Y. Tabata, and Y. Ikada, *Growth factor release from gelatin hydrogel for tissue engineering.* Journal of bioactive and compatible polymers, 1999. **14**(6): p. 474-489.
118. Madihally, S.V. and H.W. Matthew, *Porous chitosan scaffolds for tissue engineering.* Biomaterials, 1999. **20**(12): p. 1133-1142.
119. Dvir-Ginzberg, M., et al., *Liver tissue engineering within alginate scaffolds: effects of cell-seeding density on hepatocyte viability, morphology, and function.* Tissue engineering, 2003. **9**(4): p. 757-766.
120. Stoop, R., *Smart biomaterials for tissue engineering of cartilage.* Injury, 2008. **39**(1): p. 77-87.
121. Uhrich, K.E., et al., *Polymeric systems for controlled drug release.* Chemical Reviews, 1999. **99**(11): p. 3181.
122. Suh, H., *Tissue restoration, tissue engineering and regenerative medicine.* Yonsei Medical Journal, 2000. **41**(6): p. 681-684.
123. Ma, P.X. and R. Langer, *Morphology and mechanical function of long-term in vitro engineered cartilage.* Journal of biomedical materials research, 1999. **44**(2): p. 217-221.
124. Pattison, M.A., et al., *Three-dimensional, nano-structured PLGA scaffolds for bladder tissue replacement applications.* Biomaterials, 2005. **26**(15): p. 2491-2500.
125. Ng, K.W., H.L. Khor, and D. Hutmacher, *In vitro characterization of natural and synthetic dermal matrices cultured with human dermal fibroblasts.* Biomaterials, 2004. **25**(14): p. 2807-2818.
126. Powell, H.M. and S.T. Boyce, *Engineered human skin fabricated using electrospun collagen–PCL blends: morphogenesis and mechanical properties.* Tissue Engineering Part A, 2009. **15**(8): p. 2177-2187.
127. Neves, A.A., N. Medcalf, and K.M. Brindle, *Influence of stirring-induced mixing on cell proliferation and extracellular matrix deposition in meniscal cartilage constructs based on polyethylene terephthalate scaffolds.* Biomaterials, 2005. **26**(23): p. 4828-4836.
128. Gupta, B., et al., *Plasma-induced graft polymerization of acrylic acid onto poly (ethylene terephthalate) films.* Journal of applied polymer science, 2001. **81**(12): p. 2993-3001.
129. Mohajeri, S., et al., *Proliferation and differentiation of mesenchymal stem cell on collagen sponge reinforced with polypropylene/polyethylene terephthalate blend fibers.* Tissue Engineering Part A, 2010. **16**(12): p. 3821-3830.
130. Ma, Z., et al., *Surface engineering of electrospun polyethylene terephthalate (PET) nanofibers towards development of a new material for blood vessel engineering.* Biomaterials, 2005. **26**(15): p. 2527-2536.
131. Jiao, Y.-P. and F.-Z. Cui, *Surface modification of polyester biomaterials for tissue engineering.* Biomedical Materials, 2007. **2**(4): p. R24.
132. Quirk, R.A., et al., *Poly (l-lysine)–GRGDS as a biomimetic surface modifier for poly (lactic acid).* Biomaterials, 2001. **22**(8): p. 865-872.

133. Bergsma, E.J., et al., *Foreign body reactions to resorbable poly (L-lactide) bone plates and screws used for the fixation of unstable zygomatic fractures.* Journal of Oral and Maxillofacial surgery, 1993. **51**(6): p. 666-670.
134. Tibbitt, M.W. and K.S. Anseth, *Hydrogels as extracellular matrix mimics for 3D cell culture.* Biotechnology and Bioengineering, 2009. **103**(4): p. 655-663.
135. Drury, J.L. and D.J. Mooney, *Hydrogels for tissue engineering: scaffold design variables and applications.* Biomaterials, 2003. **24**(24): p. 4337-4351.
136. Almany, L. and D. Seliktar, *Biosynthetic hydrogel scaffolds made from fibrinogen and polyethylene glycol for 3D cell cultures.* Biomaterials, 2005. **26**(15): p. 2467-2477.
137. Von Recum, H.A., et al., *Novel thermally reversible hydrogel as detachable cell culture substrate.* Journal of biomedical materials research, 1998. **40**(4): p. 631-639.
138. Sahoo, S.K., A.K. Panda, and V. Labhasetwar, *Characterization of porous PLGA/PLA microparticles as a scaffold for three dimensional growth of breast cancer cells.* Biomacromolecules, 2005. **6**(2): p. 1132-1139.
139. Horning, J.L., et al., *3-D tumor model for in vitro evaluation of anticancer drugs.* Molecular pharmaceutics, 2008. **5**(5): p. 849-862.
140. Malafaya, P., et al., *Chitosan particles agglomerated scaffolds for cartilage and osteochondral tissue engineering approaches with adipose tissue derived stem cells.* Journal of Materials Science: Materials in Medicine, 2005. **16**(12): p. 1077-1085.
141. Bokhari, M., et al., *Emulsion-templated porous polymers as scaffolds for three dimensional cell culture: effect of synthesis parameters on scaffold formation and homogeneity.* Journal of Materials Chemistry, 2007. **17**(38): p. 4088-4094.
142. Carnachan, R.J., et al., *Tailoring the morphology of emulsion-templated porous polymers.* Soft Matter, 2006. **2**(7): p. 608-616.
143. Note, A.S.A., *AN-SC-13–Three Dimensional Culture of HaCaT Keratinocytes Using Alvetex Scaffold.*
144. Mooney, D.J., et al., *Novel approach to fabricate porous sponges of poly (D, L-lactic-co-glycolic acid) without the use of organic solvents.* Biomaterials, 1996. **17**(14): p. 1417-1422.
145. Watson, M.S., et al., *Incorporation of proteins into polymer materials by a novel supercritical fluid processing method.* Advanced Materials, 2002. **14**(24): p. 1802-1804.
146. Harris, L.D., B.-S. Kim, and D.J. Mooney, *Open pore biodegradable matrices formed with gas foaming.* 1998.
147. Sachlos, E. and J. Czernuszka, *Making tissue engineering scaffolds work. Review: the application of solid freeform fabrication technology to the production of tissue engineering scaffolds.* Eur Cell Mater, 2003. **5**(29): p. 39-40.
148. Ma, Z., et al., *Potential of nanofiber matrix as tissue-engineering scaffolds.* Tissue engineering, 2005. **11**(1-2): p. 101-109.
149. Ramakrishna, S., *An introduction to electrospinning and nanofibers*. 2005: World Scientific Publishing Company.
150. Lu, T., Y. Li, and T. Chen, *Techniques for fabrication and construction of three-dimensional scaffolds for tissue engineering.* International journal of nanomedicine, 2013. **8**: p. 337.
151. Yu, Y.-C., M. Tirrell, and G.B. Fields, *Minimal lipidation stabilizes protein-like molecular architecture.* Journal of the American Chemical Society, 1998. **120**(39): p. 9979-9987.
152. Frenot, A. and I.S. Chronakis, *Polymer nanofibers assembled by electrospinning.* Current opinion in colloid & interface science, 2003. **8**(1): p. 64-75.
153. Greiner, A. and J.H. Wendorff, *Electrospinning: a fascinating method for the preparation of ultrathin fibers.* Angewandte Chemie International Edition, 2007. **46**(30): p. 5670-5703.

154. Taylor, G., *Electrically driven jets.* Proceedings of the Royal Society of London. A. Mathematical and Physical Sciences, 1969. **313**(1515): p. 453-475.
155. Baumgarten, P.K., *Electrostatic spinning of acrylic microfibers.* Journal of Colloid and Interface Science, 1971. **36**(1): p. 71-79.
156. Hayati, I., A.I. Bailey, and T.F. Tadros, *Investigations into the mechanisms of electrohydrodynamic spraying of liquids: I. Effect of electric field and the environment on pendant drops and factors affecting the formation of stable jets and atomization.* Journal of Colloid and Interface Science, 1987. **117**(1): p. 205-221.
157. Simons, H.L., *Process and apparatus for producing patterned non-woven fabrics*. 1966, US Patent 3,280,229.
158. Doshi, J. and D.H. Reneker, *Electrospinning process and applications of electrospun fibers.* Journal of Electrostatics, 1995. **35**(2–3): p. 151-160.
159. Deitzel, J.M., et al., *The effect of processing variables on the morphology of electrospun nanofibers and textiles.* Polymer, 2001. **42**(1): p. 261-272.
160. Hohman, M.M., et al., *Electrospinning and electrically forced jets. II. Applications.* Physics of Fluids, 2001. **13**(8): p. 2221-2236.
161. Yarin, A., S. Koombhongse, and D. Reneker, *Bending instability in electrospinning of nanofibers*. Journal of Applied Physics, 2001. **89**(5): p. 3018-3026.
162. Warner, S.B., et al., *A fundamental investigation of the formation and properties of electrospun fibers.* National textile center annual report, 1998: p. 83-90.
163. Li, M., et al. *Electrospun blends of natural and synthetic polymers as scaffolds for tissue engineering*. in *Engineering in Medicine and Biology Society, 2005. IEEE-EMBS 2005. 27th Annual International Conference of the*. 2006. IEEE.
164. Huang, Z.-M., et al., *A review on polymer nanofibers by electrospinning and their applications in nanocomposites.* Composites science and technology, 2003. **63**(15): p. 2223-2253.
165. Sajeev, U., et al., *Control of nanostructures in PVA, PVA/chitosan blends and PCL through electrospinning.* Bulletin of Materials Science, 2008. **31**(3): p. 343-351.
166. Zong, X., et al., *Control of structure, morphology and property in electrospun poly (glycolide-< i> co</i>-lactide) non-woven membranes via post-draw treatments.* Polymer, 2003. **44**(17): p. 4959-4967.
167. Li, D. and Y. Xia, *Electrospinning of nanofibers: reinventing the wheel?* Advanced Materials, 2004. **16**(14): p. 1151-1170.
168. Hadjizadeh, A., A. Ajji, and M.N. Bureau, *Nano/micro electro-spun polyethylene terephthalate fibrous mat preparation and characterization.* Journal of the Mechanical Behavior of Biomedical Materials, 2011. **4**(3): p. 340-351.
169. Garg, K. and G.L. Bowlin, *Electrospinning jets and nanofibrous structures.* Biomicrofluidics, 2011. **5**: p. 013403.
170. Norman, J.J. and T.A. Desai, *Methods for fabrication of nanoscale topography for tissue engineering scaffolds.* Annals of biomedical engineering, 2006. **34**(1): p. 89-101.
171. Burger, C., B.S. Hsiao, and B. Chu, *Nanofibrous materials and their applications.* Annu. Rev. Mater. Res., 2006. **36**: p. 333-368.
172. Liu, H. and Y.L. Hsieh, *Ultrafine fibrous cellulose membranes from electrospinning of cellulose acetate.* Journal of Polymer Science Part B: Polymer Physics, 2002. **40**(18): p. 2119-2129.
173. Lee, K., et al., *The change of bead morphology formed on electrospun polystyrene fibers.* Polymer, 2003. **44**(14): p. 4029-4034.
174. Stanger, J., N. Tuckerand, and M. Staiger, *Electrospinning*. Vol. 16. 2009: Shropshire, UK : Smithers Rapra, 2009.
175. Liu, Y., et al., *Controlling numbers and sizes of beads in electrospun nanofibers.* Polymer International, 2008. **57**(4): p. 632-636.

176. Pham, Q.P., U. Sharma, and A.G. Mikos, *Electrospinning of polymeric nanofibers for tissue engineering applications: a review.* Tissue engineering, 2006. **12**(5): p. 1197-1211.
177. Demir, M.M., et al., *Electrospinning of polyurethane fibers.* Polymer, 2002. **43**(11): p. 3303-3309.
178. Sill, T.J. and H.A. von Recum, *Electrospinning: applications in drug delivery and tissue engineering.* Biomaterials, 2008. **29**(13): p. 1989.
179. De Vrieze, S., et al., *The effect of temperature and humidity on electrospinning.* Journal of materials science, 2009. **44**(5): p. 1357-1362.
180. Shin, M., et al., *Contractile cardiac grafts using a novel nanofibrous mesh.* Biomaterials, 2004. **25**(17): p. 3717-3723.
181. Shields, K.J., et al., *Mechanical properties and cellular proliferation of electrospun collagen type II.* Tissue engineering, 2004. **10**(9-10): p. 1510-1517.
182. Lu, H., et al., *Growth of outgrowth endothelial cells on aligned PLLA nanofibrous scaffolds.* Journal of Materials Science: Materials in Medicine, 2009. **20**(9): p. 1937-1944.
183. Prabhakaran, M.P., et al., *Stem cells and nanostructures for advanced tissue regeneration*, in *Biomedical Applications of Polymeric Nanofibers*. 2012, Springer. p. 21-62.
184. Schnell, E., et al., *Guidance of glial cell migration and axonal growth on electrospun nanofibers of poly-< i> ε</i>-caprolactone and a collagen/poly-< i> ε</i>-caprolactone blend.* Biomaterials, 2007. **28**(19): p. 3012-3025.
185. Zong, X., et al., *Electrospun fine-textured scaffolds for heart tissue constructs.* Biomaterials, 2005. **26**(26): p. 5330-5338.
186. Yang, F., et al., *Electrospinning of nano/micro scale poly (L-lactic acid) aligned fibers and their potential in neural tissue engineering.* Biomaterials, 2005. **26**(15): p. 2603-2610.
187. Corey, J.M., et al., *Aligned electrospun nanofibers specify the direction of dorsal root ganglia neurite growth.* Journal of Biomedical Materials Research Part A, 2007. **83**(3): p. 636-645.
188. Xu, C., et al., *Aligned biodegradable nanofibrous structure: a potential scaffold for blood vessel engineering.* Biomaterials, 2004. **25**(5): p. 877-886.
189. Patel, S., et al., *Bioactive nanofibers: synergistic effects of nanotopography and chemical signaling on cell guidance.* Nano letters, 2007. **7**(7): p. 2122-2128.
190. Mo, X., et al., *Electrospun P (LLA-CL) nanofiber: a biomimetic extracellular matrix for smooth muscle cell and endothelial cell proliferation.* Biomaterials, 2004. **25**(10): p. 1883-1890.
191. He, W., et al., *Biodegradable polymer nanofiber mesh to maintain functions of endothelial cells.* Tissue engineering, 2006. **12**(9): p. 2457-2466.
192. Jeong, S.I., et al., *Tissue-engineered vascular grafts composed of marine collagen and PLGA fibers using pulsatile perfusion bioreactors.* Biomaterials, 2007. **28**(6): p. 1115-1122.
193. Zhang, X., C.B. Baughman, and D.L. Kaplan, *In vitro evaluation of electrospun silk fibroin scaffolds for vascular cell growth.* Biomaterials, 2008. **29**(14): p. 2217-2227.
194. Hu, Z., T. Cai, and C. Chi, *Thermoresponsive oligo (ethylene glycol)-methacrylate-based polymers and microgels.* Soft Matter, 2010. **6**(10): p. 2115-2123.
195. You, Y., et al., *Effect of solution properties on nanofibrous structure of electrospun poly (lactic-co-glycolic acid).* Journal of applied polymer science, 2006. **99**(3): p. 1214-1221.
196. Shin, M., H. Yoshimoto, and J.P. Vacanti, *In vivo bone tissue engineering using mesenchymal stem cells on a novel electrospun nanofibrous scaffold.* Tissue engineering, 2004. **10**(1-2): p. 33-41.

197. Mouthuy, P.-A., et al., *Physico-chemical characterization of functional electrospun scaffolds for bone and cartilage tissue engineering.* Proceedings of the Institution of Mechanical Engineers, Part H: Journal of Engineering in Medicine, 2010. **224**(12): p. 1401-1414.
198. Chew, S., et al., *The role of electrospinning in the emerging field of nanomedicine.* Current pharmaceutical design, 2006. **12**(36): p. 4751.
199. Feng, C. and Y.-m. Xu, *Tissue Engineering in Low Urinary Tract Reconstruction.*
200. Yoo, H.S., T.G. Kim, and T.G. Park, *Surface-functionalized electrospun nanofibers for tissue engineering and drug delivery.* Advanced Drug Delivery Reviews, 2009. **61**(12): p. 1033-1042.
201. Powell, H.M., D.M. Supp, and S.T. Boyce, *Influence of electrospun collagen on wound contraction of engineered skin substitutes.* Biomaterials, 2008. **29**(7): p. 834-843.
202. Khil, M.S., et al., *Electrospun nanofibrous polyurethane membrane as wound dressing.* Journal of Biomedical Materials Research Part B: Applied Biomaterials, 2003. **67**(2): p. 675-679.
203. de las Heras Alarcón, C., S. Pennadam, and C. Alexander, *Stimuli responsive polymers for biomedical applications.* Chemical Society Reviews, 2005. **34**(3): p. 276-285.
204. Um, I.C., et al., *Electro-spinning and electro-blowing of hyaluronic acid.* Biomacromolecules, 2004. **5**(4): p. 1428-1436.
205. Dey, S., et al., *Enzyme-passage free culture of mouse embryonic stem cells on thermo-responsive polymer surfaces.* Journal of Materials Chemistry, 2011. **21**(19): p. 6883-6890.
206. Yamato, M., et al., *Thermo-responsive culture dishes allow the intact harvest of multilayered keratinocyte sheets without dispase by reducing temperature.* Tissue engineering, 2001. **7**(4): p. 473-480.
207. Nash, M.E., et al., *Cell and cell sheet recovery from pNIPAm coatings; motivation and history to present day approaches.* Journal of Materials Chemistry, 2012. **22**(37): p. 19376-19389.
208. Elloumi-Hannachi, I., M. Yamato, and T. Okano, *Cell sheet engineering: a unique nanotechnology for scaffold-free tissue reconstruction with clinical applications in regenerative medicine.* Journal of internal medicine, 2010. **267**(1): p. 54-70.
209. Jones, D.M., et al., *Variable adhesion of micropatterned thermoresponsive polymer brushes: AFM investigations of poly (N-isopropylacrylamide) brushes prepared by surface-initiated polymerizations.* Advanced Materials, 2002. **14**(16): p. 1130.
210. Twaites, B.R., et al., *Thermo and pH responsive polymers as gene delivery vectors: effect of polymer architecture on DNA complexation in vitro.* Journal of Controlled Release, 2004. **97**(3): p. 551-566.
211. Xu, F., et al., *Thermoresponsive poly (< i> N</i>-isopropyl acrylamide)-grafted polycaprolactone films with surface immobilization of collagen.* Colloids and Surfaces B: Biointerfaces, 2011. **85**(1): p. 40-47.
212. Biazar, E., et al., *Cell engineering: nanometric grafting of poly-N-isopropylacrylamide onto polystyrene film by different doses of gamma radiation.* International journal of nanomedicine, 2010. **5**: p. 549.
213. Shimizu, T., et al., *Two-dimensional manipulation of cardiac myocyte sheets utilizing temperature-responsive culture dishes augments the pulsatile amplitude.* Tissue engineering, 2001. **7**(2): p. 141-151.
214. Harimoto, M., et al., *Novel approach for achieving double-layered cell sheets co-culture: overlaying endothelial cell sheets onto monolayer hepatocytes utilizing temperature-responsive culture dishes.* Journal of biomedical materials research, 2002. **62**(3): p. 464-470.

215. Ide, T., et al., *Structural characterization of bioengineered human corneal endothelial cell sheets fabricated on temperature-responsive culture dishes.* Biomaterials, 2006. **27**(4): p. 607-614.
216. Rose, F.R. and N.L. Tint, *Use of Thermoreversible Hydrogels in Corneal Wound Repair.* 2009.
217. Rayatpisheh, S., P. Li, and M.B. Chan-Park, *Argon-Plasma-Induced Ultrathin Thermal Grafting of Thermoresponsive pNIPAm Coating for Contractile Patterned Human SMC Sheet Engineering.* Macromolecular bioscience, 2012. **12**(7): p. 937-945.
218. Matsuda, T., *Poly (N-isopropylacrylamide)-grafted gelatin as a thermoresponsive cell-adhesive, mold-releasable material for shape-engineered tissues.* Journal of Biomaterials Science, Polymer Edition, 2004. **15**(7): p. 947-955.
219. Okano, M.N.T. and F.M. Winnik, *Poly (N-isopropylacrylamide)-based Smart Surfaces for Cell Sheet Tissue Engineering.*
220. Wang, X., X. Qiu, and C. Wu, *Comparison of the coil-to-globule and the globule-to-coil transitions of a single poly (N-isopropylacrylamide) homopolymer chain in water.* Macromolecules, 1998. **31**(9): p. 2972-2976.
221. Kujawa, P., et al., *Impact of end-group association and main-chain hydration on the thermosensitive properties of hydrophobically modified telechelic poly (N-isopropylacrylamides) in water.* Macromolecules, 2006. **39**(1): p. 341-348.
222. Bianco-Peled, H. and S. Gryc, *Binding of Amino Acids to "Smart" Sorbents: Where Does Hydrophobicity Come into Play?* Langmuir, 2004. **20**(1): p. 169-174.
223. Wu, J.-Y., et al., *Evaluating proteins release from, and their interactions with, thermosensitive poly (N-isopropylacrylamide) hydrogels.* Journal of Controlled Release, 2005. **102**(2): p. 361-372.
224. Lutz, J.F., *Polymerization of oligo (ethylene glycol)(meth) acrylates: toward new generations of smart biocompatible materials.* Journal of Polymer Science Part A: Polymer Chemistry, 2008. **46**(11): p. 3459-3470.
225. Jonas, A.M., et al., *Thermo-responsive polymer brushes with tunable collapse temperatures in the physiological range.* Macromolecules, 2007. **40**(13): p. 4403-4405.
226. Wischerhoff, E., et al., *Controlled Cell Adhesion on PEG-Based Switchable Surfaces.* Angewandte Chemie International Edition, 2008. **47**(30): p. 5666-5668.
227. Wang, W., et al., *Biodegradable Thermoresponsive Microparticle Dispersions for Injectable Cell Delivery Prepared Using a Single-Step Process.* Advanced Materials, 2009. **21**(18): p. 1809-1813.
228. Wang, H., et al., *Fabrication of PU/PEGMA crosslinked hybrid scaffolds by in situ UV photopolymerization favoring human endothelial cells growth for vascular tissue engineering.* Journal of Materials Science: Materials in Medicine, 2012. **23**(6): p. 1499-1510.
229. Yang, J., et al., *Cell sheet engineering: recreating tissues without biodegradable scaffolds.* Biomaterials, 2005. **26**(33): p. 6415-6422.
230. Yamato, M. and T. Okano, *Cell sheet engineering.* Materials today, 2004. **7**(5): p. 42-47.
231. Kushida, A., et al., *Decrease in culture temperature releases monolayer endothelial cell sheets together with deposited fibronectin matrix from temperature-responsive culture surfaces.* Journal of biomedical materials research, 1999. **45**(4): p. 355-362.
232. Hirose, M., et al., *Creation of designed shape cell sheets that are noninvasively harvested and moved onto another surface.* Biomacromolecules, 2000. **1**(3): p. 377-381.
233. Miyahara, Y., et al., *Monolayered mesenchymal stem cells repair scarred myocardium after myocardial infarction.* Nature medicine, 2006. **12**(4): p. 459-465.
234. Ohashi, K., et al., *Engineering functional two-and three-dimensional liver systems in vivo using hepatic tissue sheets.* Nature medicine, 2007. **13**(7): p. 880-885.

235. Shimazaki, J., et al., *Transplantation of human limbal epithelium cultivated on amniotic membrane for the treatment of severe ocular surface disorders.* Ophthalmology, 2002. **109**(7): p. 1285-1290.
236. Han, B., et al., *A fibrin-based bioengineered ocular surface with human corneal epithelial stem cells.* Cornea, 2002. **21**(5): p. 505-510.
237. Okano, T., K. Nishida, and M. Yamato, *Cell sheets for ectocornea formation, method of producing the same and method of using the same*. 2004, Google Patents.
238. Sumide, T., et al., *Functional human corneal endothelial cell sheets harvested from temperature-responsive culture surfaces.* The FASEB Journal, 2006. **20**(2): p. 392-394.
239. Masuda, S., et al., *Cell sheet engineering for heart tissue repair.* Advanced drug delivery reviews, 2008. **60**(2): p. 277-285.
240. Shimizu, T., et al., *Cell sheet engineering for myocardial tissue reconstruction.* Biomaterials, 2003. **24**(13): p. 2309-2316.
241. Shimizu, T., et al., *Fabrication of pulsatile cardiac tissue grafts using a novel 3-dimensional cell sheet manipulation technique and temperature-responsive cell culture surfaces.* Circulation research, 2002. **90**(3): p. e40-e48.
242. Kawamura, M., et al., *Feasibility, safety, and therapeutic efficacy of human induced pluripotent stem cell-derived cardiomyocyte sheets in a porcine ischemic cardiomyopathy model.* Circulation, 2012. **126**(11 suppl 1): p. S29-S37.
243. Iwata, T., et al., *Periodontal regeneration with multi-layered periodontal ligament-derived cell sheets in a canine model.* Biomaterials, 2009. **30**(14): p. 2716-2723.
244. Duncan, R., *The dawning era of polymer therapeutics.* Nature Reviews Drug Discovery, 2003. **2**(5): p. 347-360.
245. Teo, W. and S. Ramakrishna, *A review on electrospinning design and nanofibre assemblies.* Nanotechnology, 2006. **17**(14): p. R89.
246. Alexander, C. and K.M. Shakesheff, *Responsive polymers at the biology/materials science interface.* Advanced Materials, 2006. **18**(24): p. 3321-3328.
247. Vihola, H., et al., *Cytotoxicity of thermosensitive polymers poly (< i> N</i>-isopropylacrylamide), poly (< i> N</i>-vinylcaprolactam) and amphiphilically modified poly (< i> N</i>-vinylcaprolactam).* Biomaterials, 2005. **26**(16): p. 3055-3064.
248. Lutz, J.-F., Ö. Akdemir, and A. Hoth, *Point by point comparison of two thermosensitive polymers exhibiting a similar LCST: is the age of poly (NIPAM) over?* Journal of the American Chemical Society, 2006. **128**(40): p. 13046-13047.
249. Lutz, J.-F., et al., *About the phase transitions in aqueous solutions of thermoresponsive copolymers and hydrogels based on 2-(2-methoxyethoxy) ethyl methacrylate and oligo (ethylene glycol) methacrylate.* Macromolecules, 2007. **40**(7): p. 2503-2508.
250. Uhlig, K., et al., *On the influence of the architecture of poly (ethylene glycol)-based thermoresponsive polymers on cell adhesion.* Biomicrofluidics, 2012. **6**: p. 024129.
251. Al Ghanami, R.C., et al., *Responsive particulate dispersions for reversible building and deconstruction of 3D cell environments.* Soft Matter, 2010. **6**(20): p. 5037-5044.
252. Ramakrishna, S., *An introduction to electrospinning and nanofibers*. 2005: World Scientific Publishing Company. 7-18.
253. Song, F., X.-L. Wang, and Y.-Z. Wang, *Fabrication of novel thermo-responsive electrospun nanofibrous mats and their application in bioseparation.* European Polymer Journal, 2011. **47**(10): p. 1885-1892.
254. Okuzaki, H., K. Kobayashi, and H. Yan, *Thermo-responsive nanofiber mats.* Macromolecules, 2009. **42**(16): p. 5916-5918.
255. Gu, S.Y., et al., *Switchable Wettability of Thermo-Responsive Biocompatible Nanofibrous Films Created by Electrospinning.* Macromolecular Materials and Engineering, 2010. **295**(1): p. 32-36.

256. Chiu, Y.-C., et al., *Thermoresponsive Luminescent Electrospun Fibers Prepared From Poly (DMAEMA-co-SA-co-StFl) Multifunctional Random Copolymers.* ACS applied materials & interfaces, 2010. **2**(11): p. 3340-3347.
257. Rockwood, D.N., et al., *Characterization of electrospun poly (N-isopropyl acrylamide) fibers.* Polymer, 2008. **49**(18): p. 4025-4032.
258. Chuang, W.-J. and W.-Y. Chiu, *Thermo-responsive nanofibers prepared from poly (N-isopropylacrylamide-co-N-methylol acrylamide).* Polymer, 2012. **53**(14): p. 2829-2838.
259. Liang, D., B.S. Hsiao, and B. Chu, *Functional electrospun nanofibrous scaffolds for biomedical applications.* Advanced drug delivery reviews, 2007. **59**(14): p. 1392-1412.
260. Gandhi, M., et al., *Post-spinning modification of electrospun nanofiber nanocomposite from Bombyx mori silk and carbon nanotubes.* Polymer, 2009. **50**(8): p. 1918-1924.
261. Cronje, L. and B. Klumperman, *Modified electrospun polymer nanofibers as affinity membranes: The effect of pre-spinning modification versus post-spinning modification.* European Polymer Journal, 2013. **49**(12): p. 3814-3824.
262. Nie, H., et al., *Three-dimensional fibrous PLGA/HAp composite scaffold for BMP-2 delivery.* Biotechnology and Bioengineering, 2008. **99**(1): p. 223-234.
263. Nie, H. and C.-H. Wang, *Fabrication and characterization of PLGA/HAp composite scaffolds for delivery of BMP-2 plasmid DNA.* Journal of Controlled Release, 2007. **120**(1): p. 111-121.
264. Chen, J.-P. and C.-H. Su, *Surface modification of electrospun PLLA nanofibers by plasma treatment and cationized gelatin immobilization for cartilage tissue engineering.* Acta biomaterialia, 2011. **7**(1): p. 234-243.
265. Ma, Z., M. Kotaki, and S. Ramakrishna, *Surface modified nonwoven polysulphone (PSU) fiber mesh by electrospinning: a novel affinity membrane.* Journal of membrane science, 2006. **272**(1): p. 179-187.
266. Agarwal, S., J.H. Wendorff, and A. Greiner, *Use of electrospinning technique for biomedical applications.* Polymer, 2008. **49**(26): p. 5603-5621.
267. Park, K., et al., *Surface modification of biodegradable electrospun nanofiber scaffolds and their interaction with fibroblasts.* Journal of Biomaterials Science, Polymer Edition, 2007. **18**(4): p. 369-382.
268. Chua, K.-N., et al., *Surface-aminated electrospun nanofibers enhance adhesion and expansion of human umbilical cord blood hematopoietic stem/progenitor cells.* Biomaterials, 2006. **27**(36): p. 6043-6051.
269. Nam, Y.S., et al., *Adhesion behaviours of hepatocytes cultured onto biodegradable polymer surface modified by alkali hydrolysis process.* Journal of Biomaterials Science, Polymer Edition, 1999. **10**(11): p. 1145-1158.
270. Yuan, X., A.F.T. Mak, and K. Yao, *Surface degradation of poly(L-lactic acid) fibres in a concentrated alkaline solution.* Polymer Degradation and Stability, 2003. **79**(1): p. 45-52.
271. Croll, T.I., et al., *Controllable surface modification of poly(lactic-co-glycolic acid) (PLGA) by hydrolysis or aminolysis I: Physical, chemical, and theoretical aspects.* Biomacromolecules, 2004. **5**(2): p. 463-473.
272. Chen, F., C.N. Lee, and S.H. Teoh, *Nanofibrous modification on ultra-thin poly(e-caprolactone) membrane via electrospinning.* Materials Science and Engineering C, 2007. **27**(2): p. 325-332.
273. Yao, C., et al., *Surface modification and antibacterial activity of electrospun polyurethane fibrous membranes with quaternary ammonium moieties.* Journal of Membrane Science, 2008. **320**(1): p. 259-267.

274. Kim, K., et al., *Incorporation and controlled release of a hydrophilic antibiotic using poly (lactide-co-glycolide)-based electrospun nanofibrous scaffolds.* Journal of Controlled Release, 2004. **98**(1): p. 47-56.
275. Shi, Q., et al., *Atmospheric plasma treatment of pre-electrospinning polymer solution: A feasible method to improve electrospinnability.* Journal of Polymer Science Part B: Polymer Physics, 2011. **49**(2): p. 115-122.
276. Choi, J.S. and H.S. Yoo, *Electrospun nanofibers surface-modified with fluorescent proteins.* Journal of Bioactive and Compatible Polymers, 2007. **22**(5): p. 508-524.
277. Song, F., X.-L. Wang, and Y.-Z. Wang, *Poly (< i> N</i>-isopropylacrylamide)/poly (ethylene oxide) blend nanofibrous scaffolds: Thermo-responsive carrier for controlled drug release.* Colloids and Surfaces B: Biointerfaces, 2011. **88**(2): p. 749-754.
278. Kim, T.G. and T.G. Park, *Biomimicking extracellular matrix: cell adhesive RGD peptide modified electrospun poly (D, L-lactic-co-glycolic acid) nanofiber mesh.* Tissue engineering, 2006. **12**(2): p. 221-233.
279. Kenawy, E.-R., et al., *Release of tetracycline hydrochloride from electrospun poly(ethylene-co-vinylacetate), poly(lactic acid), and a blend.* Journal of Controlled Release, 2002. **81**(1–2): p. 57-64.
280. Xu, X., et al., *Preparation of Core-Sheath Composite Nanofibers by Emulsion Electrospinning.* Macromolecular rapid communications, 2006. **27**(19): p. 1637-1642.
281. Sun, Z., et al., *Compound Core–Shell Polymer Nanofibers by Co-Electrospinning.* Advanced Materials, 2003. **15**(22): p. 1929-1932.
282. Zhang, Y., et al., *Preparation of core-shell structured PCL-r-gelatin bi-component nanofibers by coaxial electrospinning.* Chemistry of Materials, 2004. **16**(18): p. 3406-3409.
283. Qin, X. and D. Wu, *Effect of different solvents on poly (caprolactone)(PCL) electrospun nonwoven membranes.* Journal of thermal analysis and calorimetry, 2011. **107**(3): p. 1007-1013.
284. Huang, Z.M., et al., *Encapsulating drugs in biodegradable ultrafine fibers through co-axial electrospinning.* Journal of Biomedical Materials Research Part A, 2006. **77**(1): p. 169-179.
285. Moghe, A. and B. Gupta, *Co-axial Electrospinning for Nanofiber Structures: Preparation and Applications.* Polymer Reviews, 2008. **48**(2): p. 353-377.
286. Zhang, Y., et al., *Characterization of the surface biocompatibility of the electrospun PCL-collagen nanofibers using fibroblasts.* Biomacromolecules, 2005. **6**(5): p. 2583-2589.
287. Hou, Q., et al., *Novel surface entrapment process for the incorporation of bioactive molecules within preformed alginate fibers.* Biomacromolecules, 2005. **6**(2): p. 734-740.
288. Zhang, J., et al., *Micro-and macrothermal analysis of a bioactive surface-engineered polymer formed by physical entrapment of poly (ethylene glycol) into poly (lactic acid).* Macromolecules, 2003. **36**(4): p. 1215-1221.
289. Christopherson, G.T., H. Song, and H.-Q. Mao, *The influence of fiber diameter of electrospun substrates on neural stem cell differentiation and proliferation.* Biomaterials, 2009. **30**(4): p. 556-564.
290. Bashur, C.A., L.A. Dahlgren, and A.S. Goldstein, *Effect of fiber diameter and orientation on fibroblast morphology and proliferation on electrospun poly (D, L-lactic-co-glycolic acid) meshes.* Biomaterials, 2006. **27**(33): p. 5681-5688.
291. Vollrath, F. and D.T. Edmonds, *Modulation of the mechanical properties of spider silk by coating with water.* 1989.
292. Fong, H., I. Chun, and D. Reneker, *Beaded nanofibers formed during electrospinning.* Polymer, 1999. **40**(16): p. 4585-4592.

293. Chen, M., et al., *Role of fiber diameter in adhesion and proliferation of NIH 3T3 fibroblast on electrospun polycaprolactone scaffolds.* Tissue Engineering, 2007. **13**(3): p. 579-587.
294. Miyoshi, T., K. Toyohara, and H. Minematsu, *Preparation of ultrafine fibrous zein membranes via electrospinning.* Polymer International, 2005. **54**(8): p. 1187-1190.
295. Yuan, X., et al., *Morphology of ultrafine polysulfone fibers prepared by electrospinning.* Polymer International, 2004. **53**(11): p. 1704-1710.
296. Yu, D., et al., *A modified coaxial electrospinning for preparing fibers from a high concentration polymer solution.* eXPRESS Polym Lett, 2011. **5**: p. 732-741.
297. Lin, T., et al., *The charge effect of cationic surfactants on the elimination of fibre beads in the electrospinning of polystyrene.* Nanotechnology, 2004. **15**(9): p. 1375.
298. Veleirinho, B., M.F. Rei, and J. Lopes-DA-Silva, *Solvent and concentration effects on the properties of electrospun poly (ethylene terephthalate) nanofiber mats.* Journal of Polymer Science Part B: Polymer Physics, 2008. **46**(5): p. 460-471.
299. Zhao, L., et al., *Preparation and cytocompatibility of PLGA scaffolds with controllable fiber morphology and diameter using electrospinning method.* Journal of Biomedical Materials Research Part B: Applied Biomaterials, 2008. **87**(1): p. 26-34.
300. Kim, K.W., et al., *The effect of molecular weight and the linear velocity of drum surface on the properties of electrospun poly (ethylene terephthalate) nonwovens.* Fibers and Polymers, 2004. **5**(2): p. 122-127.
301. Li, W.J., et al., *Electrospun nanofibrous structure: a novel scaffold for tissue engineering.* Journal of biomedical materials research, 2002. **60**(4): p. 613-621.
302. Megelski, S., et al., *Micro-and nanostructured surface morphology on electrospun polymer fibers.* Macromolecules, 2002. **35**(22): p. 8456-8466.
303. Demir, M.M., et al., *Electrospinning of polyurethane fibers.* Polymer, 2002. **43**(11): p. 3303-3309.
304. Zong, X., et al., *Structure and process relationship of electrospun bioabsorbable nanofiber membranes.* Polymer, 2002. **43**(16): p. 4403-4412.
305. Vickerman, V., et al., *Design, fabrication and implementation of a novel multi-parameter control microfluidic platform for three-dimensional cell culture and real-time imaging.* Lab on a Chip, 2008. **8**(9): p. 1468-1477.
306. Li, A.D., et al., *Electrospun Chitosan-graft-PLGA nanofibres with significantly enhanced hydrophilicity and improved mechanical property.* Colloids and Surfaces B: Biointerfaces, 2012.
307. Ajalloueian, F., et al., *Emulsion Electrospinning as an Approach to Fabricate PLGA/Chitosan Nanofibers for Biomedical Applications.* BioMed Research International, 2014. **2014**: p. 13.
308. Seo, E.-D., *AFM and specular reflectance IR studies on the surface structure of poly (ethylene terephthalate) films upon treatment with argon and oxygen plasmas.* Macromolecular Research, 2004. **12**(1): p. 134-140.
309. Constantin, M., et al., *Lower critical solution temperature versus volume phase transition temperature in thermoresponsive drug delivery systems.* Express Polym Lett, 2011. **5**(10): p. 839-848.
310. Ward, M.A. and T.K. Georgiou, *Thermoresponsive polymers for biomedical applications.* Polymers, 2011. **3**(3): p. 1215-1242.
311. Porsch, C., et al., *Thermo-responsive cellulose-based architectures: tailoring LCST using poly(ethylene glycol) methacrylates.* Polymer Chemistry, 2011. **2**(5): p. 1114-1123.
312. Becer, C.R., et al., *Libraries of methacrylic acid and oligo (ethylene glycol) methacrylate copolymers with LCST behavior.* Journal of Polymer Science Part A: Polymer Chemistry, 2008. **46**(21): p. 7138-7147.

313. Yoshida, M., et al., *From advanced biomedical coatings to multi-functionalized biomaterials.* Journal of Macromolecular Science, Part C: Polymer Reviews, 2006. **46**(4): p. 347-375.
314. Chen, J., B. Chu, and B.S. Hsiao, *Mineralization of hydroxyapatite in electrospun nanofibrous poly (L-lactic acid) scaffolds.* Journal of Biomedical Materials Research Part A, 2006. **79**(2): p. 307-317.
315. Hadjizadeh, A., A. Ajji, and M.N. Bureau, *Preparation and characterization of NaOH treated micro-fibrous polyethylene terephthalate nonwovens for biomedical application.* Journal of the Mechanical Behavior of Biomedical Materials, 2010. **3**(8): p. 574-583.
316. Park, G.E., et al., *Accelerated chondrocyte functions on NaOH-treated PLGA scaffolds.* Biomaterials, 2005. **26**(16): p. 3075-3082.
317. Ng, R., et al., *Modifications of nonwoven polyethylene terephthalate fibrous matrices via NaOH hydrolysis: Effects on pore size, fiber diameter, cell seeding and proliferation.* Process biochemistry, 2009. **44**(9): p. 992-998.
318. Donelli, I., et al., *Enzymatic surface modification and functionalization of PET: a water contact angle, FTIR, and fluorescence spectroscopy study.* Biotechnology and Bioengineering, 2009. **103**(5): p. 845-856.
319. Basu, S. and S.-T. Yang, *Astrocyte growth and glial cell line-derived neurotrophic factor secretion in three-dimensional polyethylene terephthalate fibrous matrices.* Tissue engineering, 2005. **11**(5-6): p. 940-952.
320. Halil İbrahim, Ü., C. İNEGÖLLÜ, and O. ŞANLI, *Graft Copolymerization of N-Vinylimidazole on Poly (Ethylene Terephthalate) Fibers in a Swelling Solvent Using Azobisisobutyronitrile as Initiator.* Turk. J. Chem, 2003. **27**: p. 403-415.
321. Hebeish, A., S. Shalaby, and A. Bayazeed, *Graft polymerization of methyl methacrylate on poly (ethylene terephthalate) fibers using H2O2 as initiator.* Journal of applied polymer science, 1981. **26**(10): p. 3253-3269.
322. Arslan, M., et al., *Kinetics of swelling assisted grafting of 4-vinyl pyridine onto poly (ethylene terephthalate) fibers using a benzoyl peroxide initiator.* Polymer Bulletin, 2003. **51**(3): p. 237-244.
323. Sicardi, S., L. Manna, and M. Banchero, *Comparison of dye diffusion in poly (ethylene terephthalate) films in the presence of a supercritical or aqueous solvent.* Industrial & engineering chemistry research, 2000. **39**(12): p. 4707-4713.
324. Meng, Z., et al., *Preparation and characterization of electrospun PLGA/gelatin nanofibers as a potential drug delivery system.* Colloids and Surfaces B: Biointerfaces, 2011. **84**(1): p. 97-102.
325. Quirk, R.A., et al., *Controlling biological interactions with poly (lactic acid) by surface entrapment modification.* Langmuir, 2001. **17**(9): p. 2817-2820.
326. Ki, C.S., et al., *Characterization of gelatin nanofiber prepared from gelatin–formic acid solution.* Polymer, 2005. **46**(14): p. 5094-5102.
327. Theron, S., E. Zussman, and A. Yarin, *Experimental investigation of the governing parameters in the electrospinning of polymer solutions.* Polymer, 2004. **45**(6): p. 2017-2030.
328. Da Silva, R.M., J.F. Mano, and R.L. Reis, *Smart thermoresponsive coatings and surfaces for tissue engineering: switching cell-material boundaries.* TRENDS in Biotechnology, 2007. **25**(12): p. 577-583.
329. Nisbet, D., et al., *Review paper: a review of the cellular response on electrospun nanofibers for tissue engineering.* Journal of biomaterials applications, 2008.
330. Batista, U., et al., *Effects of different detachment procedures on viability, nitroxide reduction kinetics and plasma membrane heterogeneity of V-79 cells.* Cell biology international, 2010. **34**(6): p. 663-668.
331. Dalen, H. and P. Todd, *Surface morphology of trypsinized human cells in vitro.* Experimental cell research, 1971. **66**(2): p. 353-361.

332. Weinstein, D., *Comparison of pronase and trypsin for detachment of human cells during serial cultivation.* Experimental cell research, 1966. **43**(1): p. 234-236.
333. Snow, C. and A. Allen, *The release of radioactive nucleic acids and mucoproteins by trypsin and ethylenediaminetetra-acetate treatment of baby-hamster cells in tissue culture.* Biochem. J, 1970. **119**: p. 707-714.
334. Hanson, C. and G. Caisander, *Human embryonic stem cells and chromosome stability.* Apmis, 2005. **113**(11-12): p. 751-755.
335. Huang, H.-L., et al., *Research Trypsin-induced proteome alteration during cell subculture in mammalian cells.* Journal of biomedical science, 2010. **17**: p. 36.
336. Tabatabaei, M., et al., *Isolation and Partial Characterization of Human Amniotic Epithelial Cells: The Effect of Trypsin.* Avicenna Journal of Medical Biotechnology. **6**(1): p. 10-20.
337. Martin, M.J., et al., *Human embryonic stem cells express an immunogenic nonhuman sialic acid.* Nature medicine, 2005. **11**(2): p. 228-232.
338. Yamada, N., et al., *Thermo-responsive polymeric surfaces; control of attachment and detachment of cultured cells.* Die Makromolekulare Chemie, Rapid Communications, 1990. **11**(11): p. 571-576.
339. Okano, T., et al., *A novel recovery system for cultured cells using plasma-treated polystyrene dishes grafted with poly (N-isopropylacrylamide).* Journal of biomedical materials research, 1993. **27**(10): p. 1243-1251.
340. Tsuda, Y., et al., *The use of patterned dual thermoresponsive surfaces for the collective recovery as co-cultured cell sheets.* Biomaterials, 2005. **26**(14): p. 1885-1893.
341. Mizutani, A., et al., *Preparation of thermoresponsive polymer brush surfaces and their interaction with cells.* Biomaterials, 2008. **29**(13): p. 2073-2081.
342. Kessel, S., et al., *Thermoresponsive PEG-based polymer layers: surface characterization with AFM force measurements.* Langmuir, 2009. **26**(5): p. 3462-3467.
343. Saeed, A., et al., *A thermoresponsive and magnetic colloid for 3D cell expansion and reconfiguration.* Advanced Materials, 2015. **27**(4): p. 662-668.
344. Braim, S., et al., *Thermoresponsive magnetic colloidal gels via surface-initiated polymerisation from functional microparticles.* Journal of Materials Chemistry B, 2016.
345. Loh, X.J., et al., *Controlled drug release from biodegradable thermoresponsive physical hydrogel nanofibers.* Journal of Controlled Release, 2010. **143**(2): p. 175-182.
346. Chen, M., et al., *Thermo-Responsive Core− Sheath Electrospun Nanofibers from Poly (N-isopropylacrylamide)/Polycaprolactone Blends.* Chemistry of Materials, 2010. **22**(14): p. 4214-4221.
347. Lin, X., et al., *Controllable drug release of electrospun thermoresponsive poly (N-isopropylacrylamide)/poly (2-acrylamido-2-methylpropanesulfonic acid) nanofibers.* Journal of Biomedical Materials Research Part A, 2012. **100**(7): p. 1839-1845.
348. Ji, W., et al., *Bioactive electrospun scaffolds delivering growth factors and genes for tissue engineering applications.* Pharmaceutical research, 2011. **28**(6): p. 1259-1272.
349. Paik, I., et al., *Rapid micropatterning of cell lines and human pluripotent stem cells on elastomeric membranes.* Biotechnology and bioengineering, 2012. **109**(10): p. 2630-2641.
350. Ahmed, S.A., R.M. Gogal, and J.E. Walsh, *A new rapid and simple non-radioactive assay to monitor and determine the proliferation of lymphocytes: an alternative to [3H] thymidine incorporation assay.* Journal of immunological methods, 1994. **170**(2): p. 211-224.
351. Riss, T.L., et al., *Cell viability assays.* 2004.

352. Sawicka, K.M. and P. Gouma, *Electrospun composite nanofibers for functional applications.* Journal of Nanoparticle Research, 2006. **8**(6): p. 769-781.
353. Song, F., X.-L. Wang, and Y.-Z. Wang, *Poly (N-isopropylacrylamide)/poly (ethylene oxide) blend nanofibrous scaffolds: Thermo-responsive carrier for controlled drug release.* Colloids and Surfaces B: Biointerfaces, 2011. **88**(2): p. 749-754.
354. Son, W.K., et al., *The effects of solution properties and polyelectrolyte on electrospinning of ultrafine poly (ethylene oxide) fibers.* Polymer, 2004. **45**(9): p. 2959-2966.
355. Jin, H.-J., et al., *Electrospinning Bombyx mori silk with poly (ethylene oxide).* Biomacromolecules, 2002. **3**(6): p. 1233-1239.
356. Buttafoco, L., et al., *Electrospinning of collagen and elastin for tissue engineering applications.* Biomaterials, 2006. **27**(5): p. 724-734.
357. Ali, M.M. and H.D. Stöver, *Well-defined amphiphilic thermosensitive copolymers based on poly (ethylene glycol monomethacrylate) and methyl methacrylate prepared by atom transfer radical polymerization.* Macromolecules, 2004. **37**(14): p. 5219-5227.
358. Bo, G., B. Wesslén, and K.B. Wessléen, *Amphiphilic comb-shaped polymers from poly (ethylene glycol) macromonomers.* Journal of Polymer Science Part A: Polymer Chemistry, 1992. **30**(9): p. 1799-1808.
359. Han, S., M. Hagiwara, and T. Ishizone, *Synthesis of thermally sensitive water-soluble polymethacrylates by living anionic polymerizations of oligo (ethylene glycol) methyl ether methacrylates.* Macromolecules, 2003. **36**(22): p. 8312-8319.
360. Arima, Y. and H. Iwata, *Effect of wettability and surface functional groups on protein adsorption and cell adhesion using well-defined mixed self-assembled monolayers.* Biomaterials, 2007. **28**(20): p. 3074-3082.
361. Webb, K., V. Hlady, and P.A. Tresco, *Relative importance of surface wettability and charged functional groups on NIH 3T3 fibroblast attachment, spreading, and cytoskeletal organization.* Journal of biomedical materials research, 1998. **41**(3): p. 422.
362. Altankov, G., F. Grinnell, and T. Groth, *Studies on the biocompatibility of materials: Fibroblast reorganization of substratum-bound fibronectin on surfaces varying in wettability.* Journal of biomedical materials research, 1996. **30**(3): p. 385-391.
363. Ghasemi-Mobarakeh, L., et al., *Electrospun poly (ε-caprolactone)/gelatin nanofibrous scaffolds for nerve tissue engineering.* Biomaterials, 2008. **29**(34): p. 4532-4539.
364. Paragkumar N, T., D. Edith, and J.-L. Six, *Surface characteristics of PLA and PLGA films.* Applied Surface Science, 2006. **253**(5): p. 2758-2764.
365. Ji, W., et al., *Fibrous scaffolds loaded with protein prepared by blend or coaxial electrospinning.* Acta Biomaterialia, 2010. **6**(11): p. 4199-4207.
366. Shin, H.J., et al., *Electrospun PLGA nanofiber scaffolds for articular cartilage reconstruction: mechanical stability, degradation and cellular responses under mechanical stimulation in vitro.* Journal of Biomaterials Science, Polymer Edition, 2006. **17**(1-2): p. 103-119.
367. Xin, X., M. Hussain, and J.J. Mao, *Continuing differentiation of human mesenchymal stem cells and induced chondrogenic and osteogenic lineages in electrospun PLGA nanofiber scaffold.* Biomaterials, 2007. **28**(2): p. 316-325.
368. Bolin, M.H., et al., *Nano-fiber scaffold electrodes based on PEDOT for cell stimulation.* Sensors and Actuators B: Chemical, 2009. **142**(2): p. 451-456.
369. Gustafsson, Y., et al., *Viability and proliferation of rat MSCs on adhesion protein-modified PET and PU scaffolds.* Biomaterials, 2012. **33**(32): p. 8094-8103.
370. Okano, T., et al., *Mechanism of cell detachment from temperature-modulated, hydrophilic-hydrophobic polymer surfaces.* Biomaterials, 1995. **16**(4): p. 297-303.

371. Canavan, H.E., et al., *Surface characterization of the extracellular matrix remaining after cell detachment from a thermoresponsive polymer.* Langmuir, 2005. **21**(5): p. 1949-1955.
372. Kumashiro, Y., M. Yamato, and T. Okano, *Cell attachment–detachment control on temperature-responsive thin surfaces for novel tissue engineering.* Annals of biomedical engineering, 2010. **38**(6): p. 1977-1988.
373. Akiyama, Y., et al., *Ultrathin poly (N-isopropylacrylamide) grafted layer on polystyrene surfaces for cell adhesion/detachment control.* Langmuir, 2004. **20**(13): p. 5506-5511.
374. Nishida, K., et al., *Functional bioengineered corneal epithelial sheet grafts from corneal stem cells expanded ex vivo on a temperature-responsive cell culture surface.* Transplantation, 2004. **77**(3): p. 379-385.
375. Nishida, K., et al., *Corneal reconstruction with tissue-engineered cell sheets composed of autologous oral mucosal epithelium.* New England Journal of Medicine, 2004. **351**(12): p. 1187-1196.
376. Ohki, T., et al., *Endoscopic Transplantation of Human Oral Mucosal Epithelial Cell Sheets-World's First Case of Regenerative Medicine Applied to Endoscopic Treatment.* Gastrointestinal Endoscopy, 2009. **69**(5): p. AB253-AB254.
377. Kwon, O.H., et al., *Accelerated cell sheet recovery by co-grafting of PEG with PIPAAm onto porous cell culture membranes.* Biomaterials, 2003. **24**(7): p. 1223-1232.
378. Kikuchi, A., et al., *Two-dimensional manipulation of confluently cultured vascular endothelial cells using temperature-responsive poly (N-isopropylacrylamide)-grafted surfaces.* Journal of Biomaterials Science, Polymer Edition, 1998. **9**(12): p. 1331-1348.
379. Ohki, T., et al., *Treatment of oesophageal ulcerations using endoscopic transplantation of tissue-engineered autologous oral mucosal epithelial cell sheets in a canine model.* Gut, 2006. **55**(12): p. 1704-1710.
380. Okamoto, T., et al., *Clonal heterogeneity in differentiation potential of immortalized human mesenchymal stem cells.* Biochemical and biophysical research communications, 2002. **295**(2): p. 354-361.
381. Schmaljohann, D., et al., *Thermo-responsive PNiPAAm-g-PEG films for controlled cell detachment.* Biomacromolecules, 2003. **4**(6): p. 1733-1739.
382. Takezawa, T., Y. Mori, and K. Yoshizato, *Cell culture on a thermo-responsive polymer surface.* Nature Biotechnology, 1990. **8**(9): p. 854-856.
383. Ebara, M., et al., *Temperature-responsive cell culture surfaces enable "on-off" affinity control between cell integrins and RGDS ligands.* Biomacromolecules, 2004. **5**(2): p. 505-510.
384. Ernst, O., et al., *Control of cell detachment in a microfluidic device using a thermo-responsive copolymer on a gold substrate.* Lab on a Chip, 2007. **7**(10): p. 1322-1329.
385. Tang, Z., Y. Akiyama, and T. Okano, *Temperature-responsive polymer modified surface for cell sheet engineering.* Polymers, 2012. **4**(3): p. 1478-1498.
386. Storm, M.P., et al., *Three-dimensional culture systems for the expansion of pluripotent embryonic stem cells.* Biotechnology and bioengineering, 2010. **107**(4): p. 683-695.
387. Sarber, R., et al., *Regulation of proliferation of fibroblasts of low and high population doubling levels grown in collagen lattices.* Mechanisms of ageing and development, 1981. **17**(2): p. 107-117.
388. Schugar, R.C., et al., *High harvest yield, high expansion, and phenotype stability of CD146 mesenchymal stromal cells from whole primitive human umbilical cord tissue.* BioMed Research International, 2009. **2009**.
389. Heidari, B., et al., *Comparison of proliferative and multilineage differentiation potential of sheep mesenchymal stem cells derived from bone marrow, liver, and adipose tissue.* Avicenna journal of medical biotechnology, 2013. **5**(2): p. 104.

390. Williams, A.R. and J.M. Hare, *Mesenchymal stem cells biology, pathophysiology, translational findings, and therapeutic implications for cardiac disease.* Circulation research, 2011. **109**(8): p. 923-940.
391. Wei, X., et al., *Mesenchymal stem cells: a new trend for cell therapy.* Acta Pharmacologica Sinica, 2013. **34**(6): p. 747-754.
392. Salucci, M., et al., *Flavonoids uptake and their effect on cell cycle of human colon adenocarcinoma cells (Caco2).* British journal of cancer, 2002. **86**(10): p. 1645-1651.
393. Artursson, P., K. Palm, and K. Luthman, *Caco-2 monolayers in experimental and theoretical predictions of drug transport.* Advanced drug delivery reviews, 2012. **64**: p. 280-289.
394. Parfitt, G.J., et al., *Three-dimensional reconstruction of collagen–proteoglycan interactions in the mouse corneal stroma by electron tomography.* Journal of structural biology, 2010. **170**(2): p. 392-397.
395. Hassell, J.R. and D.E. Birk, *The molecular basis of corneal transparency.* Experimental eye research, 2010. **91**(3): p. 326-335.
396. West-Mays, J.A. and D.J. Dwivedi, *The keratocyte: corneal stromal cell with variable repair phenotypes.* Int J Biochem Cell Biol, 2006. **38**(10): p. 1625-31.
397. Poole, C.A., N.H. Brookes, and G.M. Clover, *Keratocyte networks visualised in the living cornea using vital dyes.* J Cell Sci, 1993. **106 ( Pt 2)**: p. 685-91.
398. Brown, T.A., et al., *Human keratinocytes express a new CD44 core protein (CD44E) as a heparan-sulfate intrinsic membrane proteoglycan with additional exons.* The Journal of cell biology, 1991. **113**(1): p. 207-221.
399. Hoar, R.M., *Embryology of the eye.* Environ Health Perspect, 1982. **44**: p. 31-4.
400. Meek, K.M. and C. Boote, *The organization of collagen in the corneal stroma.* Exp Eye Res, 2004. **78**(3): p. 503-512.
401. Scott, J.E. and A.M. Thomlinson, *The structure of interfibrillar proteoglycan bridges (shape modules') in extracellular matrix of fibrous connective tissues and their stability in various chemical environments.* J Anat, 1998. **192 ( Pt 3)**: p. 391-405.
402. Michelacci, Y.M., *Collagens and proteoglycans of the corneal extracellular matrix.* Braz J Med Biol Res, 2003. **36**(8): p. 1037-46.
403. Snyder, M.C., J. Bergmanson, and M.J. Doughty, *Keratocytes: no more the quiet cells.* Journal of the American Optometric Association, 1998. **69**(3): p. 180-187.
404. Whitcher, J.P., M. Srinivasan, and M.P. Upadhyay, *Corneal blindness: a global perspective.* Bull World Health Organ, 2001. **79**(3): p. 214-21.
405. Tabbara, K.F., *Blindness in the eastern Mediterranean countries.* Br J Ophthalmol, 2001. **85**(7): p. 771-5.
406. Dua, H.S., A. Miri, and D.G. Said, *Contemporary limbal stem cell transplantation - a review.* Clin Experiment Ophthalmol, 2010. **38**(2): p. 104-17.
407. Johnson, G.J., *Vision 2020: The right to sight: Report on the Sixth General Assembly of the International Agency for the Prevention of Blindness (IAPB).* Community Eye Health, 1999. **12**(32): p. 59.
408. Pinnamaneni, N. and J.L. Funderburgh, *Concise review: Stem cells in the corneal stroma.* Stem cells, 2012. **30**(6): p. 1059-1063.
409. Wilson, S.A. and A. Last, *Management of corneal abrasions.* American family physician, 2004. **70**: p. 123-132.
410. Matsuda, H. and G.K. Smelser, *Electron microscopy of corneal wound healing.* Experimental eye research, 1973. **16**(6): p. 427-442.
411. Funderburgh, J.L., M.M. Mann, and M.L. Funderburgh, *Keratocyte phenotype mediates proteoglycan structure: a role for fibroblasts in corneal fibrosis.* J Biol Chem, 2003. **278**(46): p. 45629-37.
412. Jester, J.V., W.M. Petroll, and H.D. Cavanagh, *Corneal stromal wound healing in refractive surgery: the role of myofibroblasts.* Progress in retinal and eye research, 1999. **18**(3): p. 311-356.

413. Jester, J.V., et al., *Expression of alpha-smooth muscle (alpha-SM) actin during corneal stromal wound healing.* Investigative ophthalmology & visual science, 1995. **36**(5): p. 809-819.
414. Helary, C., et al., *Dense fibrillar collagen matrices: a model to study myofibroblast behaviour during wound healing.* Biomaterials, 2006. **27**(25): p. 4443-52.
415. Beales, M.P., et al., *Proteoglycan synthesis by bovine keratocytes and corneal fibroblasts: maintenance of the keratocyte phenotype in culture.* Invest Ophthalmol Vis Sci, 1999. **40**(8): p. 1658-63.
416. Masur, S.K., et al., *Myofibroblasts differentiate from fibroblasts when plated at low density.* Proc Natl Acad Sci U S A, 1996. **93**(9): p. 4219-23.
417. Branch, M.J., et al., *Mesenchymal stem cells in the human corneal limbal stroma.* Invest Ophthalmol Vis Sci, 2012. **53**(9): p. 5109-16.
418. Du, Y., et al., *Stem cell therapy restores transparency to defective murine corneas.* Stem Cells, 2009. **27**(7): p. 1635-42.
419. Long, C.J., et al., *Fibroblast growth factor-2 promotes keratan sulfate proteoglycan expression by keratocytes in vitro.* Journal of Biological Chemistry, 2000. **275**(18): p. 13918-13923.
420. Jester, J.V., et al., *The cellular basis of corneal transparency: evidence for 'corneal crystallins'.* J Cell Sci, 1999. **112 ( Pt 5)**: p. 613-22.
421. Joseph, A., et al., *Expression of CD34 and L-selectin on human corneal keratocytes.* Invest Ophthalmol Vis Sci, 2003. **44**(11): p. 4689-92.
422. Perrella, G., et al., *Expression of haematopoietic stem cell markers, CD133 and CD34 on human corneal keratocytes.* Br J Ophthalmol, 2007. **91**(1): p. 94-9.
423. Pei, Y., R.Y. Reins, and A.M. McDermott, *Aldehyde dehydrogenase (ALDH) 3A1 expression by the human keratocyte and its repair phenotypes.* Experimental eye research, 2006. **83**(5): p. 1063-1073.
424. Lassen, N., et al., *Antioxidant function of corneal ALDH3A1 in cultured stromal fibroblasts.* Free Radical Biology and Medicine, 2006. **41**(9): p. 1459-1469.
425. Choong, P.F., et al., *Mesenchymal stromal cell-like characteristics of corneal keratocytes.* Cytotherapy, 2007. **9**(3): p. 252-8.
426. Polisetty, N., et al., *Mesenchymal cells from limbal stroma of human eye.* Mol Vis, 2008. **14**: p. 431-42.
427. Bray, L.J., et al., *Evaluation of methods for cultivating limbal mesenchymal stromal cells.* Cytotherapy, 2012. **14**(8): p. 936-47.
428. Li, G.G., et al., *Mesenchymal stem cells derived from human limbal niche cells.* Invest Ophthalmol Vis Sci, 2012. **53**(9): p. 5686-97.
429. Pinnamaneni, N. and J.L. Funderburgh, *Concise review: Stem cells in the corneal stroma.* Stem Cells, 2012. **30**(6): p. 1059-63.
430. Shortt, A.J., et al., *Characterization of the limbal epithelial stem cell niche: novel imaging techniques permit in vivo observation and targeted biopsy of limbal epithelial stem cells.* Stem cells, 2007. **25**(6): p. 1402-1409.
431. Ezhkova, E. and E. Fuchs, *Regenerative medicine: An eye to treating blindness.* Nature, 2010. **466**(7306): p. 567-568.
432. Carlson, E.C., et al., *Altered KSPG expression by keratocytes following corneal injury.* Mol Vis, 2003. **9**: p. 615-623.
433. WOLLENSAK, G. and W.R. GREEN, *Analysis of sex-mismatched human corneal transplants by fluorescence in situ hybridization of the sex-chromosomes.* Experimental eye research, 1999. **68**(3): p. 341-346.
434. Dunphy, S., *Development and evaluation of a bilayered electrospun scaffold for the anterior cornea*, in *School of Pharmacy*. 2015, University of Nottingham.
435. Hashmani, K., et al., *Characterization of corneal stromal stem cells with the potential for epithelial transdifferentiation.* Stem Cell Res Ther, 2013. **4**(75): p. 927-936.

436. Zhao, S. and R.D. Fernald, *Comprehensive algorithm for quantitative real-time polymerase chain reaction.* Journal of computational biology, 2005. **12**(8): p. 1047-1064.
437. Schindler, M., et al., *A synthetic nanofibrillar matrix promotes in vivo-like organization and morphogenesis for cells in culture.* Biomaterials, 2005. **26**(28): p. 5624-5631.
438. Kuruvilla, D.J. and A.K. Salem, *Nanotechnology and Nanomedicine in Diabetes: An Overview.* Nanotechnology and Nanomedicine in Diabetes, 2012: p. 1.
439. Kwon, I.K., S. Kidoaki, and T. Matsuda, *Electrospun nano-to microfiber fabrics made of biodegradable copolyesters: structural characteristics, mechanical properties and cell adhesion potential.* Biomaterials, 2005. **26**(18): p. 3929-3939.
440. Basu, S., *Effects of three dimensional structure of tissue scaffolds on animal cell culture*. 2004, The Ohio State University.
441. Ortega, Í., et al., *Combined microfabrication and electrospinning to produce 3-D architectures for corneal repair.* Acta biomaterialia, 2013. **9**(3): p. 5511-5520.
442. Shah, A., et al., *The development of a tissue-engineered cornea: biomaterials and culture methods.* Pediatric research, 2008. **63**(5): p. 535-544.
443. Bondar, B., et al., *Functionality of endothelial cells on silk fibroin nets: comparative study of micro-and nanometric fibre size.* Biomaterials, 2008. **29**(5): p. 561-572.
444. Sidney, L.E., et al., *Effect of culture medium on propagation and phenotype of corneal stroma–derived stem cells.* Cytotherapy, 2015. **17**(12): p. 1706-1722.
445. Sidney, L.E., O.D. McIntosh, and A. Hopkinson, *Phenotypic Change and Induction of Cytokeratin Expression During In Vitro Culture of Corneal Stromal CellsCytokeratin Expression by Corneal Stromal Cells.* Investigative ophthalmology & visual science, 2015. **56**(12): p. 7225-7235.
446. Hashmani, K., et al., *Characterisation of corneal stromal stem cells with the potential for epithelial transdifferentiation.* Stem Cell Res Ther, 2013. **4**(3): p. 75.
447. Sidney, L.E., et al., *Concise review: evidence for CD34 as a common marker for diverse progenitors.* Stem Cells, 2014. **32**(6): p. 1380-9.
448. Liu, H., et al., *Cell therapy of congenital corneal diseases with umbilical mesenchymal stem cells: lumican null mice.* PloS one, 2010. **5**(5): p. e10707.
449. Jester, J.V., M.M. Rodrigues, and I.M. Herman, *Characterization of avascular corneal wound healing fibroblasts. New insights into the myofibroblast.* The American journal of pathology, 1987. **127**(1): p. 140.
450. Nishida, T., et al., *The network structure of corneal fibroblasts in the rat as revealed by scanning electron microscopy.* Investigative ophthalmology & visual science, 1988. **29**(12): p. 1887-1890.
451. Jester, J.V., et al., *Corneal keratocytes: in situ and in vitro organization of cytoskeletal contractile proteins.* Investigative Ophthalmology and Visual Science, 1994. **35**: p. 730-730.
452. Pei, Y., D.M. Sherry, and A.M. McDermott, *Thy-1 distinguishes human corneal fibroblasts and myofibroblasts from keratocytes.* Experimental eye research, 2004. **79**(5): p. 705-712.
453. Ng, R., et al., *Three-dimensional fibrous scaffolds with microstructures and nanotextures for tissue engineering.* Rsc Advances, 2012. **2**(27): p. 10110-10124.
454. von der Mark, K., et al., *Relationship between cell shape and type of collagen synthesised as chondrocytes lose their cartilage phenotype in culture.* 1977.
455. Benya, P.D. and J.D. Shaffer, *Dedifferentiated chondrocytes reexpress the differentiated collagen phenotype when cultured in agarose gels.* Cell, 1982. **30**(1): p. 215-224.
456. Emerman, J.T. and D.R. Pitelka, *Maintenance and induction of morphological differentiation in dissociated mammary epithelium on floating collagen membranes.* In vitro, 1977. **13**(5): p. 316-328.

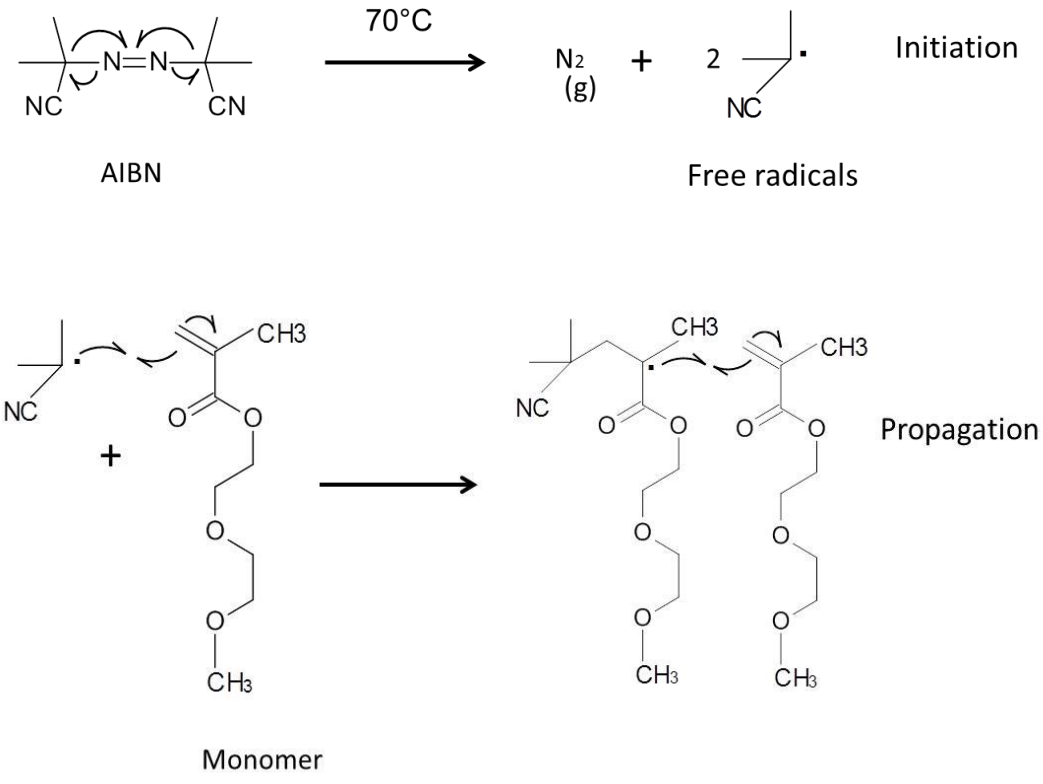
457. Vrana, N.E., et al., *Development of a reconstructed cornea from collagen–chondroitin sulfate foams and human cell cultures.* Investigative ophthalmology & visual science, 2008. **49**(12): p. 5325-5331.
458. Liu, H., J. Lin, and K. Roy, *Effect of 3D scaffold and dynamic culture condition on the global gene expression profile of mouse embryonic stem cells.* Biomaterials, 2006. **27**(36): p. 5978-5989.
459. Ru, C., et al., *A suspending, shrinkage-free electrospun PLGA nanofibrous scaffold for skin tissue engineering.* ACS applied materials & interfaces, 2015.
460. Liu, Y.-j., et al., *Control of dimensional stability and degradation rate in electrospun composite scaffolds composed of poly (d, l-lactide-co-glycolide) and poly (ε-caprolactone).* Chinese Journal of Polymer Science, 2008. **26**(01): p. 63-71.
461. Cui, W., et al., *Evaluation of electrospun fibrous scaffolds of poly (dl-lactide) and poly (ethylene glycol) for skin tissue engineering.* Materials Science and Engineering: C, 2009. **29**(6): p. 1869-1876.
462. Gualandi, C., et al., *Ethanol disinfection affects physical properties and cell response of electrospun poly (l-lactic acid) scaffolds.* European Polymer Journal, 2012. **48**(12): p. 2008-2018.
463. Sung, H.-J., et al., *The effect of scaffold degradation rate on three-dimensional cell growth and angiogenesis.* Biomaterials, 2004. **25**(26): p. 5735-5742.
464. Blakeney, B.A., et al., *Cell infiltration and growth in a low density, uncompressed three-dimensional electrospun nanofibrous scaffold.* Biomaterials, 2011. **32**(6): p. 1583-1590.
465. Sosnova, M., M. Bradl, and J.V. Forrester, *CD34+ corneal stromal cells are bone marrow-derived and express hemopoietic stem cell markers.* Stem Cells, 2005. **23**(4): p. 507-15.
466. Ainscough, S.L., et al., *Effects of fibroblast origin and phenotype on the proliferative potential of limbal epithelial progenitor cells.* Exp Eye Res, 2011. **92**(1): p. 10-9.
467. Wu, J., et al., *Bioengineering organized, multilamellar human corneal stromal tissue by growth factor supplementation on highly aligned synthetic substrates.* Tissue Eng Part A, 2013. **19**(17-18): p. 2063-75.
468. Jester, J.V., et al., *Induction of alpha-smooth muscle actin expression and myofibroblast transformation in cultured corneal keratocytes.* Cornea, 1996. **15**(5): p. 505-16.
469. Park, S.H., et al., *Human mesenchymal stem cells differentiate into keratocyte-like cells in keratocyte-conditioned medium.* Exp Eye Res, 2012. **101**: p. 16-26.
470. Pei, Y., D.M. Sherry, and A.M. McDermott, *Thy-1 distinguishes human corneal fibroblasts and myofibroblasts from keratocytes.* Exp Eye Res, 2004. **79**(5): p. 705-12.
471. Du, Y., et al., *Multipotent stem cells in human corneal stroma.* Stem Cells, 2005. **23**(9): p. 1266-75.
472. Du, Y., et al., *Multipotent stem cells in human corneal stroma.* Stem Cells, 2005. **23**(9): p. 1266-1275.
473. Garcia-Gonzalo, F.R. and J.C. Izpisua Belmonte, *Albumin-associated lipids regulate human embryonic stem cell self-renewal.* PLoS One, 2008. **3**(1): p. e1384.
474. Funderburgh, M.L., M.M. Mann, and J.L. Funderburgh, *Keratocyte phenotype is enhanced in the absence of attachment to the substratum.* Molecular vision, 2008. **14**: p. 308.
475. Scott, S.-G., A.S. Jun, and S. Chakravarti, *Sphere formation from corneal keratocytes and phenotype specific markers.* Experimental eye research, 2011. **93**(6): p. 898-905.
476. Wu, J., et al., *The engineering of organized human corneal tissue through the spatial guidance of corneal stromal stem cells.* Biomaterials, 2012. **33**(5): p. 1343-1352.
477. Said, D.G., et al., *Histologic features of transplanted amniotic membrane: implications for corneal wound healing.* Ophthalmology, 2009. **116**(7): p. 1287-95.

478. Jester, J.V., et al., *Corneal keratocytes: phenotypic and species differences in abundant protein expression and in vitro light-scattering.* Investigative ophthalmology & visual science, 2005. **46**(7): p. 2369.
479. Masur, S., J. Cheung, and S. Antohi, *Identification of integrins in cultured corneal fibroblasts and in isolated keratocytes.* Investigative ophthalmology & visual science, 1993. **34**(9): p. 2690-2698.
480. Yoshida, R., et al., *Pulsatile drug delivery systems using hydrogels.* Advanced drug delivery reviews, 1993. **11**(1-2): p. 85-108.
481. Kumoda, M., Y. Takeoka, and M. Watanabe, *Template synthesis of poly (N-isopropylacrylamide) minigels using interconnecting macroporous polystyrene.* Langmuir, 2003. **19**(3): p. 525-528.
482. Sahoo, S., et al., *Growth factor delivery through electrospun nanofibers in scaffolds for tissue engineering applications.* Journal of biomedical materials research Part A, 2010. **93**(4): p. 1539-1550.
483. Nubile, M., et al., *In vivo analysis of stromal integration of multilayer amniotic membrane transplantation in corneal ulcers.* Am J Ophthalmol, 2011. **151**(5): p. 809-822 e1.
484. Musselmann, K., et al., *Maintenance of the keratocyte phenotype during cell proliferation stimulated by insulin.* Journal of Biological Chemistry, 2005. **280**(38): p. 32634-32639.
485. Yoshida, S., et al., *Serum-free spheroid culture of mouse corneal keratocytes.* Investigative ophthalmology & visual science, 2005. **46**(5): p. 1653-1658.
486. Yamaji, S., et al., *A novel integrin-linked Kinase–Binding protein, affixin, is involved in the early stage of Cell–Substrate interaction.* The Journal of cell biology, 2001. **153**(6): p. 1251-1264.
487. Gronthos, S., et al., *Integrin-mediated interactions between human bone marrow stromal precursor cells and the extracellular matrix.* Bone, 2001. **28**(2): p. 174-181.
488. Azarin, S.M. and S.P. Palecek, *Development of scalable culture systems for human embryonic stem cells.* Biochemical engineering journal, 2010. **48**(3): p. 378-384.
489. Ma, Z., K. Masaya, and S. Ramakrishna, *Immobilization of Cibacron blue F3GA on electrospun polysulphone ultra-fine fiber surfaces towards developing an affinity membrane for albumin adsorption.* Journal of membrane science, 2006. **282**(1): p. 237-244.

# Appendixes

## Appendix A

Poly ($PEGMA_{188}$) was prepared by free radical polymerization following a published method [251], as shown in Figure A-1. In brief, initiation of the reaction started at a temperature of 70°C when the azobisisobutyronitrile (AIBN) initiator's double bond was cleaved, which resulted in the formation of two free radicals. The formed free radicals then interacted with the unstable double bond of the monomer di (ethylene glycol) methyl ether methacrylate, which resulted in the formation of a monomer free radical. This then propagated the reaction by attaching to other monomers in the solution for 1 h until the reaction was terminated by cooling the solution. Finally, the prepared poly ($PEGMA_{188}$) was precipitated three times in 500 mL of hexane and dissolved in 50 mL of 2-butanone to be cleared from the $PEGMA_{188}$ monomer.



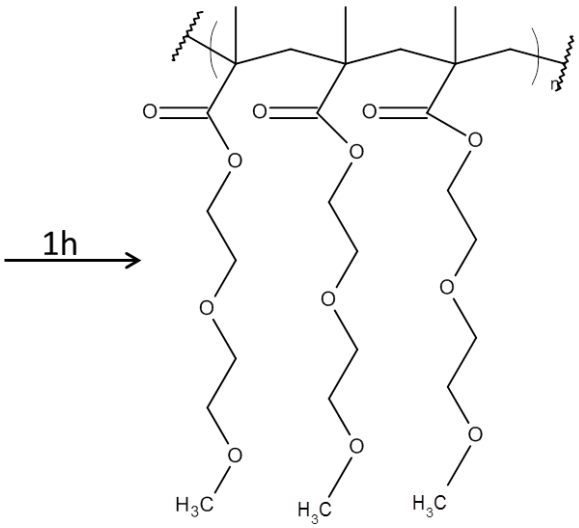
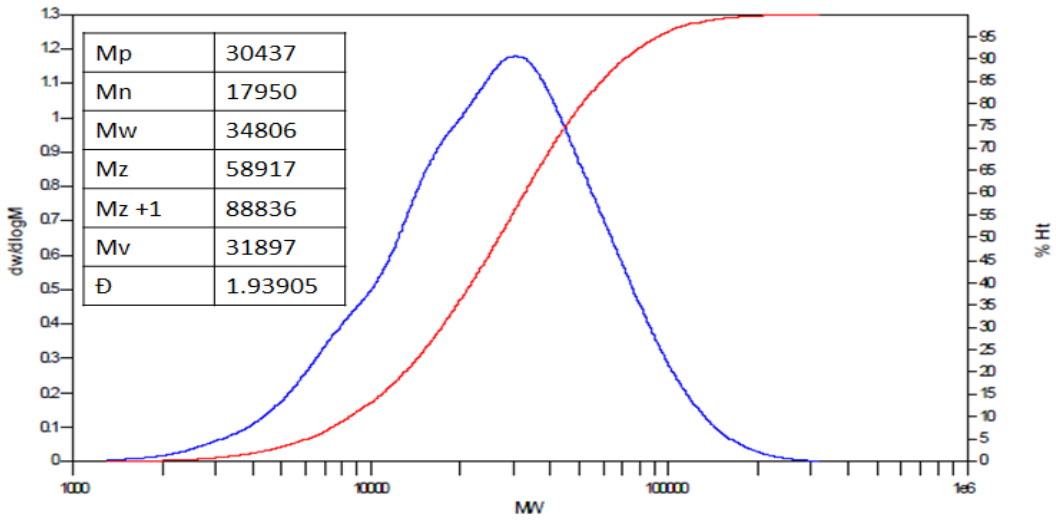



**Figure A-1:** Free radical polymerization of poly ($PEGMA_{188}$)

Figure A-2 (A and B) showed the GPC characterization of batches 2 and 3 of poly ($PEGMA_{188}$) polymer, which indicated a molar mass of 54.7 kDa (Đ = 1.9) and 34.8 kDa (Đ = 1.9), respectively.

**A**



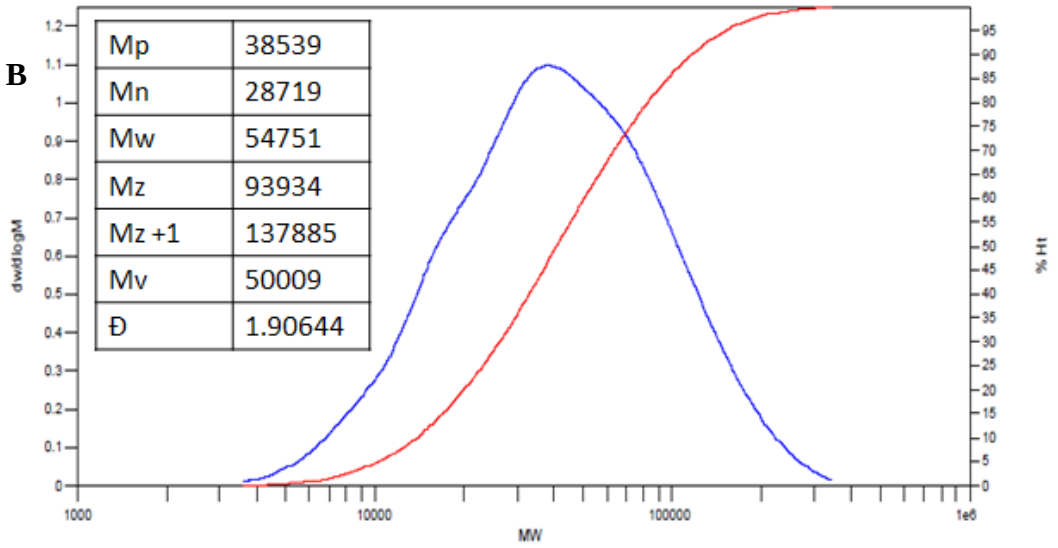



**Figure A-2:** GPC chromatogram showing the molar mass distribution of poly ($PEGMA_{188}$), A) batch 2 and B) batch 3.

SEM analysis for fibre scaffolds fabricated from PET pellets in Figure A-3 reveled that at a concentration of 9% *(w/v)*, PET scaffolds were composed of large and numerous beads, with average fibre diameter of 149.1 ± 54.1 nm. By increasing the concentration of the PET polymer to 10%, 10.5% and 11.5% (*w/v*) and maintaining the same electrospinning parameters, the resultant scaffolds overall had the same large beads but were fewer in number, and a more fibrous mat resulted. The average fibre diameters were increased by increasing the PET polymer solution concentrations with 177.6 ± 82.4 nm, 169.1 ± 95.2 nm and 253.1 ± 102.5 nm respectively.

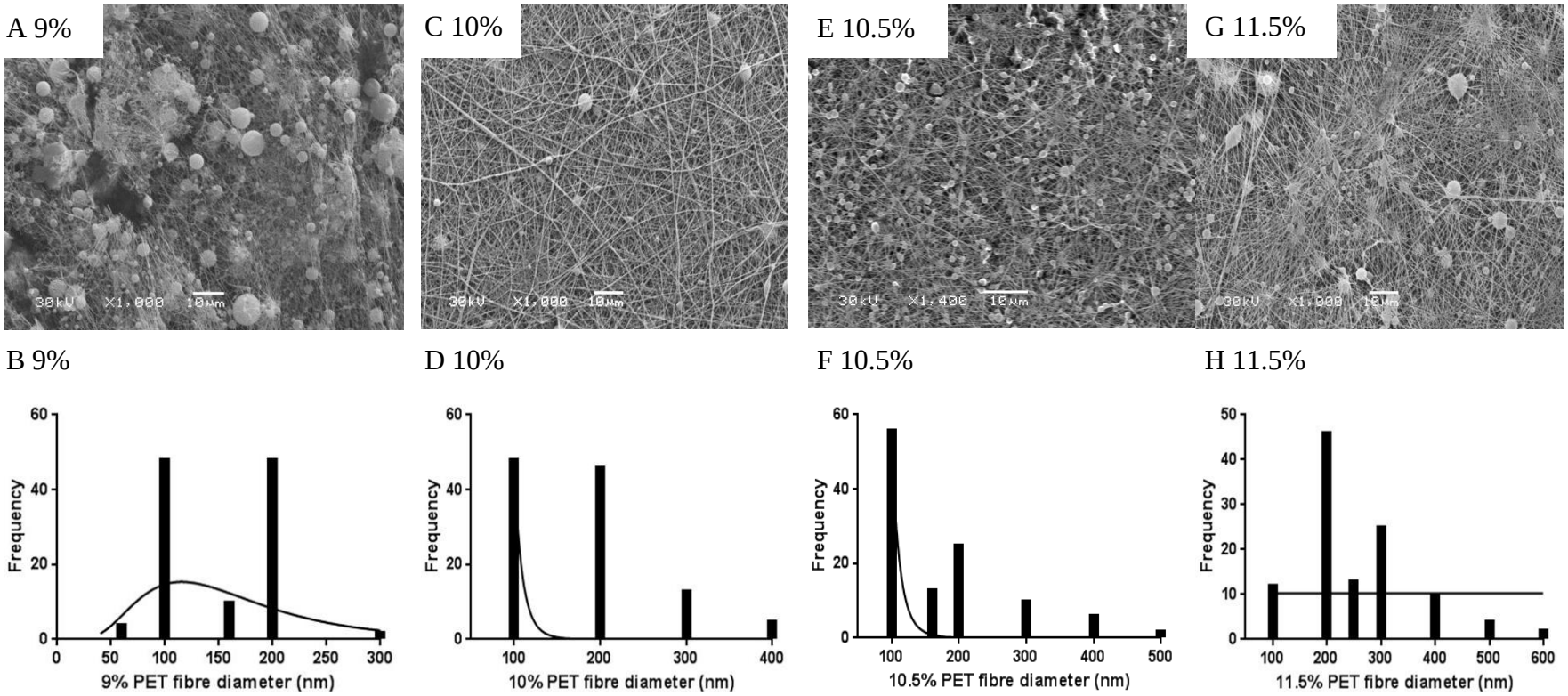



**Figure A-3:** Representative SEM images and histogram charts of pellets PET fibres showing the surface morphology at magnification powers of x1000, and frequency of fibre diameter (nm), of four different polymer solution concentrations A-B) 9% (*w/v*), C-D) 10% (*w/v*), E-F) 10.5% (*w/v*), and G-H) 11.5% (*w/v*). For histogram charts 20 measurements from each SEM image were recorded (100 in total), n = 5, n represent the number of replicates were taken from one batch of each scaffolds.

**Table A-1:** A summary table of electrospinning parameters for pellet PET polymer and fibre characterizations

| PET concentration (*w/v* %) | Solvent (1:1) (mL) | Collector distance (cm) | Voltage (KV) | Flow rate (mL/h) | Needle gauge | Fibre morphology | Diameter (mean ±SD) nm | WCA (mean ±SD) ($^{o}$) |
|---|---|---|---|---|---|---|---|---|
| 9 | DCM/TFA | 15 | 14 | 0.5 | 18 | Large numerous beads | 149.1 ± 54.1 | Hydrophobic surface |
| 10 | DCM/TFA | 15 | 14 | 0.5 | 18 | More fibres, less beads | 177.6 ± 82.4, | |
| 10.5 | DCM/TFA | 15 | 14 | 0.5 | 18 | More fibres, less beads | 169.1 ± 95.2 | |
| 11.5 | DCM/TFA | 15 | 14 | 0.5 | 18 | More fibres, less beads | 253.1 ± 102.5 | |

$^1$H NMR was conducted for PLGA and PET electrospun scaffolds as showen in Figure A-4, and resulted for PLGA (400 MHz, $CDCl_3$): δ 1.6 (br s, 3H,CHC$H_3$ ), 4.8 (br m, 2H, $CH_2O$ ), 5.2 (br m, 1H, C$H$CH$_3$ ). $^1$H NMR for PET (400 MHz, $CDCl_3$): δ 4.8 (br s, 4H, 2 $CH_2$ ), 8.1 (br s, 4H, $CH_{aromatic}$).

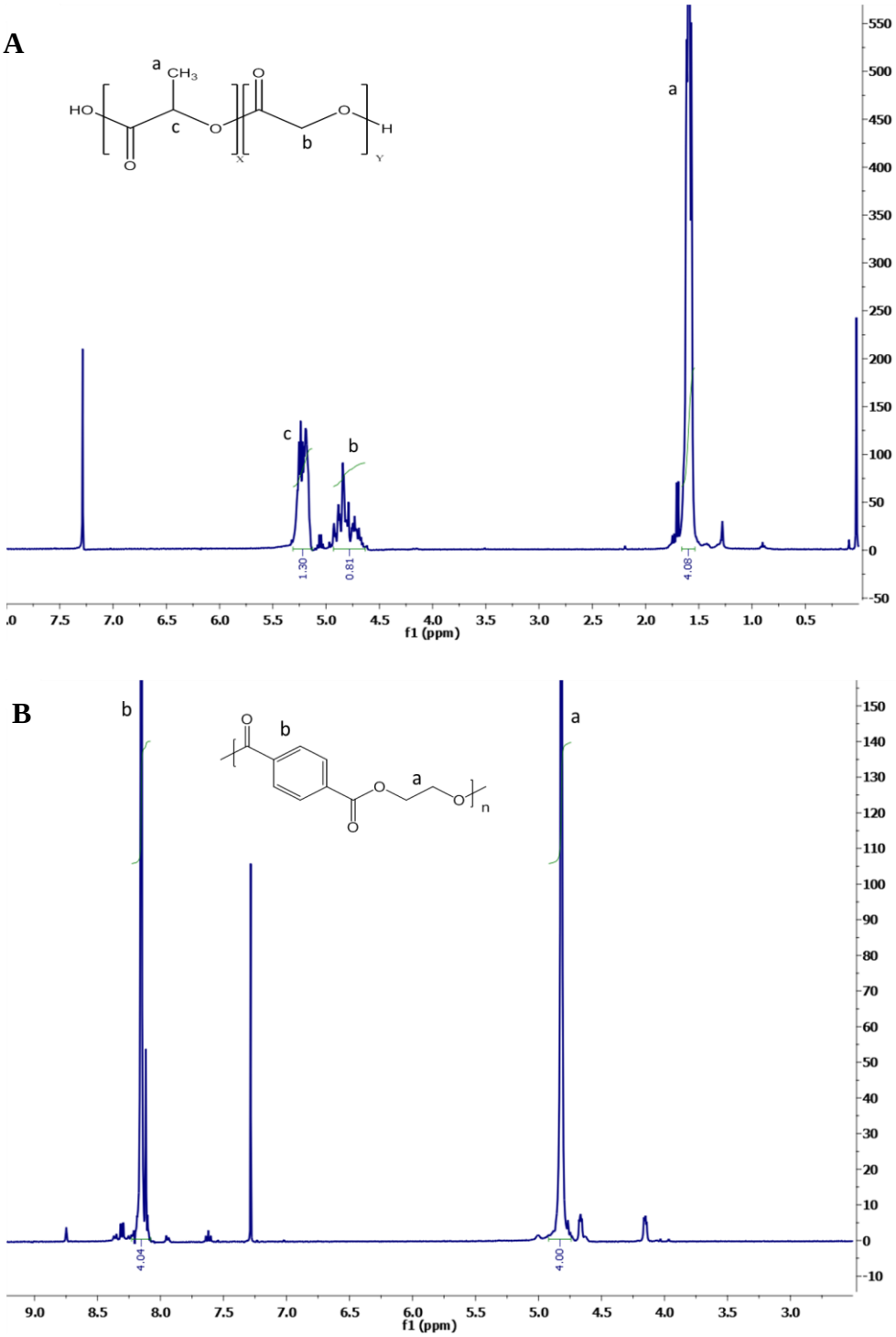



**Figure A-4:** $^1$H NMR for electrospun A) poly (lactic-co-glycolic acid) (PLGA) and B) poly (ethylene terephthalate) (PET).

# Appendix B

Calibration curve of NIH 3T3 red fluorescent shown in Figure B-1 was used to calculate the cell number after performing the cell viability AB assay.

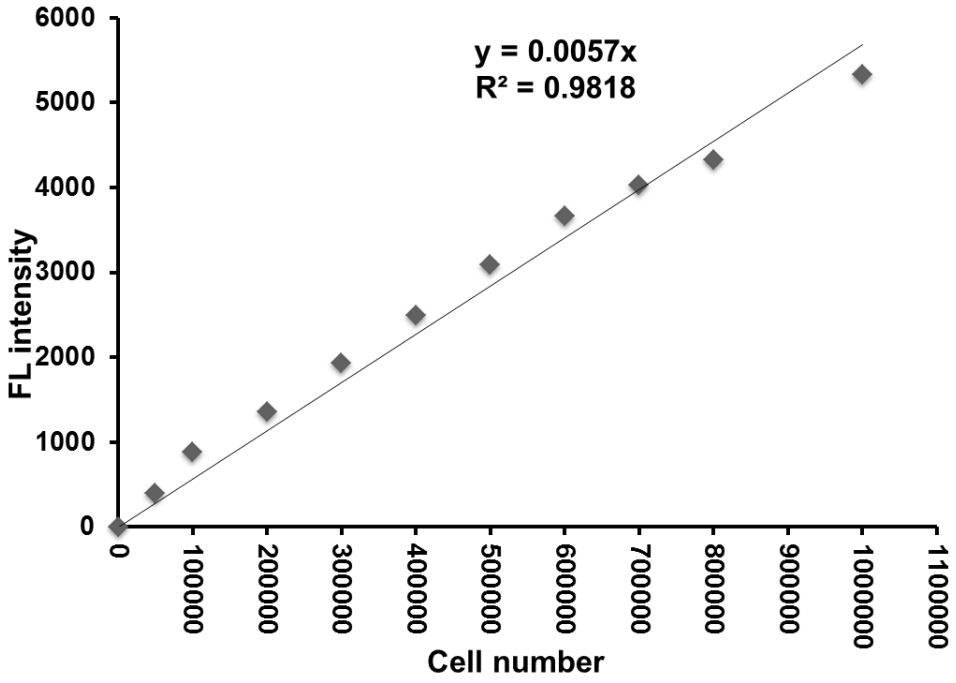



**Figure B-1:** Calibration curve of NIH 3T3 red fluorescent protein (RFP) expressing 3T3 fibroblast cells, using the AB assay. Data are shown as mean ± SD, (n = 3, average of three readings).

# Appendix C

Calibration curve of Caco2 cells and ihMSC shown in Figure C-1 (A and B) was used to calculate the cell number after performing the cell viability AB assay.

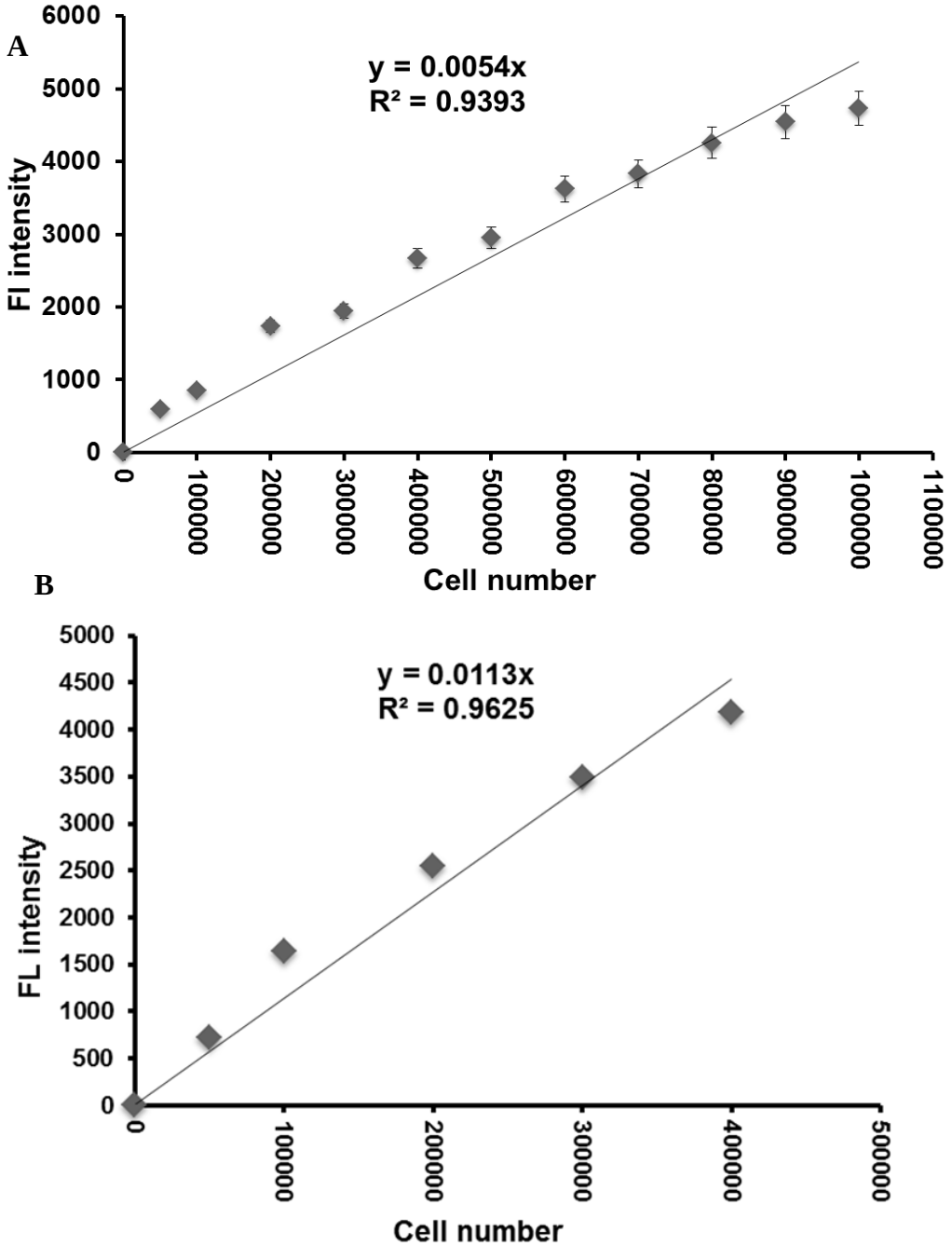



**Figure C-1:** Calibration curve of A) Caco2 cells and B) ihMSC, using the AB assay. Data are shown as mean ± SD, (n = 3, average of three readings)

# Appendix D

Calibration curve of hCSSCs shown in Figure D-1 was used to calculate the cell number after performing the cell viability AB assay.

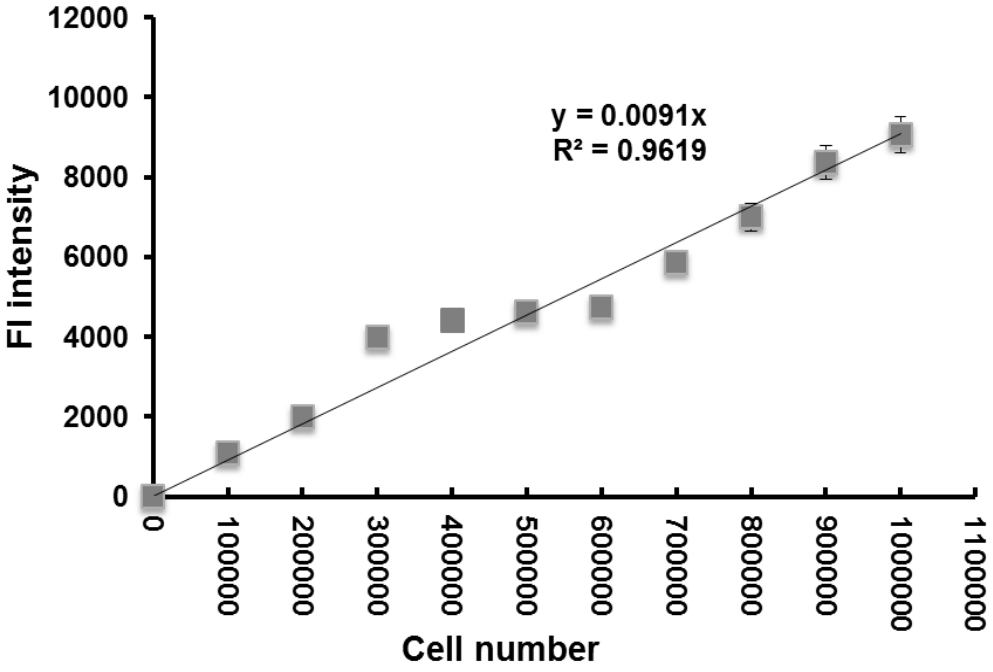



**Figure D-1:** Calibration curve of hCSSCs, using the AB assay. Data are shown as mean ± SD, (n = 3, average of three readings)

The RT-qPCR data is shown in Figure D-2, all the genes *CD34* and *ALDH3A1* (keratocytes markers), *TYH1* (fibroblast/MSC marker) or *ACTA2* (myofibroblast marker) at each passage are presented. These data show there was a significant increase in *CD34* and *ALDH3A1* expression in the cells on 3D electrospun scaffolds at all passages when compared with the 2D TCPS. Additionally, no significant difference in the *TYH1* expression was observed and there was a significant decrease in the *ACTA2* marker expression on the 3D responsive scaffolds at passage 6 and 9 when compared with the expressions in cells on the 2D TCPS.

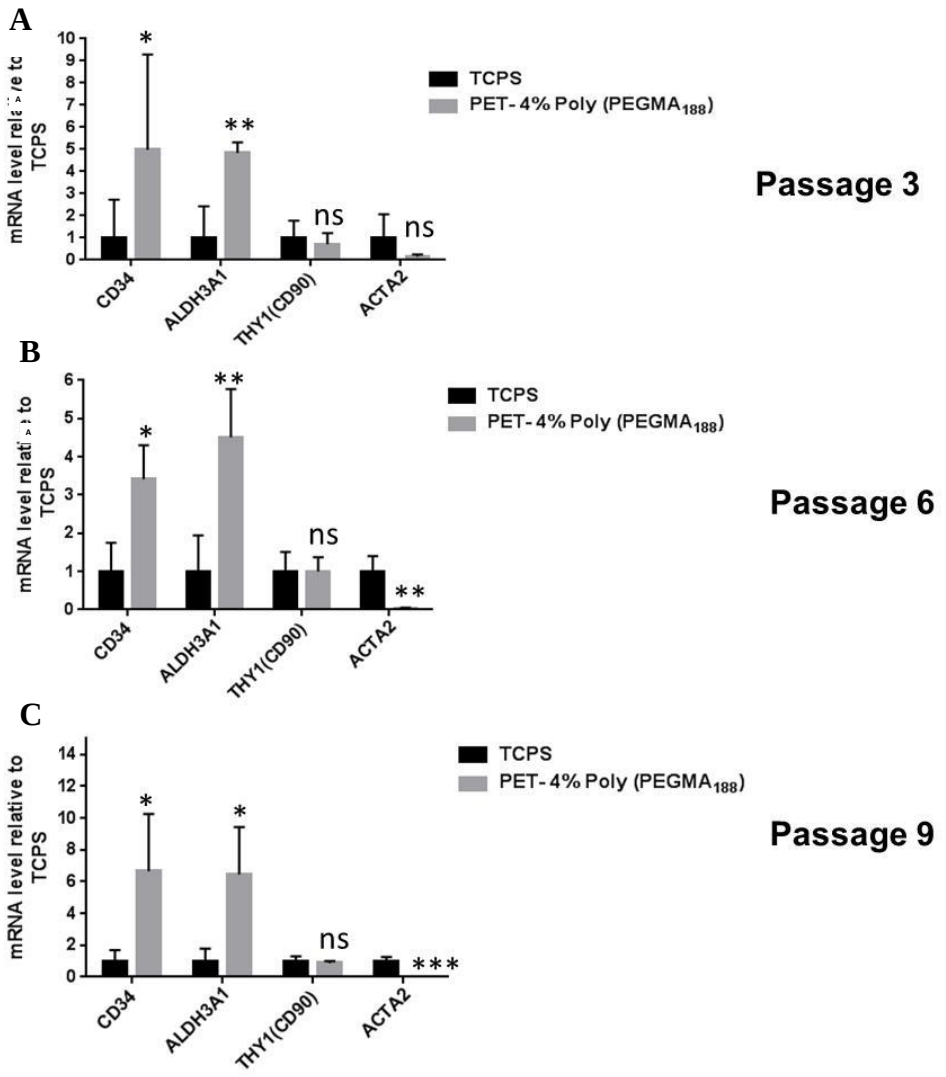



**Figure D-2:** Comparative effects of culture environment TCPS and PET- 4% poly ($PEGMA_{188}$) on gene expression of hCSSCs at different thermal and enzymatic passages of (A) 3, (B) 6 and (C) 9. Relative levels of mRNA were determined by means of RT-qPCR for the following genes: *CD34*, *ALDH3A1*, *THY1* and *ACTA2*. Expression of each target gene is normalized to *GAPDH* (housekeeping gene) and represented relative to mRNA expression in TCPS of each passage. Data are shown as mean ± standard error of the mean of three independent experiments (n = 3), each with two replicates. Statistical significance versus TCPS: $^{*}P \leq 0.05$, $^{**}P \leq 0.01$, $^{***}P \leq 0.001$ (Student's t-test). Note: after passage 3, *CD34* gene expression of TCPS is equal to n = 2 for passage 6 and passage 9.

The same data are presented in Figure D-3, however, the differences in gene expression between passages 3, 6 and 9 were relative to the mRNA expression in TCPS and in PET-4% poly ($PEGMA_{188}$) for TCPS and PET-4% poly ($PEGMA_{188}$),

respectively, at passage 3. The 3D thermo-responsive electrospun scaffolds promoted the expression of the keratocyte markers, *CD34* and *ALDH3A1* (inactivated phenotype), along with significantly reducing the expression of the myofibroblastic marker, *ACTA2* (activated phenotype), and the expression of the MSC/fibroblast marker CD90 on both scaffolds and TCPS.

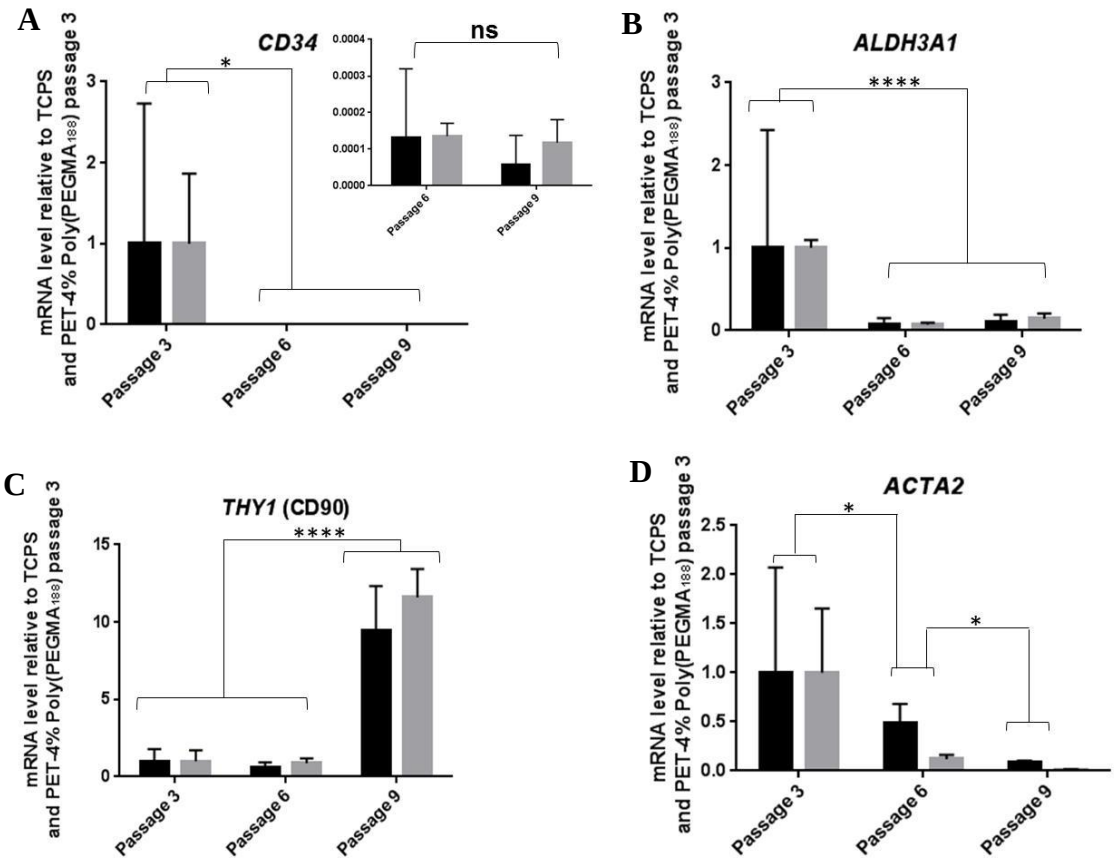



**Figure D-3:** Comparative effects of increasing passage number on gene expression of hCSSCs culture on TCPS and PET- 4% poly ($PEGMA_{188}$) at different thermal and enzymatic passages of 3, 6 and 9. Relative levels of mRNA were determined by means of RT-qPCR for the following genes: (A) *CD34*, (B) *ALDH3A1*, (C) *THY1* and (D) *ACTA2*. Expression of each target gene is normalized to *GAPDH* (housekeeping gene) and represented relative to mRNA expression in TCPS for TCPS and in PET- 4% poly ($PEGMA_{188}$) for scaffolds of passage 3. Data are shown as mean ± standard error of the mean of three independent experiments (n = 3), each with two replicates. Statistical significance versus TCPS: $^{*}P \leq 0.05$, $^{****}P \leq 0.0001$ (one-way ANOVA). Note: after passage 3, *CD34* gene expression of TCPS is equal to n = 2 for passage 6 and passage 9.